University of Naples Federico II

Polytechnic and Basic Science School

Department of Chemical Sciences

Ph.D. in Chemical Sciences

Semi synthetic polysaccharides for *drug-discovery*

Fabiana Esposito

Advisor:

prof. Emiliano Bedini

Examiner:

prof. Paola Manini

XXXVII Cycle 2022 – 2025

Coordinator: prof. Angela Lombardi

La borsa di dottorato è stata cofinanziata con risorse del
Programma Operativo Nazionale Ricerca e Innovazione 2014-2020,
risorse FSE REACT-EU
Azione IV.4 “Dottorati e contratti di ricerca su tematiche dell’innovazione”
e Azione IV.5 “Dottorati su tematiche Green”

Table of Contents

List of publications

1) Vessella G., **Esposito F.**, Traboni S., Di Meo C., Iadonisi A., Schiraldi C., Bedini E.* Exploiting Diol Reactivity for the Access to Unprecedented Low Molecular Weight Curdlan Sulfate Polysaccharides. *Carbohydrate Polymers* **2021**, *269*, 118324. doi: 10.1016/j.carbpol.2021.118324

2) **Esposito F.**, Vessella G., Sinquin C., Traboni S., Iadonisi A., Colliec-Jouault S., Zykwinska A.* Bedini E.* Glycosaminoglycan-like sulfated polysaccharides from *Vibrio diabolicus* bacterium: Semi-synthesis and characterization. *Carbohydrate Polymers* **2022**, *283*, 119054. doi: 10.1016/j.carbpol.2021.119054

3) Pizzolitto C., **Esposito F.**, Sacco P., Marsich E., Gargiulo V., Bedini E.*, Donati I.* Sulfated lactose-modified chitosan. A novel synthetic glycosaminoglycan-like polysaccharide inducing chondrocyte aggregation, *Carbohydrate Polymers* **2022**, *288*, 119379. doi: 10.1016/j.carbpol.2022.119379

4) Colliec-Jouault S., **Esposito F.**, Ledru H., Sinquin C., Marchand L., FIllaudeau A., Routier S., Buron F., Lopin-Bon C., Cuenot S., Bedini E. *, Zykwinska A. * Glycosaminoglycan mimetics obtained by microwave-assisted sulfation of marine bacterium sourced infernan exopolysaccharide, *Biomacromolecules* **2023**, *24 (1)*, 462-470. doi: 10.1021/acs.biomac.2c01277

5**)** Traboni S.,* **Esposito F.**, Ziaco M., Bedini E., Iadonisi A. A comprehensive solvent-free approach for the esterification and amidation of carboxylic acids mediated by carbodiimides. *Tetrahedron* **2023**, *133*, 133291. doi: 10.1016/j.tet.2023.133291

6) Traboni S., Bedini E., Capasso D., **Esposito F.**, Iadonisi A.* Adaptation of Zemplén's conditions for a simple and highly selective approach to methyl 1,2−trans glycosides. *Carbohydrate Research* **2023**, *528*, 108824. doi: 10.1016/j.carres.2023.108824

7) **Esposito F.**, Laezza A., Gargiulo V., Traboni S., Iadonisi A., La Gatta A., Schiraldi C., Bedini E.* Multi-step Strategies Toward Regioselectively Sulfated M-Rich Alginates. *Biomacromolecules* **2023**, *24*, 2522. doi: 10.1021/acs.biomac.3c00045

8) **Esposito F.**, Traboni S**.**, Iadonisi A., Bedini E.* Towards the semi-synthesis of phosphorylated mimics of glycosaminoglycans: Screening of methods for the regioselective phosphorylation of chondroitin. *Carbohydrate Polymers* **2024**, 3*24*, 121517. doi: 10.1016/j.carbpol.2023.121517

9) **Esposito F.**, Sinquin C., Colliec-Jouault S., Cuenot S., Pugnière M., Ngo G., Traboni S., Zykwinska A.* Bedini E.* Multi-step semi-synthesis, structural characterization and growth factor interaction study of regiochemically sulfated diabolican polysaccharides. *International Journal of Biological Macromolecules* **2024**, *260*, 129483. doi: 10.1016/j.ijbiomac.2024.129483

10) Traboni S.*, **Esposito F**., Ziaco M., De Cesare N., Bedini E., Iadonisi A. Catalytic Cleavage of the 9-Fluorenylmethoxycarbonyl (Fmoc) Protecting Group under Neat Conditions. *Organic Letters* **2024**, *26*, 3284-3288. doi: 10.1021/acs.orglett.4c00918

List of abbreviations

Ac	Acetyl
Ac_2O	Acetic anhydride
AcOH	Acetic acid
AS	Alginate sulfate
BC	Biotechnological chondroitin
BDDE	1,4-butanediol diglycidyl ether
BDPE	1,4-butanediol di-(propan-2,3-diolyl) ether
BMP-2	Bone Morphogenetic Protein-2
BTH	Bovine testicular hyaluronidase
BTSA	*N*,*O*-bis(trimethylsilyl)acetamide
Bz	Benzoyl
Bz_2O	Benzoic anhydride
BzCN	Benzoyl cyanide
CdS	Curdlan sulfate
$(CH_3O)_3PO$	Trimethyl phosphate
$CHCl_3$	Chloroform
COSY	COrrelation SpectroscopY
CP	Chondroitin phosphate
CPG	Cyclic protecting group
CS	Chondroitin sulfate
CSA	(+)-camphor-10-sulfonic acid
CtP	Chitosan phosphate
$Cu(OAc)_2$	Copper (II) acetate
DBU	1,8-Diazabicyclo(5.4.0)undec-7-ene
DeP	Dermatan sulfate
DIPEA	*N*,*N*-diisopropylethylamine

DMAP	4-dimethylaminopyridine
DMF	*N,N*-dimethylformamide
DMSO	Dimethylsulfoxide
DMT-Cl	dimethoxytrityl chloride
DOSY	Diffusion Ordered SpettroscopY
DPh	Degree of phosphorylation
DS	Degree of sulfation
EGF	Epidermal Growth Factor
Et_2O	Diethyl ether
Et_3N	Triethylamine
FGF-2	Fibroblast Growth Factor-2
GAG	Glycosaminoglycan
GalNAc, N	2-Acetamido-2-deoxy-galactose (*N*-acetyl-galactosamine)
GDF-5	Growth/Differentiation Factor-5
Glc	Glucose
GlcA, U	Glucuronic Acid
GlcNAc	2-Acetamido-2-deoxy-glucose (*N*-acetyl-glucosamine)
GulA, G	Guluronic acid
H_3PO_4	Phosphoric acid
HA	Hyaluronic acid
HBr	Hydrogen bromide
HeP	Heparin
HMBC	Heteronuclear Multiple Bond Correlation
HPLC	High Performance Liquid Chromatography
HP-SEC	High Performance Size Exclusion Chromatography
HS	Heparan sulfate
HSQC	Heteronuclear Single Quantum Coherence
i-Pr_2O	Diisopropyl ether
K_d	Dissociation constant

KS	Keratan sulfate
LMW	Low molecular weight
MALS	Multiangle Light Scattering
ManA, M	Mannuronic acid
MTSTFA	*N*-methyl-*N*-(trimethylsilyl)-trifluoroacetamide
M_w	Molecular weight
n.d.	Not determined
$N_2H_4 \cdot H_2O$	Hydrazine monohydrate
$N_2H_4 \cdot H_2SO_4$	Hydrazine sulfate salt
$Na_2S_2O_4$	Sodium dithionite
$NaBH_4$	Sodium borohydride
$NaBrO_3$	Sodium bromate
NaOAc	Sodium acetate
NOESY	Nuclear Overhauser Enhancement SpectroscopY
o.n.	overnight
P_2O_5	Phosphorus pentoxide
PEP-K	Monopotassium salt of phosphoenolpyruvate
PG	Protecting group
$PhC(OCH_3)_3$	Trimethyl orthobenzoate
$PhCH(OCH_3)_2$	α,α-dimethoxytoluene
$POCl_3$	Phosphorus oxychloride
p-OMe-$PhCH(OCH_3)_2$	Anisaldehyde dimethyl acetal
PS	Polysaccharide
py	Pyridine
r.t.	Room temperature
SD	Sulfated diabolican
$SO_3 \cdot DMF$	*N*,*N*-dimethylformamide-sulfur trioxide complex
$SO_3 \cdot Me_3N$	Trimethylamine-sulfur trioxide complex

SO_3·py	Pyridine-sulfur trioxide complex
SPR	Surface Plasmon Resonance
TBA	Tetrabutylammonium
TBAHS	*n*-tetrabutyl-ammonium bisulfate
TBAOH	Tetrabutylammonium hydroxide
TBDMSCl	*t*-butyl-dimethylsilyl chloride
TGF-β1	Transforming Growth Factor
TIPSCl	Triisopropylsilyl chloride
TLC	Silica-gel thin-layer chromatography
TMOF	Trimethyl orthoformate
$TMSCHN_2$	Trimethylsilyldiazomethane
TOCSY	TOtal Correlation SpectroscopY
VEGF	Vascular Endothelial Growth Factor
Ψ^0	(2*S*,3a*S*,6*R*,7a*S*)- -methyl-2-(4-bromophenyl)thio)-6-(prop-2-yl)hexahydrobenzo[*d*][1,3,2]oxathiaphosphole 2-oxide

Portions of this work have been adapted from the following articles that were co-written by the author:

Esposito F., Vessella G., Sinquin C., Traboni S., Iadonisi A., Colliec-Jouault S., Zykwinska A.* Bedini E.* Glycosaminoglycan-like sulfated polysaccharides from *Vibrio diabolicus* bacterium: Semi-synthesis and characterization. *Carbohydrate Polymers* **2022**, *283*, 119054. doi: 10.1016/j.carbpol.2021.119054

Esposito F., Sinquin C., Colliec-Jouault S., Cuenot S., Pugnière M., Ngo G., Traboni S., Zykwinska A.* Bedini E.* Multi-step semi-synthesis, structural characterization and growth factor interaction study of regiochemically sulfated diabolican polysaccharides. *International Journal of Biological Macromolecules* **2024**, *260*, 129483. doi: 10.1016/j.ijbiomac.2024.129483

Esposito F., Laezza A., Gargiulo V., Traboni S., Iadonisi A., La Gatta A., Schiraldi C., Bedini E.* Multi-step Strategies Toward Regioselectively Sulfated M-Rich Alginates. *Biomacromolecules* **2023**, *24*, 2522. doi: 10.1021/acs.biomac.3c00045

Vessella G., **Esposito F.**, Traboni S., Di Meo C., Iadonisi A., Schiraldi C., Bedini E.* Exploiting Diol Reactivity for the Access to Unprecedented Low Molecular Weight Curdlan Sulfate Polysaccharides. *Carbohydrate Polymers* **2021**, *269*, 118324. doi: 10.1016/j.carbpol.2021.118324

Esposito F., Traboni S**.**, Iadonisi A., Bedini E.* Towards the semi-synthesis of phosphorylated mimics of glycosaminoglycans: Screening of methods for the regioselective phosphorylation of chondroitin. *Carbohydrate Polymers* **2024**, 3*24*, 121517. doi: 10.1016/j.carbpol.2023.121517

Abstract

Polysaccharides are the most abundant biomacromolecules on our planet, possessing enormous structural diversity and functional versatility. They are currently employed for several purposes, both in their natural and structurally modified forms. An important class of natural polysaccharides includes the sulfated ones, ubiquitous in living systems, which play key roles in several biological functions. Among them, sulfated glycosaminoglycans (GAGs), extracted from animals sources, are the most studied ones. They have a lots of biological activities and play pivotal roles in several physio-pathological processes. Thus, various applications as biomaterials and therapeutics have been developed. Despite this, their employment for the formulation of novel drugs may exhibit limitations connected to production costs, batch standardization, immunogenicity, degradability, or other aspects. The biological activities of sulfated polysaccharides often depend on the selective interaction between the sulfate group(s) on polysaccharide backbone and proteins. This suggested that the sulfation pattern might be able to encode specific functional information.

The obtainment of semi-synthetic sulfated polysaccharides, by chemical or enzymatic modifications of natural ones, can lead to structures with a controlled and well-defined distribution of sulfate groups within polysaccharide repeating units (also called sulfation pattern), which can facilitate the studies about structure-activity relationships. Besides, semi-synthetic polysaccharides can exhibit new and enhanced biological properties compared to their unmodified counterparts and can also be produced in large quantities at low costs from sustainable sources.

In this frame, this project investigated the possibility to obtain regioselective sulfated polysaccharides by chemical modification of natural unsulfated ones. To this aim, three biopolymers were considered: (1) diabolican, a marine-sourced bacterial exopolysaccharide, resembling GAG structure due to the presence, in its backbone, of aminosugars and uronic acids; (2) alginate polysaccharides, produced, for commercial purposes, from brown algae and (3) curdlan, a β-1→3-glucan produced, for

commercial purposes, from mutant *Agrobacterium* strains. Species with unprecedented sulfation pattern, some of them showing a well-defined structure, were obtained both by direct regioselective sulfation/desulfation reactions and by multi-step methods, including the use of either cyclic or acyclic protecting groups.

Furthermore, the possibility to obtain anionic analogues of sulfated polysaccharides was investigated by functionalization of some hydroxyls with phosphate groups. *In silico* studies recently appeared in literature suggested that phosphorylated polysaccharides could bind proteins generally with a stronger affinity than sulfated ones, but, to the best of our knowledge, they have been poorly investigated, despite of their interesting perspectives. To fill this gap, a screening of different phosphorylating reagents and/or reaction conditions was performed towards the semi-synthesis of regioselectively phosphorylated bacterial sourced chondroitin and chitosan polysaccharides.

Lastly, in collaboration with IBSA Farmaceutici Italia Srl, cross-linked GAGs, characterized by high biocompatibility and optimized for use both in regenerative and aesthetic medicine (*e.g.* for use in injectable fillers) and in the orthopedic/physiatric field as intrarticular gels for viscosupplementation, have been studied.

CHAPTER 1

INTRODUCTION

1

INTRODUCTION

1.1 Carbohydrates

Carbohydrates are classified as the most abundant classes of organic compounds in nature, playing crucial roles in living organisms as a primary source of energy and as structural components. They represent the most information-rich class of biomacromolecules and exhibit high structural diversity compared to DNA or proteins. The building blocks of carbohydrates are known as monosaccharides, which are polyhydroxyaldehydes or polyhydroxyketones with at least three carbon atoms. Monosaccharides are classified according to the number of carbon atoms they contain and the arrangement of the hydrogen and oxygen atoms attached to the carbons. In particular, they are classified by the stereochemical configuration of the asymmetric carbon atom farthest from the carbonyl group. Two different groups can be distinguished depending on whether the hydroxyl group on the last asymmetric carbon is on the right (D-series) or on the left (L-series) in the Fischer projection. Most of the naturally occurring sugars belong to the D-series, with some exceptions (*e.g.* fucose) that have been found in the L-form. Monosaccharides can also exist in acyclic (represented by Fisher's projection) or cyclic forms, the latter characterized by a hemiacetal (or hemiketal) group formed by the reaction between one of the hydroxyl groups of the chain and the carbonyl function. The formation of the cyclic structure creates an additional asymmetric carbon, called anomeric carbon. Therefore, two diastereoisomeric forms can exist for each cyclic sugar and these are designated as α- and β-anomers whether the absolute configurations at the anomeric carbon and the farthest stereogenic centre are the same (α anomer) or different (β anomer) (Seeberger, **2015**).

Carbohydrates exist also in more complicated structures called oligosaccharides (composed by less than a dozen monomers) or polysaccharides (composed by more than dozen monomers), resulting from the linkage of different monosaccharides through acetal bonds (also called glycosidic bonds).

These compounds can be structurally very different, not only for the type of constituent monomers but also for the ways they are linked. Indeed, different linkage positions are available since each sugar typically has more than one unmodified hydroxyl group to which the anomeric carbon of another moiety can bind: this allows the construction both of linear and branched products. In addition, each anomeric carbon is a stereogenic centre and therefore each glycosidic linkage can be constructed having either the α- or β-configuration. This structural variability results in a wide range of biological properties.

Carbohydrates are very often involved in cell communication, playing key roles in immune response, viral replication, cell-cell adhesion, fertilisation, parasitic infection, cell growth and differentiation, and inflammation. Thanks to these characteristics, they have applications in different fields. For example, these bioactivities have prompted their application in pharmaceutical industry, leading to the development of various carbohydrate-based drugs, vaccines and nutrients (Brown et al., **2007**; Hudak and Bertozzi, **2014**; Mettu et al., **2020**).

1.2 Polysaccharides

Polysaccharides (PSs) are polymeric carbohydrates, composed of monosaccharide monomers joined together by glycosidic bonds. They are the most abundant biomacromolecules on our planet, possessing enormous structural diversity and functional versatility, currently employed for several purposes in biomedical field, both in their natural and structurally modified forms. These structures are often linear, but may contain various degrees of branching. PSs are often classified as homopolysaccharides, if the repeating unit is composed of a single type of sugar

monomers, and heteropolysaccharides if it is composed of different types of monomers. Some of these biomacromolecules are characterized by high natural availability (*e.g.* starch, cellulose) and they also have a great biological importance, since they can be a source of energy for animal species. Moreover, they are structural elements of cellular walls and identification sites of cellular surfaces. Depending on the structure, these biomacromolecules can have distinct and promising properties like hydrophilicity, biocompatibility, biodegradability, polyfunctionality (*i.e.* functional groups that can be modified by chemical manipulation) (Heinze et al., **2006a**). Thanks to that, PSs have great potential applications in the fields of tissue engineering, medicine, food industry. For example, alginates can be used as a biomaterial in wound healing, tissue engineering orthopedics, and dental implant surgery because of their low toxicity, relatively low cost, good biocompatibility, and osteoconductivity (Venkatesan et al., **2015**). Curdlan, is used as a gelling agent and thickener in various food applications, contributing to the texture and stability of food products (Su et al., **2022**) and chitosan, for instance, has been studied for its antimicrobial properties, making it a valuable component in wound dressings and drug delivery systems (Mohammed et al., **2021**).

1.2.1 Sulfated polysaccharides

An important class of PSs includes the sulfated ones, which play pivotal roles in several biological processes including the coagulation cascade, viral transmission, and antioxidation (Clausen et al., **2020**). Furthermore, sulfated polysaccharides are structural components of tissues and/or signaling agents in physiological processes (Zhao et al., **2015**). Thus, their composition and structure, as well as their physicochemical, biomechanical, and biological properties are of keen interest for development of new products in the pharmaceutical, medical device, food, beauty, and health industries. The activity of sulfated polysaccharides depends on the carbohydrate backbone composition, molecular mass, the position of sulfate groups

(also called sulfation pattern) and the amount or degree of sulfation. From a structural point of view, they display both branched and linear polymeric architectures.

In nature, sulfated polysaccharides are distributed in marine algae and in animals, both mammals and invertebrates. Marine sulfated polysaccharides are classified, in galactans, ulvans and fucans (Jiao et al., **2011**). Galactans are generally found in red seaweed and are characterized by a linear polysaccharide backbone composed almost exclusively of L- and/or D-galactose and 3,6-anhydro-D- or L-galactose units, that are variously sulfated (Campo et al., **2009**). Ulvans are composed of 3-*O*-sulfated-L-rhamnose residues linked to an uronic acid or, in minor extent, to xylose, either sulfated or not at its *O*-2 position (Lahaye and Robic, **2007**). They are commonly extracted from green algae. Finally, fucans, found in brown seaweed, are characterized by highly heterogeneous structures, composed of variously sulfated L-fucose units (Pomin and Mourão, **2008**).

Some of these species have been found also in animals, especially sulfated fucans and galactans have been isolated from several marine invertebrates, showing a more regular structure than their analogues from seaweeds. The most common sulfated polysaccharides in animal kingdom are glycosaminoglycans that will be discussed in paragraph 1.2.2. The relevance of sulfated polysaccharides is due to the extraordinary biological activity that they show in different fields; indeed, many of them are currently employed for the treatment of different diseases (Linhardt et al., **2003**).

The biological activities of sulfated polysaccharides include: anticoagulation, anti-thrombotic, antiviral, antioxidant, antitumor, anti-inflammatory, and are highly dependent on structure and composition. In addition, a significant number of novel drugs, medical devices and nutraceuticals based on their bioactivities are under development. These properties depend on polysaccharide-protein interactions (*e.g.* anticoagulation) as well as coordination and storage of water molecules (*e.g.* lubricity). Furthermore, they deeply depend on the carbohydrate backbone composition, molecular mass, and, importantly, the position of sulfate groups and amount or degree of sulfation (Mestechkina and Shcherbukhin, **2010**). Moreover, it

has been suggested that the sulfation pattern sequence might be able to encode specific functional information but, except for few cases, this has been not unveiled yet. Thanks to their promising bioactivities, in the last years significant research efforts have been spent to synthesize sulfated polysaccharides by chemical modification of natural unsulfated ones (see paragraph 1.3.2 and chapter 2).

1.2.2 Glycosaminoglycans

An important class of natural sulfated polysaccharides are glycosaminoglycans (GAGs). GAGs are a family of linear, complex polysaccharides ubiquitously distributed on the cell surface or in the extracellular matrix (ECM) of animal cells, where they play crucial roles in several biological events. GAGs are usually conjugated with proteins, resulting in structures called proteoglycans (PGs). They are generally constituted of a core protein and GAG chains, covalently attached through their reducing ends to the side chains of serine, threonine or asparagine residues in the protein (Lindahl et al., **2015**). PGs have key roles in several physiopathological processes, such as angiogenesis, cancer, immunity, and infectious diseases (Iozzo and Karamanos, **2010**). From a structural point of view, GAGs are highly negatively charged heteropolysaccharides, characterized by disaccharide repeating units, composed of an amino sugar (glucosamine or galactosamine) and a hexose (galactose) or an uronic (D-glucuronic or L-iduronic) acid. The saccharide backbone can be decorated with acetyl groups on the nitrogen atoms of the aminosugars, and sulfate groups on aminosugar nitrogen atoms and/or on the hydroxyl oxygen atoms of both aminosugar and uronic acid moieties. Different families of GAGs can be classified according to the nature of these disaccharide blocks, including hyaluronic acid (HA), chondroitin sulfate (CS), dermatan sulfate (DeS), keratan sulfate (KS), heparin (HeP), and heparan sulfate (HS). Noteworthy, HA is the only unsulfated GAG (Figure 1.1)

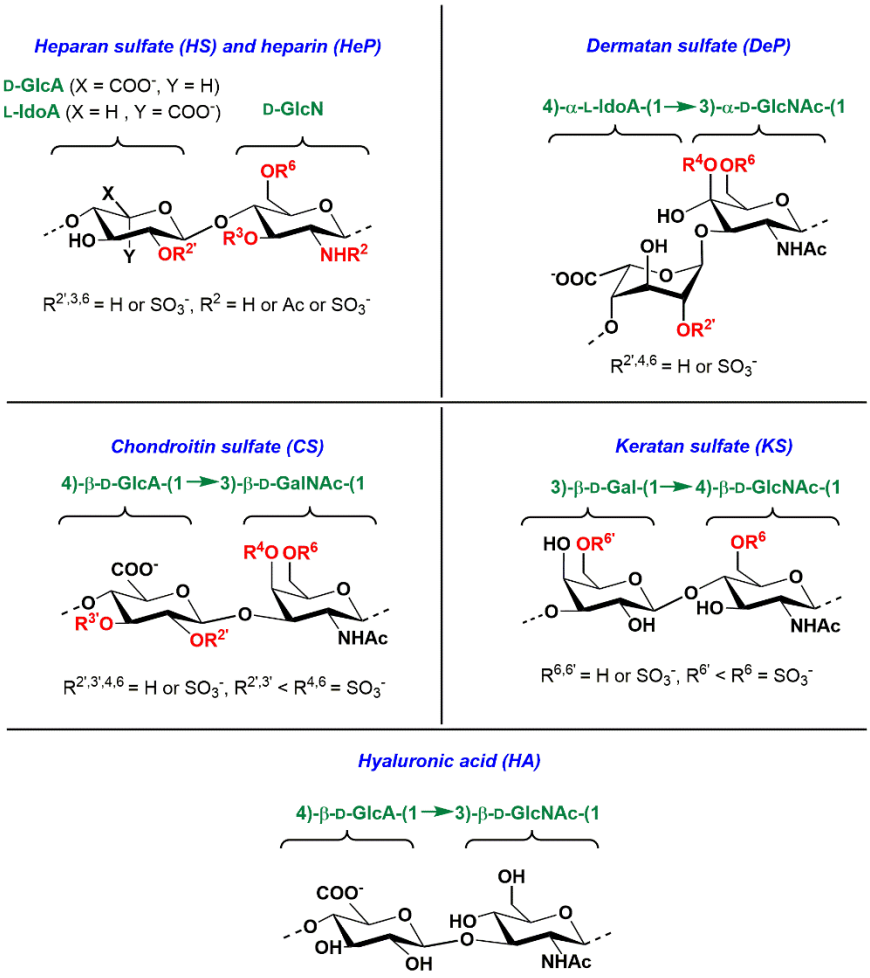

Figure 1.1. GAGs repeating units

The extraordinary structural diversity of GAGs results in highly diverse functions and allows them to modulate interactions with various molecules involved in several biological processes. For example, GAGs are involved in extracellular matrix assembly, cell−matrix and cell−cell interactions, ligand−receptor binding, and downstream cellular signalling. They control chemokine and cytokine activities and growth factor sequestration. They regulate multiple processes in a physiological context, but they also participate in the progression of many diseases. Besides their biological roles, their physical properties are of major interest for biomaterials and

tissue engineering applications (Perez et al., **2023**). Except for HA, the other GAGs are decorated with sulfate groups, that can be distributed along the polymeric chain in a particularly high number of diverse combinations. This creates an enormous structural diversity and potential variation in biological activity. The sulfate group distribution, also called sulfation pattern, seems to be strictly regulated in *vivo*, is tissue- and age-specific, and also depends on the physiological or pathological state of the organism (Bedini et al., **2019**). It has been even suggested that the sulfation pattern sequence might be able to encode specific functional information, but this "GAG sulfation code" has been not unveiled yet, except for few cases, where its functions in controlling blood clotting, guiding neuronal growth, and controlling adhesion of pathogens, have been elucidated (Gama et al., **2006**; Martín et al., **2013**; Rogers et al., **2011**; Swarup et al., **2013**; Zhao et al., **2020**).

1.3 Polysaccharides chemistry and their modification

Despite their abundance in nature, PSs (expecially sulfated ones) produced in biological systems are often heterogeneous, and the extraction/purification processes afford them in small amounts. In this frame, chemical manipulation of PSs can overtake these limitations, obtaining homogeneous structures in larger quantities.

By comparison with monosaccharides and short oligosaccharides chemistry, the development of reliable methods for structurally modification of PSs is still unexplored for all the difficulties related to polysaccharides chemistry. Firstly, they are poorly soluble in common low boiling, organic solvents and high boiling, polar solvents, such as formamide, *N,N*-dimethylformamide (DMF), dimethyl sulfoxide (DMSO) and water, are often required (Table 1.1).

Polysaccharide	Solubility in DMF	DMSO	py	H_2O
Cellulose	-	+ (TBAF)	-	-
Chitin	-	-	-	-
Starch	-	+ (80 °C)	-	-
Amylopectin	-	+ (80 °C)	-	+
Curdlan	-	+	-	-
Schizophyllan	+ (80 °C, LiCl)	+	-	-
Scleroglucan	-	-	-	-
Pullulan	+ (80 °C)	+	+	+
Xylan	+ LiCl	+	-	- (NaOH)
Guar	-	-	-	-
Alginate	-	-	-	+
Inulin	+	+	+	+
Dextran	+ (LiCl)	+ (40 °C)	-	+

Table 1.1. PSs solubility in some common organic solvents

Another issue is related to the possibility to achieve derivatization at selected hydroxyl positions in each subunit of the polymeric chain, avoiding harsh reaction conditions that might break the polymeric structure by cleaving glycosidic linkages. Finally, a detailed structural characterization of the polysaccharide structure is not trivial. For some of the most important polysaccharides, (Fox et al., **2011**; Pawar and Edgar, **2012**) these limitations have been already overtaken, by exploiting *ad hoc* solvent systems (*e.g.* mixture of a polar aprotic solvent and a chaotropic salt or ionic liquids) or suitably developed protection/deprotection reaction sequences, together with advanced 2D-NMR and mass spectrometry techniques (Bedini et al., **2016**).

1.3.1 Protecting groups in carbohydrate chemistry

Protecting groups (PGs) are commonly used in carbohydrate chemistry in particular for saccharides regioselective modification. PGs mask some reactive functionalities on the saccharide backbone to avoid reaction with other chemical reagents. Moreover, the installation of PGs promotes the chemical alteration of some functionalities

enhancing or decreasing their reactivity. The protecting groups used in carbohydrate chemistry are usually the same used in the other areas of organic synthesis. The methods for their installation and removal are often the same as those developed for non-carbohydrate molecules. In addition, several protecting groups developed *ad hoc* for sugar species have been reported (Wuts, **2014**). The most important protecting groups in carbohydrate chemistry are the hydroxyl protecting groups. Moreover, amino- and carboxy- protecting groups for the manipulation of structures which contain aminosugars and uronic acid are used too.

1.3.1.1. Protecting groups for hydroxyl moieties

The most investigated PGs in the synthesis of carbohydrates are hydroxyls protecting groups, because they are the most present moieties in glycan structures. The regioselective approach obviously requires a differentiation between two or more hydroxyl groups on the same structures. The hydroxyls moieties can be distinguished according to the different nucleophilicity of the four possible hydroxyl types on a carbohydrate backbone (hemiacetal, primary, secondary equatorial, secondary axial). Their reactivity scale is influenced by steric and electronic effects and generally follows this order: primary OH > hemiacetal OH > equatorial OH > axial OH. Another approach for regioselective protection of hydroxyl moieties can be to consider them as diols (1,2- and 1,3-diols), that can be protected together with a cyclic group. Generally, 1,3-diols involve positions 4 and 6, that can be protected together generating sufficiently not-tensed cycles, as the hydroxyl on the latter position is a primary conformationally-free OH. The 1,2-diols involve positions 2 and 3 or positions 3 and 4 and, according to their stereochemistry, they can be distinguished in *trans* (*e.g.* two axial or two equatorial OHs) and *cis* (*e.g.* an equatorial and an axial OH) (Figure 1.2).

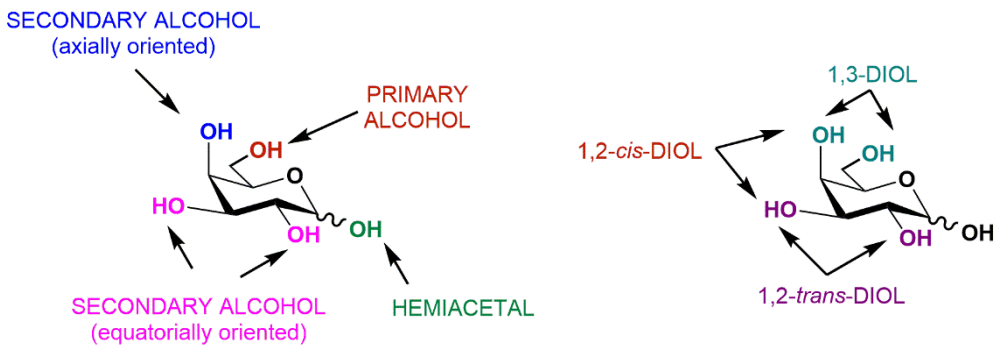

Figure 1.2. Classification of hydroxyl groups (left) and diols (right)

Hydroxyl PGs commonly used for the regioselective modification of polysaccharides, and more in general in carbohydrate chemistry, can be divided into three macro-categories: acyclic ethers and esters and cyclic PGs.

Ether-type protecting groups

Ethers are some of the most commonly used protecting groups for carbohydrate synthesis, consisting of both ethereal (such as methyl, benzyl, trityl) and silyl ether functionalities as depicted in Figure 1.3.

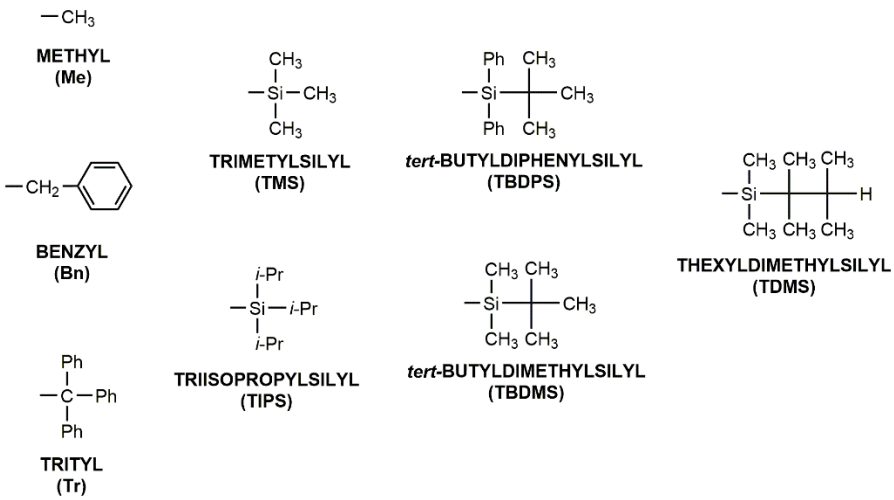

Figure 1.3. Example of ether-type protecting groups

These protecting groups have been employed not only in the synthesis of oligosaccharides and glycoconjugates, but also in the structure manipulation of polysaccharides. Alkyl ethers can be installed by alkylation: for example, they are largely employed for the modification of cellulose in the presence of alkyl halides under basic conditions in different solvents such as 1,3-dimethyl-2-imidazolidinone (DMI)/LiCl, (Takaragi et al., **1999**) *N,N*-dimethylacetamide (DMA)/LiCl (McCormick and Callais, **1987**), DMSO/LiCl mixtures (Petrus et al., **1995**) and SO_2/DEA/DMSO system (Isogai et al., **1986**), getting 2,3,6-tri-*O*-alkylated cellulose quantitatively.

Benzyl ethers are widely used as permanent protecting groups in carbohydrate synthesis for their well-known stability together with a variety of selective cleavage reactions. Their installation can be carried out under strongly basic conditions, as reported for benzylation of chitin using sodium hydride or sodium hydroxide, obtaining a perbenzylated or selectively *O*-6 protected polysaccharide, respectively (Somorin et al., **1979**; Umemura et al., **2012**). Benzyl ethers removal can be performed under hydrogenolytic, reductive (Na/ liquid ammonia) (Iseloh et al., **2002**) or oxidative conditions (Adinolfi et al., **1999**), which have been used also for polysaccharide derivatives (Laezza et al., **2015**).

Trityl ethers are regioselectively formed, for their steric demands, on primary hydroxyl positions of polysaccharides, by working in a weakly basic environment. This property has been extensively exploited for polysaccharide modification as reported for cellulose (Green, **1963**), chitin (Umemura et al., **2012**), chitosan (Holappa et al., **2005**) and curdlan (Chien and Iwata, **2018**). Trityl ethers can be easily removed using mild aqueous acid conditions.

Silyl groups are largely employed for derivatization of polysaccharides, especially to convert alcohol moieties into more hydrophobic and, often, more reactive groups as reported for the per-*O*-silylation of cellulose (Baumann et al., **2000**; Cooper et al., **1981**; Richter and Klemm, **2003**; Schultz and Lüning, **2002**). Their installation can be performed using the corresponding silyl chlorides under milder basic conditions (*e.g.*

using pyridine or imidazole) than alkyl ether insertion. In particular, it has been reported that TBDMS group can be selectively inserted on cellulose either at *O*-6 or both at *O*-2 and *O*-6, depending on the reaction conditions (Koschella et al., **2001**; Koschella and Klemm, **1997**; Petzold et al., **2003**). Their removal can be easily performed with fluoride ions (TBAF/THF).

Ester-type protecting groups

Another way to protect hydroxyl functionalities in carbohydrate synthesis is based on the installation of ester-type PGs (Figure 1.4).

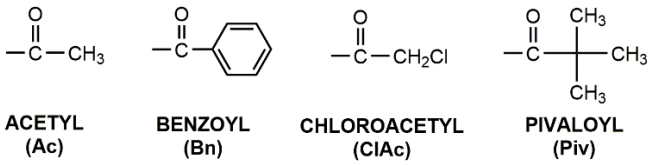

Figure 1.4. Example of ester-type protecting groups

Standard conditions for the installation of ester PGs are based on the employment of the acyl chloride or the anhydride in pyridine or other tertiary amines, often with DMAP as a catalyst. In addition, the acetylation can be performed also in acid conditions using *in situ* generated HI for the activation of the acetic anhydride (Ravindranathan Kartha and Field, **1997**).

Esterification of polysaccharides was performed on starch (Grote et al., **2005**) and cellulose (McCormick and Callais, **1987**) under basic conditions, obtaining in both cases an almost quantitative degree of substitution. Moreover, alginates were subjected to hydroxyl protection by esterification too. (Pawar et al., **2011**) Regioselective esterification at the primary position of a polysaccharide was investigated mainly on cellulose, displaying a lower regioselectivity than ether protection. (Fox et al., **2011**).

Cyclic protecting groups

As mentioned above, another approach for the regioselective protection of hydroxyl functionalities could be to consider them as diols that can be protected together with a cyclic group as acetal or ketal moieties. In this frame, acetal benzylidene and the ketal isopropylidene are the most widely used in carbohydrate synthesis (Figure 1.5).

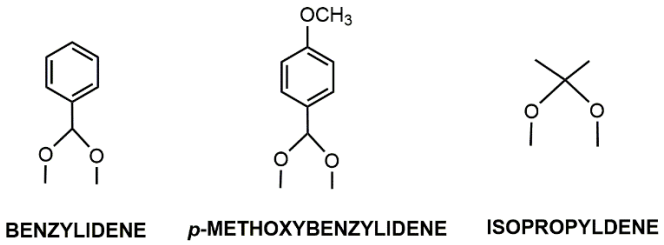

Figure 1.5. Example of cyclic protecting groups

The advantage of these protecting groups lies in the possibility of controlling the regioselectivity of protection depending on the choice of the protecting group. For example, benzylidene acetals are formed preferentially as six-membered dioxane cycles, reacting with 1,3-diols and forming 4,6-*O*-benzylidene derivatives; conversely, isopropylidene ketals are more stable as five-membered dioxolane rings, formed by reaction on 1,2-*cis*-diols. The installation of acetal/ketal moieties requires the presence of the corresponding aldehyde/ketone or a suitable acetal/ketal reagent under acid catalytic conditions. Their cleavage is usually performed under acid hydrolysis restoring the free diol. Another advantage in the manipulation of benzylidene acetals lies in the possibility to perform a regioselective opening. Reductive opening of acetals relies on a combination of a hydride reagent with a Lewis (or a Brønsted) acid. These methods are highly sensitive to the employed reaction conditions (*e.g.* solvent, temperature, reagent concentration) and the structure of the substrate, which influence regioselectivity and yields. By carefully choosing the reagent system combination, 6-*O*-benzyl or 4-*O*-benzyl ethers can be selectively prepared over the corresponding regioisomer from 4,6-*O*-benzylidene-protected

hexopyranosides. For example, the most common methods to obtain 6-*O*-benzyl protected derivatives are based on the employment of $NaCNBH_3$-HCl-THF (Garegg et al., **1982**.; Garegg and Hultberg., **1981**) and $BH_3 \cdot NMe_3$-$AlCl_3$-THF mixtures (Ek et al., **1983**). Conversely, to achieve 4-*O*-benzyl protected derivatives the use of $BH_3 \cdot$THF in THF with several different acids is a common method (Shie et al., **2009**; Daragics et al., **2009**; Tani et al., **2007**; Shie et al., **2005**; Wang et al., **2002**; Jiang and Chan, **1998**). Finally, benzylidene acetals can be also opened under oxidative conditions, using sodium bromate and sodium dithionite in a biphasic mixture (Adinolfi et al., **1999**). These conditions are sufficiently mild and efficient that can be applied also on some polysaccharide structures.

1.3.1.2 Amino protecting groups

In carbohydrate manipulation, the amino functionalities are often temporarily converted into electron-withdrawing species in order to decrease their reactivity. In particular, they are transformed into amide, carbamate or imide (Figure 1.6). Among amide-type protecting groups, haloacetil are generally introduced by reaction with the corresponding acyl chloride or anhydride and can be removed by heating in strongly acidic or basic conditions (Wuts, **2014b**). Carbamate groups, are also very common for amine protection: the installation is usually accomplished by condensation of the free amine and the appropriate chloroformate in the presence of a mild base (Boullanger et al., **1990**). Amino function can be also masked with bivalent cyclic groups. The employment of the typical phtalimido group is limitated by the strongly basic conditions of the deprotection step, to overcome this limitation, other phtaloyl-based protecting groups, such as tetrachlorophtalimides (TCP) (Debenham et al., **1996**) and dimethylmaleoides (DMM) (Aly et al., **1998**) were used: they require less strong conditions for the deprotection step. Finally, the amine functionality can be protected as an azido group. The azido group can be introduced through a diazo-transfer reaction using triflyl azide (Titz et al., **2006**; Yan et al., **2005**) or imidazole-1-

sulfonyl azide hydrochloride (Goddard-Borger and Stick, **2007**) and is converted into the free amine under hydrogenolysis conditions.

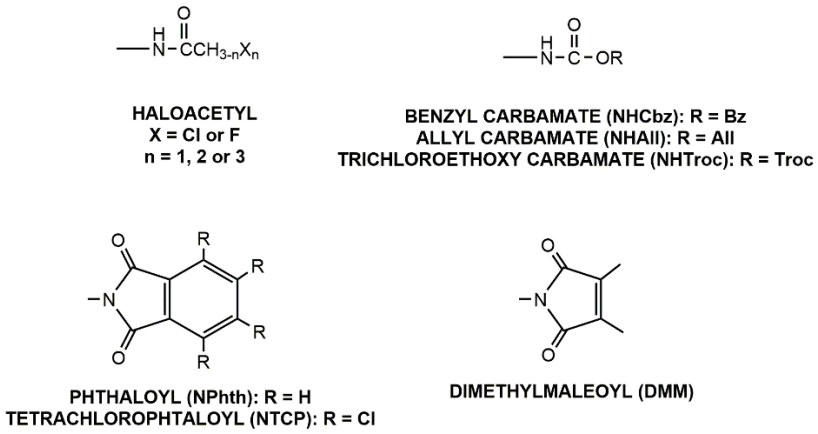

Figure 1.6. Example of amino protecting groups

1.3.1.3 Carboxyl protecting groups

Natural saccharides can present uronic acid residues that can be protected at *C*-6 position by formation of esters. The carboxyl group can react both as electrophile or as a nucleophile. In the first case, it can be activated under strongly acid conditions and then a reaction with a suitable alcohol gives the ester. These reaction conditions could be harsh for PSs chemistry, causing a possible cleavage of the glycosidic bonds and an undesirable depolymerization. Alternatively, the carboxylic acid can react as a nucleophile: it can be converted in a carboxylate ion and then alkylated by a suitable alkylating agent to give the ester, as reported for alginates (Pawar and Edgar, **2013**; Pelletier et al., **2000**) and pectins (Pappas et al., **2004**).

1.3.2 Sulfation reaction

Sulfated polysaccharides are a class of biomacromolecules characterized by promising biological activities. This has given a great impulse to the development of methods for the production of chemically or chemoenzymatically sulfated derivatives. Natural sulfated polysaccharides, particularly GAGs, are already employed for the formulation of several drugs. In most cases these compounds are extracted from animal sources (*e.g*. heparin from pig intestinal mucosa, chondroitin sulfate from bovine trachea). This raises not only ethical issues, but also severe problems in terms of product safety, as demonstrated by hundreds of serious adverse events, including 149 deaths, occurred some years ago after the contamination of some heparin lots (Kishimoto et al., **2008**). Instead, artificially sulfated polysaccharides can be produced from renewable, largely available raw materials, thus standing as a more environmentally and economically sustainable alternative to GAGs. Moreover, these compounds could have the same biological properties of natural GAGs but without risks derived from their typical animal source. In this frame, in the last years several research efforts have been spent to synthetize sulfated polysaccharides by chemical modification of natural unsulfated ones.

Usually, sulfation reactions are performed in a non-regioselective way, obtaining compounds with sulfate groups randomly distributed along PSs backbone. The tipical reagents used for this purpose are sulfuric acid or chlorosulfuric acid to generate *in situ* an active sulfur trioxide reagent (Yoshida et al., **1995**) or alternatively chlorosulfuric acid–pyridine (Mähner et al., **2001**), piperidine-*N*-sulfonic acid (Nagasawa et al., **1972**), and sulfamic acid–pyridine reagents (Zhou et al., **2014**). Nevertheless, all of these sulfating agents require harsh reaction conditions that can cause a breakage of glycosidic bonds and a consequent depolymerization of the PSs. Currently, the most widely employed method requires sulfur trioxide–amine (or amide) complexes in highly polar organic solvent such as *N,N*-dimethylformammide (DMF) or dimethylacetamide (DMAc): these reagents are relatively stable, easily handled, and compatible with highly polar solvents, thus favouring the solubility of

polysaccharides (Figure 1.6). Nonetheless, since the resulting randomly sulfated compounds give few information about the influence of the sulfation pattern in the biological processes, other sulfation methods have been developed.

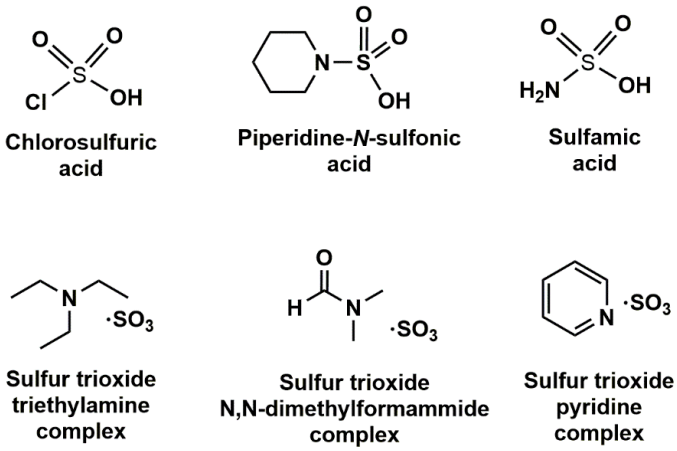

Figure 1.7. Sulfating agents

In particular, enzymatic or chemical methods have been carried out, in order to introduce sulfate groups in a regioselective way. The enzymatic approaches are highly regioselective and have produced interesting results (Sugiura et al., **2012**; Xu et al., **2017**, **2014**; Badri et al., **2021**). For example, Badri and co-authors designed a microbial platform for the sustainable production of sulfated chondroitin using *E. coli* as a host organism. Nevertheless, these methods present some limitations linked to the scarce availability and high costs of the enzymes (sulfotransferases) and their poor applicability on structures that are not very similar to the natural substrate of these enzymes. Another approach is based on the development of chemical multi-step methods based on protection/sulfation/deprotection steps involving the employment of appropriate PGs. Some advancements in this field will be examined in chapter 2.

1.3.3 Phosphorylation reaction

Phosphorylated polysaccharides are anionic analogues of sulfated ones, wherein the phosphorylation reactions typically occur through the functionalization of some hydroxyls with phosphate groups. Despite the crucial roles played by anionic polysaccharides in biological processes, and the abundant presence of anionic phosphate groups in nature in the form of structural compounds (*e.g.* phospholipids), genetic materials (*e.g.* DNA and RNA), and energy storage materials (*e.g.* ATP), studies related to carbohydrate-based phosphorylated polymers, particularly phosphorylated GAGs, remain underdeveloped.

Phosphorylation of native polysaccharides can enhance their biological activities or even impart novel ones. For example, the presence of phosphate groups along the polysaccharide backbone reduces high viscosity and improves water solubility and chelating properties (Shunli et al., **2021**). In addition, an interesting research on polysaccharide modification via phosphorylation suggests that the obtained phosphorylated polysaccharides can prevent hydroxyl radical chain reactions, thus exhibiting high antioxidant activity and enhanced hydroxyl radical-scavenging ability (Xie et al., **2020**; Chen and Huang., **2019**). Other biological activities of natural polysaccharides improved by the presence of phosphorylated moieties include antitumor, antiviral, hepatoprotective, antibacterial, anticoagulant and antihyperlipidemic properties (Shunli et al., **2021**; Laffargue et al., **2023**) (Figure 1.7).

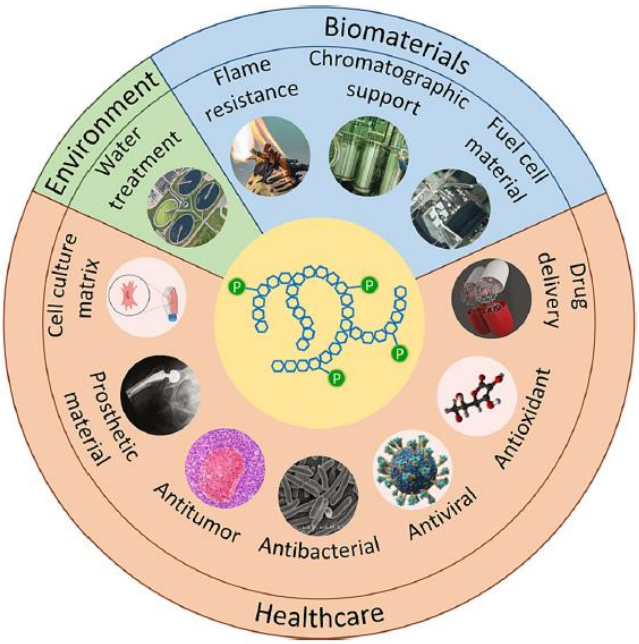

Figure 1.8. Possible applications of phosphorylated polysaccharides

In this frame, the possibility to obtain phosphorylated mimics of GAGs could open an access to a class of compounds with new or enhanced biological properties compared to their natural counterparts.

For example, by replacing the sulfate groups of GAGs with phosphates, their differences in size, polarity, acid-base and chelation properties could lend unreported activities to such phosphorylated GAGs (pGAGs), as indicated by a recent *in silico* study comparing the structural flexibility and intra- and intermolecular interaction patterns of native chondroitin sulfate (CS) and hyaluronic acid (HA) with their phosphorylated counterparts (Bojarski et al., **2019**). Indeed, this theoretical investigation suggested that phosphorylated GAGs could bind proteins generally with a stronger affinity than their sulfated counterparts and the differences in the binding modes might be highly protein target-dependent.

Therefore, the substitution of the sulfate groups of GAGs with phosphates could be attractive due to the unreported activities that pGAGs might confer to the investigated

biochemical system through interactions with GAG protein targets. Since a phosphate group can exist in two protonation states at physiological pH values, corresponding to net charges of -1 and -2, pGAGs could establish electrostatic interactions over a wider range in comparison to the natural GAGs: indeed, the charge variability of phosphate groups can lead to a greater modulation of electrostatic interactions depending on the pH range. Moreover, pGAGs can establish additional hydrogen bonding networks as well as being linked via polycondensation of the phosphate groups and can participate in cation chelation.

Nonetheless, the preparation of pGAG species is still rather unexplored compared to the semi-synthesis of sulfated species, with only few, very recently reported examples (Khaybrakhmanova et al., **2022**; Uchimura et al., **2022**; Bojarski et al., **2019**).

The introduction of phosphate groups on polysaccharide backbones currently presents several concerns:

i) harsh conditions required by the commonly employed methods (*e.g.* phosphoric acid and urea at temperatures up to 160°C);

ii) low degrees of derivatization that are generally achieved on common polysaccharides such as cellulose, dextran, alginate (Illy et al., **2015**; Wang et al., **2022**; Zhou and Huang, **2021**);

iii) the much lower control of the regiochemistry in phosphate groups installation with respect to the sulfate one.

To fill this gap, part of this thesis work was focused on the screening of different phosphorylating reagents and/or reaction conditions towards the semi-synthesis of regioselectively phosphorylated GAGs. The latest advances in this field will be discussed in detail in the following chapters.

1.4 Aim of the thesis

In this thesis work, the development of new semi-synthetic strategies for the regioselective modification of polysaccharides was carried out. The final aim is to

obtain new compounds with potential applications in the pharmaceutical field. The starting materials were obtained from eco-sustainable natural and/or biotechnological sources (algae, fungi, plants, bacteria). In particular, the attention was focused on polysaccharides already used in the biomedical and/or food fields. The purpose was to improve their biological properties or to introduce new ones through chemical modifications and in particular with the installation of chemical functionalities in a highly controlled and regioselective way. The derivatization that was carried out was focused on the insertion of negatively charged functionalities (sulfate, phosphate groups), in order to mimic the structural characteristics of natural sulfated GAGs.

Chapter 2 discusses a semi-synthetic approach for the transformation of some polysaccharides (diabolican from *V. diabolicus*, alginates, curdlan) in their sulfated derivatives, developing regioselective methods relied upon odirect protocols or multi-step strategies based on protection-sulfation-deprotection sequences.

In chapter 3 the regioselective functionalization of polysaccharides towards pGAG derivatives equipped with well-defined phosphorylated patterns was investigated. Part of these studies were conducted in collaboration with the BioGlycoChem group of the Institute of General Organic Chemistry of the Spanish National Research Council.

Finally, in collaboration with IBSA Farmaceutici Italia Srl, cross-linked GAGs, characterized by high biocompatibility and optimized for use both in regenerative and aesthetic medicine (*e.g.* for use in injectable fillers) and in the orthopedic/physiatric field as intrarticular gels for viscosupplementation, have been developed. These results will be discussed in chapter 4.

References

Adinolfi, M., Barone, G., Guariniello, L., Iadonisi, A., **1999**. *Tetrahedron Lett. 40*, 8439–8441.

Aly, M.R.E., Castro-Palomino, J.C., Ibrahim, E.-S.I., El-Ashry, E.-S.H., Schmidt, R.R., **1998**. *Eur. J. Org. Chem. 1998*, 2305–2316.

Badri, A., Williams, A., Awofiranye, A., Datta, P., Xia, K., He, W., Fraser, K., Dordick, J. S., Linhardt, R. J., Koffas, M. A. G., **2021**. *Nat. Commun. 12*, 1389.

Baumann, H., Richter, A., Klemm, D.O., Faust, V., **2000**. *Macromol. Chem. Phys. 201*, 1950–1962.

Bedini, E., Corsaro, M.M., Fernández-Mayoralas, A., Iadonisi, A., **2019**. Chondroitin, Dermatan, Heparan, and Keratan Sulfate: Structure and Functions, in: Cohen, E., Merzendorfer, H. (Eds.), *Extracellular Sugar-Based Biopolymers Matrices*. Springer Nature Switzerland, Cham, Switzerland, pp. 187–233.

Bedini, E., De Castro, C., De Rosa, M., Di Nola, A., Iadonisi, A., Restaino, O.F., Schiraldi, C., Parrilli, M., **2011**. *Angew. Chem., Int. Ed. 50*, 6160–6163.

Bedini, E., Laezza, A., Iadonisi, A., **2016**. *Eur. J. Org. Chem*, 3018-3042.

Bojarski, K. K., Becher, J., Riemer, T., Lemmnitzer, K., Möller, S., Schiller, J., Schnabelrauch, M., Samsonov, S. A., **2019**. *J. Mol. Struct. 1197*, 401–416.

Boullanger, P., Jouineau, M., Bouammali, B., Lafont, D., Descotes, G., **1990**. *Carbohydr. Res. 202*, 151–164.

Brown, J.R., Crawford, B.E., Esko, J.D., **2007**. *Crit. Rev. Biochem. Mol. Biol. 42*, 481–515.

Campo, V.L., Kawano, D.F., da Silva, D.B., Carvalho, I., **2009**. *Carbohydr. Polym. 77*, 167–180.

Chen L., Huang G., **2019**. *Int. J. Biol. Macromol. 125*, 256–261.

Chien, C.Y., Iwata, T., **2018**. *Carbohydr. Polym. 181*, 300–306.

Clausen, T.M., Sandoval, D.R., Spliid, C.B., Pihl, J., Perrett, H.R., Painter, C.D., Narayanan, A., Majowicz, S.A., Kwong, E.M., McVicar, R.N., Thacker, B.E., Glass, C.A., Yang, Z., Torres, J.L., Golden, G.J., Bartels, P.L., Porell, R.N., Garretson, A.F., Laubach, L., Feldman, J., Yin, X., Pu, Y., Hauser, B.M., Caradonna, T.M., Kellman, B.P., Martino, C., Gordts, P.L.S.M., Chanda, S.K., Schmidt, A.G., Godula, K., Leibel, S.L., Jose, J., Corbett, K.D., Ward, A.B., Carlin, A.F., Esko, J.D., **2020**. *Cell 183*, 1043–1057.

Cooper, G.K., Sandberg, K.R., Hinck, J.F., **1981**. *J. Appl. Polym. Sci. 26*, 3827–3836.

Daragics, K.; Fügedi, P., **2009**. *Tetrahedron Lett. 50, 2914-2916.*

Debenham, J.S., Debenham, S.D., Fraser-Reid, B., **1996**. N-tetrachlorophthaloyl (TCP) for ready protection/deprotection of amino sugar glycosides, in: *Bioorganic and Medicinal Chemistry*. Pergamon, pp. 1909–1918.

Ek, M., Garegg, P.J., Hultberg, H., Oscarson, S. J., **1983**. *Carbohydr. Chem. 2*, 305-311.

Fox, S.C., Li, B., Xu, D., Edgar, K.J., **2011**. *Biomacromolecules 12*, 1956-1972.

Gama, C.I., Tully, S.E., Sotogaku, N., Clark, P.M., Rawat, M., Vaidehi, N., Goddard, W.A., Nishi, A., Hsieh-Wilson, L.C., **2006**. *Nat. Chem. Biol. 2*, 467–473.

Garegg, P.J., Hultberg, H., **1981**. *Carbohydr. Res. 93*, C10-C11.

Garegg, P.J., Hultberg, H., Wallin, S., **1982**. *Carbohydr. Res. 108*, 97-101.

Goddard-Borger, E.D., Stick, R. V., **2007**. *Org. Lett. 9*, 3797–3800.

Green, J.W., **1963**. *in* Methods in Carbohydrate Chemistry, Vol III, Cellulose. (Whistler Ed.), Academic Press, New York, (NY), USA, 327.

Grote, C., Heinze, T., **2005**. *Cellulose 12*, 435–444.

Heinze, T., Liebert, T., Koschella, A., **2006a**. Esterification of Polysaccharides, 1st ed. Springer-Verlag Berlin Heidelberg, Germany.

Holappa, J.; Nevalainen, T.; Soininen, P.; Elomaa, M.; Safin, R.; Másson, M; Järvinen, T. *Biomacromolecules* **2005**, *6*, 858-863.

Hudak, J.E., Bertozzi, C.R., **2014**. *Chem. Biol. 21*, 16–37.

Iozzo, R. V., Karamanos, N., **2010**. *FEBS J. 277*, 3863–3863.

Iserloh, U., Dudkin, V., Wang, Z.G., Danishefsky, S.J., **2002**. *Tetrahedron Lett. 43*, 7027–7030.

Isogai, A., Ishizu, A., Nakano, J., **1986**. *J. Appl. Polym. Sci. 31*, 341–352.

Jiang, L., Chan, T.-H., **1998**. *Tetrahedron Lett.*, *39*, 355-358.

Jiao, G., Yu, G., Zhang, J., Ewart, H., **2011**. *Mar. Drugs 9*, 196–223.

Khaybrakhmanova, E. A., Kozyrev, S. V., Tyumkina, T. V., & Ponedel'kina, I. Y., **2022**. *Chem. Proc. 12*, 39.

Koschella, A., Klemm, D.O., **1997**. *Macromol. Symp. 120*, 115–125.

Laezza, A., Iadonisi, A., De Castro, C., De Rosa, M., Schiraldi, C., Parrilli, M., Bedini, E., **2015**. *Biomacromolecules 16*, 2237–2245.

Laezza, A., Iadonisi, A., Pirozzi, A.V.A., Diana, P., De Rosa, M., Schiraldi, C., Parrilli, M., Bedini, E., **2016**. *Chem. Eur. J. 22*, 18215–18226.

Laffargue, T., Moulis, C., & Remaud-Siméon, M., **2023**. *Biotech. Adv. 65*, 108140.

Lahaye, M., Robic, A., **2007**. *Biomacromolecules 8*, 1765–1774.

Lindahl, U., Couchman, J., Kimata, K., Esko, J.D., **2015**. Proteoglycans and Sulfated Glycosaminoglycans, in: Varki, A., Cummings, R.D., Esko, J.D., Stanley, P., Hart, G.W., Aebi, M., Darvill, A.G., Kinoshita, T., Packer, N.H., Prestegard, J.H., Schnaar, R.L., Seeberger, P.H. (Eds.), *Essentials of Glycobiology*. Cold Spring Harbor Laboratory Press, Cold Spring Harbor (NY).

Linhardt, R. J., **2003**. *J. Med. Chem.*, *46*, 2551–2564.

Martín, R., Martín, C., Escobedo, S., Suárez, J.E., Quirós, L.M., **2013**. *BMC Microbiol. 13*, 210.

McCormick, C.L., Callais, P.A., **1987**. *Polymer 28*, 2317–2323.

McCormick, C.L., Callais, P.A., **1987**. *Polymer 28*, 2317–2323.

Mestechkina, N.M., Shcherbukhin, V.D., **2010**. *Appl. Biochem. Microbiol. 46*, 267–273.

Mettu, R., Chen, C.Y., Wu, C.Y., **2020**. *J. Biomed. Sci. 27*, 9–31.

Mohammed, A., Naveed, M., Jost, N., **2021.** *J. Polym. Environ. 29(8)*, 2359-2371.

Pappas, C.S., Malovikova, A., Hromadkova, Z., Tarantilis, P.A., Ebringerova, A., Polissiou, M.G., **2004**. *Carbohydr. Polym. 56*, 465–469.

Pawar, S.N., Edgar, K.J., **2012**. *Biomaterials 33*, 3279-3305.

Pawar, S.N., Edgar, K.J., **2013**. *Carbohydr. Polym. 98*, 1288–1296.

Pelletier, S., Hubert, P., Lapicque, F., Payan, E., Dellacherie, E., **2000**. *Carbohydr. Polym. 43*, 343–349.

Perez, S., Makshakova, O., Angulo, J., Bedini, E., Bisio, A., de Paz, J.L., Fadda, E., Guerrini, M., Hricovini, M., Hricovini, M., Lisacek, F., Nieto, P.M., Pagel, K., Paiardi, G., Richter, R., Samsonov, S.A., Vivès, R.R., Nikitovic, D., Ricard Blum, S., **2023**. *JACS Au 3* (3), 628-656.

Petruš, L., Gray, D.G., BeMiller, J.N., **1995**. *Carbohydr. Res. 268*, 319–323.

Petzold, K., Koschella, A., Klemm, D.O., Heublein, B., **2003**. *Cellulose 10*, 251–269.

Pomin, V.H., Mourão, P.A.S., **2008**. *Glycobiology 18*, 1016–1027.

Ravindranathan Kartha, K.P., Field, R.A., **1997**. *Tetrahedron 53*, 11753–11766.

Richter, A., Klemm, D.O., **2003**. *Cellulose 10*, 133–138.

Rogers, C.J., Clark, P.M., Tully, S.E., Abrol, R., Garcia, K.C., Goddard, W.A., Hsieh-Wilson, L.C., **2011**. *Proc. Natl. Acad. Sci. U.S.A 108*, 9747–9752.

Schultz, P., Lüning, U., **2002**. *Macromol. Chem. Phys. 203*, 961–967.

Seeberger, P.H., **2015**. Monosaccharide Diversity, in: Varki, A., Cummings, R.D., Esko, J.D., Stanley, P., Hart, G.W., Aebi, M., Darvill, A.G., Kinoshita, T., Packer, N.H., Prestegard, J.H., Schnaar, R.L., Seeberger, P.H. (Eds.), *Essentials of Glycobiology*. Cold Spring Harbor Laboratory Press, Cold Spring Harbor (NY).

Shie, C.R., Tzeng, Z.H., Kulkarni, S.S., Uang, B.J., Hsu, C.Y., Hung, S.C., **2005**. *Angew. Chem., Int. Ed. 44*, 1665–1668.

Shie, C.-R., Tzeng, Z.-H., Wang, C.-C., Hung S.-C., **2009**. *J. Chin. Chem. Soc. 56,* 510-523.

Shunli X., Yongcong Z., Xue W., Qirui F., Xiaoyi D., Mei C., Tao H., **2021**. *Int. J. Biol. Macromol. 184*, 946−954.

Somorin, O., Nishi, N., Tokura, S., Noguchi, J., **1979**. *Polym. J. 11*, 391–396.

Su, C., Chen, Y., Tian, S., Lu, C., & Lv, Q., **2022.** *Polymers 14(16)*, 3268.

Swarup, V.P., Hsiao, T.W., Zhang, J., Prestwich, G.D., Kuberan, B., Hlady, V., **2013**. *J. Am. Chem. Soc. 135*, 13488–13494.

Takaragi, A., Minoda, M., Miyamoto, T., Liu, H.Q., Zhang, L.N., **1999**. *Cellulose 6*, 93–102.

Tani, S., Sawadi, S., Kojima, M., Akai, S., Sato, K. ichi, **2007**. *Tetrahedron Lett. 48,* 3103–3104.

Titz, A., Radic, Z., Schwardt, O., Ernst, B., **2006**. *Tetrahedron Lett. 47*, 2383–2385.

Uchimura, K., Nishitsuji, K., Chiu, L.-T., Ohgita, T., Saito, H., Allain, F., Gannedi, V., Wong, C.-H., Hung, S.-C. **2022**. *ChemBioChem 23*, e202200191.

Umemura, T., Hirakawa, M., Yoshida, Y., Kurita, K., **2012**. *Polym. Bull. 69*, 303–312.

Venkatesan, J., Lowe, B., Anil, S., Manivasagan, P., Kheraif, A. A. A., Kang, K. H., Kim, S. K., **2015.** *Starch 67*, 381–390.

Wang, C.C., Luo, S.Y., Shie, C.R., Hung, S.C., **2002**. *Org. Lett. 4*, 847–849.

Wuts, P.G.M., **2014**. Protection for the amino group, in: *Greene's Protective Groups in Organic Synthesis*. John Wiley & Sons, Inc., Hoboken, New Jersey, pp. 895–1193.

Wuts, P.G.M., **2014b**. Protection for the amino group, in: *Greene's Protective Groups in Organic Synthesis*. John Wiley & Sons, Inc., Hoboken, New Jersey, pp. 895–1193.

Xie L., Shen M., Wen P., Hong Y., Liu X., Xie J., **2020**. *Food Chem. Toxicol. 145*, 111754.

Yan, R.B., Yang, F., Wu, Y., Zhang, L.H., Ye, X.S., **2005**. *Tetrahedron Lett. 46*, 8993–8995.

Zhao, J., Zhu, Y., Song, X., Xiao, Y., Su, G., Liu, X., Wang, Z., Xu, Y., Liu, J., Eliezer, D., Ramlall, T.F., Lippens, G., Gibson, J., Zhang, F., Linhardt, R.J., Wang, L., Wang, C., **2020**. *Angew. Chem., Int. Ed. 59*, 1818–1827.

Zhao, L., Wu, M., Xiao, C., Yang, L., Zhou, L., Gao, N., Li, Z., **2015**. *Proc. Natl. Acad. Sci. U.S.A.*, *112*, 8284–8289.

CHAPTER 2

REGIOSELECTIVE SULFATION OF POLYSACCHARIDES FROM SUSTAINABLE SOURCES

2

REGIOSELECTIVE SULFATION OF POLYSACCHARIDES FROM SUSTAINABLE SOURCES

Introduction

Sulfated polysaccharides are ubiquitous in living systems and play pivotal roles in several biological processes (see also Paragraph 1.2.1). Among them, sulfated glycosaminoglycans, particulary aboundant in animal tissues, are the most studied. They have a lot of biological activities and play key roles in several physio-pathological processes. Thanks to that, various applications as therapeutics and biomaterials have been developed for sulfated polysaccharides. An example is heparin, the most used anticoagulant drug in the world since its discovery in the early 1900s (Wardrop and Keeling, **2008**), or chondroitin sulfate that is currently used for the treatment of knee and hip osteoarthritis (Bishnoi et al., **2016**). Other applications for GAGs are under development too (Kowitsch et al., **2018**). Despite this, for most medical uses, native GAGs may exhibit limitations with respect to production cost, batch standardization, immunogenicity, degradability. Within this frame, the semi-synthesis of sulfated polysaccharides by chemical or enzymatic methods can overcome some of these issues and simultaneously unveil novel biomedical applications of sulfated polysaccharides. Indeed, since these artificially sulfated species show unique structural features, they may display altered pharmacokinetic properties with respect to natural sulfated polysaccharides, revealing new possibilities for their use in biomaterials, drug delivery vehicles, and more (Arlov et al., **2021**). Besides, in several cases these compounds can be produced in large amounts and at

moderately low cost, starting from renewable and/or underutilized raw materials or from microbial production, thus being a more environmentally and economically sustainable alternative to isolation of GAGs from animal tissues (Arlov and Skjåk-Bræk, **2017**; Wang et al., **2015**). For these reasons, in the last decades significant research efforts have been spent to synthesize sulfated polysaccharides, by chemical modification of natural unsulfated ones (Caputo et al., **2019**; Wang et al., **2018**; Zeng et al., **2019**). These derivatives could have the same biological properties of the natural GAGs but without the risks derived from their typical animal sources. Several efforts have been focused on the development of regioselective strategies in order to obtain structures with a well-defined sulfation pattern, starting from unsulfated polysaccharides with wide availability and ease of purification from non-animal sources. Moreover, the presence of regular repeating units along the polymeric chain can facilitate the studies about the structure-activity relationships. To do this, two different approaches can be distinguished (Bedini et al., **2017**): unsulfated polysaccharides can be subjected to direct, regioselective sulfation reactions to install sulfate groups on the most reactive hydroxyl(s) of the polysaccharides or they can be subjected to multi-step strategies, all relying upon protection-sulfation-deprotection sequences, which allow to enlarge the scope of achievable sulfation patterns. Within this frame, in this chapter the possibility to achieve the regioselective sulfation of naturally occurring polysaccharides was investigated. In particular, three polysaccharides (marine-sourced bacterial diabolican EPS, alginates and curdlan) have been selected. These compounds already in their native (unsulfated) form, exhibit interesting properties. We supposed that their regioselective sulfation could be one of the most cost-effective ways to achieve both an improvement of their intrinsic properties and to introduce new ones.

References

Arlov, Ø., Rütsche, D., Korayem, M.A., Öztürk, E., Zenobi-wong, M., **2021**. *Adv. Funct. Mater. 2010732*.

Arlov, Ø., Skjåk-Bræk, G., **2017**. *Molecules 22*, 793.

Bedini, E., Laezza, A., Parrilli, M., Iadonisi, A., **2017**. *Carbohydr. Polym. 174*, 1224–1239.

Bishnoi, M., Jain, A., Hurkat, P., Jain, S.K., **2016**. *Glycoconjugate J. 33*, 693–705.

Caputo, H.E., Straub, J.E., Grinstaff, M.W., **2019**. *Chem. Soc. Rev. 48*, 2338–2365.

Kowitsch, A., Zhou, G., Groth, T., **2018**. *J. Tissue Eng. Regen. Med. 12*, e23–e41.

Wang, Junlong, Yang, W., Wang, Jiancheng, Wang, X., Wu, F., Yao, J., Zhang, J., Lei, Z., **2015**. *Carbohydr. Polym. 133*, 320–327.

Wang, Z., Xie, J., Shen, M., Nie, S., Xie, M., **2018**. *Trends Food Sci. Technol. 74*, 147–157.

Wardrop, D., Keeling, D., **2008**. *Br. J. Haematol. 141*, 757–763.

Zeng, K., Groth, T., Zhang, K., **2019**. *ChemBioChem 20*, 737–74

SECTION 2.1 – REGIOSELECTIVE SULFATION OF LOW MOLECULAR WEIGHT DIABOLICAN POLYSACCHARIDE FROM *V. DIABOLICUS* BACTERIUM

2.1
REGIOSELECTIVE SULFATION OF LOW MOLECULAR WEIGHT DIABOLICAN POLYSACCHARIDE FROM *V. DIABOLICUS* BACTERIUM

2.1.1. Diabolican polysaccharide from *V. diabolicus* bacterium: structure and activities

Diabolican is the exopolysaccharide (EPS) produced by *Vibrio diabolicus* HE800 strain, a mesophilic bacterium collected from a deep-sea hydrothermal field.

EPSs are high molecular weight carbohydrate biopolymers that microorganisms produce in their surrounding environment, which have different structure and are secreted by a wide range of bacteria. Depending on their localization, bacterial EPS are divided into capsular polysaccharides if attached to the cell membrane through the lipopolysaccharides anchored in the membrane or through other specific proteins (Decho, **1990**), and free slime polysaccharides loosely attached or even totally secreted into the extracellular environment (Netrusov, **2023**).

These polysaccharides have mostly a protective role and permit resistance under extreme environmental conditions by participating in the cell membrane integrity, trapping nutrients, allowing adhesion to surfaces, protecting from toxic compounds and adverse conditions, such as freezing (Decho, **1990**; Finore et al., **2014**).

A particular attention has been focused on polysaccharide-producing marine bacteria; indeed, the existence of various extreme habitats in marine ecosystem (*e.g.* deep-sea, hydrothermal vents, volcanic and hydrothermal marine areas, marine salterns, salt lakes, and sea ice in polar regions) leads to the presence of unusual microorganisms,

secreting very different and peculiar EPS structures with interesting chemical and rheological properties (Casillo et al., **2018**).

In particular, *Vibrio diabolicus* is a facultatively anaerobic, heterotrophic, mesophilic bacterium isolated from the polychaete annelid *Alvinella pompejana* collected from a deep-sea hydrothermal field in the East Pacific Rise (Raguénès et al., **1997**). As many other *Vibrio* bacteria (Bramhachari et al., **2007**; Drouillard et al., **2015**; Jiang et al., **2011**), it secretes an EPS. This polysaccharide has showed interesting bioactive properties for skincare applications, *i.e.* promotion of fibroblast proliferation and migration and production of extracellular matrix (Benhadda et al., **2023**). From the structural point of view, the polymer backbone consists of a linear tetrasaccharide repeating unit, including two D-GlcA residues, one D-GlcNAc and one D-GalNAc (Figure 2.1**)**

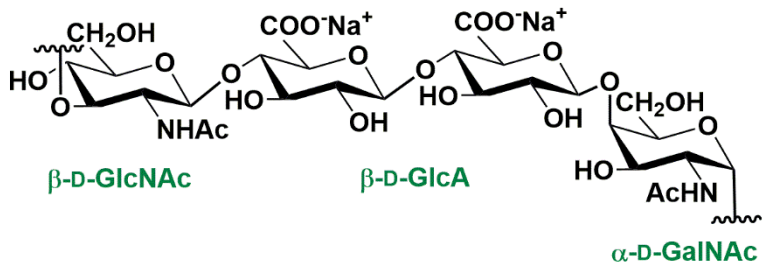

Figure 2.1. Repeating unit of diabolican polysaccharide from *V. diabolicus*

The resemblance of diabolican chain to GAG structures, due to the presence of both aminosugars and uronic acids, makes it of potential interest in term of biological and biomedical properties and applications.

The polysaccharide chain may be structurally modified, opening the way to semi-synthetic macromolecules with new or enhanced bioactivity. To the best of our knowledge, this approach is still almost unexplored on diabolican and only few reports, dealing with chemical modifications of marine EPSs, can be found in literature (Gomez D'Ayala et al., **2008**). In the case of diabolican EPS, only low-

molecular weight oversulfated derivatives thereof have been obtained through chain-shortening of the native polysaccharide, followed by a quantitative, non-regioselective sulfation, and they have shown to exhibit biological activities similar to heparin and other GAGs (Senni et al., **2015**, **2013**). Furthermore, a per-*O*-sulfated derivative was very recently shown to be efficient in preventing brain inflammation and metabolism failure in mucopolysaccharidosis IIIA mice (Veraldi et al., **2023**). However, less sulfated diabolican derivatives with specific sulfation patterns may offer the possibility to finely tune the binding affinity towards signaling proteins with more selective interactions when compared to oversulfated derivatives. To this aim, the semi-synthesis of a new set of diabolican derivatives with intermediate degree of sulfation (DS) values leading to specific sulfation patterns has been investigated in order to obtain new compounds which could act as GAG-mimics.

2.1.2. Results and discussion

Several semi-synthetic pathways for the regioselective sulfation of diabolican polysaccharide from *V. diabolicus* bacterium were investigated. Both direct methods or multi-step strategies were developed for a controlled installation of sulfate groups on specific positions of the polysaccharide backbone. Direct, regioselective sulfation or desulfation reactions were carried out for the manipulation of the most reactive alcohol moieties; multi-step procedures, based on the installation of protecting groups on selected positions of the polysaccharide structure, followed by sulfation of the unprotected hydroxyls and then global deprotection (Bedini, Laezza, Parrilli, & Iadonisi, **2017**) were used to have access to other sulfation patterns.

Since sulfated polysaccharides can cause adverse effects associated with high molecular weight sulfated species (Fonseca et al., **2010**), the polysaccharide was partially depolymerized through a H_2O_2-mediated free radical reaction to give a LMW derivative before any reaction.

Firstly, the attention was focused on the regioselective sulfation of the most reactive, primary alcohol moieties of GlcNAc and GalNAc. For this purpose, a direct reaction under mild conditions was attempted. A cation exchange step was performed to obtain tetrabutylammonium salt **1**, that was then solubilized in DMF and treated with $SO_3 \cdot py$ at 4 °C. Then, a cation re-exchange step could afford sulfated polysaccharide sodium salt **SD-1**, presumably with sulfate groups exclusively at position *O*-6 of GlcNAc and GalNAc units (Figure 2.2).

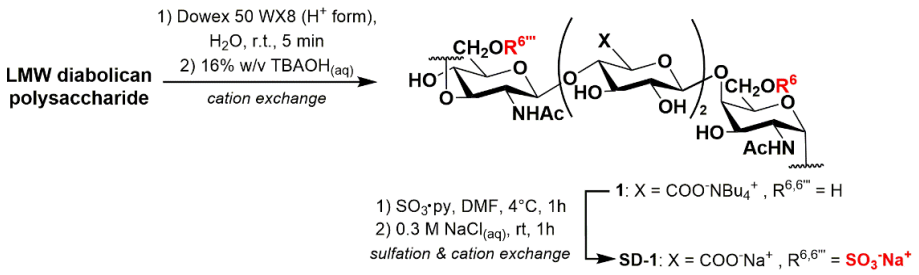

Figure 2.2. Semi-synthesis of **SD-1** using a mild sulfation strategy.

Derivative **SD-1** was characterized by a complete set of ^1H and 2D-NMR spectra. $^1H,^{13}C$-DEPT-HSQC spectrum of polysaccharide **SD-1** (Figure 2.3) showed two groups of methylene signals at $\delta_{H/C}$ 4.25, 4.34/67.8 and 4.17-4.25/69.6 ppm, associated to *CH₂* atoms at GlcNAc6S and GalNAc6S 6-position, respectively. The degree of sulfation (DS) at primary position of GlcNAc residues could be evaluated by relative integration of methylene signals at $\delta_{H/C}$ 4.34/67.8 and 3.90/61.8 ppm. A DS equal to 0.64 was estimated for GlcNAc 6-*O*-sulfation. Regarding GalNAc 6-*O*-sulfation, DS could be not evaluated by integration of methylene signals due to signal overlapping. By looking for alternative signals to be integrated, three different signals were assigned to anomeric α-linked *CH* atoms of GalNAc units, at $\delta_{H/C}$ 5.61/98.0, 5.54/98.3 and 5.42/98.8, that suggested the presence of three different subunits within the polysaccharide backbone. The most ^1H-upfield shifted signal was assigned to unsulfated GalNAc units, by comparison with starting diabolican (Rougeaux et al.,

1999), while using a full set of 2D-NMR spectra (COSY, TOCSY, HMBC and HSQC-TOCSY) it was possible to assign the middle one to GalNAc6S residues. Similarly, the most ^{1}H-downfield shifted signal was associated to α-linked GalNAc units with a different sulfation pattern, in particular with an additional sulfate group at *O*-3 position as indicated by the marked downfield shift of related *CH* signal with respect to starting diabolican. A relative integration of GalNAc, GalNAc6S and GalNAc3,6S anomeric signals in ^{1}H-NMR spectrum of **SD-1** gave DS values equal to 0.65 and 0.16 for 6-*O*- and 3-*O*-sulfation, respectively.

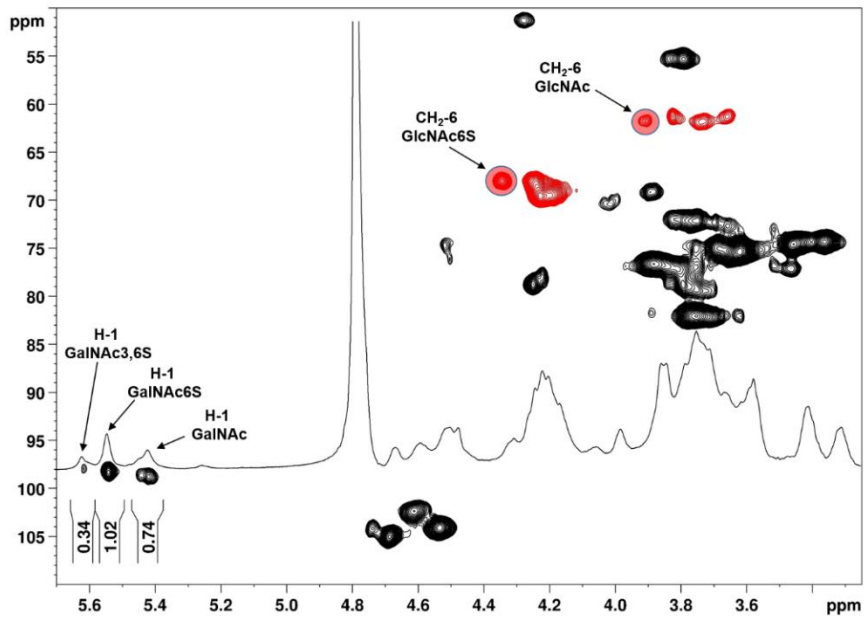

Figure 2.3. Zoom of ^{1}H and ^{1}H,^{13}C-DEPT-HSQC NMR spectra (600 MHz, 298 K, D_2O) of **SD-1** (indicated signals and densities were integrated for estimation of relative amounts of differently sulfated units; only some of the assignments are shown)

To obtain a derivative with complementary sulfation pattern, with sulfate groups at each hydroxyl positions except for the primary ones, a selective desulfation reaction on per-*O*-sulfated derivative **SD-2**, obtained by sulfation of the pyridinium salt **2** with SO_3·py in DMF at 45°C, was attempted. The desulfation reaction was performed on

the pyridinium salt of **3** with MTSTFA, a reagent known to cleave selectively sulfate groups placed at *O*-6 position of polysaccharides and converts the released primary hydroxyl groups into trimethylsilyl ethers that can be then easily cleaved by an aqueous work-up (Takano et al., **1995**) to obtain derivative **SD-3** (Figure 2.4).

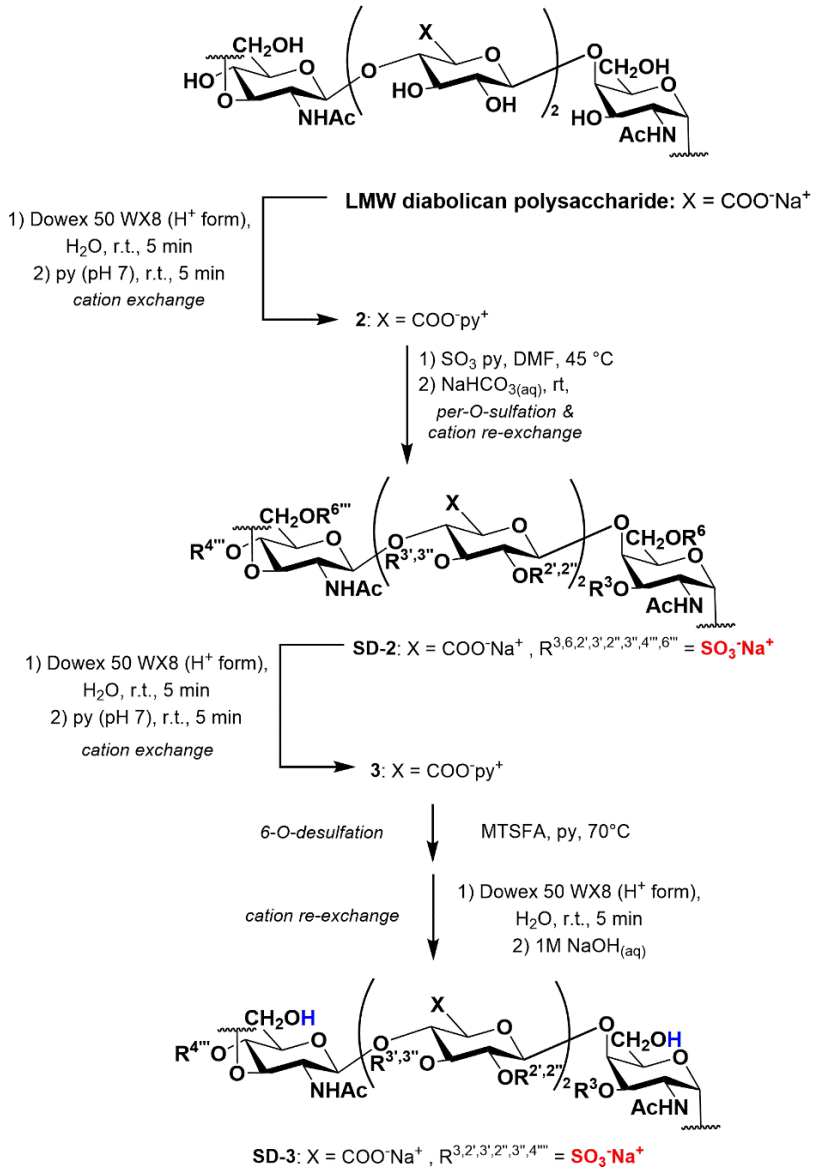

Figure 2.4. Semi-synthesis of **SD-3** using de-*O*-sulfation approach.

Per-*O*-sulfation of derivative **SD-2** was confirmed by 2D-NMR analysis, giving a single pattern of signals for every monosaccharide constituent of the repeating unit, with a marked ^{1}H and ^{13}C downfield shift of chemical shift values related to every CH and CH_2 atoms. Unfortunately, 2D-NMR analysis of **SD-3** showed no particular difference with respect to the starting oversulfated product (Figure 2.5).

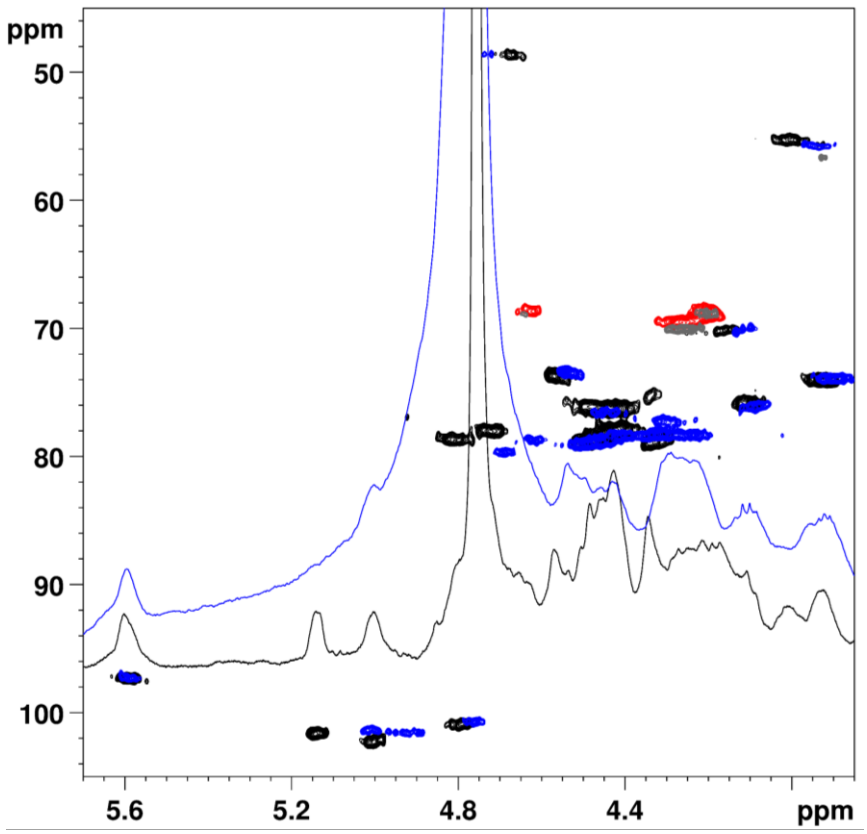

Figure 2.5. Superimposition of ^{1}H and $^{1}H,^{13}C$-DEPT-HSQC NMR zoomed spectra (400 MHz, 298K, D2O) of **SD-2** (black and red) and **SD-3** (blue and grey)

A third, direct strategy was based on the substitution of the acetamido moieties of GlcNAc and GalNAc units with *N*-linked sulfate groups. To this aim, the *N*-acetyl groups of the GlcNAc and GalNAc unites should be first cleaved under appropriate conditions, then the free amino functions should be chemoselectively sulfated. This

strategy required the optimization of the *N*-deacetylation reaction conditions. Hydrazinolysis is the common method employed for GAG *N*-deacetylation (Nadkarni et al., **1996**). Reaction parameters, such as temperature, catalyst, hydrazine content and reaction time, play a pivotal role in determining its efficiency and avoiding side-reactions (Guo & Conrad, 1989; Zhao et al., **2013**). Indeed, GAG structures are quite labile under the required alkaline condition, that could cause a β-eliminative cleavage at the glycosidic bonds involving *O*-4 linked uronic units, thus resulting in an undesired depolymerization. In particular, the reaction temperature (not higher than 90°C) and hydrazine content (not higher than 70% in water) are already well-established parameters (Yan et al., **2017**; Zhao et al., **2013**). The reaction is often performed in the presence of a catalyst, commonly hydrazine sulfate, which provides protons to accelerate the *N*-deacetylation rate, again avoiding the β-elimination. For these reasons, the optimization study was focused exclusively on reaction time (Figure 2.6).

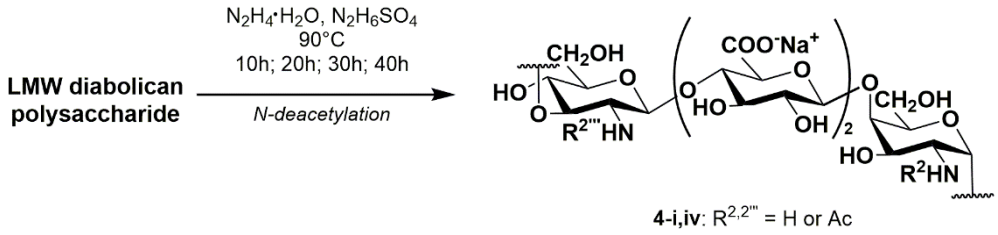

Figure 2.6. *N*-deacetylation step on **LMW diabolican**

The reaction was conducted with $N_2H_4 \cdot H_2O$ and $N_2H_4 \cdot H_2SO_4$ at 90°C for different times (10, 20, 30 and 40 hours). After the work-up with ethanol and some drops of saturated aqueous NaCl solution, each aliquot was dialysed at 4 °C and freeze-dried, then the obtained derivatives **4-i,iv** were analysed by ^{1}H-NMR spectroscopy.

A comparison of ^{1}H-NMR spectra of starting LMW diabolican polysaccharide and of the obtained derivatives (Figure 2.7) clearly showed a lowering of the intensity of the α-linked GalNAc *H*-1 signal at δ 5.42 ppm with the reaction time, together with the

concomitant appearance of a new resonance at δ 5.67 ppm, which could be attributed to the anomeric proton of the *N*-deacetylated GalN units. However, at reaction times higher than 20 hours (Figure 2.7b), overlapped peaks could be observed in the range 5.62–5.72 ppm, reasonably due to anomeric signals of GalN units in shorter and/or differently degraded polysaccharide chains. For these reasons, a reaction time of 20 h was considered adequate both to have a good deacetylation degree and to avoid polysaccharide depolymerization and/or by-products.

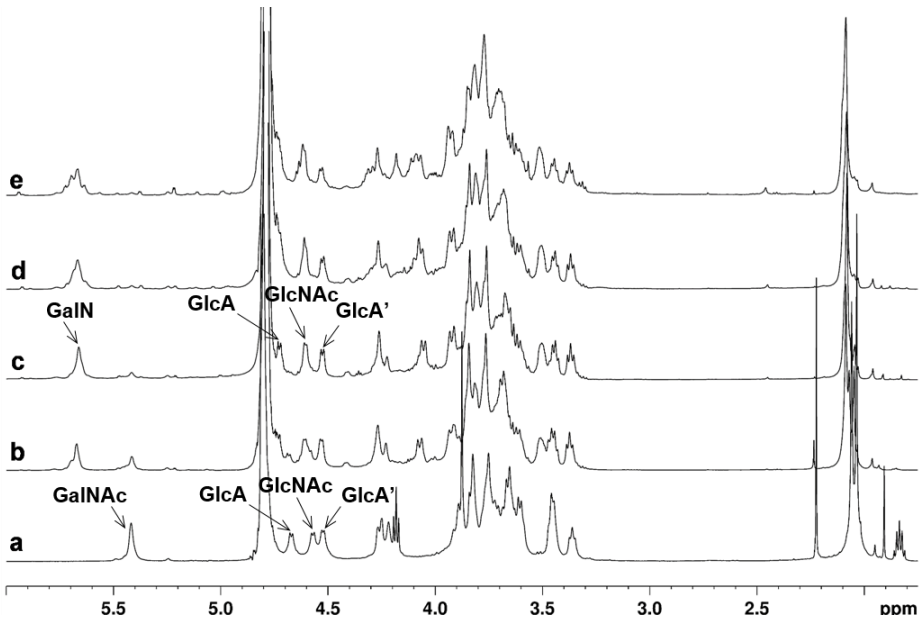

Figure 2.7. ^{1}H NMR spectra (zoom, 600 MHz, 298 K, D_2O) of (a) LMW-HE800 EPS and (b-e) derivative **4-i,iv** obtained after 10, 20, 30 or 40 hours, respectively, under hydrazinolysis reaction (only anomeric signals assignment is displayed)

A detailed 2D-NMR analysis of the polysaccharide derivative **4-ii** was performed in order to have a fully characterization (Figure 2.8). The ^{1}H,^{13}C-DEPT-HSQC spectrum displayed four anomeric signals ($\delta_{H,C}$ 5.67/97.2, 4.72/104.2, 4.60/101.5 and 4.52/103.9 ppm), that could be assigned to GalN, GlcA, GlcNAc and GlcA' residues, respectively. This revealed that the *CH*-1 signal of glucosamine residues underwent

no significant ^{1}H and ^{13}C shifts with respect to starting LMW-diabolican values. Similarly, the *CH*-2 resonance of the glucosamine units remained unaffected after the *N*-deacetylation reaction, while its galactosamine counterpart was significantly upfield shifted in the ^{1}H dimension (from 4.27 to 3.68 ppm) and slightly downfield shifted in the ^{13}C one (from 51.3 to 52.4 ppm). The observed NMR shifts, in agreement with reported data on *N*-deacetylation of GAGs (Li et al., **2014**; Mans et al., **2015**), suggested that the *N*-deacetylation reaction involved exclusively GalNAc units, leaving unaltered the GlcNAc residues. The latter could not be deacetylated even under prolonged reaction times. Presumably, the acetamido moiety of GalNAc units is more labile to hydrazinolysis with respect to GlcNAc one.

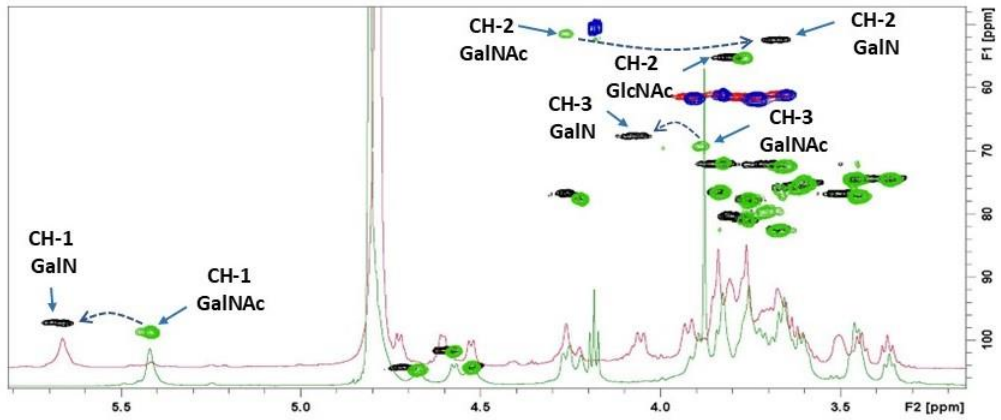

Figure 2.8. Superimposition of ^{1}H and $^{1}H,^{13}C$-DEPT-HSQC NMR zoomed spectra of Diabolican EPS (green and blue, 600 MHz, 298K, D_2O) and **4-ii** (black and red, 400 MHz, 298K, D_2O)

Derivative **4-ii**, obtained through hydrazinolysis after 20 hours reaction, was subjected to sulfation reaction of the single free amine (Figure 2.9). The reaction was conducted with $SO_3 \cdot Me_3N$ as sulfating agent, selected for its lower reactivity with respect to other commonly employed ones (*e.g.* $SO_3 \cdot py$, $SO_3 \cdot DMF$). This can be ascribed to the higher Lewis base strength of trimethylamine. *N*-sulfation was conducted in water at 45°C in the presence of Na_2CO_3 (Li et al. **2014**).

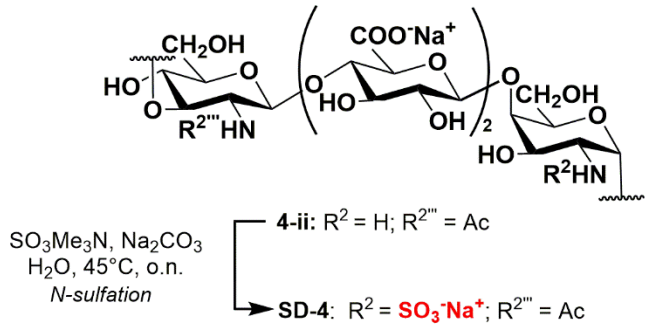

Figure 2.9. Semi-synthesis of **SD-4** through *N*-sulfation step

2D-NMR spectra analysis of derivative **SD-4** confirmed the postulated structure with a single sulfate group linked to the nitrogen atom of GalN units, as evidenced by the ^{13}C-downfield shift of their *CH*-2 signal with respect to starting derivative **4-ii** (Figure 2.10).

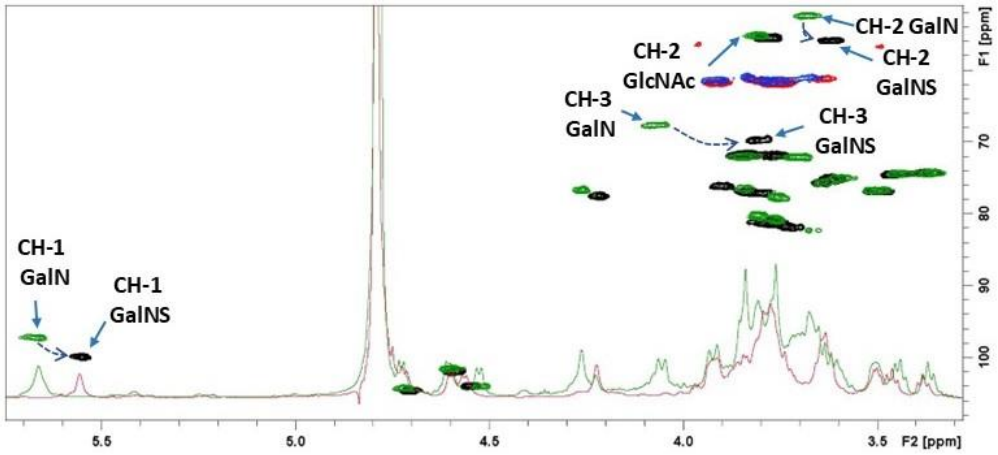

Figure 2.10. Superimposition of ^{1}H and ^{1}H,^{13}C-DEPT-HSQC NMR zoomed spectra of **4-ii** (green and blue, 400 MHz, 298K, D_2O) and **SD-4** (black and red, 400 MHz, 298K, D_2O)

To sum up, direct sulfation methods were exploited to have access to new LMW diabolican sulfated compounds with unprecedent sulfation pattern. The degree of sulfation (DS) of derivatives **SD-1,4** are resumed in Table 2.1. Furthermore, in

collaboration with Dr. Zykwinska from the Institut Français de Recherche pour l'Exploitation de la Mer (IFREMER) in Nantes (France), in order to complete the structural characterization of the obtained products, the weight-averaged molecular weight (M_w) and dispersity were measured by HP-SEC-MALLS analysis. A significant chain shortening with respect to starting LMW diabolican EPS was detected for derivative **SD-4**, as expected from the employed strategies (*e.g. N*-deacetylation step), even if no dramatic increase of polydispersity index was noted (Esposito et al. **2022**).

	Yield[a]	**DS**[b]	**M_w**[c] **(kDa)**	**M_n**[d] **(kDa)**	**M_w/M_n**[e]
LMW Diabolican	--	0	24.0 ± 0.1	17.6 ± 0.3	1.36 ± 0.02
SD-1	50%	1.48 ± 0.15 / 1.45 (GlcNAc 6-sulfation: 0.64 GalNAc 6-sulfation: 0.65 GalNAc 3-sulfation: 0.16)	27.2 ± 0.1	18.8 ± 0.2	1.44 ± 0.02
SD-2	204%	6.90 ± 0.25 / 7.00 (fully *O*-sulfated)	38.9 ± 0.2	31.8 ± 0.3	1.22 ± 0.04
SD-3	133%	6.95 ± 0.15 / 7.00 (fully *O*-sulfated)	31.1 ± 0.7	23.1 ± 0.8	1.35 ± 0.06
SD-4	53%	0.98 ± 0.02 / 1.00 (GalNS *N*-sulfation)	5.4 ± 0.1	4.2 ± 0.1	1.29 ± 0.05

[a] Overall mass yield calculated from starting diabolican EPS.

[b] Degree of sulfation (as average percentage amount of sulfate groups per diabolican repeating unit) evaluated by CHNS elemental analysis (first value) or estimated by 2D-NMR analysis (second value, also the sulfation patterns are included).

[c] Weight averaged molecular mass.

[d] Number-averaged molecular mass.

[e] Polydispersity index

Table 2.1. Yield and structural data for semi-synthetic polysaccharides **SD-1,4**

Another semi-synthetic approach was based on the development of multi-step pathways: these strategies are based on the regioselective installation of protecting groups followed by the sulfation of the unprotected position and then by the global deprotection of the sulfated product. The first methods were focused on the insertion of sterically hindered acyclic protecting groups for the protection of the most accessible and reactive positions of the polysaccharide. To this aim, two silyl ether protecting groups (*t*-butyldimethylsilyl, TBDMS and triisopropylsilyl, TIPS) were selected on the basis of their successful employment on other polysaccharides (Koschella et al. **1997**) Firstly, LMW diabolican was converted into its *n*-tetrabutylammonium (TBA) salt **5-i** (Esposito et al., **2022**), that was then treated with TBDMSCl or TIPSCl in the presence of imidazole in DMF (Figure 2.11).

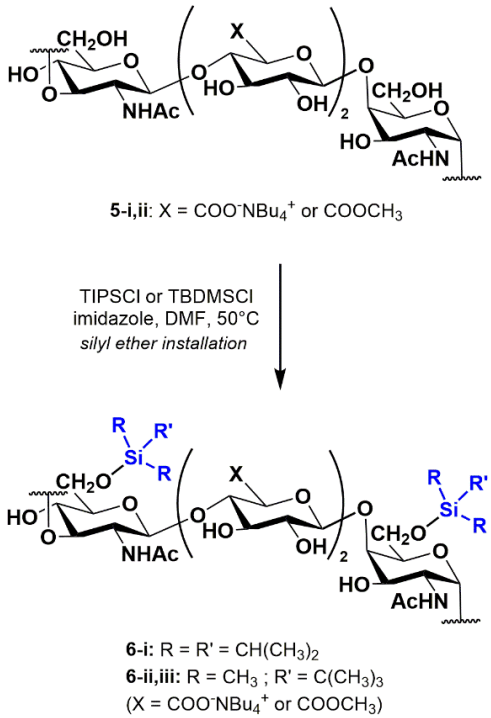

Figure 2.11. Silyl ethers installation on LMW diabolican derivatives **5-i,ii**

After purification by precipitation, the obtained compounds **6-i,ii** were subjected to ^{1}H-NMR analysis. Both spectra showed the absence of any silyl ether moiety covalently linked to the polysaccharide, as no significant signal was detected in the typical regions (approx. 0-1 ppm) for Si-CH_3 and Si-$CH(CH_3)_2$ moieties of TBDMS and TIPS groups, respectively. The same result was observed by performing the reaction with TBDMSCl on diabolican methyl ester derivative **5-ii**, which gave compound **6-iii**. The regioselective protection of diabolican could be also performed using cyclic protecting groups in order to protect two alcoholic moieties in a single step (Figure 2.12). For this purpose, a *p*-methoxy-benzylidene acetal group was selected for the protection of the positions 4 and 6 of GlcNAc residue. Therefore, the *p*-methoxy-benzylidenation reaction on LMW diabolican was conducted with *p*-OMe-PhCH$(OCH_3)_2$ and CSA in DMF at 80°C to afford the regioselective protection of GlcNAc hydroxyls without any reaction on the other six alcohol moieties of diabolican repeating unit.

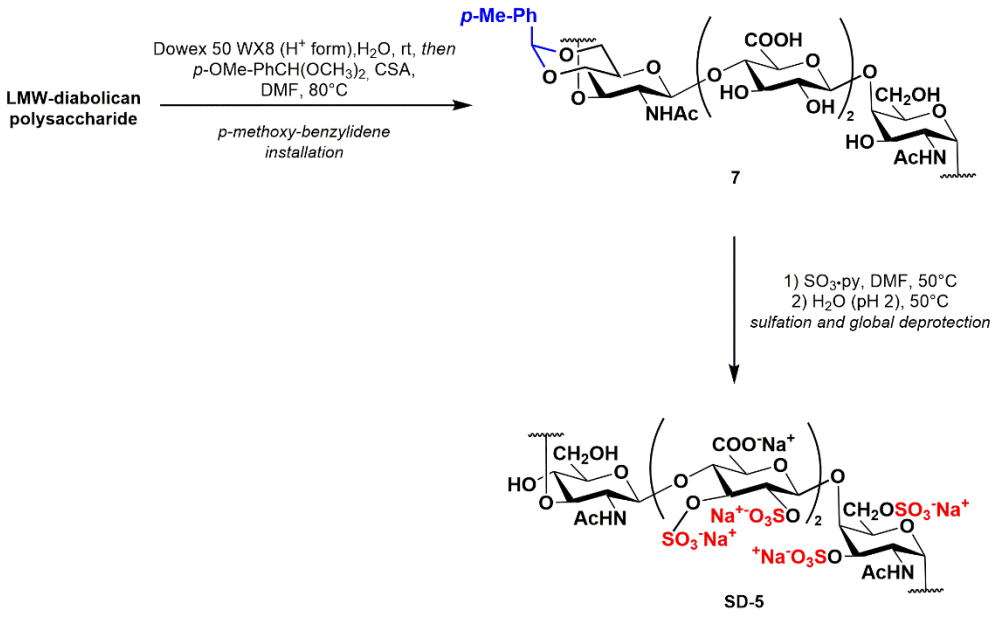

Figure 2.12. Semi-synthesis of **SD-5**

The presence of *p*-methoxy-benzylidene rings on **7** was confirmed by its ^{1}H-NMR spectrum, that showed some signals in the region between 6.80 and 7.60 ppm, typical of the aromatic ring of the cyclic protecting group (Figure 2.13).

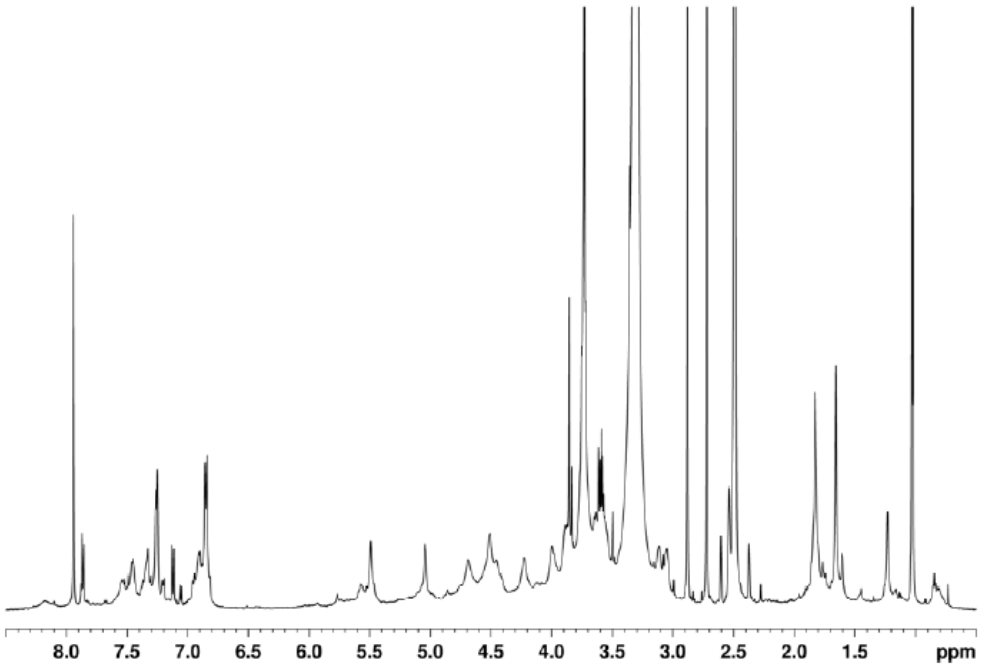

Figure 2.13. ^{1}H-NMR spectrum (600 MHz, 298 K, DMSO-*d6*) of **7**

Derivative **7** was subjected to sulfation under standard conditions with SO_3· py in DMF at 50 °C, followed by a treatment under acid aqueous conditions, in order to remove the *p*-methoxy-benzylidene rings and afford compound **SD-5**. It was subjected to a complete set of ^{1}H and 2D-NMR spectra for a fully structural characterization (Figure 2.14). A comparison between the ^{1}H,^{13}C-DEPT-HSQC spectrum of **SD-5** and starting LMW diabolican showed the ^{1}H- and ^{13}C-downfield shift of a single methylene signal associated to primary positions of aminosugars, in particular the one related to CH_2 atoms at position 6 of GalNAc residues. This suggested that this position was decorated with sulfate groups. The most ^{1}H-downfield

shifted anomeric signal at $\delta_{H/C}$ 5.56/96.2 could be assigned to GalNAc units due to their α-configuration. The study of HSQC-TOCSY spectrum displayed a correlation of a single signal related to CH atoms at position 3 of GalNAc units ($\delta_{H/C}$ 4.44/74.7) with GalNAc anomeric signal. Its marked ^{1}H- and ^{13}C- downfield shift with respect to the signal associated to the same CH atoms in the starting LMW diabolican, revealed that GalNAc *O*-3 atom was quantitatively decorated with a sulfate group in agreement with the method. As regards the GlcNAc residues, all the signals were neither ^{1}H- nor ^{13}C-downfield shifted with respect to the starting polysaccharide. This suggested the absence of any sulfate group installed on GlcNAc units.

The anomeric signals of the two GlcA residues were split in three different peaks (the most intense $GlcA_I$ at $\delta_{H/C}$ 4.93/100.0 and the other two $GlcA_{II}$ and $GlcA_{III}$ at $\delta_{H/C}$ 5.07/100.2 and 4.80/102.2), all ^{1}H-downfield and ^{13}C-upfield shifted with respect to the starting LMW diabolican. This suggested that GlcA units were all derivatized with sulfate groups at positions 2 and/or 3. Since the anomeric signals for $GlcA_{II}$ and $GlcA_{III}$ showed a similar, lower intensity with respect to the $GlcA_I$ one, a heterogeneous sulfation pattern for one of the two GlcA residues of **SD-5** could be hypothesized. This was confirmed by detecting the $GlcA_{I\text{-}III}$ H-1-H-2 cross-peaks in COSY spectrum and the HSQC-TOCSY signals correlating with $GlcA_{I\text{-}III}$ anomeric signals. Indeed, it was possible to locate the CH-2 signal of $GlcA_I$ and $GlcA_{II}$ at much higher ^{1}H and ^{13}C chemical shift values ($\delta_{H/C}$ 4.33/77.2) with respect to $GlcA_{III}$ one ($\delta_{H/C}$ 3.60/72.2). Since the ^{1}H chemical shift value assigned to the former was close to the one reported for LMW per-*O*-sulfated diabolican, $GlcA_I$ and $GlcA_{II}$ were both assigned as 2,3-disulfated residues. $GlcA_{III}$ could be recognized as a 3-sulfated unit because its CH-3 atoms – but not CH at position 2 - showed a marked ^{1}H- and ^{13}C-downfield shifted signal at $\delta_{H/C}$ 4.49/81.6 with respect to unsulfated LMW diabolican. To summarize, by 2D-NMR analysis **SD-5** was detected to have sulfate groups placed on both GalNAc and the two GlcA residues of diabolican repeating unit, and no sulfation on GlcNAc residues.

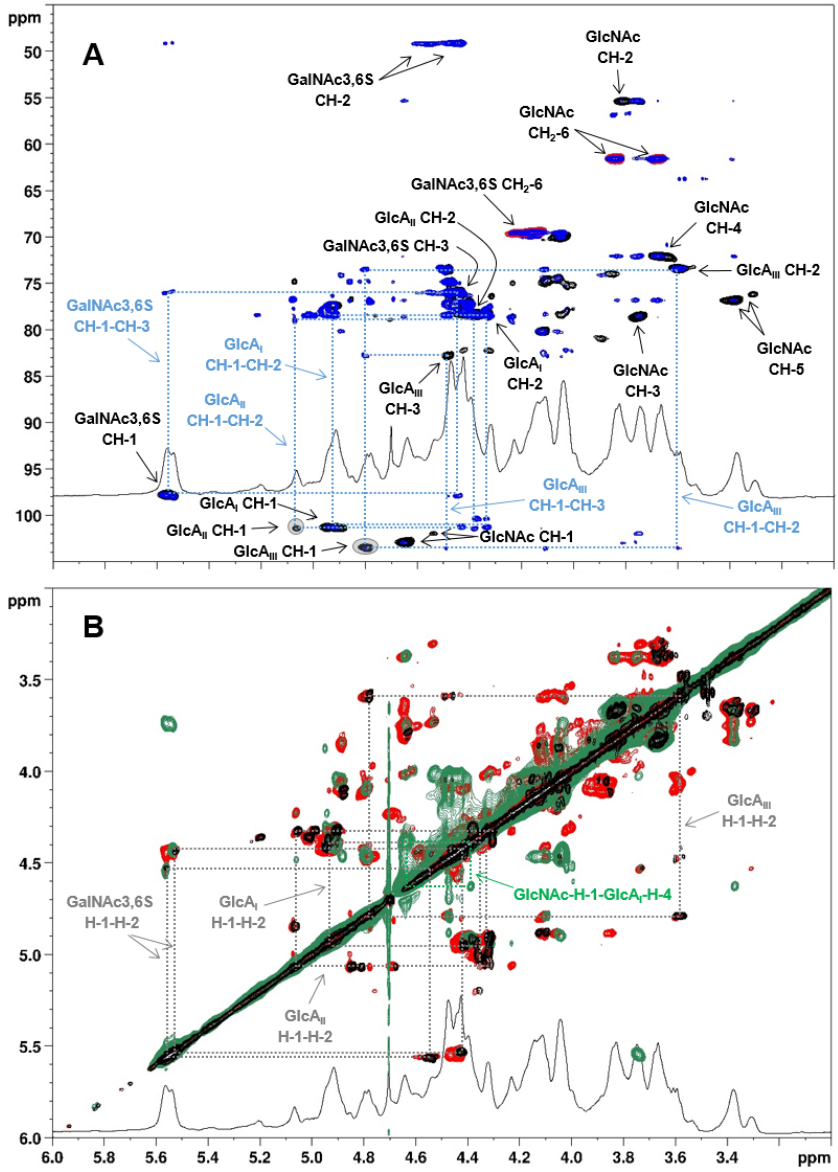

Figure 2.14. Zoomed superimposition of A) ^{1}H NMR, ^{1}H,^{13}C-DEPT-HSQC (black and red) and ^{1}H,^{13}C– HSQC-TOCSY (blue and green) and B) ^{1}H NMR, COSY (black), TOCSY (red) and NOESY (green) 2D-NMR spectra (600 MHz, 298 K, D_2O) of sulfated derivative **SD-5** (*GlcA$_I$* = GlcNAc-1 → 4-*GlcA2,3S*, *GlcA$_{II}$* = *GlcA2,3S*-1 → 4- GalNAc, *GlcA$_{III}$* = *GlcA3S*-1 → 4-GalNAc; densities enclosed in dotted lines were integrated for $GlcA_{II}$- $GlcA_{III}$ ratio estimation; only some assignments and correlations are indicated)

The *p*-methoxy-benzylidene installation was also included in a three-step, two-pot sequence (Vessella et al. **2021**), based on the cyclic protecting group installation, followed by acetylation of the secondary hydroxyl groups on GlcA and GalNAc residues and then by chemoselective cleavage of the *p*-methoxybenzylidene rings to restore the diol moiety on GlcNAc units. This sequence was expected to afford derivative **9**. The presence of acetyl ester groups in the structure of **9** was confirmed by the typical signals at 1.96-2.15 ppm in its ^{1}H-NMR spectrum. Instead, no signals were detected in the aromatic region, thus confirming the successful cleavage of the *p*-methoxybenzylidene protecting groups (Figure 2.15).

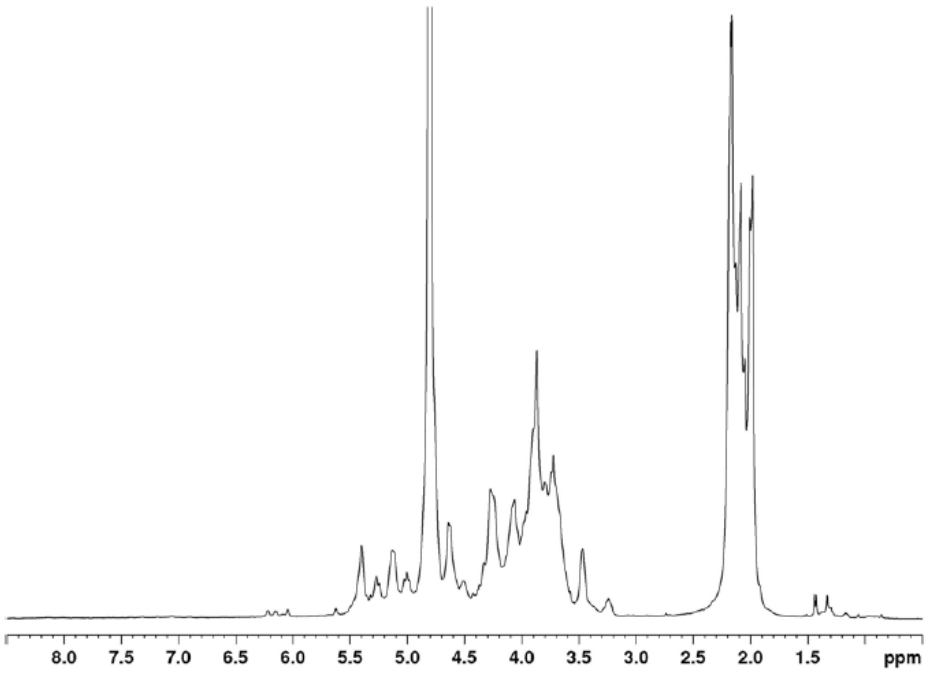

Figure 2.15. ^{1}H-NMR spectrum (600 MHz, 298 K, D_2O) of **9**

Derivative **9** was then subjected to a sulfation and global deprotection reaction under alkaline aqueous conditions to remove the ester moieties, obtaining derivative **SD-6** with a sulfation pattern complementary to derivative **SD-5** (Figure 2.16).

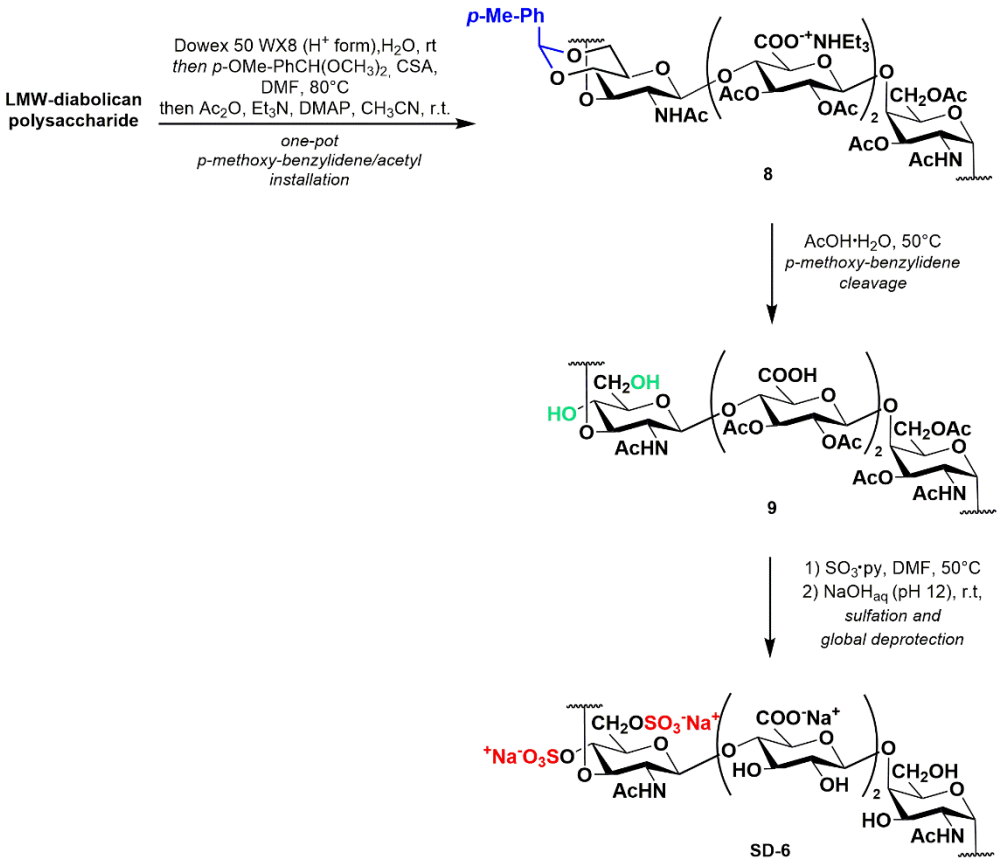

Figure 2.16. Semi-synthesis of **SD-6**

A detailed 2D-NMR analysis of the polysaccharide derivative **SD-6** was performed to confirm the presence of sulfate groups on position 4 and 6 of GlcNAc units (Figure 2.17). By integration of $^{1}H,^{13}C$-DEPT-HSQC peak volumes, a quantitative derivatization was found only for the primary position, while only a 48% average amount of sulfate groups was estimated for the GlcNAc *O*-4 site. Furthermore, an unexpected 51% average amount of sulfate groups was found on GlcA *O*-2 positions, together with a minor amount (19%) for GlcA *O*-3 sites. The partial sulfation of GlcA *O*-2 positions was in agreement with the non-quantitative sulfation at the same sites in derivative **SD-5**. These complementary results could be hypothetically ascribed to

the formation of acyclic acetals protecting some GlcA units during the *p*-methoxy-benzylidenation of LMW diabolican, as already reported for the acetalation of other polysaccharides (Bachelder et al **2017**; Laezza et al **2014**).

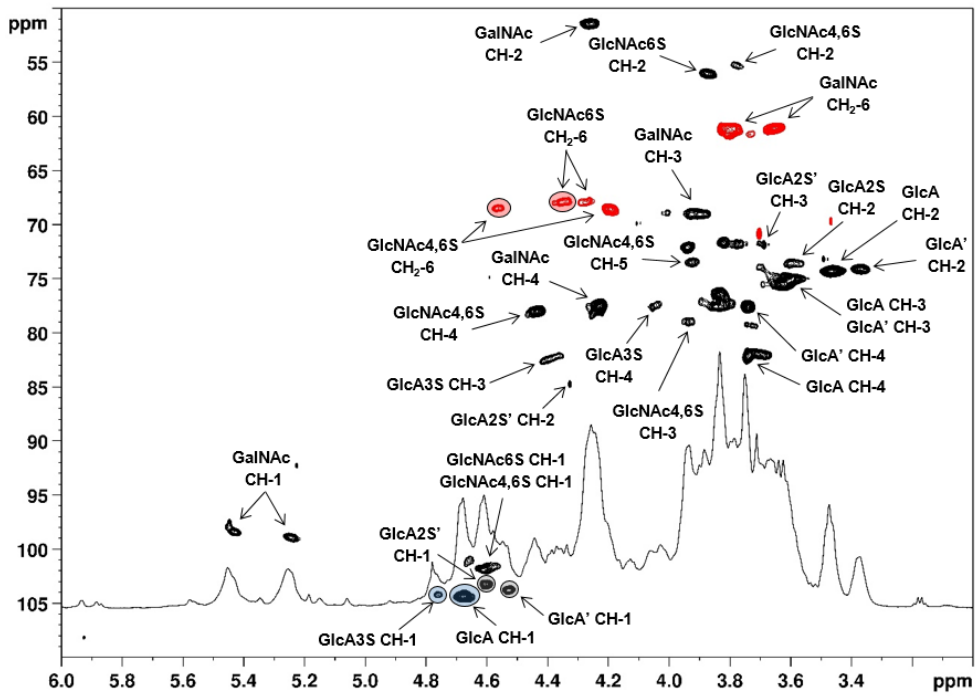

Figure 2.17. ^{1}H-NMR and ^{1}H,^{13}C-DEPT-HSQC spectra (600 MHz, 298K, D_2O, zoom) of **SD-6** (GlcA = GlcA-1→4-GalNAc, GlcA' = GlcNAc-1→4-GlcA; densities enclosed in circles were integrated for GlcNAc4S, GlcNAc4,6S, GlcA-GlcA3S and GlcA'-GlcA2S' estimation; only some assignments are indicated)

A third multi-step approach was focused on an intramolecular reaction, involving the carboxylic acid and the alcohol group at position 3 of GlcA residues, to form a lactone ring. This reaction (Vessella et al. **2019**) has been conducted by employing Bz_2O in DMF at 85°C, followed by one-pot treatments firstly with DMAP and pyridine at room temperature to allow the benzoylation of all the free hydroxyls and then with sodium acetate and methanol to cleave the lactone rings on GlcA units. This three-

step, one-pot procedure was expected to afford derivative **11**, having all the reactive moieties of diabolican repeating unit protected as esters but the hydroxyls at position 3 of the two GlcA residues (Figure 2.18).

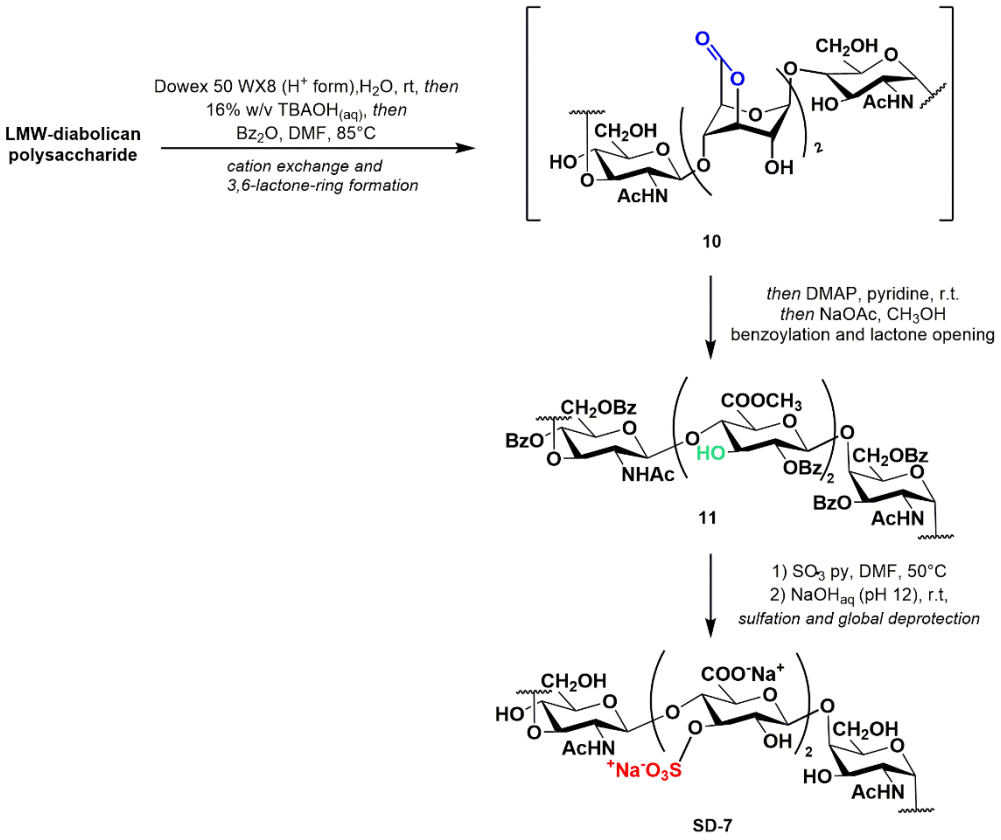

Figure 2.18. Semi-synthesis of **SD-7**

The presence of benzoyl esters in the structure of **11** was confirmed by its ^{1}H-NMR spectrum, displaying the typical Bz esters phenyl rings signals in the region between 7.2 and 8.1 ppm, (Figure 2.19).

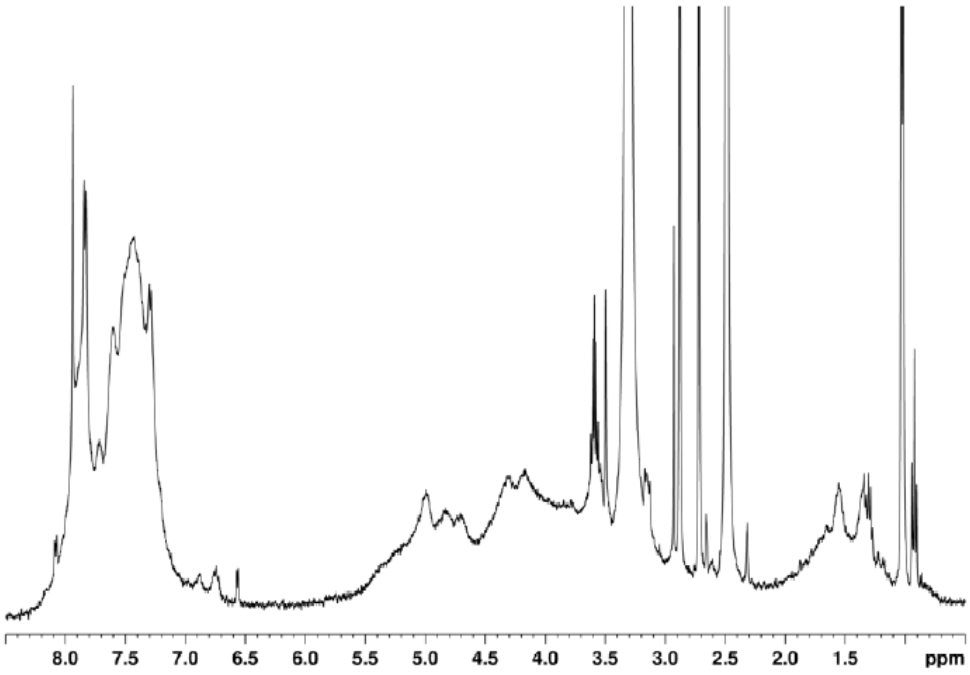

Figure 2.19 ^{1}H-NMR spectrum (600 MHz, 298 K, DMSO-*d6*) of **10**

Therefore, derivative **11** was subjected to sulfation reaction under the same conditions of derivatives **SD-5,6** followed by ester moieties cleavage, affording compound **SD-7**. The study of a complete set of 2D-NMR spectra of derivative **SD-7** (Figure 2.20) suggested the presence of sulfate groups at position 3 of some GalNAc residues and at position 4 of some GlcNAc units. This unexpected sulfation pattern could be attributed to the absence of any 3,6-lactone rings in compound **10**. Therefore, the following benzoylation reaction was allowed to protect all the hydroxyls of diabolican backbone, leaving the alcohol functionality still free only on some of the most plausibly hindered positions, *i.e.* GalNAc *O*-3 and GlcNAc *O*-4 sites. Such unprotected positions were in turn derivatized with sulfate groups in the subsequent reaction from derivative **11** to product **SD-7**.

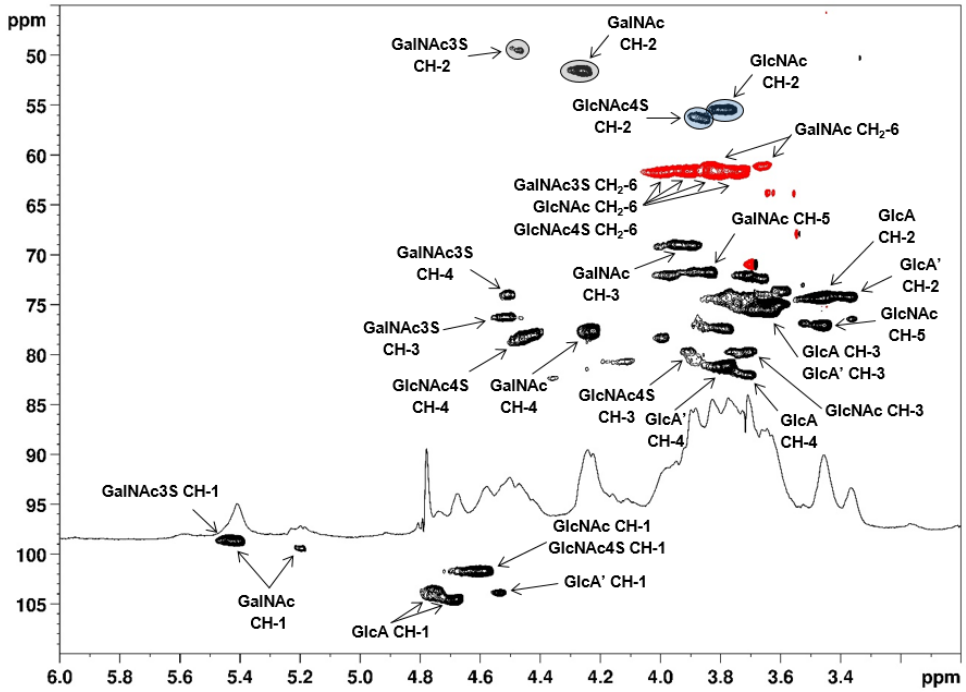

Figure 2.20. ^{1}H-NMR and ^{1}H,^{13}C-DEPT-HSQC spectra (600 MHz, 298K, D_2O, zoom) of **SD-7** (GlcA = GlcA-1→4-GalNAc, GlcA' = GlcNAc-1→4-GlcA; densities enclosed in circles were integrated for GalNAc-GalNAc3S and GlcNAc-GlcNAc4S estimation; only some assignments are indicated)

The DS of derivatives **SD-5,7** were also estimated through elemental analysis. Furthermore, their weight-averaged molecular weight (M_w) and dispersity were evaluated by HP-SEC-MALLS analysis. M_w values were found to be slightly to significantly shortened with respect to starting LMW diabolican, although a dramatic fragmentation of the polysaccharide chain was not detected in all cases. Similarly, a slight to significant increase of dispersity was noted. The distribution of sulfated groups was evaluated from 2D-NMR data, as discussed above (Table 2.2).

	Semi-synthetic precursor	Yield[a]	M_w [kDa]	$Đ$[b]	DS[c]	Sulfation pattern
LMW diabolican	--	--	24.0 ± 0.1	1.36 ± 0.02	0	--
SD-5	**7**	132%	15.8 ± 0.6	1.58 ± 0.11	3.85 ± 0.25 / 5.31	GalNAc-*O*-3 (1; 1) GalNAc-*O*-6 (1; 1) GlcA-*O*-2 (2; 1.31) GlcA-*O*-3 (2; 2)
SD-6	**9**	72%	6.7 ± 0.6	1.39 ± 0.17	2.80 ± 0.03 / 2.18	GlcA-*O*-3 (0; 0.19) GlcA-*O*-2 (0; 0.51) GlcNAc-*O*-4 (1; 0.48) GlcNAc-*O*-6 (1; 1)
SD-7	**11**	41%	11.5 ± 1.2	1.78 ± 0.28	1.27 ± 0.16 / 0.62	GalNAc-*O*-3 (0; 0.20) GlcA-*O*-3 (2; 0) GlcNAc-*O*-4 (0; 0.42)

[a] Overall weight yield calculated from starting LMW diabolican.

[b] Calculated as the ratio between M_w and M_n.

[c] Degree of sulfation (as average percentage amount of sulfate groups per diabolican repeating unit) evaluated by CHNS elemental analysis (first value) or estimated by 2D-NMR analysis (second value).

Table 2.2. Global yield and structural features of derivatives **SD-5-7**

Biological activities of sulfated GAGs depend on their protein-binding ability, which allow the regulation of physiological and pathological processes (Gandhi et al. **2008**; Vallet et al. **2022**) including organogenesis, wound healing, coagulation, inflammation, thrombosis, cancer growth and metastasis (Köwitsch, Zhou, & Groth, **2018**). By interacting with growth factors, GAGs protect them from undesired degradation and enhance both their local concentration up to levels required for

signaling and their stability, thus facilitating the growth factor binding to their cell receptors.

The main contribution to binding affinity comes from electrostatic interactions between negatively charged sulfate groups of GAGs and positively charged, basic amino acids, such as arginine, lysine and histidine, of growth factors (Gandhi & Mancera, **2008**). However, the presence of two uronic acids, possessing negatively charged carboxylate moieties together with free hydroxyls in the diabolican structure, may promote the polysaccharide/growth factor binding thanks also to non-covalent interactions, such as hydrogen bonding. GAG-protein interactions are influenced by several factors like molecular weight, DS and sulfation pattern. The impact of these parameters on the growth factor binding affinity was investigated through Surface Plasmon Resonance (SPR) by Dr. Zykwinska and collaborators. Firstly, the interaction of derivatives **SD-1,4** with five basic growth factors, namely TGF-β1, BMP-2, VEGF, GDF-5 and FGF-2, and one acidic growth factor, EGF, was tested (Table 2.3).

	TGF-β1	**BMP-2**	**VEGF**	**GDF-5**	**FGF-2**	**EGF**
LMW diabolican	$9.1\ 10^{-8}$	$3.5\ 10^{-8}$	$1.7\ 10^{-8}$	$5.8\ 10^{-8}$	$4.0\ 10^{-8}$	$>10^{-5}$
SD-1	$5.2\ 10^{-7}$	$5.0\ 10^{-7}$	$2.2\ 10^{-7}$	$1.2\ 10^{-7}$	$4.1\ 10^{-7}$	$>10^{-5}$
SD-2	$2.2\ 10^{-9}$	$7.6\ 10^{-9}$	$1.3\ 10^{-8}$	$1.4\ 10^{-9}$	$5.9\ 10^{-9}$	$>10^{-5}$
SD-3	$>10^{-5}$	$>10^{-5}$	$>10^{-5}$	$9.4\ 10^{-7}$	$>10^{-5}$	$>10^{-5}$
SD-4	$>10^{-5}$	$3.1\ 10^{-6}$	$1.8\ 10^{-5}$	$2.3\ 10^{-7}$	$2.9\ 10^{-6}$	$>10^{-5}$

Table 2.3. Dissociation constant (K_d [M]) values for the interaction between LMW diabolican EPS derivatives and growth factors

Firstly, no binding affinity was measured between the acidic Epidermal Growth Factor (EGF) and all the LMW diabolican derivatives. Due to electrostatic repulsion between negatively charged (sulfated) diabolican samples and negatively charged EGF (negative global charge, even if it has few positively charged lysins), there is no interaction between these two entities (in the conditions of the SPR experiment). Instead, for the tested basic growth factors (*e.g.* BMP-2, TGF-β1), the overall protein

charge is positive (pI > 7), despite of the negatively charged amino acids present in the protein structure (Asp, D and Glu, E). In these growth factors there is a specific sequence with clustered basic residues (heparin binding domains), responsible for heparin/heparan sulfate binding (and for the binding with sulfated diabolican derivatives).

This demonstrated the electrostatic origin of the interactions between the LMW diabolican derivatives and basic growth factors. The binding strength is primarily depending on polysaccharide sulfation degree. In particular, a much stronger binding was detected for per-*O*-sulfated derivative **SD-2** with respect to the rest of derivatives which show DS ranging from 0 to 1.5. The polysaccharide molecular weight also highly impacts the association with proteins: for the same sulfation pattern, the binding affinity was higher for the derivative with lower molecular weight.

Derivatives **SD-5,7** were also subjected to SPR investigations to evaluate their interaction with TGF-β1, BMP-2, VEGF and FGF-2 growth factors. The binding affinity between diabolican derivative **SD-5** and TGF-β1 and BMP-2 was only slightly decreased in comparison with per-*O*-sulfated derivative **SD-2** (Table 2.3). Conversely, a much stronger binding was measured for FGF-2, not only with respect to **SD-2** but also to heparin (Ibrahimi et al. **2004**). Derivatives **SD-6,7**, showed similar binding affinities in comparison to **SD-5** as regards the interaction with TGF-β1, BMP-2 and VEGF, while their interaction with FGF-2 was considerably decreased (Table 2.4).

	***Kd (M)* TGF-β1**	***Kd (M)* BMP-2**	***Kd (M)* VEGF**	***Kd (M)* FGF-2**
LMW diabolican	$9.1\ 10^{-8}$	$3.5\ 10^{-8}$	$1.7\ 10^{-8}$	$4.0\ 10^{-8}$
SD-5	$3.4\ 10^{-9}$	$2.3\ 10^{-9}$	$2.9\ 10^{-8}$	$9.6\ 10^{-10}$
SD-6	$3.1\ 10^{-9}$	$5.8\ 10^{-9}$	$4.1\ 10^{-8}$	$>10^{-5}$
SD-7	$2.2\ 10^{-9}$	$4.2\ 10^{-9}$	$1.3\ 10^{-8}$	$4.6\ 10^{-8}$

Table 2.4. Dissociation constant (K_d) values showing the binding affinity between LMW diabolican and its sulfated derivatives and growth factors.

2.1.3. Conclusions

In this section, the study of the regioselective sulfation of LMW diabolican EPS from *V. diabolicus* bacterium was carried out. Both direct methods and multi-step strategies were investigated to have access to new sulfated compounds with DS ranging from 1.5 to 8. Several sulfation patterns were achieved, with molecular weights ranging from 5 to 40 kDa. Then the binding affinity for some growth factors was measured. The resulting structure-affinity correlation revealed that the installation of sulfate groups within diabolican backbone is generally able to increase the binding strength. Noteworthy, within this frame some sulfation sites seemed to be much more effective than others to trigger the protein-polysaccharide interaction, at least with the FGF-2 growth factor (derivative **SD-5**). This result suggested that the sulfation pattern could be a key structural element for the selective interaction with signalling proteins not only in the case of native GAGs, as already known, but also for GAG-like structures obtained by regioselective sulfation of naturally unsulfated polysaccharides. However, more details about the interaction between growth factors and sulfated diabolican derivatives will be investigated in a near future through several other techniques.

2.1.4. Experimental section

General methods. Commercial grade reagents and solvents (HPLC-grade pure, including water) were used without further purification, except where differently indicated. Dialyses were conducted on Spectra/Por 3.5 kDa cut-off membranes at 4°C. Centrifugations were performed with an Eppendorf (Hamburg, Germany) Centrifuge 5804R instrument at 4°C (4600 g, 5 min). Freeze-dryings were performed with a 5Pascal (Trezzano sul Naviglio, Italy) Lio 5P 4K freeze dryer. Elemental analyses were performed on a ThermoFisher Scientific (Waltham, MA, USA) Flash Smart V CHNS/CHNS instrument, using sulfanilamide as calibration standard.

The weight-average (M_w) and number-average (M_n) molecular weights were determined using high-performance size-exclusion chromatography (HP-SEC) coupled with a multi-angle laser light scattering detector (MALLS, Dawn Heleos-II, Wyatt Technology, Santa Barbara, CA, USA) and a differential refractive index (RI) detector (Optilab Wyatt technology, Santa Barbara, CA, USA). HP-SEC system was composed of an HPLC system Prominence (Shimadzu, Kyoto, Japan), a PL aquagel-OH MIXED, 8 µm guard column (7.5 × 50 mm, Agilent Technologies, Santa Clara, CA, USA), and a PL aquagel-OH MIXED separation column (7.5 × 300 mm, Agilent Technologies, Santa Clara, CA, USA). Samples (in duplicate) were eluted with aqueous 0.1 M NH_4OAc at 1 mL/min flow rate. Molecular weights were calculated using a refractive index increment characteristic of polysaccharides (dn/dc = 0.145 mL/g) and taking into consideration the typical variability of such value among unsulfated and differently sulfated polysaccharides (dn/dc = 0.140-0.160 mL/g) in the error bar.

NMR spectra were recorded on a Bruker (Billerica, MA, USA) Avance-III HD (^{1}H: 400 MHz, ^{13}C: 100 MHz) or on a Bruker Avance-III (^{1}H: 600 MHz, ^{13}C: 150 MHz) instrument – the latter equipped with a cryo-probe – in D_2O (acetone as internal standard, ^{1}H: $(CH_3)_2CO$ at δ 2.22 ppm; ^{13}C:$(CH_3)_2CO$ at δ 31.5 ppm) or DMSO-*d*$_6$ (^{1}H: CHD_2SOCD_3 at δ 2.49 ppm; ^{13}C: CD_3SOCD_3 at δ 39.5 ppm). Data were processed using the data analysis packages integrated with Bruker TopSpin® 4.0.5 software. Gradient-selected COSY, TOCSY and NOESY experiments were performed using spectral widths of 6000 Hz in both dimensions, using data sets of 2048 × 256 points. TOCSY mixing time was set to 120 ms. ^{1}H,^{13}C-DEPT-HSQC and ^{1}H,^{13}C-HSQC-TOCSY experiments were measured in the ^{1}H-detected mode via single quantum coherence with proton decoupling in the ^{13}C domain, using data sets of 2048 × 256 points and typically 100 increments. The mixing time for ^{1}H,^{13}C-HSQC-TOCSY was set to 120 ms.

Transforming Growth Factor-β1 (TGF-β1), Bone Morphogenetic Protein-2 (BMP-2), Vascular Endothelial Growth Factor ($VEGF_{165}$) and Fibroblast Growth Factor-2 (FGF-

2_{146}) from PeproTech (ThermoFisher Scientific, Waltham, MA, USA) were covalently immobilized (3400-4800 RU) to the dextran matrix of a CM5 sensor chip (Cytiva, Washington, DC, USA) by amine coupling, as recommended by the manufacturer at a flow rate of 5 µL/min. Binding assays of diabolican derivatives were performed in 10 mM HEPES at pH 7.4 containing 150 mM NaCl and 0.005% P20 surfactant (HBS-P buffer, Cytiva, Washington, DC, USA) by one-cycle kinetic titration. Five increasing concentrations (12 – 37 – 111 - 333 – 1000 nM) were injected (injection time =180s) at 30 µL/min. After a dissociation time of 600 s coated surface was regenerated using 4.5 mM NaOH. All the sensorgrams were corrected by subtracting the low signal from the control reference surface and buffer blank injections. From the resulting sensorgrams, KD were evaluated using a bivalent fitting model from T200 evaluation software (Cytiva, Washington, DC, USA).

Production of the native diabolican EPS. V. diabolicus was cultured at 25°C in Marine Broth 2216 medium at pH 7.2 in a 2L fermenter. Glucose at 30 g/L was added as a carbon source. After 48 h of fermentation, the culture medium was centrifuged at 9000 g for 45 min, the supernatant containing soluble EPS was ultrafiltrated on a 100 kDa cut-off membrane and freeze-dried.

LMW diabolican EPS. The native EPS (2.5 g) solubilized in pure water (350 mL) was depolymerized at 60°C for 45 min using H_2O_2 added dropwise (530 µL at 30%) in the presence of copper (II) acetate ($Cu(OAc)_2$, 18 mg), used as catalyst. After overnight reduction by sodium borohydride ($NaBH_4$) at rt and purification on Chelex® 20 resin, the solution containing depolymerized EPS was ultrafiltrated on a 10 kDa cut-off membrane and freeze-dried. To obtain a homogeneous fraction with low dispersity, a predominant population of the polysaccharide chains was selected by a gel filtration chromatography on Superdex® 30, using an AKTA FPLC system coupled with a refractometric detector. Samples eluted with pure water were pooled and freeze-dried.

Polysaccharide ***SD-1.*** LMW diabolican EPS (33.9 mg, 34.4 μmol repeating unit) was dissolved in pure water (750 μL) and passed through a short Dowex 50 WX8 column (H^+ form, 20-50 mesh, approx. 4 cm^3). Elution with deionized water was continued until a neutral pH of the eluate was detected. The eluted fraction was then neutralized with some drops of an aqueous solution of tetrabutylammonium hydroxide (16% w/v TBAOH in H_2O). After freeze-drying, polysaccharide **1** (43.8 mg, 129% mass yield) was obtained as a white waxy solid. A suspension of **1** (41.2 mg, 33.2 μmol repeating unit) in dry DMF (2.5 mL) was then treated with a 0.40 M solution of pyridine-sulfur trioxide complex (SO_3·py) in dry *N,N*-dimethylformamide (DMF, 550 μL, 199 μmol). After 1 h stirring at 4 °C, some drops of aqueous 1 M $NaHCO_3$ were added to adjust pH to 7 and then aqueous 0.3 M NaCl (5 mL) was added. The mixture was stirred for 1 h at rt, then dialyzed and freeze-dried. The obtained product was dissolved in pure water and passed through a short Dowex 50 WX8 column (H^+ form, 20-50 mesh, approx. 4 cm^3), continuing the elution with pure water until a neutral pH of the eluate was detected. The eluted solution was adjusted to pH 10 with aqueous 1 M NaOH(aq), then dialyzed and freeze-dried to afford **SD-1** (15.9 mg, 39% mass yield) as a white solid.

Polysaccharide ***SD-2****.* LMW diabolican EPS (50.0 mg, 50.7 μmol repeating unit) was dissolved in pure water (5 mL) and passed through a Dowex 50 WX8 column (H^+ form, 20-50 mesh, approx. 8 cm^3). After elution with pure water, the fraction was neutralized with pyridine added dropwise. After freeze-drying, LMW diabolican EPS pyridinium salt **2** was firstly solubilized in dry DMF (25 mL) at 45°C for 2 h under continuous stirring and then sulfated for the next 2 h at 45°C in the presence of SO_3.py (250 mg, 1.57 mmol). Some drops of aqueous $NaHCO_3$ were then added to adjust pH to 7. The mixture was then dialyzed against pure water for three days prior to be freeze-dried to afford **SD-2** (101.8 mg, 204% mass overall yield) as a white solid.

*Polysaccharide **SD-3***. Per-*O*-sulfated derivative **SD-2** (18.8 mg, 9.13 μmol repeating unit) was dissolved in pure water (1.0 mL) and passed through a short Dowex-50 WX8 column (H^+ form, 20–50 mesh, approx. 4 cm^3). Elution with pure water was continued until pH of the eluate was neutral. The obtained eluate was treated with some drops of pyridine to neutralize the solution. Freeze-drying of the collected eluate gave per-*O*-sulfated pyridinium salt **3**, that was in turn suspended in pyridine (1.7 mL) and treated with *N*-methyl-*N*-(trimethylsilyl)-trifluoroacetamide for a 6-*O*-desulfation in order to convert the released hydroxyl groups into trimethylsilyl ethers (MTSTFA, 31 μL, 0.16 mmol). After 20 h stirring at 70°C, the mixture was cooled to rt, then pure water (3 mL) was added giving a turbid mixture that was dialyzed for one day. Thereafter, the mixture was passed through a short Dowex-50 WX8 column (H^+ form, 20–50 mesh, approx. 4 cm^3), continuing the elution with pure water until a neutral pH of the eluate was reached. Then some drops of aqueous 1 M NaOH were added to neutralize the solution. Dialysis and subsequent freeze-drying gave **SD-3** (12.2 mg, 65% mass overall yield) as a white solid.

*Polysaccharides **4-i,iv***. LMW diabolican EPS (40.5 mg, 50.5 μmol repeating unit) was dissolved in hydrazine monohydrate ($N_2H_4 \cdot H_2O$, 64-65% hydrazine in water, 1.0 mL), then hydrazine sulfate salt ($N_2H_4 \cdot H_2SO_4$, 10.0 mg, 76.8 μmol) was added. The suspension was flushed under Ar atmosphere and heated at 90 °C. At different times (10, 20, 30 and 40 hours), 250 μL aliquots were collected, cooled to rt and treated with ethanol (1.0 mL) and a few drops of brine. The mixtures were dialyzed and freeze-dried. The sample obtained from a 20 hours *N*-deacetylation reaction was named as **4-ii** and employed for further reaction to polysaccharide **SD-4**.

*Polysaccharide **SD-4.*** Polysaccharide **4-ii** (15.6 mg, 19.3 μmol repeating unit) was dissolved in pure water (3.9 mL) and treated with Na_2CO_3 (25.0 mg, 23.6 μmol) and trimethylamine-sulfur trioxide complex ($SO_3 \cdot Me_3N$, 25.0 mg, 18.0 μmol) and heated at 45°C. After 4 h stirring, a second aliquot of $SO_3 \cdot Me_3N$ (25.0 mg, 18.0 μmol) was

added to the solution. After 20 h stirring at 45°C, the obtained solution was cooled to rt, dialyzed and freeze-dried to yield **SD-4** (12.4 mg, 79% mass yield) as a white solid.

*Derivative **5-ii***. LMW diabolican TBA salt (27.3 mg) was suspended in dry methanol (3.5 mL) and then treated with a 2.0 M solution (0.7 mL) of (trimethylsilyl)diazomethane ($TMSCHN_2$) in diethyl ether (Et_2O). After 2 hours stirring at room temperature, a second aliquot (0.7 mL) of the $TMSCHN_2$ solution was added. After further 2 hours stirring, the yellow reaction mixture was treated with diisopropyl ether (20 mL) to afford a white precipitate that was collected by centrifugation and dried under vacuum to give derivative **5-ii** (11.6 mg, 42% weight yield).

*Derivatives **6-i,iii***. Derivative **5-i** (20.8 mg) (or **5-ii** for the semi-synthesis of **6-iii**) was suspended in dry DMF (0.8 mL) and then treated with triisopropylsilyl chloride (TIPSCl, 15.8 mg) or *t*-butyl-dimethylsilyl chloride (TBDMSCl, 12.5 mg) and imidazole (16.3 mg). The reaction mixture was stirred overnight at 50°C. Thereafter, it was cooled to room temperature and treated with diisopropyl ether (*i*-Pr_2O, 3.5 mL). The obtained precipitate was collected by centrifugation and dried under vacuum to give derivative **6-i** (16.1 mg, 77% weight yield) or **6-ii** (30.8 mg, 148% weight yield) or **6-iii** (14.5 mg, 70% weight yield).

*Derivatives **7**-**8***. LMW diabolican (20.5 mg) was dissolved in water (1.0 mL) and passed through a short Dowex 50 WX8 column (H^+ form, 20–50 mesh, approx. 4 cm^3). Elution with water was continued until a neutral pH of the eluate was detected. The eluted fraction was freeze-dried to give a white solid (20.5 mg), that was stirred at 80 °C for 1 hour in dry DMF (1.0 mL) to give a homogeneous solution. This was then treated at room temperature with anisaldehyde dimethyl acetal (*p*-OMe-$PhCH(OCH_3)_2$, 45 μL), that was dried over freshly activated AW-300 4Å molecular sieves. A freshly prepared 0.87 M solution of (+)-camphor-10-sulfonic acid (CSA) in

dry DMF (7.3 μL) was then added and the reaction mixture was heated at 80 °C. After overnight stirring, it was cooled to room temperature and, for the semi-synthesis of **7**, treated with diisopropyl ether (5 mL) to give a yellowish precipitate. The mixture was stored at −28 °C for some hours, then the solid was collected by centrifugation and dried under vacuum to afford derivative **7** (26.6 mg, 130% weight yield).
Conversely, for the semi-synthesis of **8**, after overnight stirring at 80°C and cooling to rt, the reaction mixture was one-pot treated with a 2:1 v/v CH_3CN-DMF mixture (750 μL) and then triethylamine (Et_3N, 74 μL), acetic anhydride (Ac_2O, 100 μL) and 4-dimethylaminopyridine (DMAP, 1.2 mg) were consecutively added. After overnight stirring at 50°C, the reaction mixture was cooled to room temperature and then treated with *i*-Pr_2O (10 mL) to afford a brownish precipitate. The mixture was stored at −28 °C for some hours, then the solid was collected by centrifugation and dried under vacuum to afford derivative **8** (25.5 mg), that was dissolved in a 9:1 v/v mixture (1.0 mL) of acetic acid (AcOH) and water and stirred at 50°C for 48 hours. The reaction mixture was then cooled to room temperature, diluted with water (3.0 mL), dialyzed and freeze-dried to afford derivative **9** (18.7 mg, 91% weight yield from LMW diabolican).

*Derivative **11***. LMW diabolican TBA salt (25.2 mg) was stirred under an argon atmosphere at 85 °C for 1 hour in dry DMF (1.0 mL) to give a homogeneous solution, that was then cooled to room temperature, treated with benzoic anhydride (Bz_2O, 138 mg) and then heated to 85°C. After 24 hours stirring, the solution was cooled to room temperature and treated with dry pyridine (870 μL) and 4-dimethylaminopyridine (DMAP, 5.0 mg). The yellowish solution was stirred for 68 hours and then treated with methanol (870 μL) and sodium acetate (NaOAc, 2.5 mg). After 26 h stirring at room temperature, the reaction mixture was diluted with methanol (2.4 mL) and then concentrated by rotoevaporation to approximately 2 mL in volume. Cold *i*-Pr_2O (5 mL) was added to the residue, to give a slightly yellow precipitate. The mixture was

stored at −28 °C for some hours, then the solid was collected by centrifugation and dried under vacuum to afford derivative **11** (32.0 mg, 127% weight yield).

*Polysaccharides **SD-5-7***. Compound **7** (24.1 mg) (or **9** or **11** for the semi-synthesis of **SD-6** or **SD-7**, respectively) was stirred for few minutes at 50 °C in dry DMF (675 mL) to give a yellowish, homogeneous solution, that was then cooled to room temperature and treated with a 0.42 M solution of SO_3·py in dry DMF (1.3 mL). After overnight stirring at 50 °C, a cold, saturated NaCl solution in acetone (7 mL) was added at room temperature and the mixture was then stored at -28 °C for some hours to give a precipitate, that was collected by centrifugation and then dissolved in pure water (2.0 mL). For the semi-synthesis of **SD-5**, the resulting acid mixture (pH ~ 2) was heated to 50 °C and stirred for 2 hours. Thereafter, the mixture was cooled to room temperature and neutralized with a 33% w/v NaOH aqueous solution. After dialysis and freeze-drying, sulfated polysaccharide **SD-5** (24.6 mg, 102% weight yield) was obtained as a slightly yellow solid, that was further purified for biological assays by consecutive filtration on two C-18 silica gel cartridges.
For the semi-synthesis of **SD-6,7**, the acid mixture resulting after suspending the sulfated precipitate in water, was directly treated with a 33% w/v NaOH aqueous solution to alkaline pH (≥ 12). After overnight stirring at room temperature, the resulting homogeneous solution was neutralized with 1M HCl, dialyzed and freeze-dried to afford **SD-6,7**. Their further purification was performed as described above for derivative **SD-5**.

Degree of sulfation. For the evaluation of the DS by CHNS elemental analysis, **SD-5-7** samples (~2-3 mg) were weighted and mixed in a tin capsule with V_2O_5 as oxidizer. They were then combusted in a furnace with the following set of parameters: temperature furnace = 950 °C, temperature oven = 65 °C, He carrier flow = 140 mL/min, O_2 flow = 250 mL/min flow, oxygen injection end = 3 s, sampling delay time = 12 s, run time = 720 s. Experiments were performed for each sample in duplicate.

DS values were calculated according to Eq. (2.1) (m_C = atomic mass carbon, m_S = atomic mass sulfur, n_C = number of carbon atoms per repeating unit).

$$DS = [(\%S \times m_C \times n_C)/(\%C \times m_S)] \qquad \text{Eq. (2.1)}$$

References

Bachelder, E.M., Pino, E.N., Ainslie, K.M., **2017**. *Chem. Rev. 117*, 1915–1926.

Bedini, E., Laezza, A., Parrilli, M., & Iadonisi, A., **2017**. *Carbohydr. Polym. 174*, 1224–1239.

Benhadda, F., Zykwinska, A., Colliec-Jouault, S., Sinquin, C., Thollas, B., Courtois, A., Fuzzati, N., Toribio, A., Delbarre-Ladrat, C., **2023.** *Mar. Drugs 21,* 582.

Bramhachari, P. V., Kavi Kishor, P.B., Ramadevi, R., Kumar, R., Rama Rao, B., Dubey, S.K., **2007**. *J. Microbiol. Biotechnol. 17*, 44–51.

Casillo, A., Lanzetta, R., Parrilli, M., Corsaro, M.M., **2018**. *Mar. Drugs 16*, 69–103.

Decho, A.W., **1990**. *Oceanogr. Mar. Biol.* 28, 73–153.

Drouillard, S., Jeacomine, I., Buon, L., Boisset, C., Courtois, A., Thollas, B., Morvan, P.Y., Vallée, R., Helbert, W., **2015**. *Mar. Drugs 13*, 6723–6739.

Esposito, F., Vessella, G., Sinquin, C., Traboni, S., Iadonisi, A., Colliec-Jouault, S., Zykwinska, A., Bedini, E., **2022**. *Carbohydr. Polym. 283,* 119054.

Finore, I., Di Donato, P., Mastascusa, V., Nicolaus, B., Poli, A., **2014**. *Mar. Drugs 12*, 3005–3024.

Fonseca, R.J.C., Oliveira, S.N.M.C.G., Pomin, V.H., Mecawi, A.S., Araujo, I.G., Mourão, P.A.S., **2010**. *Thromb. Haemostasis 103*, 994–1004.

Gandhi, N. S., & Mancera, R. L., **2008**. *Chem. Biol. Drug Des. 72*, 455–482

Gandhi, N.S., Mancera, R.L., **2008**. *Chem. Biol. Drug Des. 72*, 455–482.

Gomez D'Ayala, G., Malinconico, M., Laurienzo, P., **2008**. *Molecules 13*, 2069–2106.

Guo, Y., & Conrad, H.E., **1989**. *Anal. Biochem. 176*, 96–104.

Ibrahimi, O.A., Zhang, F.M., Hrstka, M. Mohammadi, S.C.L., Linhardt, R.J., **2004.** *Biochemistry 43*, 4724–4730.

Jiang, P., Li, J., Han, F., Duan, G., Lu, X., Gu, Y., Yu, W., **2011**. *PLoS One 6*, e18514.

Koschella, A., Klemm, D., **1997**. *Macromol. Symp. 120,* 115−125.

Köwitsch, A., Zhou, G., & Groth, T., **2018**. *J. Tissue Eng. Regen. Med. 12*, e23–e41.

Laezza, A., De Castro, C., Parrilli, M., Bedini, E., **2014.** *Carbohydr. Polym. 112*, 546–555.

Li, G., Cai, C., Li, L., Fu, L., Chang, Y., Zhang, F., Toida, T., Xue, C., & Linhardt, R.J., **2014**. *Anal. Chem. 86*, 326–330.

Mans, D.J., Ye, H., Dunn, J.D., Kolinski, R.E., Long, D.S., Phatak, N.L., Ghasriani, H., Buhse, L.F., Kauffman, J.F., & Keire, D.A., **2015**. *Anal. Biochem*. *490*, 52–54.

Nadkarni, V.D., Toida, T., Van Gorp, C.L., Schubert, R.L., Weiler, J.M., Hansen, K.P., Caldwell, E.E.O., & Linhardt, R.J., **1996**. *Carbohydr. Res. 290*, 87–96.

Netrusov, A.I.; Liyaskina, E.V.; Kurgaeva, I.V.; Liyaskina, A.U.; Yang, G.; Revin, V.V., **2023**. *Microorganisms 11*, 1541.

Raguénès, G., Christen, R., Guezennec, J., Pignet, P., Barbier, G., **1997**. *Int. J. Syst. Bacteriol. 47*, 989–995.

Rougeaux, H., Kervarec, N., Pichon, R., & Guezennec, J., **1999**. *Carbohydr. Res. 322*, 40–45.

Senni, K., Gueniche, F., Changotade, S., Septier, D., Sinquin, C., Ratiskol, J., Lutomski, D., Godeau, G., Guezennec, J., Colliec-Jouault, S., **2013**. *Mar. Drugs 11*, 1351–1369.

Senni, K., Gueniche, F., Fioretti, F., Godeau, G.J., Colliec-Jouault, S., Ratiskol, J., Sinquin, C., Raguénès, G., Courtois, J., Guézennec, J., **2015**. Sulfated depolymerized

derivatives of exopolysaccharides from mesophilic marine bacteria, method for preparing same, and uses thereof in tissue regeneration. US 9,125,883.

Takano, R., Kanda, T., Hayashi, K., Yoshida, K., & Hara, S., **1995**. *J. Carbohydr. Chem. 14*, 885–888.

Vallet, S.D., Berthollier, C., Ricard-Blum, S., **2022**. *Am. J. Physiol. Cell Physiol. 322*, 1271–1278.

Veraldi, N., Dentand Quadri, I., van de Looij, Y., Malaguti Modernell, L., Sinquin, C., Zykwinska, A., Tournier, B.B., Dalonneau, F., Li, H., Li, J.-P., Millet, P., Vives, R., Colliec-Jouault, S., de Agostini, A., Farias Sanches, E., Sizonenko, S. V., **2023**. *Carbohydr. Polym. 320*, 121214.

Vessella, G., Esposito, F., Traboni, S., Di Meo, C., Iadonisi, A., Schiraldi, C., Bedini, E., **2021**. *Carbohydr. Polym. 269*, 118324.

Vessella, G., Traboni, S., Cimini, D., Iadonisi, A., Schiraldi, C., Bedini, E., **2019**. *Biomacromolecules 20*, 3021−3030.

Yan, L., Li, J., Wang, D., Ding, T., Hu, Y., Ye, X., Linhardt, R.J. & Chen, S., **2017**. *Carbohydr. Polym. 178*, 180–189.

Zhao, L., Lai, S., Huang, R., Wu, M., Gao, N., Xu, L., Qin, H., Peng, W., & Zhao, J., **2013**. *Carbohydr. Polym. 98*, 1514–152

SECTION 2.2 - REGIOSELECTIVE SULFATION OF ALGINATE POLYSACCHARIDES FROM BROWN ALGAE

2.2
REGIOSELECTIVE SULFATION OF ALGINATE POLYSACCHARIDES FROM BROWN ALGAE

2.2.1. Alginates: structure and activities

Alginates are polysaccharides quite widespread in nature, composed of β-1-4-linked D-mannuronic acid (ManA, M) and its *C*-5 epimer L-guluronic acid (GulA, G) units. These residues are distributed along the polysaccharide chain in a block-copolymer fashion with homopolymeric regions composed of M-blocks and G-blocks, respectively, and heteropolymeric ones with MG alternating structures (MG-blocks) or more complex sequences (*e.g.* GGM- and MMG-) (Aarstad et al., **2012**) (Figure 2.21).

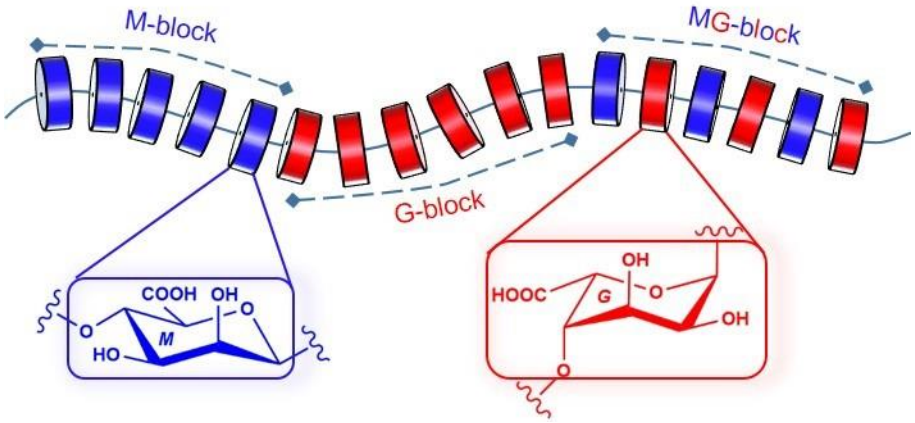

Figure 2.21. Schematic representation of the chemical structure of alginate polysaccharides

Alginates are present both in marine brown algae as structural components and in soil bacteria as capsular polysaccharides. Thanks to their properties (*e.g.* viscosity enhancement, gel-forming ability, stabilization of aqueous mixtures, dispersions, and emulsions, as well as encapsulation of drugs and cells), they have several employments in food, pharmaceutical and textile industry (Draget et. al, **2006**). Apart the already established applications for alginates, also several others are currently under development (Lee and Mooney, **2012**; Szekalska et al., **2016**)

The amount of alginate biosynthesized annually in algae is estimated to be at least ten times higher than the amount produced and employed by industry in the same time period. This large availability has pushed the investigation of the possibility to obtain structurally modified alginate derivatives as novel, sustainable materials with enhanced properties with respect to the native polysaccharide or completely new ones. Several kinds of transformations have been reported to this aim (Fernando et al., **2019**; Pawar and Edgar, **2012**; Yang et al., **2011**). Among them, one of the most investigated is the installation of sulfate groups on alginate backbone (Arlov and Skjåk-Bræk, **2017**). Sulfated alginates (ASs), as well as several other artificially sulfated polysaccharides (Arlov et al., **2021**; Caputo et al., **2019**; Wang et al., **2018**; Zeng et al., **2019**), show interesting anti-coagulant, anti-inflammatory and wound dressing activities, often associated with unique characteristics with respect to GAGs. Furthermore, ASs can be produced from renewable, largely available raw materials, thus standing as a more environmentally and economically sustainable alternative to GAGs. Notably, a low molecular weight alginate sulfated derivative (propylene glycol alginate sodium sulfate, PSS) has been used for more than 30 years in China as a heparin-like drug for the treatment of cardiovascular diseases. Nonetheless, a not negligible number of adverse effects has been recorded during the clinical application of PSS (Xue et al., **2016**). The M/G ratio is known to play an important role in both anticoagulant and side effects of PSS (Wu et al., **2014**), but the key factors for SAR studies, not only for PSS but also for alginate sulfate species as well as for sulfated polysaccharides in general, are the DS and the sulfation pattern (Freeman et al., **2008**).

In semi-synthetic sulfated polysaccharides, the former parameter can be often controlled through stoichiometry, while the latter requires, as discussed above, the development of chemical or enzymatic methods for the regioselective insertion of sulfate groups exclusively on determined positions. This goal has been achieved for several polysaccharides up to now, while, to the best of our knowledge, such result is still missing for any alginate sulfate derivative (Bedini et al., **2017**). Indeed, a quite good control of DS on alginates with homogeneous monosaccharide sequences (poly-M, poly-G and poly-MG) could be gained (Arlov et al., **2014**), whereas no control of sulfation pattern — neither between nor within M and G units (*i.e.* M- *vs.* G-, and *O*-2 *vs. O*-3, respectively) — has been reported. Only a slight preference for sulfation of M- over G-units and of *O*-3 over *O*-2 positions has been observed, anyway in the context of an undoubtedly random sulfation pattern (Cong et al., **2014**).

To this aim, the semi-synthesis of a new set of ASs derivatives with a homogeneous and well defined sulfation pattern has been attempted in order to shed new light on the molecular details of alginate sulfate properties and applications particularly in biomedical field. For this purpose, commercially available M-rich and G-rich alginic acids, containing a 83% and 87% amount of M- and G-units, respectively, and a non-G/M-enriched species, composed of an approximately equal amount of M and G residues, have been selected.

2.2.2. Results and discussion

In this section, different protecting groups have been tested to open for the first time an access to regioselectively sulfated derivatives of commercially available M-rich and G-rich alginic acids as well as of a non-G/M-enriched species. In particular, both 2-*O*- and 3-*O*- selectively protected polysaccharide derivatives have been pursued, in order to obtain AS products differently sulfated at 3-*O*- or 2-*O*-positions, respectively. The first investigations have been carried out on a commercial M-rich derivative.

Firstly, a direct regioselective protection was performed using acyclic protecting groups such as trialkylsilyl ethers or benzoyl esters (Figure 2.22).

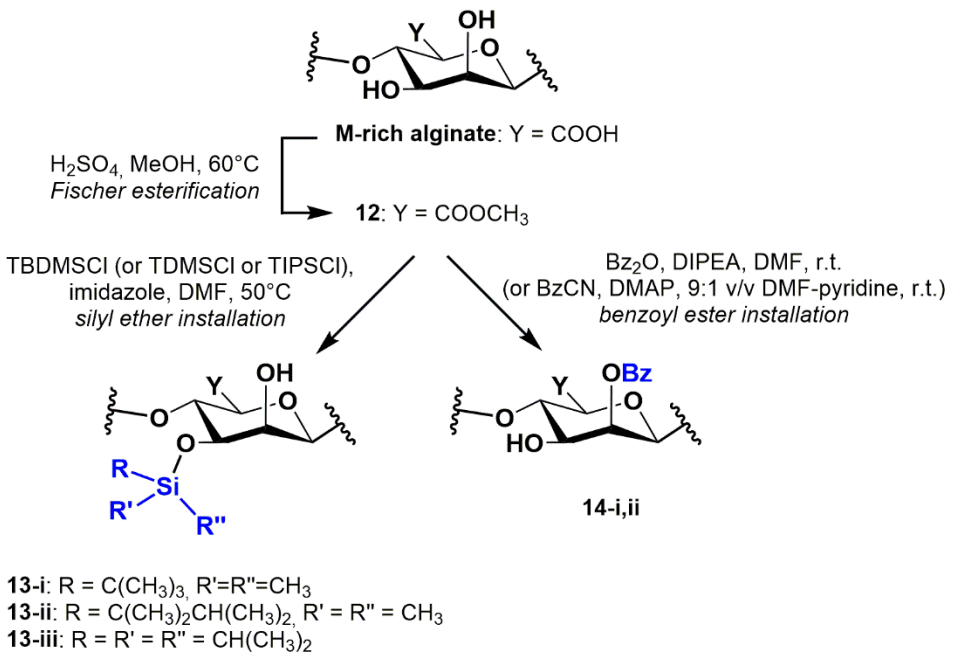

Figure 2.22. 2-*O* vs 3-*O* sites protection strategies through acyclic PGs on M-rich alginate

Regioselective protection of the equatorial hydroxyl at 3-*O*-positions was first attempted by screening medium-size trialkylsilyl ether protecting groups (*t*-butyl-dimethylsilyl, TBDMS; thexyldimethylsilyl, TDMS; triisopropylsilyl, TIPS). The typical use of a slightly basic compound such as imidazole, in combination with trialkylsilyl chlorides for hydroxyl silylation, suggested to perform the protection reaction not on M-rich alginic acid itself but on its methyl ester derivative **12**, that could be obtained by treatment with H_2SO_4 in dry methanol at 60°C (Sanchez-Ballester et al., **2020**).

Typical signals for TBDMS and TIPS ether groups could be detected at δ 0.8-0.0 and 1.0 ppm, respectively, in the ^{1}H-NMR spectra of derivatives **13-i** and **13-iii**, while no

significant signals related to TDMS ethers could be found in the ^{1}H-NMR spectrum of **13-ii**, that was therefore not considered further (Figure 2.23).

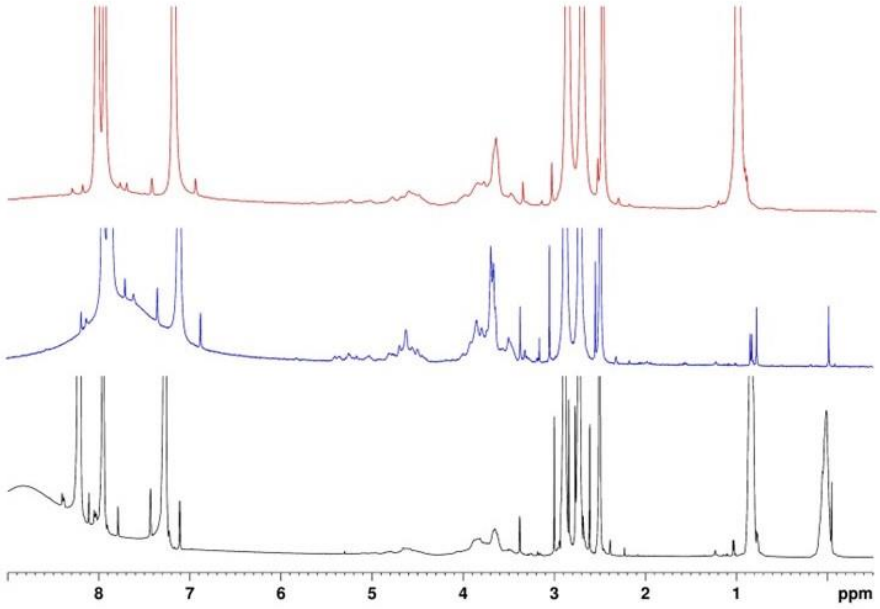

Figure 2.23. ^{1}H NMR spectra (zoom, 600 MHz, 298 K, DMSO-*d6*) of **13-i** (black), **13-ii** (blue), **13-iii** (red)

Regioselective protection of the axial hydroxyl at 2-*O*-positions was performed using two different methods reported for the installation of benzoyl (Bz) esters preferentially on the axial position of *cis*-1,2-diols in pyranosides. They combine either Bz_2O and DIPEA (Ren et al., **2018**) or BzCN and DMAP (Peng et al., **2016**). These procedures were adapted to our polysaccharide case, giving derivatives **14-i,ii** from **12**, both showing ^{1}H-NMR spectra with characteristic signals for benzoylated species in the aromatic region and at chemical shifts between δ 4.8 and 5.5 ppm (Figure 2.24).

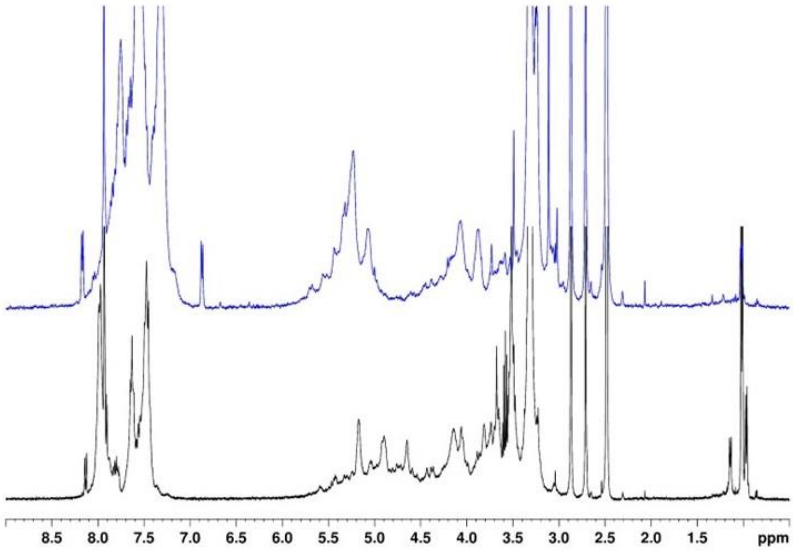

Figure 2.24 ^{1}H NMR spectra (zoom, 600 MHz, 298 K, DMSO-*d6*) of **14-i** (black), **14-ii** (blue)

Derivatives **13-i,ii** and **14-i,ii** were subjected to sulfation under standard conditions (Bedini et al., **2017**) with $SO_3 \cdot py$ in DMF at 50°C, followed by a global deprotection under aqueous, slightly acid conditions to remove acid-labile TBDMS and TIPS ethers and then by an alkaline treatment to hydrolyze methyl and benzoate esters affording derivatives **AS-1,4** (Figure 2.25).

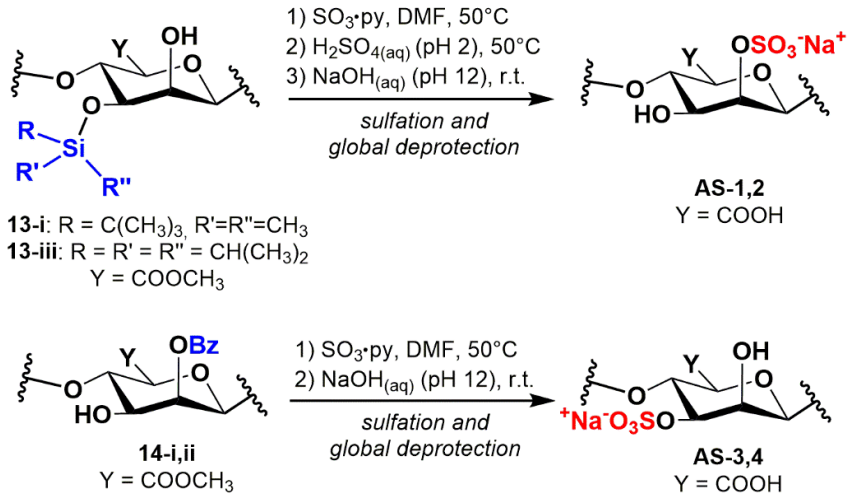

Figure 2.25. Sulfation and global deprotection steps to derivatives **AS-1,4**

Derivatives **AS-1,4** were structurally characterized by a complete set of ^{1}H and 2D-NMR spectra. Firstly, as regards compound **AS-1** the superimposition of $^{1}H,^{13}C$-HSQC and $^{1}H,^{13}C$-HMBC spectra (Figure 2.26) allowed the assignment of two groups of CH signals in the $^{1}H,^{13}C$-HSQC spectrum to M-2 positions, at $\delta_{H/C}$ 3.98/71.4 and 4.35-4.23/70.0-70.6 ppm respectively, from their HMBC correlation with anomeric CH signals. By comparison with the $^{1}H,^{13}C$-HSQC spectrum of starting M-rich alginic acid, the *CH*-2 signal at $\delta_{H/C}$ 3.98/71.4 could be assigned to unsulfated M units. The downfield shift of *CH*-2 signal at $\delta_{H/C}$ 4.35-4.23/70.0-70.6 ppm was due to the presence of a sulfate group at *O*-2 site. Moreover, the most ^{1}H-downfield shifted signal in the $^{1}H,^{13}C$-HSQC spectrum at $\delta_{H/C}$ 4.96/77.1 ppm was indicative for the presence of additional sulfate groups at position 3 of some M units. The discrimination between M3S and 2,3-disulfated (M2S3S) units was possible on the basis of the presence or the absence, respectively, of the typical signal for M3S *CH*-3 atoms at $\delta_{H/C}$ 4.73/79.3 ppm. Therefore, the contemporary presence of unsulfated M, M2S and M2S3S along the polysaccharide chain could be inferred for **AS-1**.

The relative integration of the well-resolved *CH*-4 signal volumes at $\delta_{H/C}$ 3.84/78.9, 4.03/74.9 and 4.47/77.1 ppm in the $^{1}H,^{13}C$-DEPT-HSQC spectrum, that could be

assigned to M, M2S and M2S3S units respectively, allowed to estimate a 20%:60%:20% ratio for M, M2S and M2S3S residues in **AS-1**. The relative M:M2S:M2S3S ratio estimated by 2D-NMR analysis returned a DS equal to 1.0 for **AS-1.**

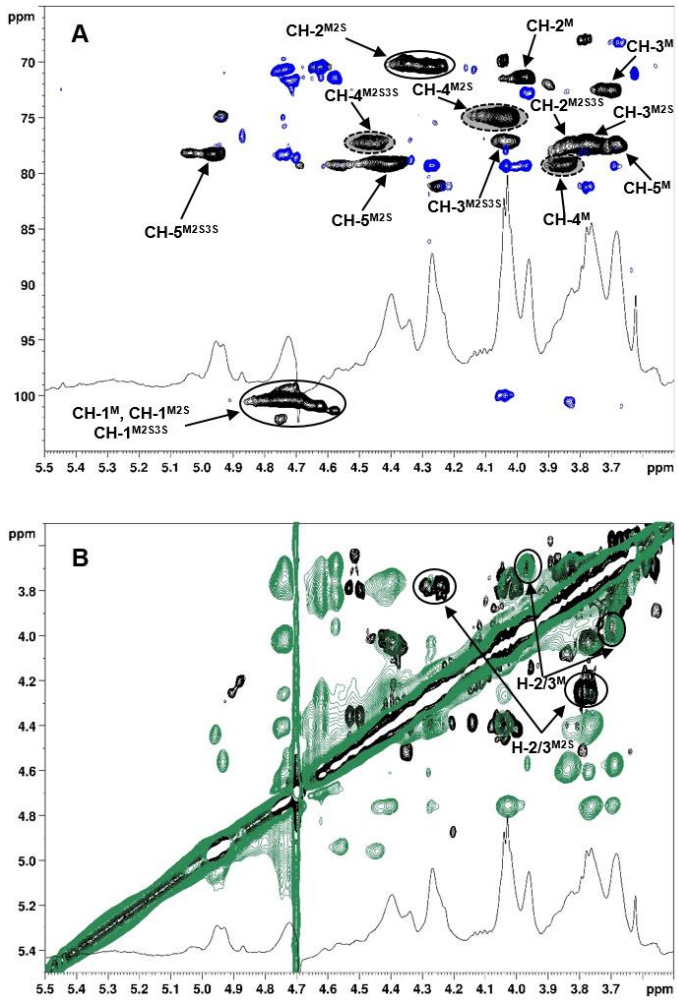

Figure 2.26. Superimposition of zoomed (A) ^{1}H-NMR, ^{1}H,^{13}C-HSQC (black) and ^{1}H,^{13}C-HMBC (blue) 2D-NMR (densities enclosed in dotted lines were integrated for DS estimation) and (B) ^{1}H-NMR, COSY (black) and NOESY (green) 2D-NMR spectra (600 MHz, 298K, D_2O) of **AS-1** (only some correlations are indicated).

A similar analysis of 2D-NMR spectra was conducted on derivative **AS-2** revealing the presence of a lower relative amount of the target M2S residues (52%) with respect to **AS-1** and a higher amount of M2S3S units (32%). Therefore, a slightly higher regioselectivity could be inferred for the semi-synthetic strategy to a 2-*O*-sulfated polysaccharide derivative employing TBDMS *vs.* TIPS ether protecting groups (Figure 2.27).

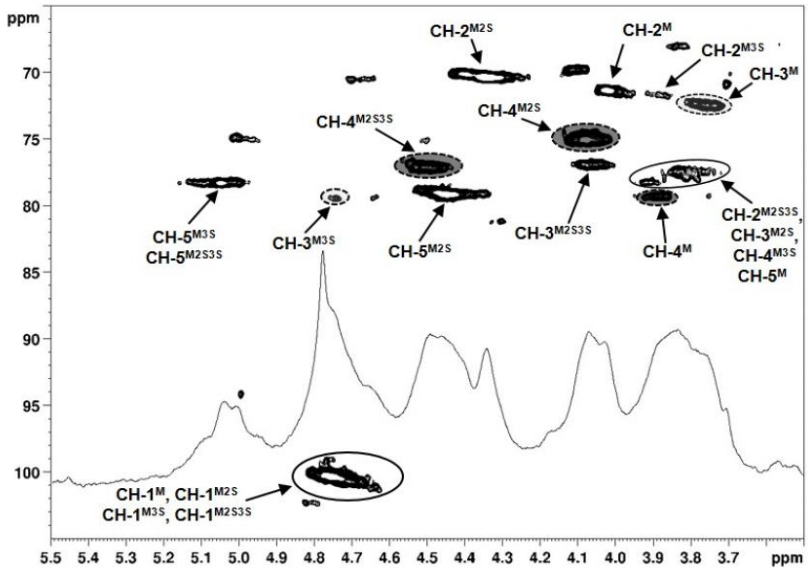

Figure 2.27. ^{1}H and $^{1}H,^{13}C$-HSQC NMR spectra (600 MHz, 298K, D_2O, zoom) of **AS-2** (densities enclosed in dotted lines and with the same filling were subjected to relative integration for DS estimation)

A higher control of sulfation pattern was achieved for derivative **AS-3**. Its precursor **14-i** was obtained through regioselective protection of the methyl esterified M units at *O*-2 position by DIPEA-promoted benzoylation with Bz_2O. Its 2D-NMR spectra revealed a marked prevalence for M3S units (75%) along the polysaccharide backbone, together with a minor amount of M2S3S residues (22%) (Figure 2.28).

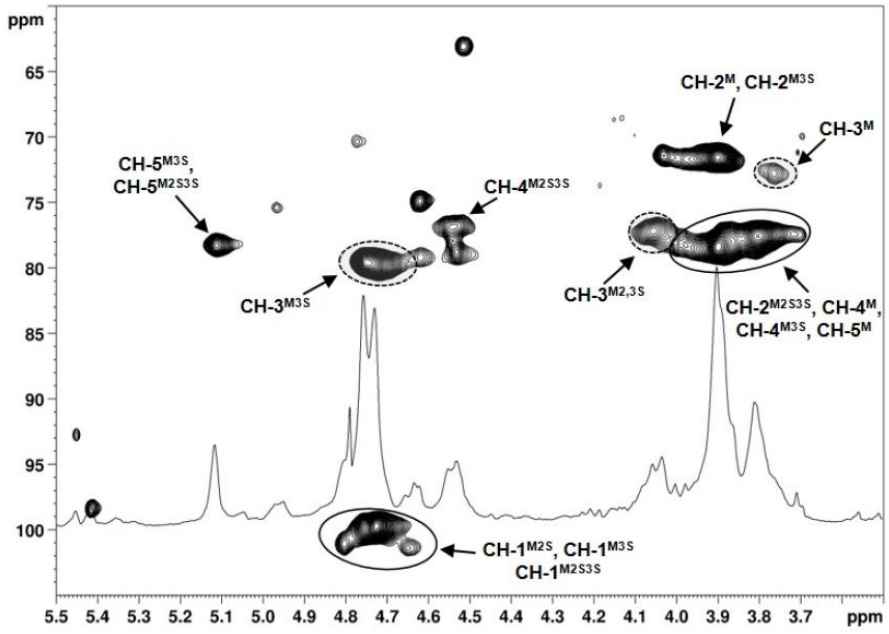

Figure 2.28. ^{1}H and $^{1}H,^{13}C$-HSQC NMR spectra (400 MHz, 298K, D_2O, zoom) of **AS-3**

On the other hand, derivative **AS-4**, obtained through a semi-synthetic pathway focused on the reaction of methyl ester derivative **14-ii** with BzCN as benzoylating reagent, gave a ^{1}H-NMR spectrum very similar to starting M-rich alginate one (Figure 2.29). This result can be explained with an almost quantitative benzoylation at both *O*-2 and *O*-3 position in the semi-synthetic intermediate **14-ii** instead of the targeted regioselective protection at the axial site.

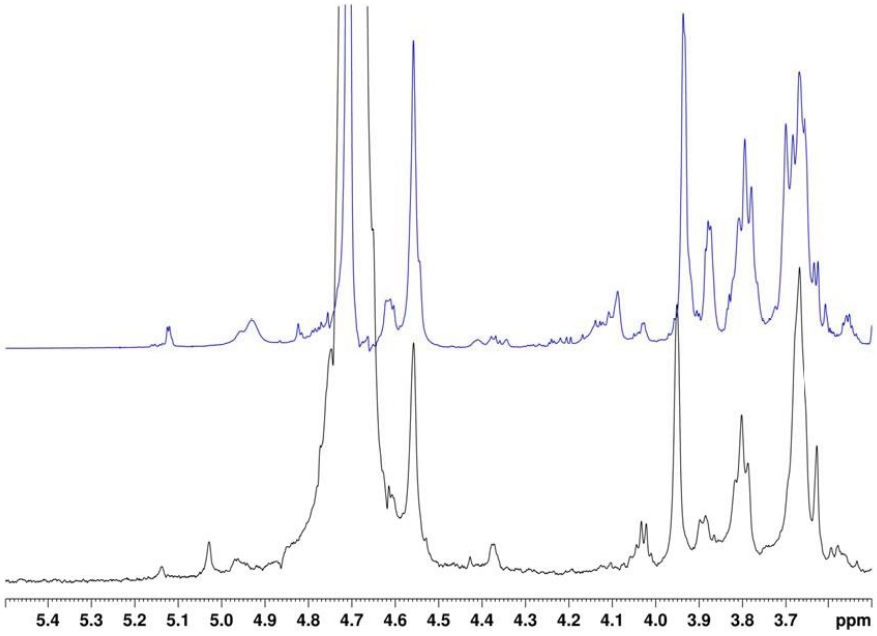

Figure 2.29. ^{1}H NMR spectra (zoom, 600 MHz, 298 K, D_2O) of **AS-4** (black) and starting PolyM (blue)

An alternative strategy to obtain 2-*O*-benzoylated alginate was based on M-2,3-diol protection with cyclic protecting groups (CPGs) followed by the regioselective opening of the latter (Figure 2.30).

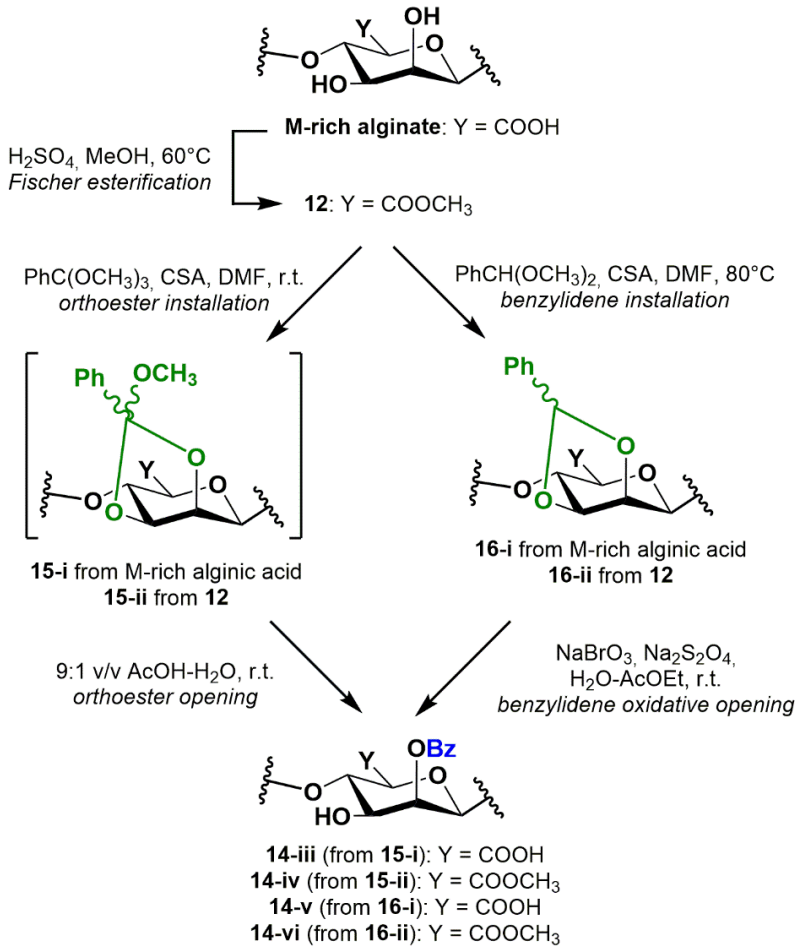

Figure 2.30. Protection strategies on M-rich alginate through CPGs employment

Firstly, an orthobenzoate ring was installed on both native M-rich alginic acid and its methylester derivative **12**, using $PhC(OCH_3)_3$ in DMF in the presence of CSA as catalyst. However, the isolation of derivatives **15-i,ii** was not attempted, due to the lability of the orthoester PG. Instead, the reaction mixture was subjected to a treatment with aqueous acetic acid, that is known to cleave the CPG and restore the alcohol moiety exclusively at equatorial sites, with the axial positions protected as Bz esters (Mukhopadhyay & Field, **2003)**. ^{1}H-NMR spectra of the obtained derivatives **14-iii,iv** confirmed the presence of Bz esters, as demonstrated by the signals at δ 8.1-7.5 ppm

related to aromatic hydrogen atoms together with signals at δ 5.2-5.7 ppm assignable to ring protons downfield shifted by an electron withdrawing group as Bz ester.

Another approach was based on the installation of benzylidene five-membered rings that could be opened under oxidative conditions to restore a free hydroxyl on the equatorial position of the diol and leave the axial oxygen atom protected as a Bz ester (Adinolfi et al., **1999**). Therefore, benzylidene rings were installed on M-rich alginic acid and its methyl ester derivative **12** by their treatment with $PhCH(OCH_3)_2$ in DMF in the presence of CSA as acid catalyst. Derivatives **16-i,ii** were isolated and purified from the reaction mixture by precipitation and the presence in their ^{1}H-NMR spectrum (Figure 2.31) of signals at δ 7.6-7.2 ppm, associated to aromatic hydrogen atoms, together with signals at δ 6.1-5.7 ppm assignable to acetal hydrogen atoms downfield shifted by the adjacent phenyl ring, demonstrated the formation of benzylidene rings. The oxidative opening was conducted with $NaBrO_3$ and $Na_2S_2O_4$ in water-ethyl acetate biphasic mixture to afford derivatives **14-v,vi**, displaying ^{1}H-NMR spectra with signal patterns similar to those detected for **14-iii,iv** samples after the orthoester installation/cleavage sequence.

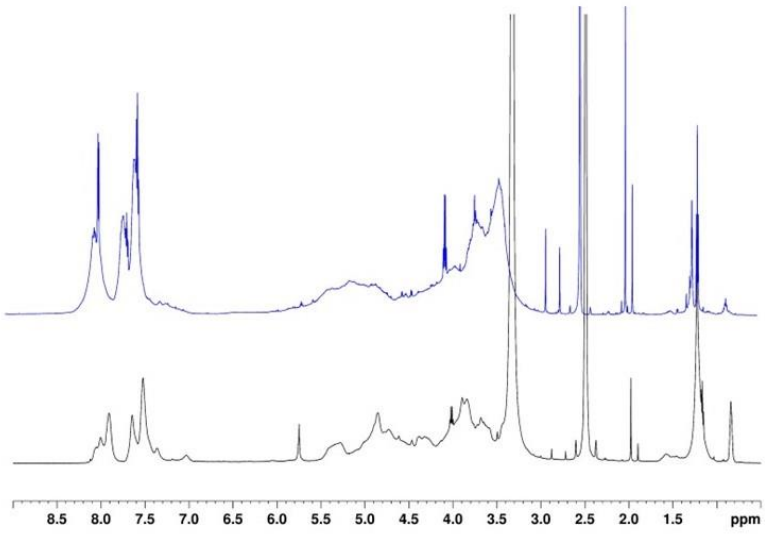

Figure 2.31. ^{1}H NMR spectra (zoom, 600 MHz, 298 K, DMSO-d_6) of **16-i** (black), **16-ii** (blue)

The last approach was based on a three-step, one-pot sequence (Figure 2.32) very recently developed on unsulfated chondroitin (Vessella et al., **2019**). This relies on the installation of a 3,6-lactone ring to link together carboxylic acid and OH-3 moieties (Elferink et al., **2019**).

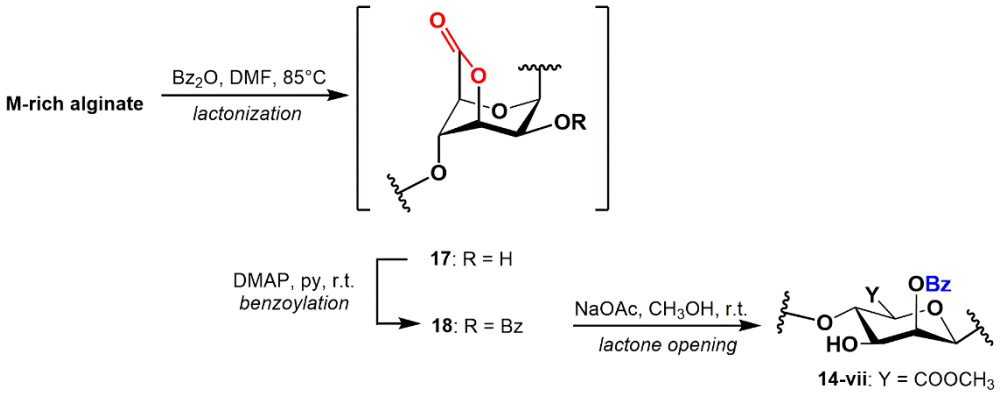

Figure 2.32. One-pot lactonization-benzoylation sequence on M-rich alginate

The lactonization reaction was performed using Bz_2O in DMF at 85 °C (Kornilov et al., **2001**), followed by one-pot addition of DMAP and pyridine to protect the unreacted hydroxyls as benzoate esters and then of sodium acetate in methanol to selectively cleave the labile lactone and restore an alcohol moiety exclusively at position *C*-3. Unfortunately, the obtained derivative **14-vii** cannot be subjected to NMR analysis as it was found to be insoluble in any deuterated solvent.

Derivatives **14-iii,vii** were subjected to sulfation under standard conditions (Bedini et al., **2017**) with $SO_3 \cdot py$ in DMF at 50°C, followed by a global deprotection under aqueous, slightly acid conditions to remove any residual presence of benzylidene and orthoester CPGs, and then by an alkaline treatment to hydrolyze methyl and benzoate esters (Figure 2.33).

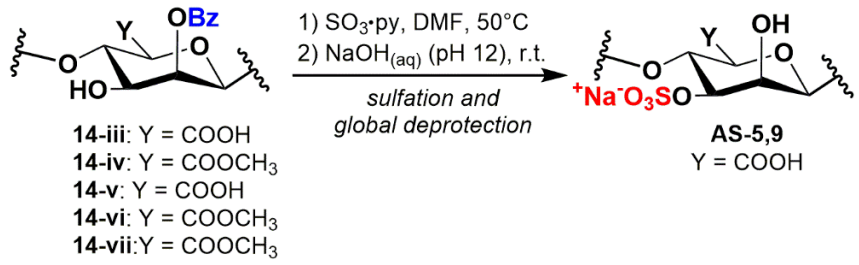

Figure 2.33. Sulfation and global deprotection steps to derivatives **AS-5,9**

The $^{1}H,^{13}C$-HSQC NMR spectra of derivatives **AS-5-9** were expected to show comparable spectra to **AS-3,4** due to the theoretical similar regioselectivity of the Bz ester on the axial *O*-2 position. **AS-5,6** showed two density volumes at $\delta_{H/C}$ 3.88/71.7 and 4.73/79.3 ppm that could be assigned with the help of $^{1}H,^{13}C$-HMBC and COSY NMR spectra to CH atoms at *O*-2 and *O*-3 positions, respectively, of M3S units. The $^{1}H,^{13}C$-HSQC NMR spectra of **AS-5,6** revealed the presence of M2S and M2S3S residues too. The M2S:M3S:M2S3S relative amounts were estimated to be equal to 43%:20%:37% (for **AS-5**) and 31%:28%:41% (for **AS-6**), by relative integration of *CH*-3^{M3S} *vs. CH*-3^{M2S3S} and *CH*-4^{M2S} *vs. CH*-4^{M2S3S} signals. Such sulfation pattern data showed that the semi-synthetic strategies based on the orthoester protecting group were not useful to achieve the targeted, regioselective sulfation at *O*-3 site (Figure 2.34).

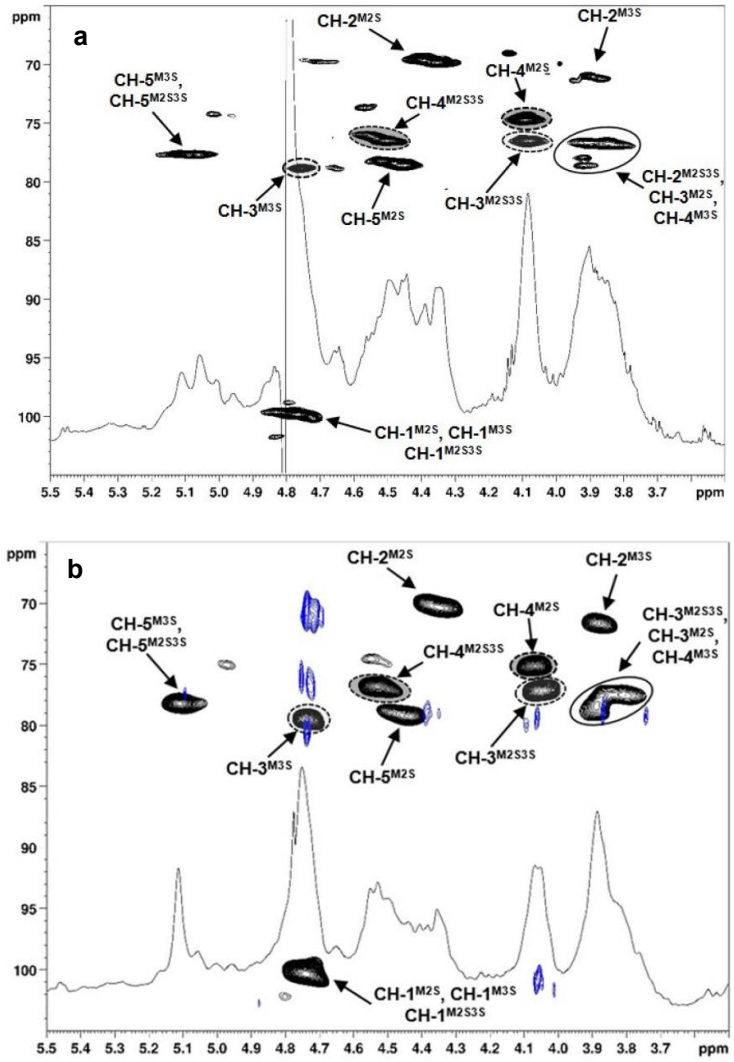

Figure 2.34. ^{1}H and $^{1}H,^{13}C$-HSQC NMR spectra (400 MHz, 298K, D_2O, zoom) of (a) **AS-5** and (b) **AS-6**

The other tested CPGs gave unsatisfying results as well: a regioselective sulfation was not detected for **AS-7,8** (Figure 2.35). Noteworthy, while orthoester CPG-derived products **AS-5,6** gave similar DS and sulfation patterns (see Table 2.5), regardless of the employed starting material (M-rich alginic acid or its methyl ester derivative **12**,

respectively), a marked difference was found for **AS-7,8**, derived by the use of a benzylidene CPG on the same precursors.

In particular, the semi-synthetic strategy developed from M-rich alginic acid afforded derivative **AS-7** having M-2,3S as major unit (63%) along the polysaccharide chain, while in **AS-8** the same disulfated residue was not found. This marked difference could be presumably ascribed to a different behavior of benzylidene-protected intermediates **16-i** and **16-ii** in the regioselective ring opening step. The reaction on **16-ii** gave derivative **14-vi** composed almost exclusively of mono-Bz ester protected M units, obtained from the bromine radical-mediated oxidative mechanism (Adinolfi et al., **1999**), although the targeted regioselective protection at *O*-2 position was not achieved, as highlighted by the very similar amount estimated for M2S and M3S units in derivative **AS-8**.

Conversely, competition by a hydrolytic mechanism was hypothesized for the benzylidene cleavage reaction on free acid derivative **16-i**, thus affording unprotected M residues as major units in the polysaccharide chain of **14-v**, and therefore explaining the predominance of disulfated M2S3S-units in derivative **AS-7**. This hydrolytic mechanism could be mediated by the carboxylic acid functionality of M units.

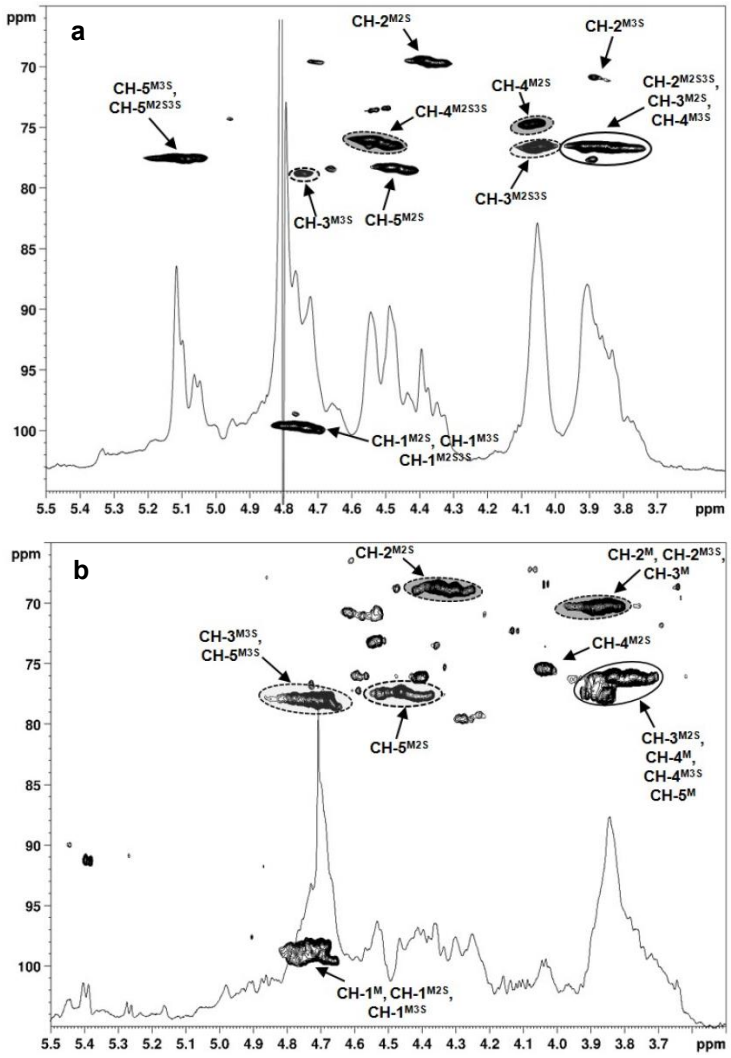

Figure 2.35. ^{1}H and $^{1}H,^{13}C$-HSQC NMR spectra (400 MHz, 298K, D_2O, zoom) of (a) **AS-7** and (b) **AS-8**

Moreover, the semi-synthetic strategy based on the installation of the intramolecular 3,6-lactone CPG that led to derivative **AS-9**, revealed an almost quantitative per-*O*-sulfation. This suggested that the one-pot 3,6-lactonization/benzoylation/lactone opening sequence was not able to protect almost any hydroxyl present on M-rich alginic acid chain (Figure 2.36).

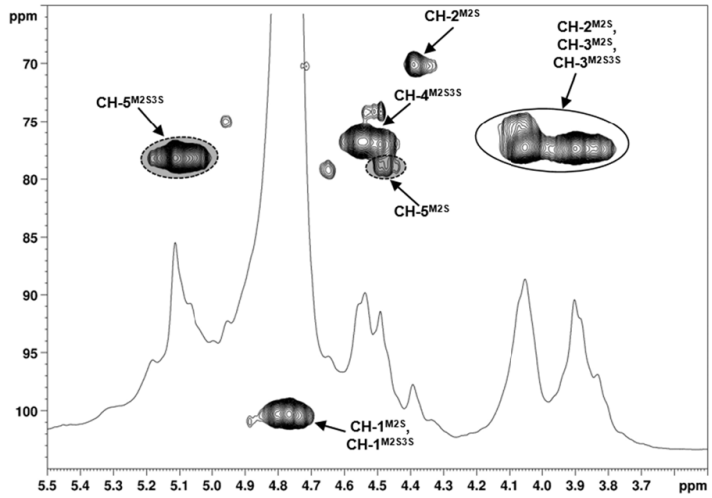

Figure 2.36. ^{1}H and $^{1}H,^{13}C$-HSQC NMR spectra (400 MHz, 298K, D_2O, zoom) of **AS-9**

In Table 2.5 are resumed the DS of derivatives **AS-1,9** as inferred from NMR assignment data and also as estimated through elemental analysis, as well as the distribution of sulfate groups along the polysaccharide backbone, as evaluated from 2D-NMR data.

	DS (El. Anal.)[a]	DS (NMR)[b]	Sulfation pattern[b]			
			M[c]	M2S[c]	M3S[c]	M2S3S[c]
M-rich alginate	0.03 ± 0.01	--	100%	--	--	--
AS-1	0.84 ± 0.01	1.0	20%	60%	n.d.[d]	20%
AS-2	1.01 ± 0.01	1.16	14%	52%	2%	32%
AS-3	0.81 ± 0.11	1.19	3%	n.d.[d]	75%	22%
AS-4	0.17 ± 0.03	n.d.[d]	n.d.[d]	n.d.[d]	n.d.[d]	n.d.[d]
AS-5	1.32 ± 0.12	1.37	n.d.[d]	43%	20%	37%
AS-6	1.20 ± 0.02	1.41	n.d.[d]	31%	28%	41%
AS-7	1.55 ± 0.01	1.63	n.d.[d]	25%	12%	63%
AS-8	0.81 ± 0.12	0.96	4%	51%	45%	n.d.[d]
AS-9	1.75 ± 0.03	1.88	n.d.[d]	12%	n.d.[d]	88%

[a] Evaluated by elemental analysis data

[b] Estimated by $^{1}H,^{13}C$-HSQC NMR signal volumes integration

[c] Data expressed as relative percentages with respect to the total amount of M, M2S, M3S and M2S3S units

[d] Not detected

Table 2.5. Degree of sulfation and sulfation patterns of derivatives **AS-1,9**

The structural characterization of **AS-1,9** also concerned the molecular weight data, which were evaluated by high-performance size-exclusion chromatography combined with a triple detector array (HP-SEC-TDA). These experiments were conducted in collaboration with our partner group (prof. Schiraldi and collaborators at the Department of Experimental Medicine of the University of Campania "L. Vanvitelli") All the semi-synthesized polysaccharides but two (**AS-3,8**) showed comparable molecular weights (Table 2.6) thus indicating that any relevant depolymerization did not occur during chemical modification. However, it is worth underlining that a low molecular weight (9 kDa) M-rich alginate sample was employed as the starting material due to the adverse effects (e.g., platelet aggregation and bleeding) typically associated with high molecular weight sulfated species.

	Semi-synthetic intermediate	Global mass yield[a]	M_w (kDa)	M_w/M_n	[η] (dL/g)	R_h (nm)
M-rich alginate	--	--	9±2	1.3±0.3	0.14±0.01	2.4±0.1
AS-1	**13-i**	11%	15±6	1.5±0.5	0.15±0.03	3.0±0.6
AS-2	**13-iii**	29%	11±5	2.0±0.5	0.12±0.03	2.4±0.4
AS-3	**14-i**	71%	7±2[d]	1.5±0.2	0.10±0.04	1.8±0.4
AS-4	**14-ii**	13%	n.d.[e]	n.d.[e]	n.d.[e]	n.d.[e]
AS-5	**14-iii**	121%	12±5	1.5±0.3	0.11±0.01	2.5±0.4
AS-6	**14-iv**	51%	10±4	1.7±0.2	0.12±0.02	2.3±0.3
AS-7	**14-v**	53%	11±2	1.5±0.1	0.14±0.01	2.8±0.1
AS-8	**14-vi**	15%	3±1[d]	1.5±0.3	0.06±0.02	1.2±0.2
AS-9	**14-vii**	134%	14±4	1.5±0.3	0.11±0.01	2.7±01

[a] Evaluated as percentage ratio between the mass of the semi-synthetic AS derivative and the mass of the starting M-rich alginic acid.

Table 2.6. Global yield, theoretical molecular weight and hydrodynamic parameters for semi-synthetic polysaccharides **AS-1-9**

The semi-synthetic methods discussed above for the M-rich alginate sample were also tested on its G-rich epimer. Indeed, similar approaches towards regioselectively sulfated derivatives were developed using both acyclic and cyclic PGs. Firstly, methods for the protection of the most reactive equatorial hydroxyl at 2-*O*-positions

were investigated (Figure 2.37). These steps were based on the installation of trialkylsilyl ethers (TBDMS and TIPS) or benzoyl esters on methyl ester derivative **19**.

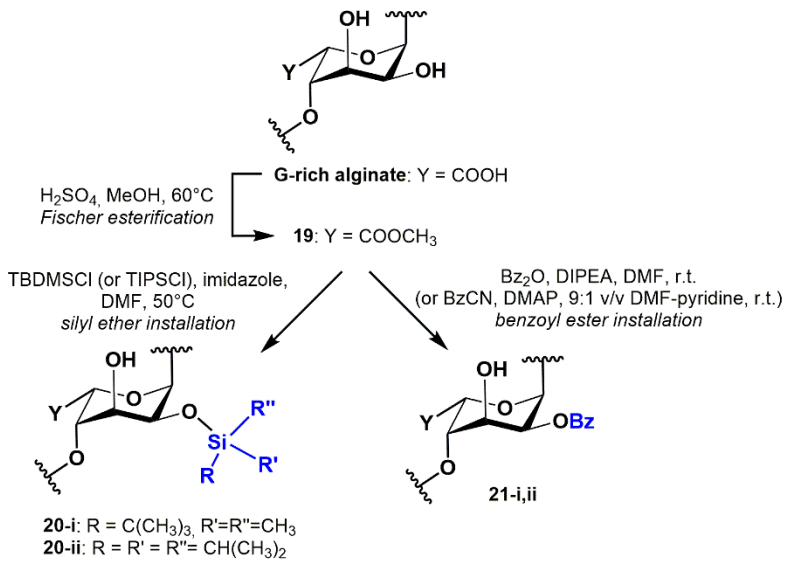

Figure 2.37. Protection strategies on G-rich alginate through acyclic PGs

These procedures gave derivatives **20-i,ii** and **21-i,ii** respectively, showing ^{1}H-NMR spectra with characteristic signals of the desired PGs. The obtained compounds were subjected to sulfation with SO_3·py in DMF at 50°C (Bedini et al., **2017**), followed by a global deprotection under aqueous acid conditions to remove acid-labile silyl ethers PGs and then by an aqueous alkaline treatment for the cleavage of methyl and benzoate esters to obtain compounds **AS-10,13** (Figure 2.38).

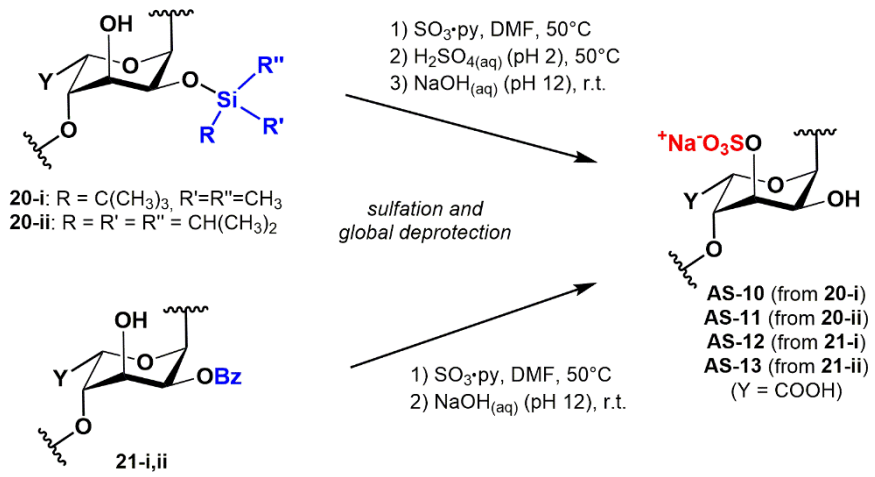

Figure 2.38. Sulfation and global deprotection to products **AS-10,13**

Derivatives **AS-10,13** were characterized by a complete set of ^{1}H and 2D-NMR spectra (Figure 2.39). Firstly, as regards compound **AS-10** the $^{1}H,^{13}C$-HSQC spectrum showed the ^{1}H- and ^{13}C-downfield shift of anomeric signals at $\delta_{H/C}$ 5.26/99.7 ppm. Its COSY correlation revealed also a downfield shifted *CH*-2 signal at $\delta_{H/C}$ 4.61/72.4 ppm that can be attributed to the presence of a sulfate group at *O*-2 site. Additional sulfate groups can be detected at position 3 of some G units for the presence of the most downfield shifted signal in the $^{1}H,^{13}C$-HSQC spectrum at $\delta_{H/C}$ 4.48/79.2 ppm. The relative integration of the well-resolved *CH*-2 signal volumes at $\delta_{H/C}$ 4.00/65.6, 4.61/72.4 and 4.05/64.9 ppm in the $^{1}H,^{13}C$-DEPT-HSQC spectrum, that could be assigned to G, G2S and G3S units respectively, allowed to estimate a 7%:63%:30%: ratio for G, G2S and G3S residues in **AS-10**. The relative G:G2S:G3S ratio estimated by 2D-NMR analysis returned a DS equal to 0.93 for **AS-10.**

A similar analysis of 2D-NMR spectra was conducted on derivative **AS-13** revealing the presence of a good relative amount of the target G3S residues (61%) with respect to **AS-10,11,12** but a higher amount of underivatized units (20%). The superimposition of the $^{1}H,^{13}C$-HSQC spectrum of **AS-13** with a per-O-sulfated G-rich derivative also revealed the presence of a little amount of G2S3S units (19%).

However, the highest regioselectivity could be inferred for the semi-synthetic strategy towards a 3-*O*-sulfated polysaccharide derivative employing benzoyl ester protecting groups using BzCN as benzoylating agent.

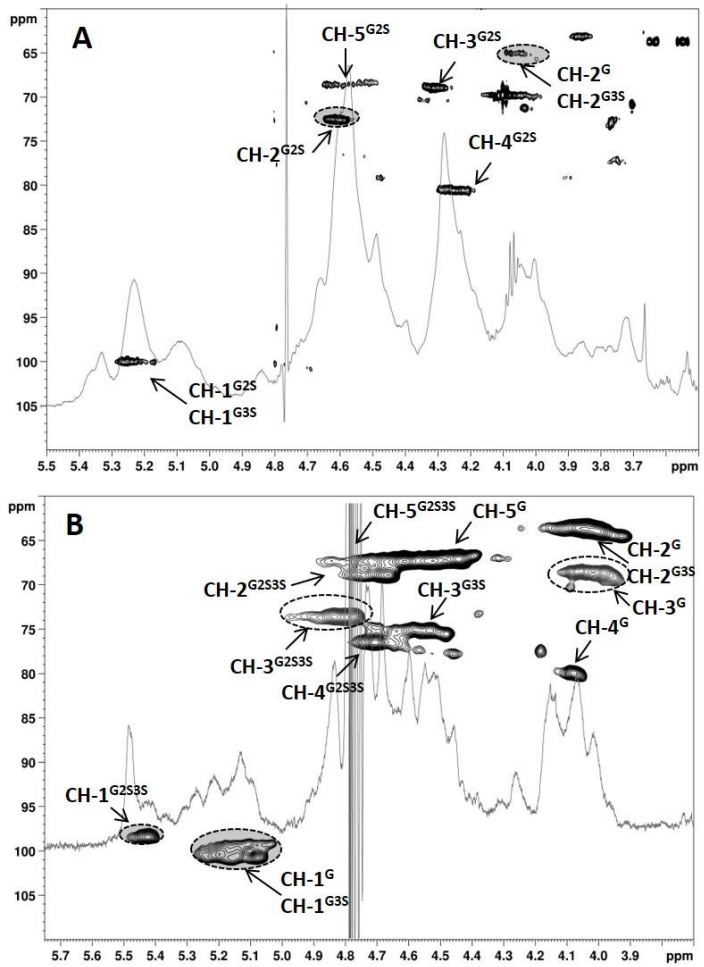

Figure 2.39. ^{1}H and $^{1}H,^{13}C$-HSQC NMR spectra (400 MHz, 298K, D_2O, zoom) of (a) **AS-10** and (b) **AS-13**

Another approach was based on the installation of CPGs such as cyclic benzylidene or orthoester followed by their regioselective opening for the protection of the axial hydroxyl at 3-*O*-positions. These reactions were performed both on both native G-rich

alginic acid and its methyl ester derivative **19** and, also in this case, using a similar approach developed for the M-rich alginic acid case discussed above (Figure 2.40).

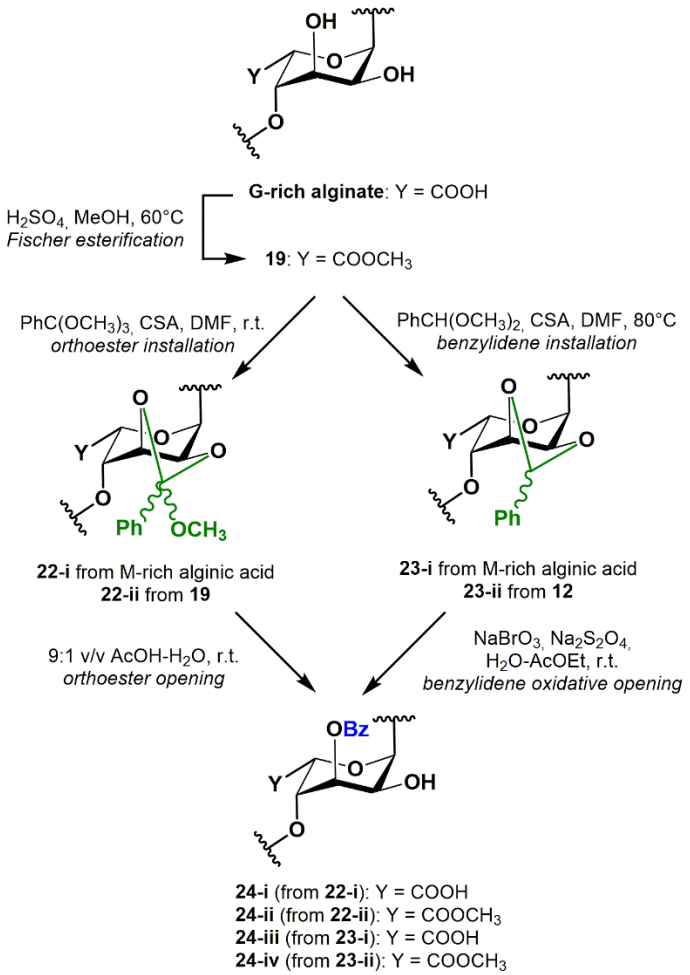

Figure 2.40. Protection strategies on G-rich alginate through cyclic PGs

Briefly, the orthobenzoate ring was installed using $PhC(OCH_3)_3$ in DMF in the presence of CSA as catalyst. The reaction mixture was subjected to a treatment with aqueous acetic acid for the cleavage of the CPG obtaining derivatives **24-i,ii**, with the axial positions protected as Bz esters (Mukhopadhyay & Field, **2003**). Another

approach was based on the installation of benzylidene five-membered rings by treatment with $PhCH(OCH_3)_2$ in DMF in the presence of CSA.

The formation of benzylidene rings was demonstrated by the presence in ^{1}H-NMR spectra of their typical signals, as already discussed above for the M-rich alginate case (derivatives **16-i,ii**). Therefore, derivatives **23-i,ii** were subjected to the oxidative opening of the benzylidene rings with $NaBrO_3$ and $Na_2S_2O_4$ in water-ethyl acetate biphasic mixture to afford derivatives **24-iii,iv** (Adinolfi et al., **1999**).

As expected, derivatives **24-i,iv**, displaying similar ^{1}H-NMR spectra with the characteristic signals of the benzoyl moieties at the aromatic region (δ 8.1-7.5 ppm) together with ring protons signals downfield shifted by an electron withdrawing group as Bz ester. Derivatives **24-i,iv** were subjected to sulfation in standard conditions (SO_3·py in DMF at 50°C) (Bedini et al., **2017**), followed by a global deprotection under aqueous, slightly acid conditions to remove any residual presence of CPGs, and then by an alkaline treatment to hydrolyze all the ester moieties (Figure 2.41).

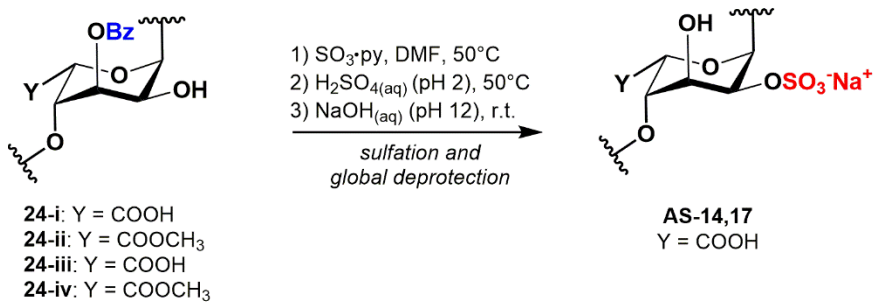

Figure 2.41. Sulfation and global deprotection to products **AS-14,17**

Derivatives **AS-14,17** were characterized by ^{1}H and 2D-NMR experiments which showed that a better control of the regioselectivity was obtained performing these strategies on the methyl ester derivative **19** (Table 2.7).

In particular, the ^{1}H,^{13}C-DEPT-HSQC spectrum of **AS-15** displayed two anomeric signals ($\delta_{H,C}$ 5.29/99.8, 5.14/102.0 ppm). The most ^{1}H- downfield shifted signal at $\delta_{H/C}$ 5.29/99.8 ppm showed a COSY correlation with a downfield shifted *CH-2* signal at

$\delta_{H/C}$ 4.61/72.4 ppm that can be assigned to G2S species. The superimposition with starting G-rich alginate also revealed the presence of unmodified G units. The relative integration of the well-resolved anomeric signal volumes at $\delta_{H/C}$ 5.29/99.8 and 5.14/102.0 ppm in the $^{1}H,^{13}C$-DEPT-HSQC spectrum allowed to estimate that only a 33% of the residues were decorated with sulfate groups on *CH*-2 positions. A higher control of the regioselectivity of the sulfation pattern was achieved for derivative **AS-17**. Its precursor **24-iv** was obtained through a benzylidene ring installation on the methyl ester derivative **19** and a regioselective opening of the CPG under oxidative conditions. Its 2D-NMR spectra revealed a marked prevalence for G2S units (92%) along the polysaccharide backbone, together with a very small amount of G residues (8%). This suggested a higher control of the regioselectivity in the benzylidene opening step (Figure 2.42).

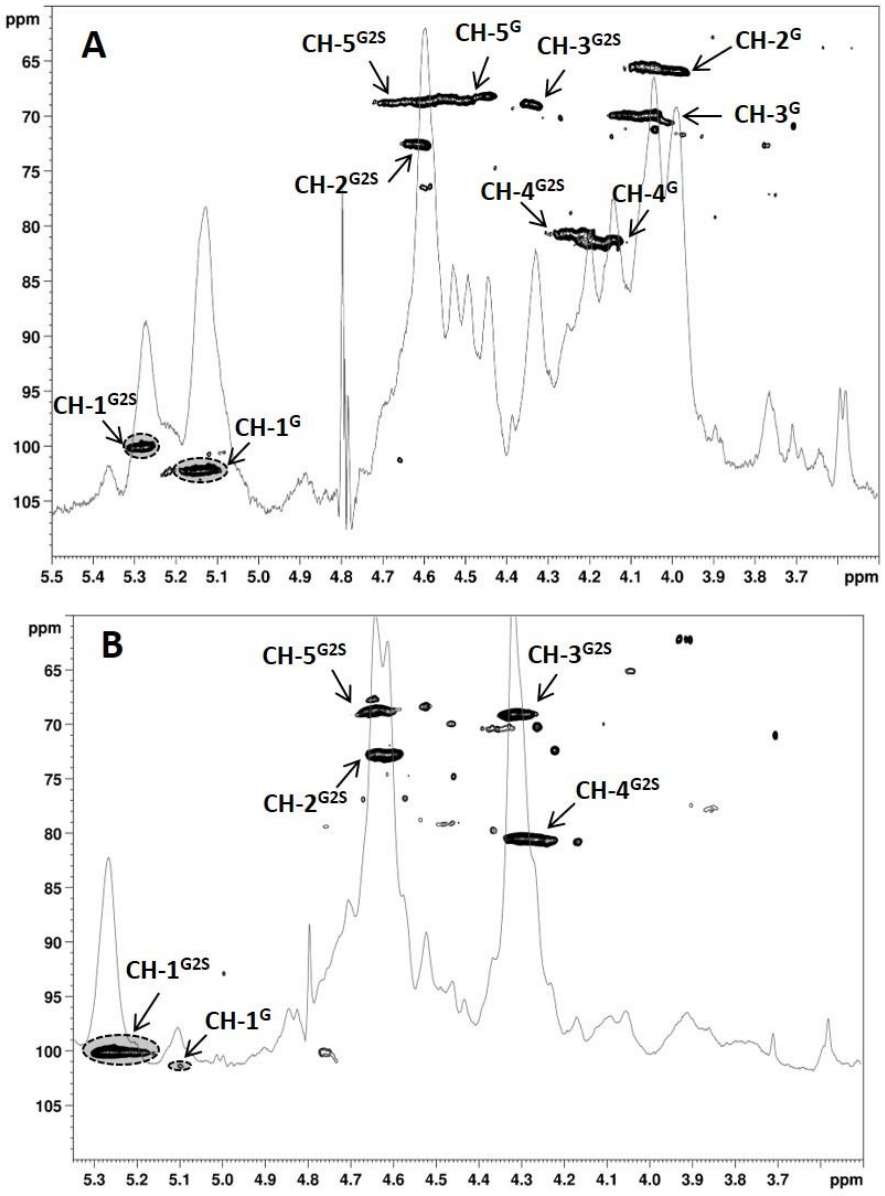

Figure 2.42. ^{1}H and $^{1}H,^{13}C$-HSQC NMR spectra (400 MHz, 298K, D_2O, zoom) of (a) **AS-15** and (b) **AS-17**

In Table 2.7 are resumed the DS of derivatives **AS-10,17** as inferred from NMR assignment data and also as estimated through elemental analysis as well as the

distribution of sulfate groups along the polysaccharide backbone, as evaluated from 2D-NMR data.

	DS (El. Anal.)[a]	DS (NMR)[b]	Sulfation pattern[b]			
			G[c]	G2S[c]	G3S[c]	G2S3S[c]
G-rich alginate	0	0	100%	--	--	--
AS-10	in progress	0.93	7 %	63 %	30 %	n.d.[d]
AS-11	in progress	in progress				
AS-12	1.12	in progress				
AS-13	in progress	0.99	20 %	n.d.[d]	61 %	19 %
AS-14	in progress	in progress				
AS-15	0.51	0.33	67 %	33 %	n.d.[d]	n.d.[d]
AS-16	0.80	0.60	40 %	39 %	21 %	n.d.[d]
AS-17	0.95	0.92	8 %	92 %	n.d.[d]	n.d.[d]

[a] Evaluated by elemental analysis data

[b] Estimated by $^{1}H,^{13}C$-HSQC NMR signal volumes integration

[c] Data expressed as relative percentages with respect to the total amount of G, G2S, G3S and G2S3S units

[d] Not detected

Table 2.7. Degree of sulfation and sulfation patterns of derivatives **AS-10,17**

Starting from these achievements, the semi-synthetic approaches used for M-rich and G-rich alginate polysaccharides were enlarged to a non-G/M-enriched starting material to study how the regioselectivity of these methods was influenced by the heterogeneity of the alginate structure. The starting material for this investigation was the methyl ester derivative **25**, that was subjected to protection steps testing both acyclic protecting groups such as a trialkylsilyl ether (TBDMS) and benzoyl esters or cyclic protecting groups (orthoester and benzylidene) followed by their regioselective opening.

In particular, on the basis of the previous results, the protection of both equatorial hydroxyls (3-*O*-positions for M units and 2-*O*-positions for G-units) could be performed through a silyl ether installation. Instead, by performing a benzoylation

reaction, it could be theoretically possible to discriminate between the axial hydroxyl on 2-*O*-positions of M units and the equatorial hydroxyl on 3-*O*-positions of G units (Ren et al., **2018**; Peng et al., **2016**) (Figure 2.43).

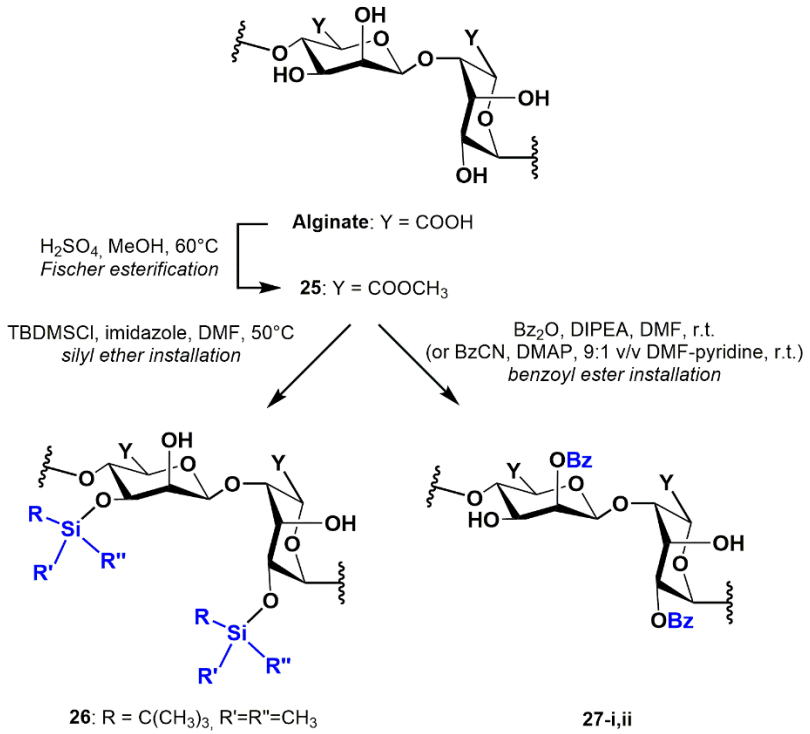

Figure 2.43. Protection strategies on non-M/G enriched alginate through acyclic PGs

These procedures gave derivatives **26** and **27-i,ii**, respectively, showing ^{1}H-NMR spectra characterized by typical signals of the desired PGs. These derivatives were subjected to sulfation reaction using SO_3·py in DMF at 50°C (Bedini et al., **2017**), followed by a global deprotection under aqueous acid conditions for the cleavage of acid-labile silyl ethers and then by an aqueous alkaline treatment to remove all the ester moieties to obtain compounds **AS-18,20** (Figure 2.44).

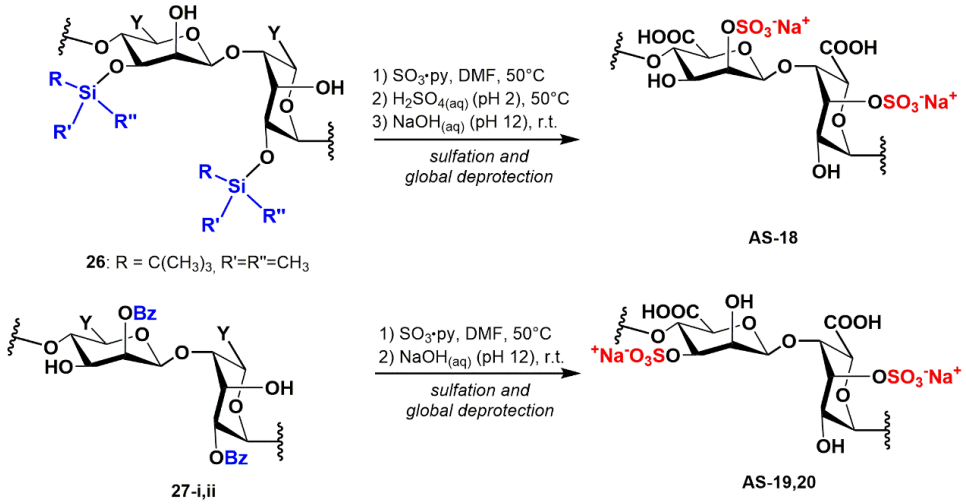

Figure 2.44. Sulfation and global deprotection to products **AS-18-20**

Similar to the AS products discussed above, derivatives **AS-18,20** were characterized by a complete 2D-NMR analysis and all the related data are reported in table x. Derivative **25** was also subjected to a protection with CPGs such as benzylidene and orthoester. In both cases, the regioselective opening of the rings could allow the protection of both axial hydroxyls (2-*O*-positions for M units and 3-*O*-positions for G-units) with benzoyl esters (Mukhopadhyay & Field, **2003**; Adinolfi et al., **1999**). ^{1}H-NMR experiments confirmed the presence of the desired ester moieties. Therefore, compounds **30-i,ii** were finally subjected to a sulfation reaction under standard conditions (Bedini et al., **2017**) followed by an aqueous alkaline step to remove the protecting groups obtaining derivatives **AS-21,22** (Figure 2.45).

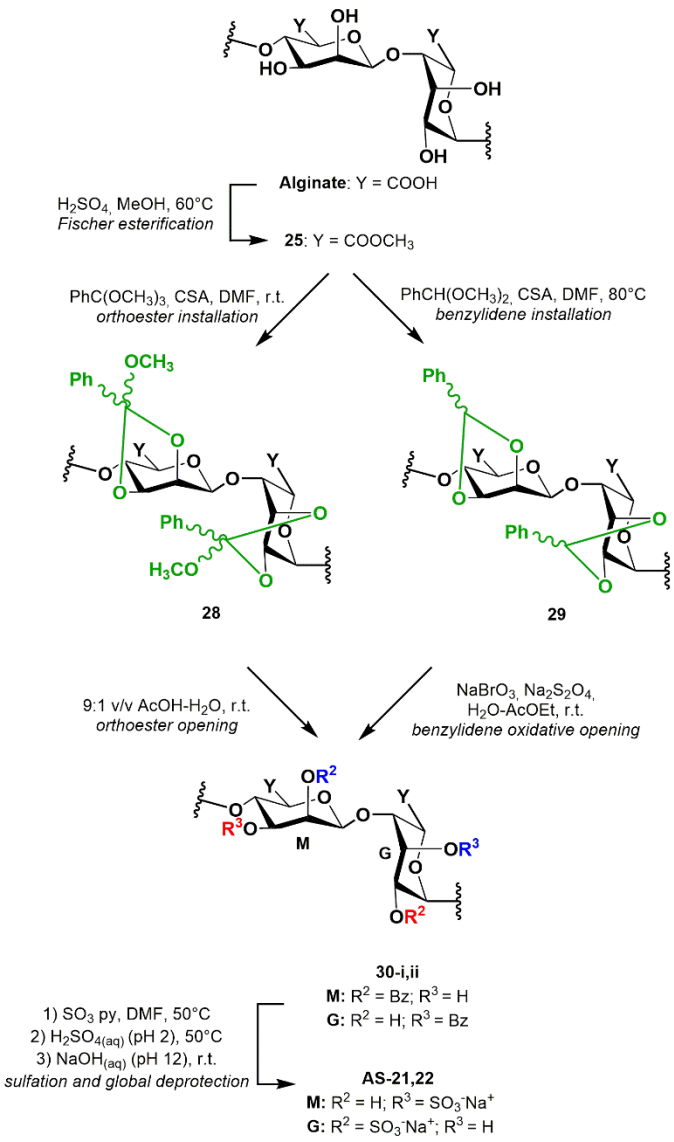

Figure 2.45. Protection strategies on non-M/G enriched alginate through cyclic PGs

Noteworthy, the 2D-NMR spectra of **AS-22,** obtained from benzylidene installation and its regioselective cleavage under oxidative conditions, revealed a marked prevalence for G2S units (93%) along the polysaccharide backbone, together with a very little amount of G2,3S residues (7%). This confirmed the very high control of

regioselectivity through this method on G units. Moreover, a better control of the regioselectivity was reached for the M units with respect to **AS-8**, that was obtained with the same approach on the homogeneous M-rich alginate starting material. Indeed, a good amount of M2S (76%) residues was estimated, together with a small quantity of M3S (24%) units. This could be explained by the presence of G units that could influence also the regioselectivity of the benzylidene ring oxidative opening on the M residues (Figure 2.46).

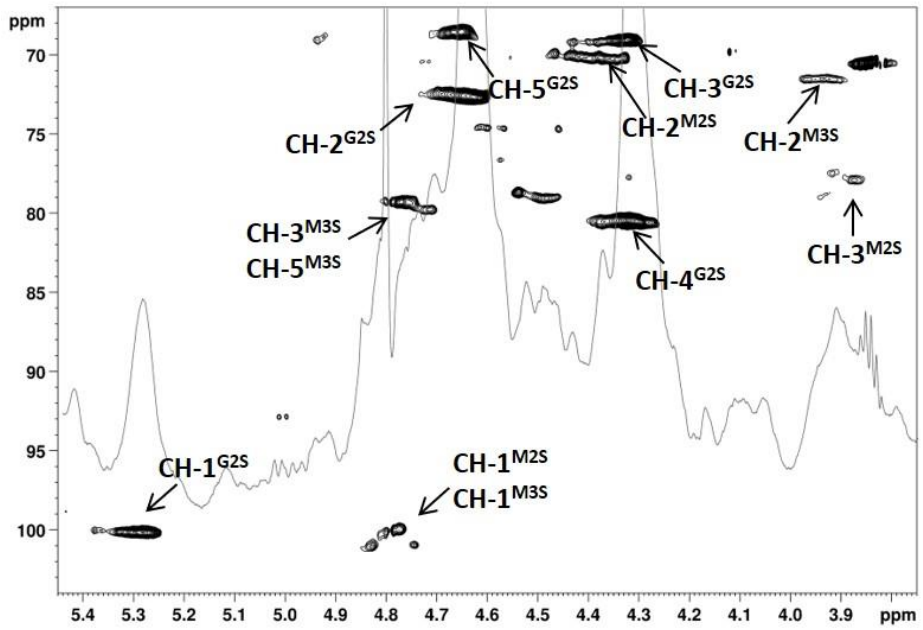

Figure 2.46. ^{1}H and $^{1}H,^{13}C$-HSQC NMR spectra (400 MHz, 298K, D_2O, zoom) of **AS-22**

In Table 2.8 are resumed the DS of derivatives **AS-18,22**, as inferred from NMR assignment data and also as estimated through elemental analysis, as well as the distribution of sulfate groups along the polysaccharide backbone, as evaluated from 2D-NMR data. It is worth underlining that, despite of the quite alkaline-lability typical of alginate compounds, no evidence of β-elimination arose from NMR spectra.

	DS (El. Anal.)[a]	DS (NMR)[b]	Monosaccarides units composition [b]
Alginate	0	0	M (52%), G (48%)
AS-18	in progress	1.04	M2S (57%), M (43%), G2S (87%), G2,3S (13%)
AS-19	1.33	1.44	M3S (73%), M2,3S (27%), G2S (38%), G2,3S (62%)
AS-20	0.93	0.90	M2,3S (56%), M (44%), G3S (51%), G2,3S (8%), G (41%)
AS-21	in progress	1.55	M2S (28%), M3S (33%), M2,3S (39%), G2S (29%), G2,3S (71%)
AS-22	1.44	1.04	M2S (76%), M3S (24%), G2S (93%), G2,3S (7%)

[a] Evaluated by elemental analysis data

[b] Estimated by $^{1}H,^{13}C$-HSQC NMR signal volumes integration

Table 2.8. Degree of sulfation and sulfation patterns of derivatives **AS-18,22**

The structural characterization of **AS-10,22** will be completed with molecular weight measurements, which will be evaluated by HP-SEC-TDA in collaboration with our partner group (prof. Schiraldi and collaborators at the Department of Experimental Medicine of the University of Campania "L. Vanvitelli"). These experiments are currently in progress. The most interesting products of these studies will be also subjected to structure-activities investigations to test, for example, their potential anti-coagulant activity. This work is scheduled for the near future and will be reported elsewhere.

2.2.3. Conclusions

In this section, the study of the regioselective sulfation of different alginate polysaccharides was attempted through several different multi-step strategies, all relying upon protection-sulfation-deprotection sequences. In particular, both acyclic and cyclic protecting groups were tested in order to obtain new alginate sulfate derivatives with a well-defined sulfation pattern. All the semi-synthesized, sulfated polysaccharides were subjected to a detailed characterization of their sulfation pattern

through a combination of elemental analysis, and 1D- and 2D-NMR spectroscopy. In the case of the M-rich polysaccharide, the employment of TBDMS ether allowed the sulfation on the axial hydroxyl at *C*-2 site. The complementary sulfation pattern was accessed by protecting the *O*-2 position with Bz_2O in the presence of DIPEA. The employment of other protecting groups gave a lower or no regiocontrol in sulfate group installation. These strategies were extended firstly to a G-rich polysaccharide: the sulfation on the axial hydroxyl at *C*-3 site was attempted with a good regiocontrol after having used BzCN in the presence of DMAP in the protection reaction, instead a complementary derivatization pattern was reached using a strategy based on the employment of cyclic benzylidene followed by its regioselective opening under oxidative condition, obtaining a product with a highly homogeneous sulfation pattern. Finally, these approaches were tested on a non-G/M enriched alginate. Also in this case, derivatives with a well-defined sulfation pattern were obtained. Some experiments to complete the structural characterization of the products are current under investigation and the most promising products will be subjected to biological investigations to test, for example, their potential anti-coagulant activity.

2.2.4. Experimental section

General methods. Commercial grade reagents and solvents were used without further purification, except where differently indicated. Starting polysaccharides were purchased from Biosynth (Thal, Switzerland). The term “pure water” refers to water purified by a Millipore Milli-Q Gradient system (Merck Millipore, Burlington, MA, USA). Dialyses were conducted on Spectra/Por 3.5 kDa cut-off membranes at 4°C. Centrifugations were performed with an Eppendorf (Hamburg, Germany) Centrifuge 5804R instrument at 4°C (4600 g, 5 min). Freeze-drying was performed with a 5Pascal (Trezzano sul Naviglio, Italy) Lio 5P 4K freeze dryer. Elemental analyses were performed on Leco 628 and Leco 144 Elemental Analyzer instruments (Leco, St.

Joseph, MI, USA). NMR spectra were recorded on a Bruker (Billerica, MA, USA) Avance-III HD (^{1}H: 400 MHz, ^{13}C: 100 MHz) or on a Bruker Avance-III (^{1}H: 600 MHz, ^{13}C: 150 MHz) instrument – the latter equipped with a cryo-probe – in D_2O (acetone as internal standard, ^{1}H: $(CH_3)_2CO$ at δ 2.22 ppm; ^{13}C:$(CH_3)_2CO$ at δ 31.5 ppm) or DMSO-*d*$_6$ (^{1}H: CHD_2SOCD_3 at δ 2.49 ppm; ^{13}C: CD_3SOCD_3 at δ 39.5 ppm). Data were processed using the data analysis packages integrated with Bruker TopSpin® 4.0.5 software. Gradient-selected COSY and NOESY experiments were performed using spectral widths of 6000 Hz in both dimensions, using data sets of 2048 × 256 points. ^{1}H,^{13}C-HSQC and ^{1}H,^{13}C-HMBC experiments were measured in the ^{1}H-detected mode via single quantum coherence with proton decoupling in the ^{13}C domain, using data sets of 2048 × 256 points and typically 80 increments (160 for HMBC). A Viscotek TDA 305 instrument (Malvern, UK) was used to determine molecular mass data.

Example of silyl ether installation. Derivative **12** (44.7 mg) was suspended in dry DMF, 1.7 mL and then treated with TBDMSCl (177 mg) and imidazole (240 mg). The mixture was stirred overnight at 50°C. Thereafter, it was cooled to rt and treated with *i*-Pr_2O (7 mL). The mixture was stored at −28 °C for some hours, then the obtained precipitate was collected by centrifugation and dried under vacuum to give polysaccharide **13-i** (120 mg, 268% weight yield).

Example of orthoester installation and cleavage. M-rich alginic acid (85.0 mg, 0.481 mmol repeating unit) was suspended in dry DMF (3.8 mL). After 90 min stirring at rt, trimethyl orthobenzoate ($PhC(OCH_3)_3$, 752 μL, 4.38 mmol) and then CSA (140 mg, 603 μmol) were added. The suspension was stirred at rt overnight, then pure water (15 mL) was added. The resulting milky suspension was stirred for 2 hours, then subjected to dialysis and freeze-drying. The whole procedure was performed twice. Compound **14-iii** (94.4 mg, 111% weight yield) was obtained as a yellowish powder.

Example of benzylidene installation. A suspension of M-rich alginic acid (196 mg, 1.11 mmol repeating unit) in dry DMF (15 mL) was briefly stirred at 80 °C and then treated at rt with α,α-dimethoxytoluene ($PhCH(OCH_3)_2$, 816 μL, 5.44 mmol) that was freshly dried over 4Å molecular sieves, and then with a 0.21M solution of CSA in dry DMF (0.77 μL). The mixture was vigorously stirred at 80 °C overnight, then cooled to rt and treated with *i*-Pr_2O (40 mL) to give a white precipitate. The mixture was stored at −28 °C for some hours, then the solid was collected by centrifugation. After overnight drying under vacuum, derivative **16-i** (175 mg, 89% weight yield) was obtained as a white powder.

Typical procedure of methyl esterification. M-rich alginic acid (520 mg, 2.95 mmol repeating unit) was treated *via cannula* with a solution obtained dissolving concentrated H_2SO_4 (535 μL) in dry methanol (103 mL) under Ar atmosphere. The mixture was stirred at 60°C for 24 hours, then the solid was collected by centrifugation followed by washing with 1:1 v/v EtOH-acetone. After drying the solid under vacuum, polysaccharide **12** (292 mg, 56% weight yield) was obtained.

Example of benzoylation with Bz_2O. Derivative **12** (61.4 mg) was dissolved in dry DMF (2.3 mL) and then treated with Bz_2O (362 mg) and *N*,*N*-diisopropylethylamine (DIPEA, 112 μL). The solution was stirred overnight at rt, then treated with *i*-Pr_2O (11 mL). The mixture was stored at −28°C for some hours, then the obtained precipitate was collected by centrifugation and dried under vacuum to give compound **14-i** (91.3 mg, 149% weight yield).

Example of benzoylation with BzCN. Derivative **12** (59.8 mg) was dissolved in 9:1 v/v DMF-pyridine (2.5 mL) and then treated with benzoyl cyanide (BzCN, 206 mg) and DMAP (10.6 mg). The solution was stirred overnight at rt, then treated with methanol (2 mL) and *i*-Pr_2O (10 mL). The mixture was stored at −28°C for some hours, then

the obtained precipitate was collected by centrifugation and dried under vacuum to give product **14-ii** (121 mg, 202% weight yield).

Example of oxidative cleavage of benzylidene CPGs. Polysaccharide **16-ii** (52.2 mg) was suspended in ethyl acetate (1.3 mL) and treated with a 0.27 M solution of sodium bromate ($NaBrO_3$) in pure water (1.3 mL) and then with a 0.24 M solution of sodium dithionite ($Na_2S_2O_4$) in pure water (1.2 mL). The addition of the latter solution was carried out in five aliquots with a few minutes intervals. The biphasic reaction mixture was vigorously stirred at rt overnight. Thereafter, the biphasic liquid mixture was partitioned by centrifugation, the organic phase collected, dried over anhydrous Na_2SO_4, filtered and concentrated by rotary evaporation to give derivative **14-vi** (34.5 mg, 66% weight yield) as a yellowish residue.

Typical procedure for sulfation and global deprotection. Polysaccharide **13-i** (180 mg) was suspended in dry DMF (5.2 mL) and then treated with a 1.45 M solution of SO_3·py in dry DMF (7.5 mL). After overnight stirring at 50 °C, a saturated NaCl solution in acetone (11 mL) was added at rt and the mixture was then stored at -28 °C for some hours. The obtained white precipitate was collected by centrifugation, then dissolved in pure water (5.0 mL) and the resulting acid mixture (pH ~ 2) was heated to 50 °C. After 2 hours stirring at 50 °C, the mixture was cooled and then treated with a 4M $NaOH_{(aq)}$ solution to adjust pH to 12. The solution was stirred at rt overnight and then neutralized with 1M $HCl_{(aq)}$. Dialysis and subsequent freeze-drying gave **AS-1** (266 mg, 148% weight yield) as a white amorphous solid.

One-pot lactonization-benzoylation-lactone opening sequence on M-rich alginic acid. M-rich alginic acid (196 mg, 1.11 mmol repeating unit) was suspended in dry DMF (8.8 mL) and briefly stirred at 85°C. The resulting, fine, yellowish suspension was treated with Bz_2O (7.57 g, 33.5 mmol) at rt under argon atmosphere. The mixture was vigorously stirred at 85 °C for 26 h, then cooled to rt and treated with pyridine (4.9

mL) and DMAP (182 mg, 1.49 mmol). After 72 h further stirring at rt, dry methanol (7.5 mL) and NaOAc (137 mg, 1.67 mmol) were added and stirring was continued for 24 h. Thereafter, a further amount of methanol (16 mL) was added and the reaction mixture was concentrated to approximately 20 mL volume by rotary evaporation. The residue was treated at 0 °C with *i*-Pr_2O (9 mL) to give a white precipitate. The mixture was stored at −28°C for some hours, then the solid was collected by centrifugation and further purified by dissolving it in dimethylsulfoxide (DMSO, 9 mL) and then precipitating with 2:1 *v/v* acetone- *i*-Pr_2O (45 mL). After overnight drying under vacuum, derivative **14-vii** (190 mg, 97% weight yield) was obtained as a white powder.

Hydrodynamic analyses. A size exclusion chromatography-triple detector array (SEC-TDA) instrument consisting of two gel-permeation columns set in series (TSK-GEL GMPWXL, 7.8 × 30.0 cm, Tosoh Bioscience, Tokyo, Japan), a refractive index detector (RI), a laser detector made of a right-angle and a low-angle light scattering (RALS and LALS, respectively), and a four-bridge viscometer (VIS) was employed. A refractive index increment (d*n*/d*c*) value of 0.138 mL/g, as reported for water solutions of native or sulfated, polymannuronate derivativeswas used for calculations. It is worth noting that the molecular weight data from SEC-TDA varied less than 10% when using 0.13−0.15 mL/g d*n*/d*c*, which is the range reported for unmodified and sulfated alginates (Bi et al., **2020**; Syanda et al., **2022**). An appropriate amount of each AS sample was dissolved in pure water and stirred at 25 °C overnight. The solution was then centrifuged, filtered on 0.22 μm filters, and analyzed for hydrodynamic characterization in triplicate. An isocratic elution with 0.1 M $NaNO_3$ aqueous solution (pH ~ 7.0) at a flow rate of 0.6 ml/min was carried out. Analyses were performed at 40 °C with a running time of 1 h (La Gatta et al., **2010**).

References

Aarstad, O. A.; Tøndervik, A.; Sletta, H.; Skjåk-Bræk, G., **2012**. *Biomacromolecules 13*, 106–116.

Adinolfi, M., Barone, G., Guariniello, L., Iadonisi, A., **1999**. *Tetrahedron Lett. 40*, 8439–8441.

Arlov, Ø.; Lillelund Aachmann, F.; Sundan, A.; Espevik, T.; Skjåk-Bræk, G., **2014**. *Biomacromolecules 15*, 2744–2750.

Arlov, Ø.; Rütsche, D.; Korayem, M. A.; Öztürk, E.; Zenobi-Wong, M., **2021**. *Adv. Funct. Mat. 31*, 2010732.

Arlov, Ø.; Skjåk-Bræk, G., **2017**. *Molecules 22*, 778.

Bedini, E.; Laezza, A.; Parrilli, M.; Iadonisi, A., **2017**. *Carbohydr. Polym.*, *174*, 1224–1239.

Bi, D., Li, X., Li, T., Li, X., Lin, Z., Yao, L.; Li, H., Xu, H., Hu, Z., Zhang, Z., Liu, Q., Xu, X., **2020**. *Front. Pharmacol. 11*, 21.

Caputo, H. E.; Straub, J. E.; Grinstaff, M., **2019**. *Chem. Soc. Rev. 48*, 2338–2365.

Cong, Q.; Xiao, F.; Liao, W.; Dung, Q.; Ding, K., **2014**. *Int. J. Biol. Macromol. 69*, 252–259.

Draget, K.I., Moe, S.T., Skjåk-Bræk, G., Smidsrød, O., **2006**. Alginates, in: Stephen, A.M., Phillips, G.O., Williams, P.A. (Eds.), *Food Polysaccharides and Their Applications*. CRC Press, Boca Raton (FL), pp. 289–334.

Elferink, H., Mensink, R. A., Castelijns, W. W. A., Jansen, O., Bruekers, J. P. J., Martens, J., Oomens, J., Rijs, A. M., Boltje, T. J., **2019**. *Angew. Chem. Int. Ed. 58*, 8746–8751.

Fernando, I. P. S.; Kim, D.; Nah, J.-W.; Jeon, Y.-J., **2019**. *Chem. Eng. J. 355*, 33–48.

Freeman, I.; Kedem, A.; Cohen, S., 2008. *Biomaterials 29*, 3260–3268.

Kornilov, A. V., Sukhova, E. V., Nifantiev, N. E., **2001**. *Carbohydr. Res. 336*, 309–313.

La Gatta, A., De Rosa, M., Marzaioli, I., Busico, T., Schiraldi, C., **2010**. *Anal. Biochem. 404*, 21−29.

Lee, K. Y.; Mooney, D. J., **2012**. *Progress Polym. Sci. 37*, 106-126.

Mukhopadhyay, B., Field, R. A. A, **2003**. *Carbohydr. Res. 338*, 2149–2152.

Pawar, S. N.; Edgar, K. J., **2012**. *Biomaterials 33*, 3279–3305.

Peng, P., Linseis, M., Winter, R. F., Schmidt, R. R., **2016**. *J. Am. Chem. Soc. 138*, 6002–6009.

Ren, B., Gan, L., Zhang, L., Yan, N., Dong, H., **2018**. *Org. Biomol. Chem. 16*, 5591–5597.

Sanchez-Ballester, N. M., Bataille, B., Benabbas, R., Alonso, B., Soulairol, I., **2020**. *Carbohydr. Polym. 240*, 116280.

Syanda, A. M. Kringstad, V. I. Blackford, S. J. I., Kjesbu, J. S., Ng, S. S., Ma, L. Xiao, F., Coron, A. E., Rokstad, A. M. A., Modi, S., Rashid, S. T., Strand, B. L., **2022**. *Front. Bioeng. Biotechnol. 9*, 816542.

Szekalska, M.; Puciłowska, A.; Szymańska, E.; Ciosek, P.; Winnicka, K., **2016.** *Int. J. Polym. Sci.*, 7697031.

Vessella, G., Traboni, S., Cimini, D., Iadonisi, A., Schiraldi, C., Bedini, E., **2019**. *Biomacromolecules 20*, 3021–3030.

Wang, Z.; Xie, J.; Shen, M.; Nie, S.; Xie, M., **2018**. *Trends Food Sci. Technol. 74*, 147–157.

Wu, J.; Zhao, X.; Ren, L.; Xue, Y.; Li, C.; Yu, G.; Guan, H., **2014**. *Carbohydr. Polym. 104*, 23–28.

Xue, Y.-T.; Ren, L.; Li, S.; Wang, L.; He, X.-X.; Zhao, X.; Yu, G.; Guan, H.-S.; Li, C.-X., **2016**. *Carbohydr. Polym. 144*, 330–337.

Yang, J.-S.; Xie, Y.-J.; He, W., **2011**. *Carbohydr. Polym. 84*, 33–39.

Zeng, K.; Groth, T.; Zhang, K., **2019**. *Chembiochem 20*, 737–746.

SECTION 2.3 –REGIOSELECTIVE SULFATION OF LOW MOLECULAR WEIGHT CURDLAN POLYSACCHARIDE

2.3
REGIOSELECTIVE SULFATION OF LOW MOLECULAR WEIGHT CURDLAN POLYSACCHARIDE

2.3.1. Curdlan: structure and activities

Curdlan is a linear homopolysaccharide composed of β-1→3-linked Glc units, and extracted from some bacteria as an exopolysaccharide (Figure 2.47). It is currently available from mutant *Agrobacterium* strains in high fermentation yield (Kalyanasundaram et al., **2012**) and employed in food industry due to its remarkable rheological and thermal behaviours. Furthermore, its ability to form gel encapsulations with several drugs and above all its roles in both innate and adaptive immunity have fueled an increasing interest in pharmaceutical applications of curdlan and derivatives thereof (Zhan et al., **2012**).

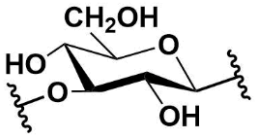

Figure 2.47. Repeating unit of curdlan polysaccharide

In particular, several curdlan semi-synthetic polysaccharides carrying well-defined structural modifications, especially at the most reactive primary *O*-6 position, have been accessed and demonstrated to have interesting biomedical and pharmaceutical applications (Zhang and Edgar, **2014**). Among them, curdlan sulfate derivatives recently emerged thanks not only to a highly enhanced water solubility with respect

to native curdlan, but also to an efficient adjuvant activity displayed in antitumor and hepatitis B virus immunotherapy both *in vitro* and *in vivo* (Jin et al., **2020**; Li et al., **2014**). Some regioselectively sulfated curdlan derivatives have been already obtained through multi-step protection-sulfation-deprotection procedures. In particular, a few years ago, we investigated the possibility to develop suitably tailored multi-step sequences based mainly on the installation of a cyclic benzylidene protecting group to have access to new LMW-curdlan derivatives with a well-defined sulfation patterns. Three different semi-synthetic pathways were investigated (Figure 2.48), one relying upon the sulfation of a benzylidene-protected intermediate and the others based on the sulfation of two polysaccharide derivatives obtained after hydrolytic or oxidative cleavage, respectively, of benzylidene protecting groups. For some of the semi-synthetic derivatives, NMR characterization revealed the presence of unprecedented Glc sulfation patterns as main motifs along the polysaccharide chain, *i.e.* 4,6-disulfated for **CdS-1,2**, 4- and 6-sulfated for **CdS-3**, and 2-sulfated for **CdS-6** (Vessella et al., **2021**). Within this frame, this project aims to extend this library to other, unprecedented, sulfation patterns in order to increase the number of LMW-curdlan sulfate polysaccharides on which structure-activity relationship studies could be done.

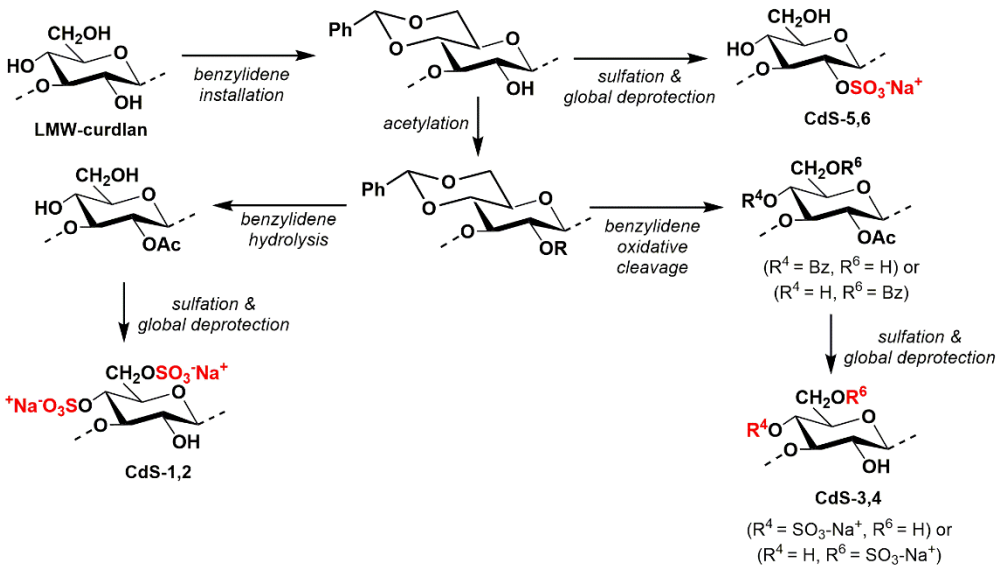

Figure 2.48. Previous multi-step methods developed for the regioselective sulfatation of LMW-curdlan polysaccharide (Vessella et al., **2021**)

2.3.2. Results and discussion

This section is focused on the study of different semi-synthetic methods in order to extend the library of curdlan sulfate compounds for future structure-activity relationship studies. To do that, both direct and multi-step methods were investigated using a LMW curdlan as starting material (Vessella et al. **2021**).

Firstly, sulfation under mild conditions was performed using a method reported in literature (Gao et al., **1997**) for the semi-synthesis of a LMW CdS 2,6-disulfate. The authors of this report used SO_3·py complex (4 equivalents) in DMSO for 75' at room temperature obtaining a quantitative derivatization on 6-*O*-position and a DS of 0.52-0.55 on 2-*O*-position. This procedure was replaced both by increasing the equivalents of SO_3·py and by using the more reactive SO_3·DMF complex (Figure 2.49).

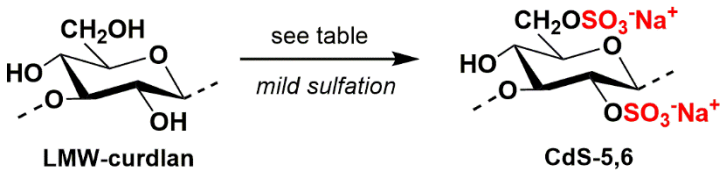

entry	product	sulfation conditions
1	**CdS-5**	SO_3·py (7 eqs), DMSO, 75', rt
2	**CdS-6**	SO_3·DMF (7 eqs), DMSO, 75', rt

Figure 2.49. Semi-synthesis of **CdS-5,6** through sulfation under mild conditions

A comparison between the ^{1}H-NMR spectra of **CdS-5** and **CdS-6** samples revealed similar results: the two spectra were found to be similar and superimposable. Both spectra showed a ^{1}H-downfield shifted signal at $\delta_{H/C}$ 4.27 ppm, assignable to new methylene groups by comparison with starting LMW-curdlan and literature data. This suggested the presence of Glc units decorated with sulfate groups on primary hydroxyls. The degree of sulfation (DS) could be evaluated by integration of these new methylene signals at $\delta_{H/C}$ 4.27 ppm with respect to the methylene signal at $\delta_{H/C}$ 3.83 ppm of the unsulfated Glc units. A DS equal to 0.69 and 0.54 were estimated for **CdS-5** and CdS-6 respectively. Unfortunately, in both cases, no derivatization at 2-*O*-position was detected (Figure 2.50).

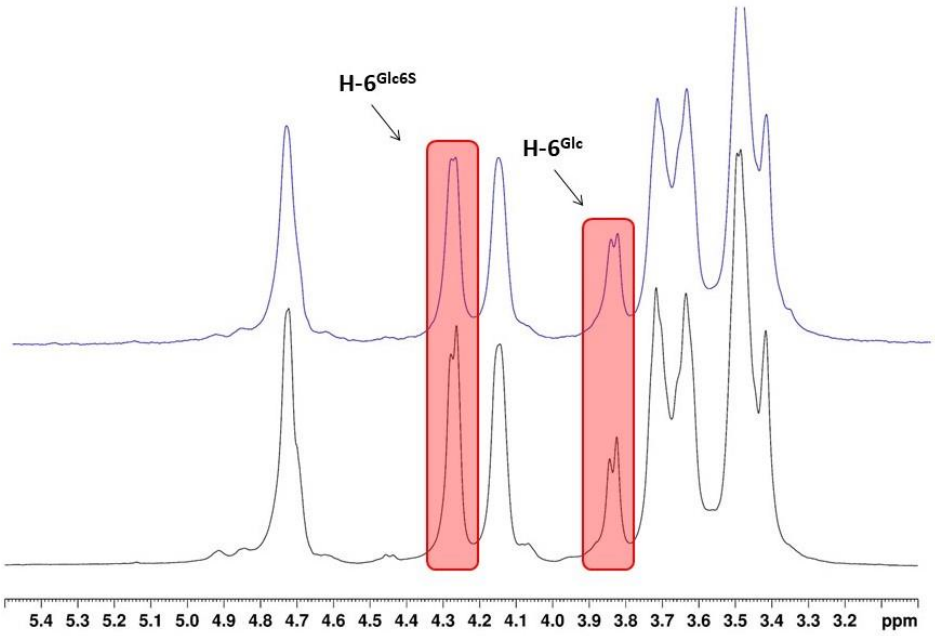

Figure 2.50. ^{1}H NMR spectra (zoom, 600 MHz, 298 K, D_2O) of **CdS-5** (black), **CdS-6** (blue)

Another approach towards regioselectively sulfated curdlan was based on a selective desulfation reaction on per-*O*-sulfated derivative **CdS-7**, obtained by sulfation of LMW-curdlan with a large excess of SO_3·DMF (10 eqs) in DMF at room temperature for 3h. The desulfation reaction was performed on the pyridinium salt of **CdS-7** with BTSA, a reagent known to cleave selectively sulfate groups placed at *O*-6 position of polysaccharides and to convert the released primary hydroxyl groups into trimethylsilyl ethers that can be then easily cleaved by an aqueous work-up (Takano et al., **1995**), to obtain derivative **CdS-8** (Figure 2.51).

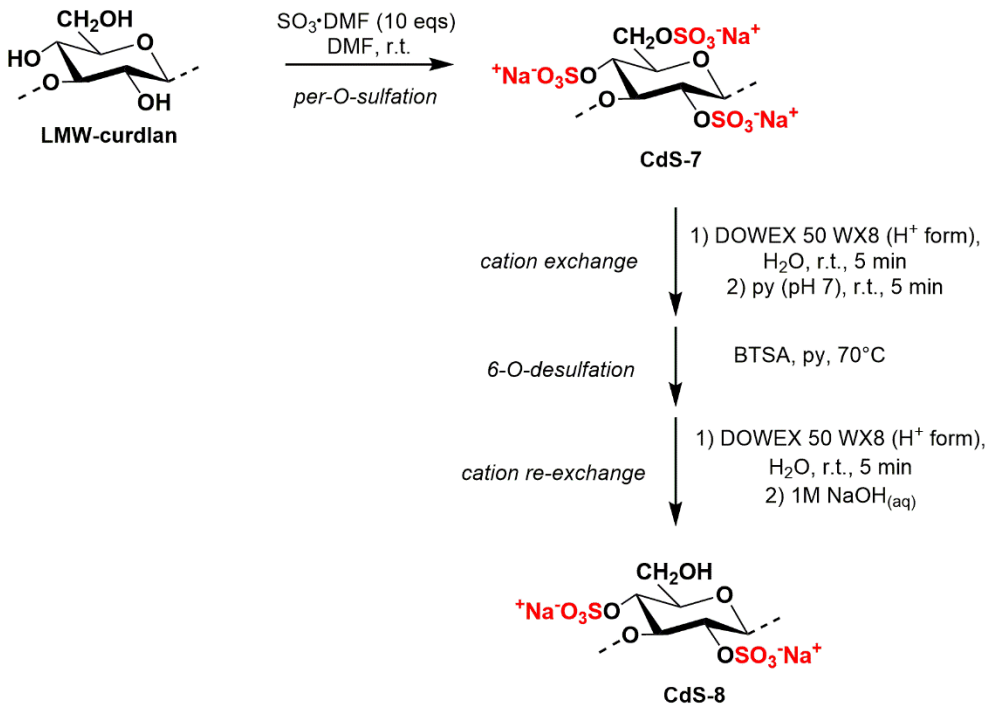

Figure 2.51. Semi-synthesis of **CdS-8** through 6-*O*-desulfation strategy

2D-NMR spectra analysis of derivative **CdS-8** confirmed the postulated quantitative desulfation on *O*-6 position: indeed, no $^{1}H,^{13}C$-downfield shift of methylene signal was detected. The analysis of a full set of 2D-NMR spectra (COSY, TOCSY, HMBC and HSQC-TOCSY) revealed a partial desulfation also on position *O*-2 and *O*-4. The relative integration of the anomeric signals at $\delta_{H/C}$ 5.14/97.5, 4.95/99.9, 4.75/100.8, 4.65/102.4 ppm revealed the presence of Glc 2,4-*O*-disulfated units (37%) together with Glc 2-*O* and 4-*O* sulfate units (30% and 10% respectively) and also a 23% of unsulfated Glc units (Figure 2.52).

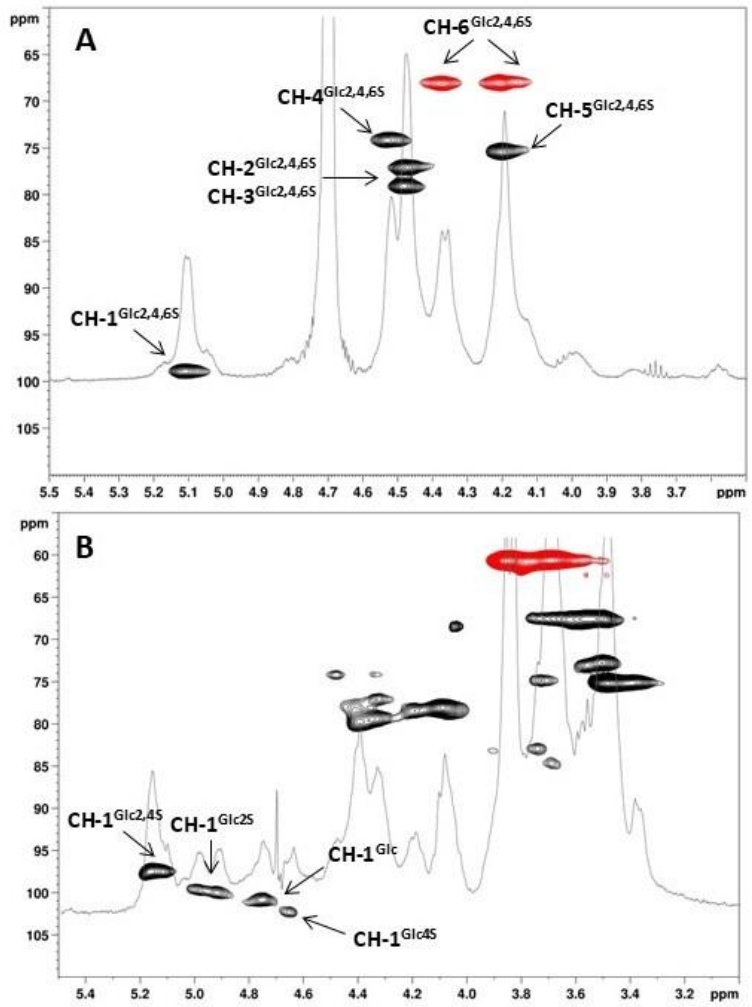

Figure 2.52. ^{1}H and $^{1}H,^{13}C$-HSQC NMR spectra (zoom, 400 MHz, 298K, D_2O) of (a) **CdS-7** and (b) **CdS-8** (only integrated signals are reported)

Another semi-synthetic approach was based on the development of multi-step pathways based on the regioselective insertion of protecting groups followed by the sulfation and then the global deprotection of the sulfated product. Within this frame, the first strategy dealt with the installation of acyclic protecting groups for the protection of the most accessible and reactive positions of the polysaccharide (Figure 2.53).

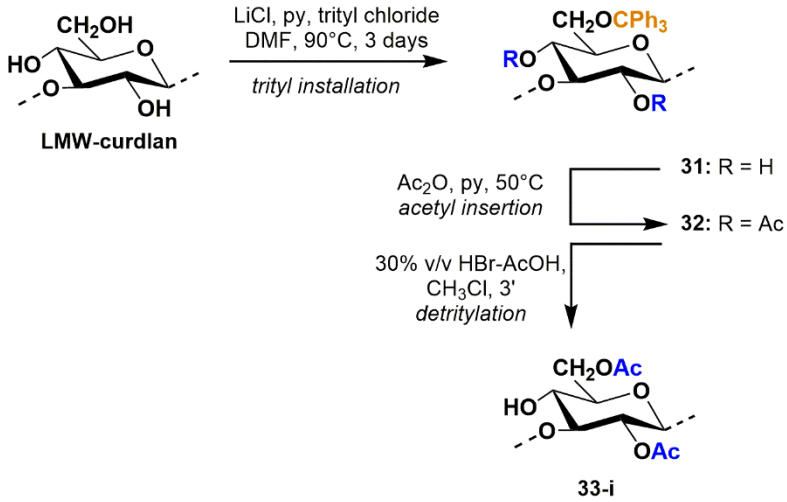

Figure 2.53. Semi-synthetic pathway to obtain 2,6 acetylated LMW-curdlan derivative **33-i**

In particular, the attention was focused on the installation of a sterically hindered trityl ether on the most reactive primary hydroxyl on position 6, by reacting LMW-curdlan with trityl chloride and pyridine in DMF using LiCl as chaotropic agent, to promote the solubility of the polysaccharide. Derivative **31** was then subjected to a global protection through an acetylation reaction using acetic anhydride in pyridine. The subsequent detrytilation reaction on derivative **32** with HBr-AcOH could promote the acetyl migration from position *O*-4 to *O*-6 (Chien and Iwata, **2018)**. The cleavage of trityl PG was confirmed by the absence of any typical signal in the aromatic region in the ^{1}H-NMR spectrum of **33-i** (Figure 2.54).

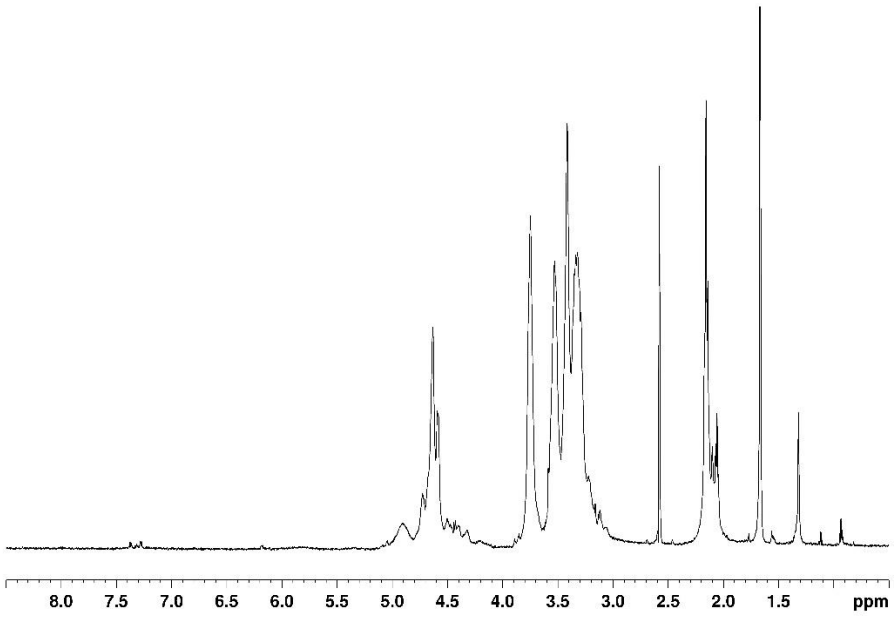

Figure 2.54. ^{1}H NMR spectra (600 MHz, 298 K, DMSO-d_6) of **33-i**

Derivative **33-i** was then subjected to sulfation under standard conditions with SO_3·py in DMF at 50 °C, followed by a treatment under alkaline aqueous conditions to remove the ester moieties which gave derivative **CdS-9**. Besides, a complementary sulfation pattern could be obtained by subjecting directly compound **31** to a sulfation reaction. In this case, the deprotection step also included a treatment under acidic conditions to remove the trityl ether PGs (Figure 2.55).

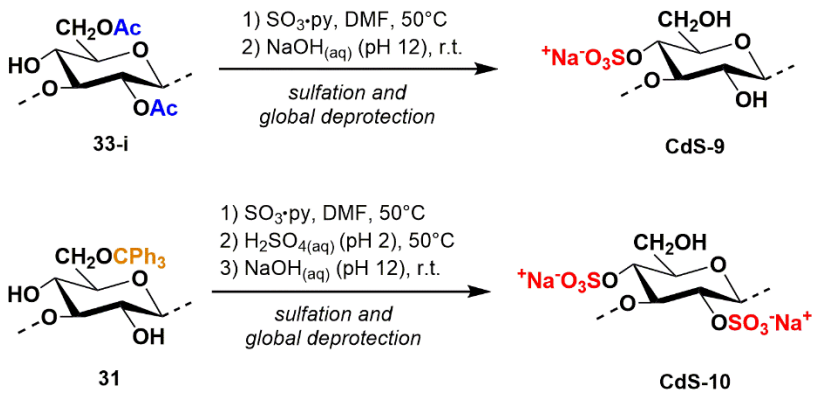

Figure 2.55. Sulfation and global deprotection of the partially protected compounds **33-i** and **31**

Derivative **CdS-9** was subjected to a ^{1}H and 2D-NMR analysis for the structural characterization. A comparison between the $^{1}H,^{13}C$-DEPT-HSQC spectrum of **CdS-9** and starting LMW curdlan showed the absence of any Glc unsulfated units. Moreover, the detection of three anomeric signals at $\delta_{H/C}$ 5.16/100.4, 5.01/101.8 and 4.82/103.4 ppm suggested a heterogeneous structure. In particular, the presence of three species with different sulfation pattern could be hypothesized (Figure 2.56).

A comparison with **CdS-7** allowed the assignment of the most ^{1}H downfield shifted anomeric signal at $\delta_{H/C}$ 5.16/100.4 ppm to per-*O*-sulfated units. Besides, the presence of a $^{1}H,^{13}C$-downfield shift for two *CH*-4 signals suggested the presence of species decorated with sulfate groups on position 4. In particular, by comparison with literature data (Vessella et al. 2021), the presence of Glc 4,6S and Glc 4S units was inferred. The relative integration of the anomeric signals at $\delta_{H/C}$ 5.16/100.4, 5.01/101.8 and 4.82/103.4 ppm revealed the presence of a 42% amount of Glc 2,4,6-*O*-sulfated units together with a 39% amount of Glc 4,6-*O*-disulfated units and a 19% amount of 4-*O* sulfate units. A similar approach was used for the characterization of **CdS-10** and also in this case a heterogeneous structure was detected (Table 2.9).

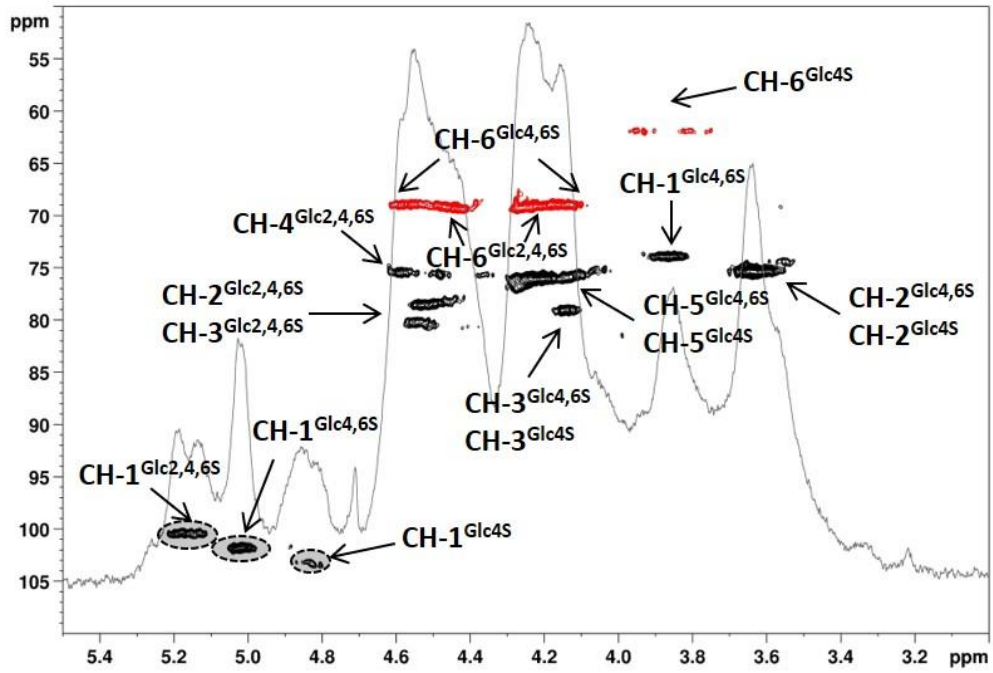

Figure 2.56. ^{1}H and $^{1}H,^{13}C$-DEPT-HSQC NMR spectra (zoom, 400 MHz, 298K, D_2O) of **CdS-9**

Derivative **33** with a 2,6-diacetyl protecting group pattern could be also obtained by performing a three-step, one-pot sequence relying upon the installation of a dimethoxytrityl (DMT) protecting group on the primary hydroxyl, using dimethoxytrityl chloride in DMF, py and LiCl as chaotropic agent. This step was followed by an acetylation reaction of the secondary hydroxyl groups to obtain fully protected compound **35**. Then, the cleavage of DMT moieties could be performed under milder acid conditions with respect to the cleavage of trityl ethers on derivative **32**, using a 80% aqueous solution of AcOH to obtain derivative **33-ii** (Figure 2.57).

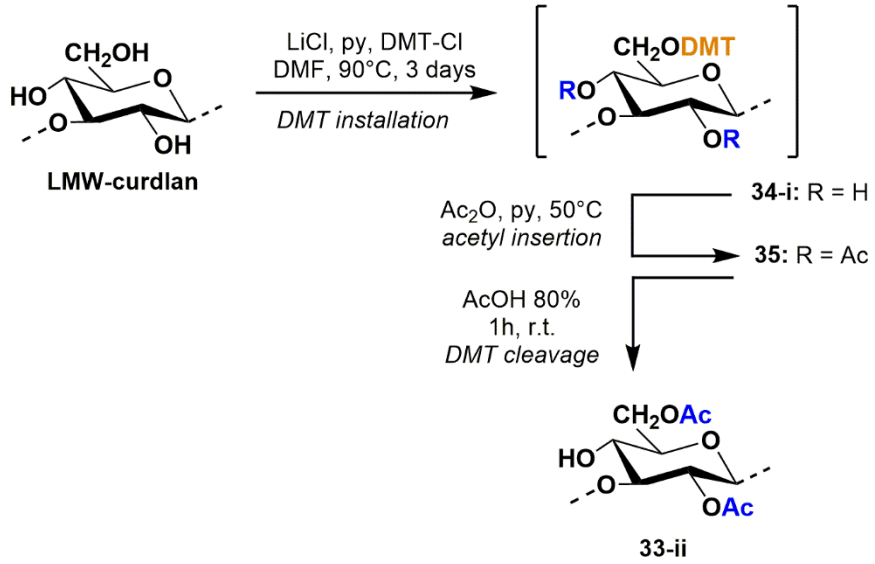

Figure 2.57. One-pot dimethoxytritylation-acetylation step followed by DMT cleavage to obtain **33-ii**

The removal of DMT protecting group was confirmed by the absence of any signals in the aromatic region in the ^{1}H-NMR spectrum. Besides, the presence of acetyl ester groups in the structure of **33-ii** was confirmed by detection of the typical signals at 1.96-2.15 ppm. The partially protected compound was subjected to sulfation under standard conditions with SO_3· py in DMF at 50 °C, followed by a treatment under alkaline aqueous conditions to remove the ester moieties which gave derivative **CdS-11**. Also in this case, the semi-synthesis of the complementary sulfation pattern was attempted by performing a one-pot reaction focused on the installation of DMT, directly followed by sulfation and deprotection steps (Figure 2.58).

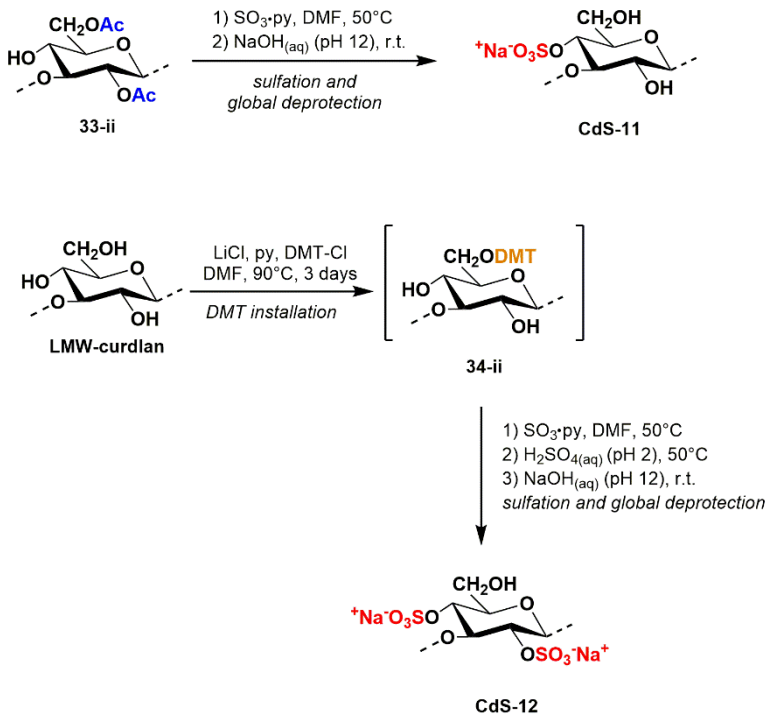

Figure 2.58. Sulfation and global deprotection of the partially protected compound **33-ii** and one-pot dimethoxytritylation-sulfation reaction

The ^{1}H,^{13}C-DEPT-HSQC spectrum of **CdS-11** clearly showed the ^{1}H- and ^{13}C-downfield shift of a methylene signal associated to primary positions of Glc units decorated with sulfate groups on 6-*O*-position. A comparison between the ^{1}H-NMR spectra of **CdS-11** and **CdS-5,6** obtained through direct methods revealed that analogous results were obtained, as the spectra were found to be very similar. The relative integration of methylene signals allowed to estimate a DS equal to 0.66 (Figure 2.60).

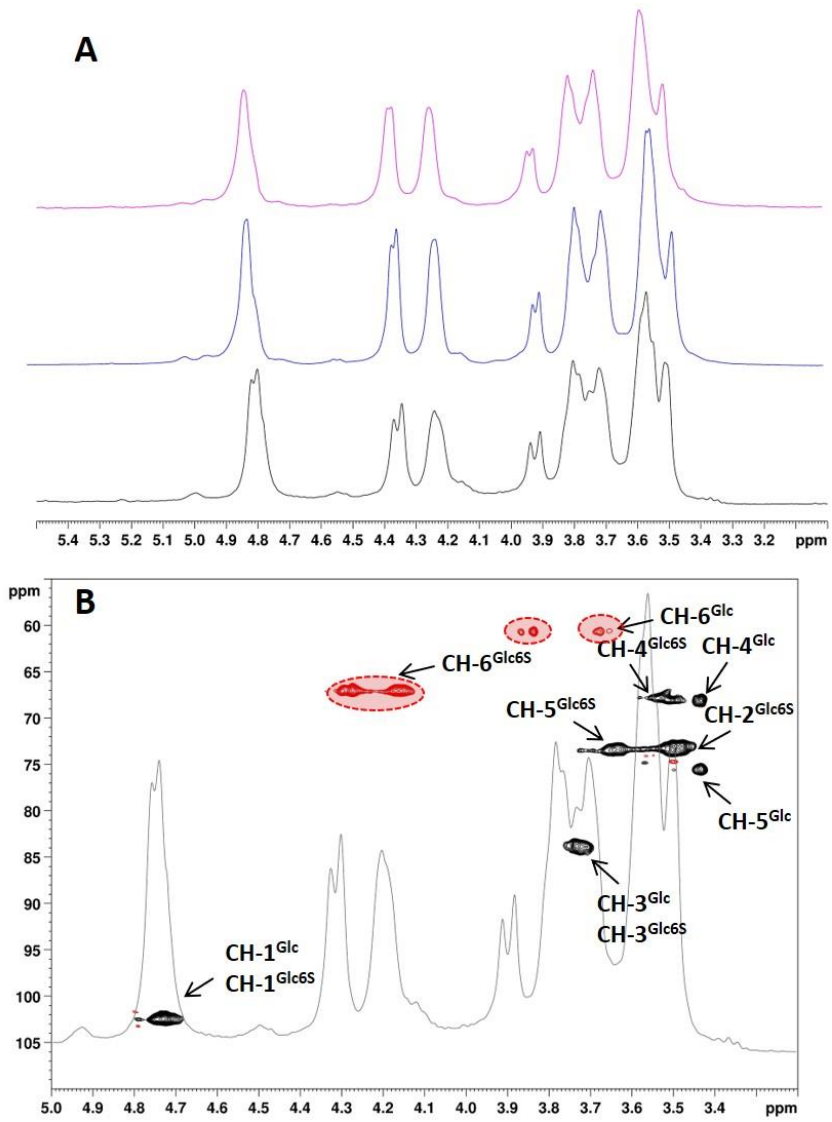

Figure 2.60. (a) ^{1}H NMR spectra (zoom, 600 MHz, 298 K, D_2O) of **CdS-11** (black), **CdS-5** (blue) and **CdS-6** (red); (b) ^{1}H and ^{1}H,^{13}C-HSQC NMR spectra (400 MHz, 298K, D_2O) of **CdS-11**

The regioselective protection of *O*-6 could be also obtained by performing a benzoylation reaction combining Bz_2O as benzoylating agent with DIPEA in DMF (Ren et al., **2018**). The derivatization was confirmed by the presence in the ^{1}H-NMR

spectrum of the typical signals of benzoylated species in the aromatic region and at chemical shifts between δ 4.8 and 5.5 ppm. Derivative **36** was then subjected to sulfation and global deprotection under standard conditions (Figure 2.61).

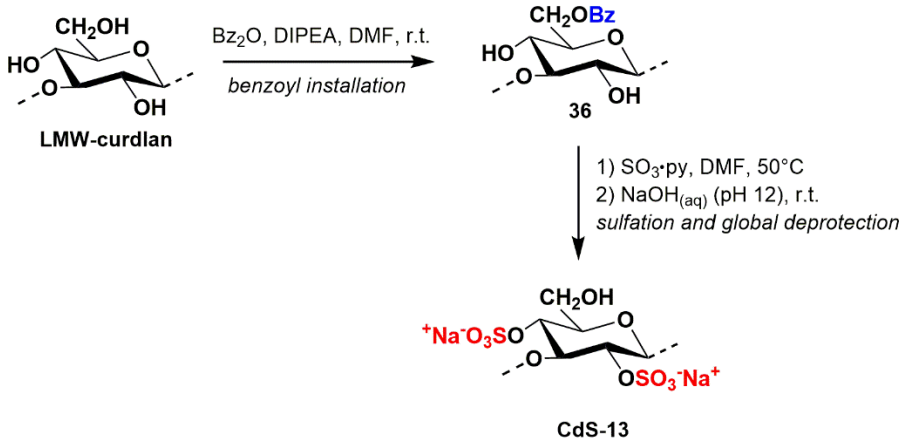

Figure 2.61. Semi-synthesis of **CdS-13**

A detailed 2D-NMR analysis of the polysaccharide derivative **CdS-13** was performed to confirm the presence of sulfate groups on position 2 and 4 of Glc units. By integration of $^{1}H,^{13}C$-DEPT-HSQC peak volumes, the desired derivatization was demonstrated: a 42% average amount of sulfate groups was found on Glc *O*-2,4 positions. Nonetheless, a 46% amount of unsulfated Glc units was also detected together with a minor amount (12%) of Glc2S residues (Figure 2.62).

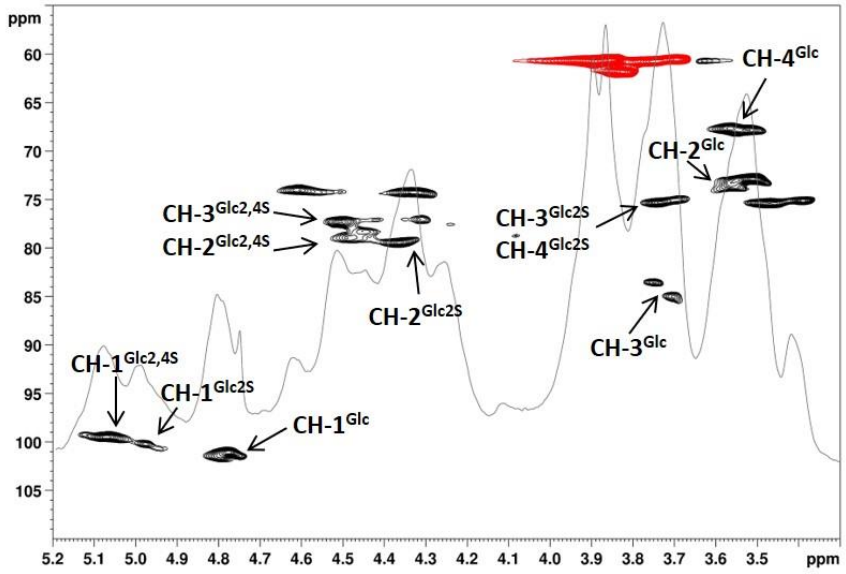

Figure 2.62. ^{1}H and $^{1}H,^{13}C$-HSQC NMR spectra (zoom, 600 MHz, 298K, D_2O) of **CdS-13** (only integrated signals are reported)

The last studies were focused on the employment of cyclic protecting groups: in particular, a different approach, with respect to the previously employed methods based on CPGs installation (Vessella et al., **2021**), was investigated for the installation of *para*-methoxy-benzylidene (PMP) moieties. The LMW curdlan *C*-4 and *C*-6 hydroxyl groups were firstly protected by acetalation under a homogeneous anisaldehyde/DMSO solution using CSA as catalyst and TMOF as dehydrating agent to generate *in situ* the anisaldehyde acetal (Chien et al., **2019**) (Figure 2.63).

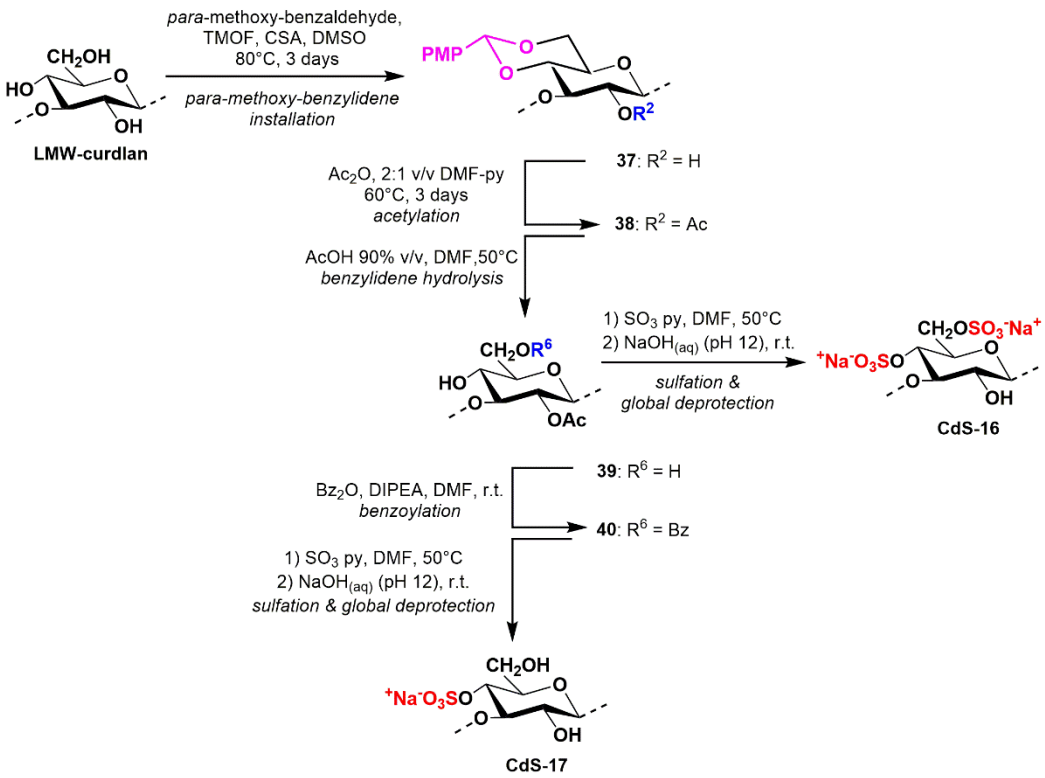

Figure 2.63. Multi-step pathway for the semi-synthesis of **CdS-14** and **CdS-15**

Derivative **37** was then subjected to acetylation reaction using acetic anhydride in a DMF/pyridine mixture. The global protection of the polysaccharide compound **38** was confirmed by the presence in the ^{1}H-NMR spectrum of the typical signals of the *para*-methoxy-benzylidene ring in the aromatic region and at 5.5 ppm and by the signals around 2 ppm assignable to the acetyl moieties. Derivative **38** was subjected to a treatment under mildly acidic conditions to restore the diol at *C*-4,6 positions, as confirmed through ^{1}H-NMR spectrum by the absence of *para*-methoxy-benzylidene signals. Derivative **39** could be directly sulfated to obtain a 4,6-disulfated compound (**CdS-14**) or subjected to regioselective benzoyl installation at primary positions, which gave derivative **40** (Ren et al., **2018**), and then sulfated to obtain a product decorated with sulfate group only on position 4 (**CdS-15**). The structural

characterization of polysaccharide **CdS-14** could be made on the basis of the assignments previously done on the already obtained CdS derivatives. Noteworthy, as expected from the employed pathway, the most abundant Glc units within the polysaccharide backbone were characterized by a 4,6-disulfation pattern (56%), but a minor amount of per-*O*-sulfated units (29%) and Glc 2,4 S units (15%) were also detected (Figure 2.64).

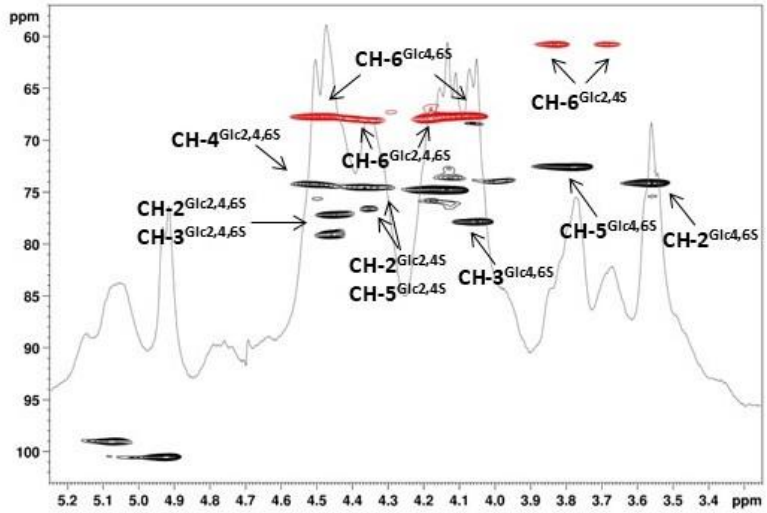

Figure 2.64. ^{1}H and $^{1}H,^{13}C$-HSQC NMR spectra (zoom, 600 MHz, 298K, D_2O) of **CdS-14**

In Table 2.9 are resumed the DS of derivatives **CdS-5-14**, as inferred from NMR assignment data and the distribution of sulfate groups along the polysaccharide backbone, as evaluated from 2D-NMR data.

	DS (NMR)[a]	Sulfation pattern
LMW curdlan	0	-
CdS-5	0.69	Glc 6S (69%); Glc (31%)
CdS-6	0.54	Glc 6S (54%); Glc (31%)
CdS-7	3.00	Glc 2,4,6S (100%)
CdS-8	1.14	Glc (23%); Glc 2S (30%); Glc 4S (10%); Glc 2,4S (37%)
CdS-9	2.23	Glc 4S (19%); Glc 4,6S (39%); Glc 2,4,6S (42%)
CdS-10	1.71	Glc 6S (27%); Glc 4,6S (42%); Glc 2,4,6S (20%)
CdS-11	0.66	Glc 6S (66%); Glc (34%)
CdS-12	1.69	Glc (24%); Glc 6S (14%); Glc 4,6S (31%); Glc 2,4,6S (31%)
CdS-13	0.96	Glc (46%); Glc 2S (12%); Glc 2,4S (42%)
CdS-14	2.29	Glc 2,4S (15%); Glc 4,6S (56%); Glc 2,4,6S (29%)

[a] Estimated by $^{1}H,^{13}C$-HSQC NMR signal volumes integration

Table 2.9. Structural data for semi-synthetic polysaccharides **CdS-5,14**

The structural characterization of **CdS-5,14** will be completed with molecular weight measurements, which will be evaluated by HP-SEC-TDA in collaboration with our partner group (prof. Schiraldi and collaborators at the Department of Experimental Medicine of the University of Campania “L. Vanvitelli).

2.3.3. Conclusions

In this section, the study of the regioselective sulfation of LMW curdlan polysaccharide was attempted. Several different semi-synthetic methods were investigated in order to extend the library of curdlan sulfate derivatives for future structure-activity relationship studies. To this aim, both direct and multi-step methods were developed. As regards direct methods, both mild sulfation and desulfation strategies were investigated. Instead, different multi-step strategies, all relying upon

protection-sulfation-deprotection sequences were carried out. In particular, both acyclic and cyclic protecting groups were tested in order to obtain new curdlan sulfate derivatives with a well-defined sulfation pattern. All the semi-synthesized sulfated polysaccharides were subjected to a detailed characterization of their sulfation pattern through 1D- and 2D-NMR spectroscopy.

For some of them, the structural analysis revealed the presence of unprecedented Glc sulfation patterns as main motifs along the curdlan polysaccharide: for example, 2,4-disulfated Glc units for **CdS-13** obtained by protecting the *O*-6 position with Bz_2O in the presence of DIPEA. This achievement actually enlarges the number of curdlan sulfate polysaccharides on which structure-activity relationship studies could be done. Some experiments to complete the structural characterization are current under investigation. Thereafter, the most interesting products of this library of curdlan sulfate derivatives will be subjected to a study of their immunological properties.

2.3.4. Experimental section

General methods. Commercial grade reagents and solvents were used without further purification, except where differently indicated. Starting curdlan was purchased from Biosynth (Thal, Switzerland). The term "pure water" refers to water purified by a Millipore Milli-Q Gradient system (Merck Millipore, Burlington, MA, USA). Dialyses were conducted on Spectra/Por 3.5 kDa cut-off membranes at 4°C. Centrifugations were performed with an Eppendorf (Hamburg, Germany) Centrifuge 5804R instrument at 4°C (4600 g, 5 min). Freeze-drying was performed with a 5Pascal (Trezzano sul Naviglio, Italy) Lio 5P 4K freeze dryer. NMR spectra were recorded on a Bruker (Billerica, MA, USA) Avance-III HD (^{1}H: 400 MHz, ^{13}C: 100 MHz) or on a Bruker Avance-III (^{1}H: 600 MHz, ^{13}C: 150 MHz) instrument – the latter equipped with a cryo-probe – in D_2O (acetone as internal standard, ^{1}H: $(CH_3)_2CO$ at δ 2.22 ppm; ^{13}C:$(CH_3)_2CO$ at δ 31.5 ppm) or DMSO-d_6 (^{1}H: CHD_2SOCD_3 at δ 2.49 ppm; ^{13}C:

CD_3SOCD_3 at δ 39.5 ppm). Data were processed using the data analysis packages integrated with Bruker TopSpin® 4.0.5 software. Gradient-selected COSY and NOESY experiments were performed using spectral widths of 6000 Hz in both dimensions, using data sets of 2048 × 256 points. $^{1}H,^{13}C$-HSQC and $^{1}H,^{13}C$-HMBC experiments were measured in the ^{1}H-detected mode via single quantum coherence with proton decoupling in the ^{13}C domain, using data sets of 2048 × 256 points and typically 80 increments (160 for HMBC).

Example of mild sulfation. A solution of LMW curdlan (52.7 mg, 0.325 mmol repeating unit) in dry DMSO (1 mL) was treated with SO_3·py (362 mg, 2.28 mmol). After 75' stirring at rt, some drops of a saturated aqueous solution of Na_2CO_3 were added to adjust pH to 7 and then the solution was diluted with 10 mL of pure water. The solution was then dialyzed and freeze-dried to afford **CdS-5** (56.3 mg, 106 % mass yield) as a white solid.

*Polysaccharide **CdS-7**.* A suspension of LMW curdlan (50.2 mg, 0.310 mmol repeating unit) in dry DMF (2 mL) was treated with 2.8 mL of a solution prepared by dissolving *N*,*N*-dimethylformamide-sulfur trioxide complex (SO_3·DMF, 494.3 mg) in 2.9 mL of dry DMF. After 75' stirring at rt, some drops of a saturated aqueous solution of Na_2CO_3 were added to adjust pH to 7 and then the solution was diluted with 15 mL of pure water. The solution was then dialyzed and freeze-dried to afford **CdS-7** (75.1 mg, 147 % mass yield) as a white solid.

*Polysaccharide **CdS-8**.* Per-*O*-sulfated derivative **CdS-7** (25.6 mg, 50.2 μmol repeating unit) was dissolved in pure water (1.0 mL) and passed through a short Dowex-50 WX8 column (H^+ form, 20–50 mesh, approx. 4 cm^3). Elution with pure water was continued until pH of the eluate was neutral. The obtained eluate was treated with some drops of pyridine to neutralize the solution. Freeze-drying of the collected eluate gave per-*O*-sulfated pyridinium salt, that was in turn suspended in

pyridine (2.5 mL) and treated with *N*,*O*-bis(trimethylsilyl)acetamide (BTSA, 422.1 μL, 1.73 mmol). After 20 h stirring at 70°C, the mixture was cooled to rt, then pure water (4.5 mL) was added giving a turbid mixture that was dialyzed for one day. Thereafter, the mixture was passed through a short Dowex-50 WX8 column (H^+ form, 20–50 mesh, approx. 4 cm^3), continuing the elution with pure water until a neutral pH of the eluate was reached. Then some drops of aqueous 1M NaOH were added to neutralize the solution. Dialysis and subsequent freeze-drying gave **CdS-8** (10.7 mg, 42% mass overall yield).

*Compound **31**.* A suspension of LMW curdlan (151 mg, 0.935 mmol repeating unit) in dry DMF (6.1 mL) was treated with LiCl (262 mg, 6.18 mmol), pyridine (1.5 mL) and trityl chloride (521 mg, 1.87 mmol) and stirred at 90°C for 3 days. Thereafter, it was cooled to room temperature and treated with ethanol (30 mL). The obtained yellowish precipitate was collected by centrifugation and dried under vacuum to give derivative **31** as yellow oil.

*Compound **32**.* A solution of **31** (0.620 mmol repeating unit) in dry pyridine (10 mL) was treated with Ac_2O (1.2 mL) and stirred at 50 °C for 20 h, then cooled to 25 °C and treated with ethanol (20 mL) to give a brownish precipitate. This was stirred at rt for 20 h, collected by centrifugation and dried under vacuum to give derivative **32** (141 mg, 44% mass yield) as a brownish powder.

*Compound **33-i**.* A solution of compound **32** (40.1 mg, 77.1 μmol repeating unit) in chloroform ($CHCl_3$, 1.6 mL) was treated with 80 μL of a hydrogen bromide (HBr) solution – 33% wt. in acetic acid and stirred at rt for 3'. The formation of a precipitate was observed. The solid was collected by centrifugation and then suspended in 1.6 mL of aqueous 1M $NaHCO_3$. After overnight stirring at rt, a precipitate was afforded. It was recovered by centrifugation and dried under vacuum to afford derivative **33-i** (30.7 mg, 77% weight yield) as brown powder.

*Compound **35**.* A suspension of LMW curdlan (141 mg, 0.870 mmol repeating unit) in dry DMF (5.6mL) was treated with LiCl (258.3 mg, 6.1 mmol), pyridine (1.3 mL) and dimethoxytrityl chloride (DMT-Cl 1.5 g, 4.35 mmol) and stirred at 90°C for 3 days. Thereafter, it was cooled to room temperature and treated with Ac_2O (1.7 mL) and pyridine (1.7 mL). The mixture was stirred at 50 °C for 20 h, then cooled to 25 °C and treated with ethanol (20 mL) to give a brownish precipitate that was collected by centrifugation and dried under vacuum to give derivative **35** as a brownish oil.

*Compound **33-ii**.* A suspension of **35** (108 mg, 0.368 mmol) in 80% v/v AcOH-pure water (25 mL) was stirred at rt for 1 h. The resulting orange solution was diluted with pure water (30 mL), dialyzed and freeze-dried to afford derivative **33-ii** (155.3 mg, 72% weight yield).

*Polysaccharide **CdS-12**.* A suspension of LMW curdlan (40.9 mg, 0.252 mmol repeating unit) in dry DMF (1.6 mL) was treated with LiCl (74.9 mg, 1.77 mmol), pyridine (380 μL) and DMT-Cl (427 mg, 1.26 mmol) and stirred at 90°C for 3 days. Thereafter, it was cooled to room temperature and treated with a 1.45 M solution of SO_3·py in dry DMF (4.4 mL). After overnight stirring at 50 °C, a saturated NaCl solution in acetone (10 mL) was added at rt and the mixture was then stored at -28 °C for some hours. The obtained white precipitate was collected by centrifugation, then dissolved in pure water (5.0 mL) and the resulting acid mixture (pH ~ 2) was heated to 50 °C. After 2 hours stirring at 50 °C, the mixture was cooled and then treated with a 4M $NaOH_{(aq)}$ solution to adjust pH to 12. The solution was stirred at rt overnight and then neutralized with 1M $HCl_{(aq)}$. Dialysis and subsequent freeze-drying gave **CdS-12** (75.7 mg, 185% weight yield).

*Compound **37**.* LMW-curdlan (1.26 g, 7.79 mmol repeating unit) was suspended in dry DMSO (42 mL) and then heated to 80 °C. After 2 h stirring, a very fine suspension

was obtained. It was cooled to 25 °C and then treated with anisaldehyde (2.8 mL, 23 μmol), trimethyl orthoformate (TMOF, 2.5 mL) and then with CSA (181 mg, 0.779 mmol). The mixture was stirred for 3 days at 80 °C. Thereafter, it was cooled to 25 °C and treated with methanol (60 mL). The obtained yellow precipitate was collected by centrifugation and then dried under vacuum. The procedure was repeated twice to afford derivative **37** (1.01 g, 79% mass yield) as a yellowish powder.

*Compound **38**.* A solution of **37** (230 mg, 0.819 mmol repeating unit) in 2:1 v/v DMF-pyridine (34.1 mL) was treated with Ac_2O (4.5 mL) and stirred at 60 °C for 3 days, then cooled to 25 °C and treated with methanol (67 mL) to give a yellowish precipitate. The mixture was stored at −28°C for some hours, then the obtained precipitate was collected by centrifugation and dried under vacuum. The procedure was repeated twice to give compound **38** (185 mg, 80% weight yield) as yellow powder.

*Compound **39**.* A suspension of **38** (185 mg, 0.572 mmol) in dry DMF (1.6 mL) was treated with 9:1 v/v AcOH-pure water (5.2 mL) and stirred at 50 °C for 24 h. The resulting milky mixture was diluted with pure water (30 mL), dialyzed and freeze-dried to obtain derivative **39** (97.1 mg, 52% mass yield).

Example of regioselective benzoylation. LMW curdlan (78.8 mg, 0.491 mmol repeating unit) was suspended in dry DMF (2.9 mL) and then treated with Bz_2O (550 mg) and DIPEA (1.7 mL). The mixture was stirred overnight at rt, then treated with *i*-Pr_2O (14 mL). The mixture was stored at −28°C for some hours, then the obtained precipitate was collected by centrifugation and dried under vacuum. to give compound **36** (86.5 mg, 109% weight yield) as white powder.

Typical procedure for sulfation and global deprotection. Polysaccharide **31** (0.312 mmol) was suspended in dry DMF (2.7 mL) and then treated with a 1.45 M solution

of SO_3·py in dry DMF (5.7 mL). After overnight stirring at 50 °C, a saturated NaCl solution in acetone (22.6 mL) was added at rt and the mixture was then stored at -28 °C for some hours. The obtained white precipitate was collected by centrifugation, then dissolved in pure water (5.0 mL) and the resulting acid mixture (pH ~ 2) was heated to 50 °C. After 2 hours stirring at 50 °C, the mixture was cooled and then treated with a 4 M $NaOH_{(aq)}$ solution to adjust pH to 12. The solution was stirred at rt overnight and then neutralized with 1 M $HCl_{(aq)}$. Dialysis and subsequent freeze-drying gave **CdS-10** (20.1 mg, 162% weight yield) as a white solid.

References

Chien, C-Y., Enomoto, K., Iwata, T., **2019**. *ACS Sustainable Chem. Eng. 7*, 9857−9864.

Chien, C-Y., Iwata, T., **2018**. *Carbohydr. Polym. 181*, 300-306.

Gao, Y., Fukuda, A., Katsuraya, K., Kaneko, Y., Mimura, T., Nakashima, H., Uryu, T., **1997**. *Macromolecules 30*, 3224–3228.

Jin, Y., Mu, Y., Zhang, S., Li, P., Wang, F., **2020**. *Int. J. Biol. Macromol.146*, 273−284.

Kalyanasundaram, G. T., Doble, M., Gummadi, S. N., **2012**. *AMB Express 2*, 31.

Li, P., Tan, H., Xu, D., Yin, F., Cheng, Y., Zhang, X., Liu, Y., Wang, F., **2014**. *Carbohydr. Polym. 110*, 446−455.

Ren, B., Gan, L., Zhang, L., Yan, N., Dong, H., **2018**. *Org. Biomol. Chem. 16*, 5591–5597.

Takano, R., Kanda, T., Hayashi, K., Yoshida, K., & Hara, S., **1995**. *J. Carbohydr. Chem. 14*, 885–888.

Vessella, G., Esposito, F., Traboni, S., Di Meo, C., Iadonisi, A., Schiraldi, C., Bedini, E., **2021**. *Carbohydr. Polym. 269*, 118324.

Zhan, X.-B., Lin, C.-C., Zhang, H.-T., **2012**. *Appl. Microbiol. Biotechnol. 93*, 525−531.

Zhang, R., & Edgar, K. J., **2014**. *Biomacromolecules 15*, 1079−1096.

CHAPTER 3

DEVELOPMENT OF METHODS FOR THE PHOSPHORYLATION OF POLYSACCHARIDES

3
DEVELOPMENT OF METHODS FOR THE PHOSPHORYLATION OF POLYSACCHARIDES

Introduction

Phosphorylated polysaccharides are anionic analogues of sulfated ones, wherein the phosphorylation reactions typically occur through the functionalization of some hydroxyls with phosphate groups (see also Paragraph 1.3.3). Despite the crucial roles played by anionic polysaccharides in biology and medicine, as previously noted for sulfated polysaccharides, and the abundant presence of anionic phosphate groups in nature in the form of structural compounds (*e.g.*, phospholipids), genetic materials (*e.g.*, DNA and RNA), and energy storage materials (*e.g.*, ATP), studies related to carbohydrate-based phosphorylated polymers remain underdeveloped. Phosphorylation of native polysaccharides can enhance their biological activities or even impart novel ones. For example, the presence of phosphate groups along the polysaccharide backbone reduces high viscosity and improves water solubility and chelating properties (Schunli et al., **2021**). In addition, an interesting research on polysaccharide modification via phosphorylation suggests that, due to this process, phosphorylated polysaccharides have been shown to prevent hydroxyl radical chain reactions, thus exhibiting better antioxidant activity and enhanced hydroxyl radical-scavenging ability (Xie et al., **2020**; Chen and Huang, **2019**). Other biological activities of natural polysaccharides improved by the presence of phosphorus include antitumor, antiviral, hepatoprotective, antibacterial, anticoagulant and antihyperlipidemic activity (Schunli et al., **2021**; Laffargue et al., **2023**).

The introduction of phosphate groups, in particular phosphoric monoester functionalities, into well-known polysaccharides has been described using different reaction systems. The most straightforward method involves esterification reactions with phosphorylating agents, wherein the phosphorus can be covalently attached to the polysaccharide chain via a reaction with hydroxyl groups. Typically, primary groups are more nucleophilic than the secondary alcohols, leading to partial or full regioselectivity in the reaction. Depending on the employed phosphorylation agent, two types of phosphorus containing moieties can be embedded into the polysaccharide chain: phosphonate or phosphonic acid groups ($ROPO_2H_2$) in the case of reactions performed with phosphorous acid (H_3PO_3) or derivatives thereof, and phosphate or phosphoric acid groups ($ROPO_3H_2$) obtained with phosphoric acid or derivatives thereof, other chemical phosphorylating agents or through enzymatic phosphorylation (Laffargue et al., **2023**).

A widely used method to introduce monophosphate moieties onto polysaccharides involves the use of phosphoric acid (H_3PO_4) as the phosphorylating agent. In literature, different reaction conditions are reported. These strategies share the common feature of using an excess of phosphoric acid at high temperature ranging between 120–155 °C. Often, urea is added to a polar solvent, especially DMF, in order to favour the phosphorylation reaction. Nonetheless, the installation of phosphate groups on a polysaccharide backbone is limited by several issues. In most cases, the insolubility of the starting polysaccharides in water and in common organic solvents, as well as their susceptibility to decomposition at high temperature, causes low degree of derivatization, typically between 0 and 0.35. An alternative method involves the use of phosphorus oxychloride ($POCl_3$). In this approach, the polysaccharide is typically treated with DMF at room temperature before being added to a $POCl_3$/pyridine solution at a specific temperature and stirred for a defined time interval. However, during the reaction the presence of $POCl_3$ can lead to polysaccharides degradation due to an increase in the concentration of hydrogen ions: for this reason, alkaline reagents are usually employed in combination with $POCl_3$,

e.g. pyridine. In addition, chlorination of the polysaccharide may occur as a side-reaction and the phosphorus content in the final product is often rather low (Illy et al., **2015**; Vigo and Welch, **1974**). Among the most common phosphorylating agents, phosphorus pentoxide (P_4O_{10}) must be mentioned too, although it is less suitable for phosphorylation of polysaccharides, as it tends to degrade the polysaccharides due to the strongly acidic reaction environment. Indeed, before taking part to the reaction, phosphoric anhydride must be dissolved in a suitable solvent, usually methanesulfonic acid, which could lead to polysaccharide degradation, drastically reducing the molecular weight of the polymer (Nishi et al., **1986**).

The degree of derivatization and phosphorylation pattern are crucial factors influencing the biological activity of phosphorylated polysaccharides. Therefore, to determine the appropriate derivatization pattern and to synthesize structurally well-defined products are essential issues for obtaining optimal biological activities. Within this frame, in this chapter the possibility to achieve the phosphorylation of naturally occurring polysaccharides was investigated testing both standard or novel methods. In particular, two polysaccharides (chondroitin from *E. coli* and chitosan) have been selected. These compounds already in their native or sulfated form, exhibit interesting properties. Therefore, we supposed that a comparison between the bioactivities of such polysaccharides in their sulfated or phosphorylated form could give interesting insights towards the discovery of polysaccharide derivatives with novel therapeutics properties.

References

Chen, L., Huang, G., **2019**. *Int. J. Biol. Macromol. 125*, 256–261

Illy, N., Fache, M., Ménard, R., Negrell, C., Caillol, S., Ghislan, D., **2015**. *Polym. Chem. 6*, 6257–6291

Laffargue, T., Moulis, C., Remaud-Siméon, M., **2023**. *Biotechnolog. Adv. 65*, 108140.

Nishi, N., Ebina, A., Nishimura, S., Tsutsumi, A., Hasegawa, O., Tokura, S., **1986**. *Int. J. Biol. Macromol. 8*, 311–317.

Shunli, X., Yongcong, Z., Xue, W., Qirui, F., Xiaoyi, D., Mei, C., Tao, H., **2021**. *Int. J. Biol. Macromol. 184*, 946−954.

Vigo, T.L., Welch, C.M. **1974**. *Carbohydr. Res. 32*, 331–338.

Xie, L., Shen, M., Wen, P., Hong, Y., Liu, X., Xie, J., **2020**. *Food Chem. Toxicol. Int. J. Publ. Br. Ind. Biol. Res. Assoc. 145*, 111754.

SECTION 3.1 – SCREENING OF REGIOSELECTIVE METHODS FOR THE PHOSPHORYLATION OF BACTERIAL CHONDROITIN

3.1
SCREENING OF REGIOSELECTIVE METHODS FOR THE PHOSPHORYLATION OF BACTERIAL CHONDROITIN

3.1.1. Chondroitin: structure and activities

Chondroitin sulfate (CS) is a typical linear sulfated glycosaminoglycan found in both vertebrates and invertebrates, composed of a hundred or more repeating disaccharide units, composed by D-GlcA and D-GalNAc residues. The resulting disaccharide repeating units can be variously sulfated. In mammals, CS is a key constituent of the ECM, where several saccharide chains are covalently attached to proteins forming large proteoglycans, and it is also abundant in bones, cartilages, skin, and nerve tissues (Mikami and Kitagawa, **2013**). Depending on CS degree of polymerization, the entire size of the proteoglycan ranges from as small 10 kDa to as large 3500 kDa (Silbert and Sugumaran, **2002**). According to the different sulfated locations and degrees, CS is classified into different types, commonly identified by a letter (Pomin, **2013**) (Figure 3.1).

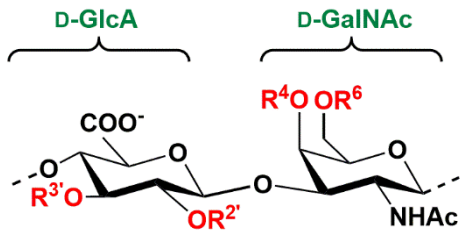

	0	A	C	U	V	B	D	E	K	L	R	M	S	S'	T
$R^{2'}$	H	H	H	*S*	H	*S*	*S*	H	H	H	*S*	H	*S*	*S*	*S*
$R^{3'}$	H	H	H	H	*S*	H	H	H	*S*	*S*	*S*	*S*	*S*	*S*	H
R^{4}	H	*S*	H	H	H	*S*	H	*S*	*S*	H	H	*S*	*S*	H	*S*
R^{6}	H	H	*S*	H	H	H	*S*	*S*	H	*S*	H	*S*	H	*S*	*S*

S = SO_3^-

Figure 3.1. Repeating unit of chondroitin sulfate (CS) and its sulfation pattern

The sulfate group distribution seems to be a result of the evolution, to let CS play key roles in complex biological processes typical of higher animals (*e.g.* central nervous system development). Indeed, simple and evolutionary more ancient organisms, such as bacteria and nematodes, possess only or mostly unsulfated chondroitin (Yamada et al., **2007**). Sulfation pattern can be subjected to variations also depending on tissue source and, in higher animals, on different physio-pathological conditions, such as aging, inflammation and tumour formation (Collin et al., **2017**).

The sulfate groups on CS backbone confer the ability to interact with other molecules, thereby influencing its multifaceted biological and pathophysiological functions. CS is recognized as cell surfaces receptor for pathogens, co-receptors, and signal modulators (Mikami and Kitagawa, **2013**), including parasites, bacteria and viruses (Uyama et al., **2006**), and several humoral factors to stimulate neurite outgrowth or the proliferation/maintenance of neural stem and progenitor cells (Mizumoto et al., **2015**). CS possesses anti-inflammation bioactivity, both directly and indirectly, that is exploited for the treatment of osteoarthritis patients (Uebelhart et al., **2004**). Additionally, according to *in vitro* and *in vivo* investigations, CS may exhibit anti-

thrombotic, anti-coagulant, anti-oxidative, anti-diabetic and anti-obesity bioactivities (Table 3.1).

Bioactivity	Component	Biological Effects
Anti-inflammation	CS	Repress the expression of genes encoding proteolytic enzymes; inhibit IL-1β-induced expression of the pro-inflammatory genes iNOS and COX-2 and restores TGF-β receptors I and II mRNA levels.
Anti-thrombus	CS-E	Enhances plasminogen activation.
Anti-coagulation	*O*-sulfonated CS	Increases anti-factor IIa activity and anti-factor Xa activity.
Anti-oxidation	CS and CS–metal complex	Enhance hydroxyl radical or superoxide radical scavenging activity.
Anti-tumor	CS-C	Influences tumor-associated inflammation; affects NF-κB signaling and cell behavior and regulates cytokine/chemokine activity.
Anti-viral	CS-E	Interferes with the binding of viral gC to a CS-E-like receptor on the cell surface.
Anti-diabetes	CS	Reduces the digestion of carbohydrates; reduces hyperglycemia.
Anti-obesity	CS	Ameliorates obesity; prevents the gaining of body weight, liver weight, and adipose tissue weight; maintains lower food consumption; inhibits the intestinal absorption of triglyceride; adjusts the serum endotoxin level.
Neuroprotective	CS sodium salt	Downregulates P-Ser129 α-synuclein and total α-synuclein expression; inhibits ROS overproduction and changes mitochondrion-mediated apoptotic pathways.
Wound healing	CS aerogel	High hydration and rapid setting to the wound bed.
Proliferation and bone formation	CS and Glucosamine	Proliferates chondrocytes; increases remaining cartilage and trabecula.
Protective bladder barrier	CS	Contributes to urothelial barrier function.

Table 3.1. List of CS bioactivities

In the biomaterial field, as a consequence of its biocompatibility, non-toxicity, good biodegradability, and anionic properties, CS can be employed as the functional component in biomaterials such as functionalized hydrogels and scaffolds for tissue engineering applications. For instance, CS-containing scaffolds are employed in nucleus pulposus, corneal stromal, tendon, bone, and cartilage tissue engineering (Qingshan et al., **2023**). Moreover, due to its non-immunogenicity, CS has attracted increasing attention for its potential use as a drug delivery system, particularly for colon-targeted drug, as it is resistant to digestion by enzymes in the stomach or small intestine and it is primarily degraded by microorganisms in the colon (Amhare et al., **2021**). Finally, chondroitin, the unsulfated precursor of CS, obtained from

biotechnological production processes, has been tested in *in vitro* models of osteoarthritis and wound healing, both alone and in combination with high molecular weight hyaluronic acid, showing promising biophysical and biological features. Indeed, it supports primary cell proliferation, prompting stem cells differentiation, and aids in wound healing (Vassallo et al., **2022a**; Vassallo et al., **2022b**). Additionally, very recently unsulfated chondroitin has been used *in vivo*, demonstrating its ability to reduce pain and pain-related proinflammatory mediators in an osteoarthritic mouse model (Cimini et al., **2022**; Cimini et al., **2023**). In this frame, numerous biotechnological methods have been developed for an alternative access to CS or CS-like products from non-animal sources, addressing these challenges through enzymatic and chemical synthesis as well as microbial fermentation. These methods provide an environmentally sustainable alternative and enable the obtainment of sulfated GAG mimics and analogues with enhanced properties and well-characterized structures. In this context, in the past years in our laboratories several research efforts have been spent towards the semi-synthesis of chondroitin sulfate derivatives starting from a microbial sourced unsulfated chondroitin.

The replacement of sulfate groups with phosphate groups in GAGs (pGAGs) is an attractive research area, as the differences between phosphate and sulfate groups (*e.g.*, size, polarity, acid-base and chelation properties) could affect protein interactions, providing pGAGs with unique biochemical activities. For these reasons, we decided to extend the research area about the chemical manipulation of bacterial chondroitin by studying the possibility to obtain a library of phosphorylated chondroitin derivatives with well-defined phosphorylation patterns. Starting from an unsulfated chondroitin (CS-0) polysaccharide, derived from the fed-batch fermentation of *Escherichia coli* O5:K4:H4, the goal was to design new semi-synthetic approaches for the regioselective installation of phosphate groups on the polysaccharide backbone in order to obtain semi-synthetic functionalized compounds with new or improved activities.

3.1.2. Results and discussion

As anticipated in paragraph 1.3.3., the possibility to obtain phosphorylated mimics of GAGs could open access to a class of compounds with new or enhanced biological properties compared to their natural counterparts. The substitution of the sulfate groups of GAGs with phosphates could be attractive due to the unreported activities that pGAGs might confer to biochemical systems. To this aim, this section is focused on the construction of a library of semi-synthetic chondroitin phosphate derivatives (CP) with various phosphorylation patterns. In this frame, the screening of different phosphorylating reagents and/or reaction conditions was investigated. In particular, a number of novel methods for the (poly)-phosphorylation of complex biomolecules such as peptides, carbohydrates, oligonucleotides and secondary metabolites recently appeared in literature (Domon et al., **2020**; Lin et al., **2022**; Ociepa et al., **2021**). They share a high chemoselectivity and the unprecedented employment of P(V) phosphorylating agents, that are not only much milder than the standard phosphorylating reagents (*e.g.* H_3PO_4 or $POCl_3$) but also more biomimetic than the classical phosphoramidite-type P(III) reagents (Knouse et al., **2021**). So, in this thesis work two of these novel methods (Domon et al., **2020**; Ociepa et al., **2021**) have been tested and compared to H_3PO_4 and $POCl_3$ standard procedures. The structures of all the employed phosphorylating reagents are shown in Figure 3.2.

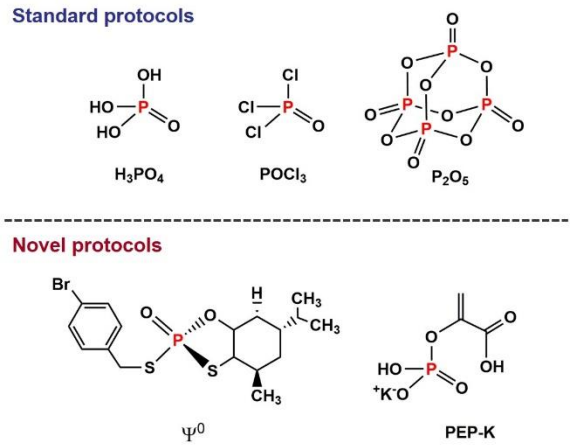

Figure 3.2. Chemical structures of P(V)-based phosphorylating agents employed on chondroitin

Moreover, some experiments were conducted using microwave irradiation. In modern organic chemistry, the use of microwaves in driving chemical reactions appears to offer rapid heating and potential rate enhancement over conventional methods, as microwave irradiation provides a highly efficient form of heating, allowing energy to be directly absorbed by the reactants (Dudley et al., **2015**). In this frame, microwave heating could lead to positive effects in the phosphorylation reactions, such as increased yield, selectivity, and accelerated rate of reaction.

First of all, this study began with the semi-synthesis of substrates employed for the regioselective phosphorylation reactions. Starting from a microbial sourced, unsulfated chondroitin (CS-0) deriving from the fed-batch fermentation of *Escherichia coli* O5:K4:H4 (Cimini et al., **2018**), a set of CS-0 derivatives, having a different pattern of protecting groups distributed within the disaccharide repeating unit, was prepared (Figure 3.3).

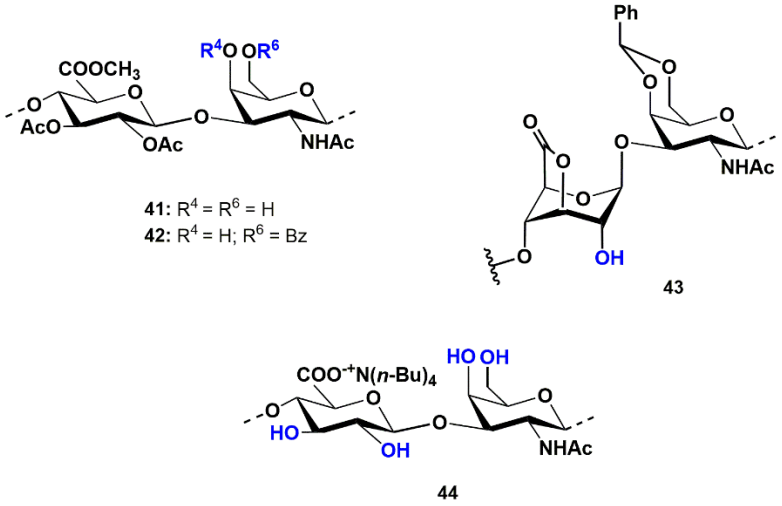

Figure 3.3. Set of CS-0 starting substrates used for phosphorylation reactions

Derivatives **41-42** were semi-synthetized from CS-0 through known procedures (Vessella et al., **2019a**; Vessella et al., **2019b**; Vessella et al. **2021a**). Briefly, compound **41** was obtained through a multi-step procedure on a methyl ester derivative of CS-0, based on the installation of cyclic benzylidene protecting groups on *O*-4 and *O*-6 position of GalNAc units followed by an acetylation step for the full protection of GlcA residues. Finally, the 4,6-diol reinstatement was possible through a hydrolysis reaction conducted in aqueous acidic solution. The obtained derivative 41 was then protected regioselectively at the primary hydroxyl position of GalNAc-6 sites by mild benzoylation to afford derivative **42**. Instead, derivative **43** was prepared using a procedure focused on the installation of a benzylidene PG on GalNAc units and then the formation of a lactone ring on GlcA units (Figure 3.4).

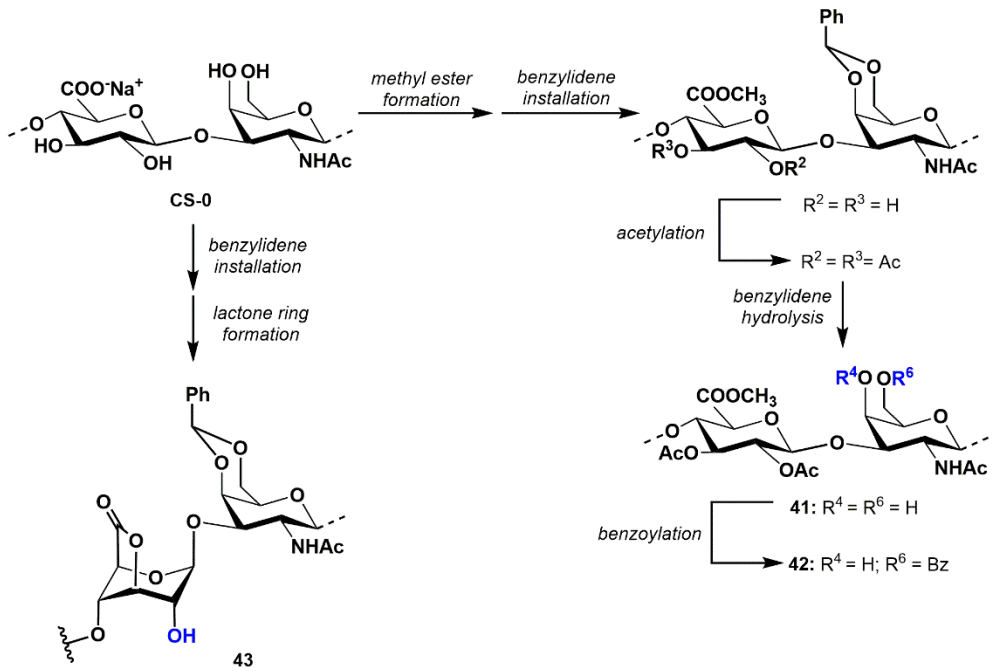

Figure 3.4. Schematic representation of protection steps (Vessella et al., **2019a**; Vessella et al., **2019b**; Vessella et al. **2021a**)

Finally, derivative **44**, without any protecting group and having a *n*-tetrabutylammonium as GlcA carboxylate counterion, was also prepared (Vessella et al., **2021b**), in order to increase the solubility in organic solvents of the unprotected CS-0 polysaccharide to be tested for the regioselective phosphorylation at the most reactive site of its repeating unit, *i.e.* primary hydroxyl at GalNAc-6 position.

The screening of phosphorylation reactions started by subjecting derivative **44** to two standard procedures using H_3PO_4 and urea in DMF at high temperatures (120-150°C) or $POCl_3$ and pyridine in DMF at room temperature. The recently introduced biomimetic procedure for alcohol phosphorylation (Domon et al., **2020**) using a combination of PEP-K and tetrabutylammonium hydrogen sulfate TBAHS in DMF at 80°C, was also tested (Table 3.2). Finally, a phosphorylation procedure, employing the chiral, limonene-derived reagent Ψ^{O} in combination with DBU as hindered base and very recently demonstrated to work efficiently on both simple and medicinally

relevant alcohols (Ociepa et al., **2021**), completed the screening. A subsequent treatment with aqueous NaOH was also performed in all cases, in order to substitute GlcA carboxylate tetrabutylammonium counterion with Na^+. Finally, a sequential purification by dialysis and size-exclusion chromatography furnished products **CP-1,4**.

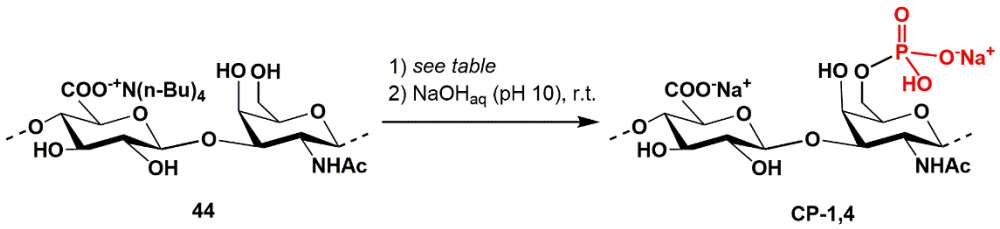

entry	product	precursor	phosphorylation conditions[a]	phosphorylation position (DPh)
1	**CP-1**	**44**	H_3PO_4, urea, 120°C, 3h	GalNAc *O*-6 (49%)
2	**CP-2**	**44**	$POCl_3$, pyridine, rt, 18h	--
3	**CP-3**	**44**	Ψ^O, DBU, rt, 1h	--
4	**CP-4**	**44**	PEP-K, TBAHS, 80°C, 48h	GalNAc *O*-6 (36%)

[a] Reactions were all conducted in dry DMF

Table 3.2. Phosphorylation tests on precursor **44** with different reagents

Firstly, derivatives **CP-1,4** were subjected to ^{1}H-NMR spectra and compared with *E. coli*-sourced CS-0 starting material. This comparison showed the presence of new signals at δ 3.87, 4.02 and 4.16 in **CP-1** and **CP-4** spectra, while no clear differences between CS-0 and **CP-2** or **CP-3** derivatives were detected. In order to have a more detailed structural characterization of derivatives **CP-1,4**, a set of ^{1}H,^{1}H-, ^{1}H,^{13}C- and ^{1}H,^{31}P-2D-NMR spectra were also measured.

The analysis of the $^{1}H,^{13}C$-DEPT-HSQC 2D-NMR spectrum (Figure 3.5) revealed the presence of two methylene signals, at $\delta_{H/C}$ 4.02/65.6 and 3.73-3.82/62.4. The former could be assigned to the CH_2 group at position *O*-6 of 6-phosphorylated GalNAc (GalNAc6P) units by the main signal detected at $\delta_{H/P}$ 4.02/0.73 in the $^{1}H,^{31}P$-HSQC 2D-NMR spectrum, while the latter was due to unsubstituted GalNAc 6-*O*-CH_2 moieties as confirmed by comparison with CS-0 spectra. A relative integration of the two methylene signals volumes in the $^{1}H,^{13}C$-DEPT-HSQC spectrum of **CP-1** and **CP-4** returned a similar degree of phosphorylation (DPh) for the two CP products (49% and 36% for **CP-1** and **CP-4**, respectively). Apart the signal at δ 0.73, the ^{31}P-NMR spectrum of **CP-4** revealed also a marked peak at δ 0.28, that could be assigned by a ^{31}P-DOSY 2D-NMR spectrum to residual, fast diffusing inorganic phosphate, in agreement with literature reporting the difficulty in dialyzing it quantitatively from phosphorylated polysaccharides (Lowman, Ensley, & Williams, **1998**).

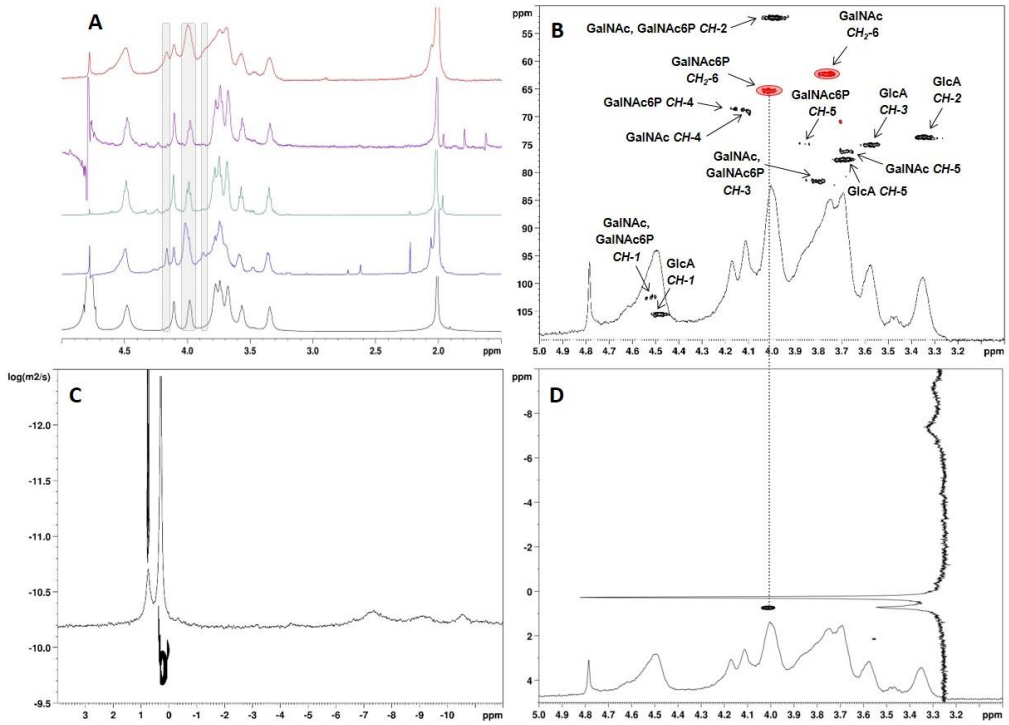

Figure 3.5. (A) ^{1}H-NMR spectra (400 MHz, 298K, D_2O) of CS-0 (black), **CP-1** (blue), **CP-2** (green), **CP-3** (purple) and **CP-4** (red) (the grey stripes highlight the main differences among the spectra); (B) superimposed ^{1}H-NMR and ^{1}H,^{13}C-DEPT-HSQC 2D-NMR spectra (400 MHz, 298K, D_2O, zoom) of **CP-4** (densities enclosed in red circles were integrated for DPh estimation); (C) ^{31}P-NMR and ^{31}P-DOSY 2D-NMR spectra (162 MHz, 298K, D_2O, zoom) of **CP-4**; (D) superimposed ^{1}H-, ^{31}P-NMR and ^{1}H,^{31}P-HSQC 2D-NMR spectra (400 and 162 MHz, 298K, D_2O, zoom) of **CP-4**

Furthermore, to increase the DPh on GalNAc 6-*O* position, the reaction under standard condition was repeated twice, getting a negligible enhancement (0.51, Table 3.3 entry 1), while an increase of temperature to 150°C (entry 2) afforded **CP-6** product with a quantitative DPh at GalNAc *O*-6 position. Starting from the latter achievement, a screening of microwave irradiation conditions for the same phosphorylation reaction was conducted in order to compare the results to the conventional heating technique. Lower reaction time (2 h) and temperature (80°C) were firstly tested to give **CP-7**

product, after *n*-tetrabutylammonium/Na^+ exchange and purification by dialysis. No derivatization was achieved under these conditions, as detected by comparing ^{1}H-NMR spectra of **CP-7** and starting CS-0.

Therefore, stronger microwave irradiation conditions were tested, increasing the temperature from 80°C to 100/120 °C, the microwave irradiation power from 13 W to 50/100W and the pressure from 20 psi to 50/300 psi (Table 3.3, entries 3, 4, 5). Finally, under the strongest microwave irradiating conditions, the regioselective installation of the phosphate group at GalNAc *O*-6 site was also attempted by prolonging the reaction of chondroitin *n*-tetrabutyl-ammonium carboxylate salt for 3 h at 120°C under 100W microwave irradiation at 300 psi, affording derivative **CP-11**.

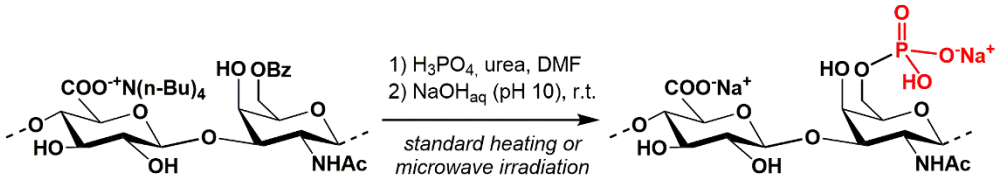

44 **CP-5,11**

entry	product	conditions	DPh[a]
1	**CP-5**	conventional heating: 120°C, 3h (twice)	0.51
2	**CP-6**	conventional heating: 150°C, 3h	1.00
3	**CP-7**	microwave irradiation: 80°C, 1h, 13W, 20 psi	0
4	**CP-8**	microwave irradiation: 100°C, 1h, 50W, 50 psi	0.12
5	**CP-9**	microwave irradiation: 120°C, 1h, 100W, 50 psi	0.20
6	**CP-10**	microwave irradiation: 120°C, 1h, 100W, 300 psi	0.27
7	**CP-11**	microwave irradiation: 120°C, 3h, 100W, 300 psi	0.83

[a] Degree of phosphorylation at GalNAc *O*-6 site, measured by relative integration of CH_2 signal at 3.92/64.5 and 3.75/62.3 ppm assigned to GalNAc-6 phosphate and GalNAc CH_2-6, respectively, in the ^{1}H,^{13}C-DEPT-HSQC 2D-NMR spectrum (Figures **3.6** a,c)

Table 3.3. Phosphorylation tests on **44** with H_3PO_4, urea and DMF under different reaction conditions

A set of 1D- and 2D-NMR experiments, comprising ^{1}H-, ^{31}P-, ^{1}H,^{31}P-HSQC and ^{1}H,^{13}C-DEPT-HSQC spectra was recorded in order to obtain a detailed structural characterization of derivatives **CP-6,11**.

As regards compound **CP-11**, the latter spectrum showed only two signals sensibly shifted to different chemical shift values with respect to starting CS-0, at $\delta_{H/C}$ 3.77/73.6. These could be assigned to CH-5 and CH_2-6 atoms of GalNAc-6-phosphate units, respectively, by comparison with previous results (see Figure 3.4). By integrating the signals at $\delta_{H/C}$ 3.92/64.5 and 3.76/62.5 – assigned to GalNAc-6-phosphate and underivatized GalNAc units, respectively – a DPh equal to 0.83 was calculated. This value was considerably higher with respect to the DPh resulting from the reaction conducted under the same conditions but with standard heating **(CP-1,5)**. As anticipated, an increase of temperature to 150°C using conventional heating (entry 2) afforded **CP-6** product with a quantitative DPh at GalNAc *O*-6 site. Nonetheless, its ^{1}H,^{13}C-DEPT-HSQC 2D-NMR spectrum showed also a remarkably downfield shifted CH signal at $\delta_{H/C}$ 4.60/73.9 (Figure 3.6c), which could be associated to the phosphorylation of a secondary OH by the cross-peak at $\delta_{H/P}$ 4.60/-0.4 in the ^{1}H,^{31}P-HSQC 2D-NMR spectrum (Figure 3.6d). The higher structural heterogeneity of **CP-6** sample was related not only to the presence of multiple phosphorylation sites but also to the detection of peaks in different regions of its ^{31}P and ^{31}P-1D-DOSY spectra. Indeed, together with broad peaks at 2.0 and -0.4 ppm assigned to monophosphate groups at the two different derivatization positions, some additional signals of similar intensity were detected at -7.0, -10.5 and -11.2 ppm. These could be assigned to diphosphate groups, as clearly evidenced by the ^{1}H,^{31}P-HSQC 2D-NMR spectrum of **CP-6** (Figure 3.6d), showing cross-peaks at $\delta_{H/P}$ 4.06/-10.5 and 4.62/-11.2. In particular, the latter could be assigned to the phosphorus atoms of diphosphate groups directly attached to the polysaccharide (α-phosphorus atoms), while the ^{31}P-signal at -7.0 ppm, that was not correlated to any ^{1}H signal in the ^{1}H,^{31}P-HSQC 2D-NMR spectrum, could be assigned to the distal phosphorus atoms of both diphosphate groups (β-phosphorus atoms) (Zhao et al., **2021**; Pondel'kina et al., **2023**) A minor

amount of triphosphate groups decorating the chondroitin backbone could be also inferred by the less intense ^{31}P signal at -20.0 ppm, that could be assigned to their middle β-phosphorus atoms, being the α- and γ-ones (closest and farthest to the attachment site on the polysaccharide backbone, respectively) overlapped with α- and β-phosphorus signals of diphosphate groups (Zhao et al., **2021)**. Interestingly, the presence of minor signals associated to diphosphate groups could be detected also in **CP-11 (**Figures 3.6 a,b) product from microwave irradiated phosphorylation. Noteworthy, increasing the DPh at higher values under conventional heating eroded the desired phosphorylation regioselectivity, while the reaction conducted under microwave irradiation did not. Moreover, in both cases high DPhs also resulted in a higher presence of diphosphate or even triphosphate moieties, in addition to the desired monophosphate groups, attached to polysaccharide chain.

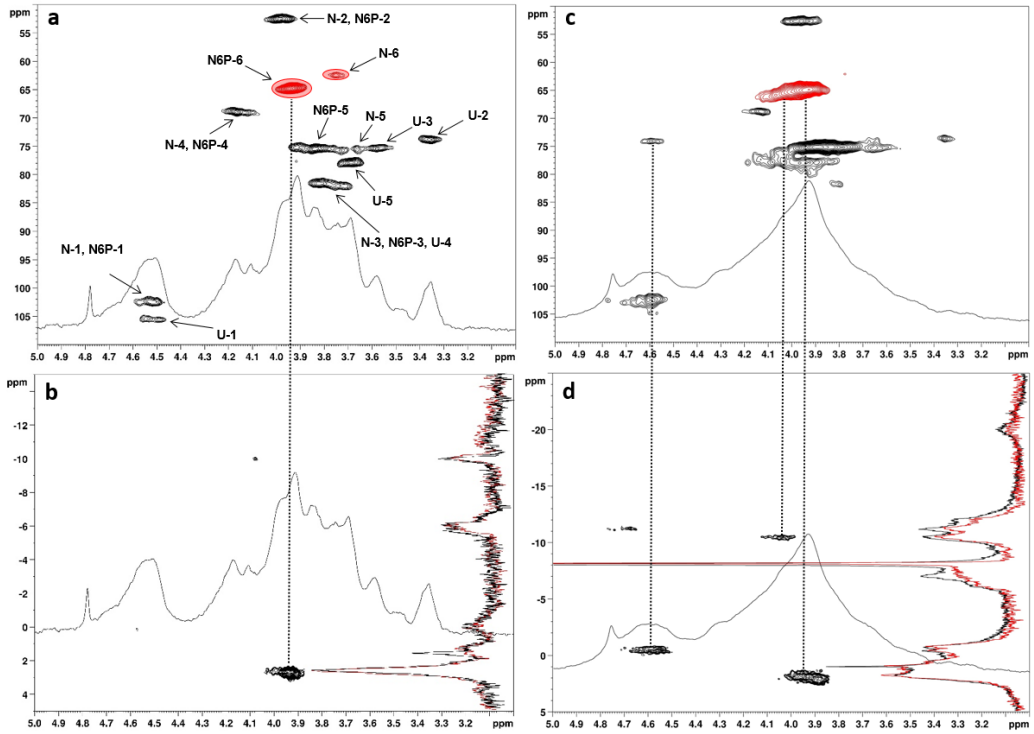

Figure 3.6. Superimposed, zoomed ^{1}H and $^{1}H,^{13}C$-DEPT-HSQC (a,c) and ^{1}H, ^{31}P, ^{31}P-1D-DOSY (in red) and $^{1}H,^{31}P$-HSQC (b,d) NMR spectra (D_2O, 400 MHz, 298K, zoom) of **CP-11** (a,b) and **CP-6** (c,d) (N = GalNAc, N6P = GalNAc-6-phosphate, U = GlcA; densities enclosed in red circles were integrated for DPh estimation)

The investigation of phosphorylation reactions was then extended to regioselectively protected substrates, starting with chondroitin derivative **42**, which had a single, free hydroxyl at position *O*-4 of GalNAc residues, with other positions protected by esters moieties.

Compound **42** was firstly subjected to phosphorylation with phosphorus pentoxide (P_2O_5), a common phosphorylating agent, commonly used for studies on cellulose phosphate (Granja et al., **2006**). It was used both in presence of only pyridine and DMF as solvent or together with other phosphorylating agents such as trimethyl

phosphate ($(CH_3O)_3PO$) and phosphoric acid obtaining derivatives **CP-12,13**, respectively.

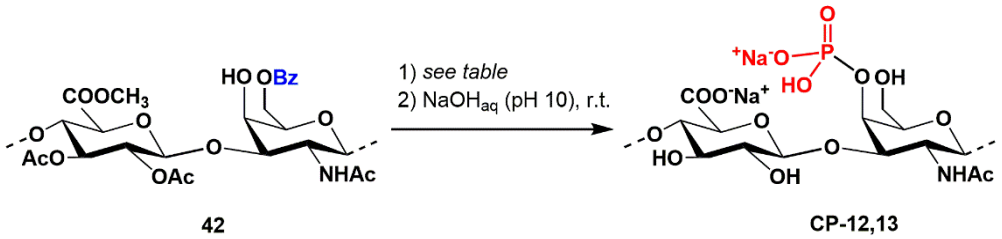

42 **CP-12,13**

entry	product	precursor	phosphorylation conditions[a]	phosphorylation position (DPh)
1	**CP-12**	**42**	P_2O_5, py, rt, 24h	--
2	**CP-13**	**42**	P_2O_5, H_3PO_4, $(CH_3O)_3PO$, 80°C for 2h and then rt for 24h	--

[a] Reactions were all conducted in dry DMF

Table 3.4. Phosphorylation tests on precursor **42** with P_2O_5

Unfortunately, a comparison of the ^{1}H-NMR spectra of *E. coli*-sourced CS-0 and **CP-12,13** samples revealed the absence of any derivatization since the ^{1}H-NMR spectra were found to be superimposable.

Compound **42** was also subjected to phosphorylation reactions under conditions similar to the ones already investigated on derivative **44**, affording derivatives **CP-14,20**.

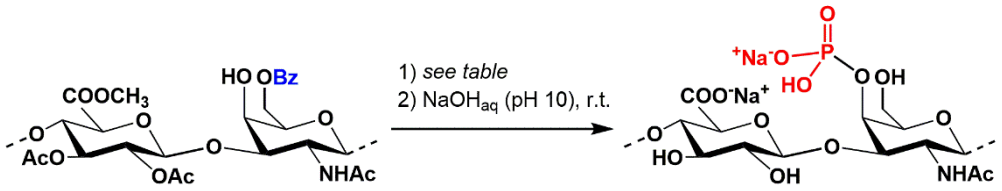

42 **CP-14,20**

entry	product	precursor	phosphorylation conditions[a]	phosphorylation position (DPh)
1	**CP-14**	**42**	H_3PO_4, urea, 150°C, 3h	n.d.[b]
2	**CP-15**	**42**	$POCl_3$, pyridine, rt, 18h	n.d.[b]
3	**CP-16**	**42**	Ψ^O, DBU, rt, 1h	--
4	**CP-17**	**42**	PEP-K (10 eqs), TBAHS (0.6 eqs), 80°C, 48h	--
5	**CP-18**	**42**	PEP-K (30 eqs), TBAHS (1.2 eqs), 100°C, 48h	--
6	**CP-19**	**42**	PEP-K (50 eqs), TBAHS (2.0 eqs), 80°C, 24h	GalNAc *N*-2 (29%)
7	**CP-20**	**42**	PEP-K (50 eqs), TBAHS (2.0 eqs), 100°C, 48h	GalNAc *N*-2 (10%)

[a] Reactions were all conducted in dry DMF

[b] Not determined

Table 3.5. Phosphorylation tests on precursor **42** with different reagents

Standard phosphorylation procedures (Table 3.5, entries 1,2) gave derivatives **CP-14,15**, which are highly heterogeneous as showed by ^{1}H-NMR spectra, characterized by broadened signals (Figure 3.7a).

Conversely, only slight differences could be found between ^{1}H-NMR spectra of starting CS-0 and **CP-16** derivative obtained by reaction of **42** with Ψ^O, but no significant peak was detected in the ^{31}P-NMR spectrum of the latter, thus concluding that no phosphate groups were installed on polysaccharide backbone (Table 3.5, entry 3).

Similarly, no differences between starting CS-0 and **CP-17** obtained with PEP-K under the conditions successfully employed to obtain **CP-4** (entry 4). An increase of PEP-K and TBAHS amounts and of reaction temperature (entries 5-7) afforded CP derivatives showing ^{1}H-NMR spectra with minor signals at δ 4.43 and 5.08, that could not be detected in the spectrum of starting CS-0. **CP-19,20** derivatives showed these signals at a much higher intensity with respect to **CP-18**. Surprisingly, the ^{1}H,^{31}P-HSQC spectrum of **CP-19** revealed that none of these signals gave cross-peaks with ^{31}P signals. A complete set of 2D-NMR spectra (Figures 3.7c,d) allowed the full assignment of ^{1}H and ^{13}C chemical shifts of **CP-19** spectrum; in particular, the anomeric signal at $\delta_{H/C}$ 5.08/100.3 gave a HMBC correlation with the signal at $\delta_{H/C}$ 4.76/72.7, which could be assigned to the CH atoms at position 5 of an uronic acid moiety by HMBC correlation with a carboxyl signal at δ_{C} 176.6. A complete set of 2D-NMR experiments (COSY, TOCSY and HSQC-TOCSY) allowed the assignment of chemical shifts also for the CH atoms at positions 2, 3 and 4 of the same residue, that could be identified by comparison with literature data (Pomin, **2014**; Sudo et al., **2001**) as an α-L-iduronic acid (IdoA) unit, *i.e.* the C-5 epimer of GlcA residues

Furthermore, the ^{1}H,^{13}C-DEPT-HSQC spectrum of **CP-19,20** revealed the presence of a low intense signal at $\delta_{H/C}$ 3.69/54.9 correlating with a ^{31}P signal at δ -9.4 in the ^{1}H,^{31}P-HSQC spectrum. This suggested the presence of a phosphate moiety linked to the nitrogen atom of some GalNAc units in **CP-19,20** polysaccharides. The relative amounts of these GalNAcNP residues with respect to unmodified GalNAc units could be estimated as 29% and 10% in **CP-19,20**, respectively, by relative integration of the GalNAc and GalNAcNP CH-2 signals volume in the ^{1}H,^{13}C-DEPT-HSQC spectrum. The presence of some unexpected GalNAcNP units in **CP-19,20** derivatives could be explained with a very low reactivity of the single unprotected hydroxyl at GalNAc *O*-4 position of starting polysaccharide **42**. Indeed, it is very well known in synthetic carbohydrate chemistry that the OH at position 4 of acetamido-sugars is a very poor nucleophile (Crich and Dudkin, **2001**). Its reactivity can be even lower than the acetamido group one (Liao and Auzanneau, **2005**), that conversely is known to react

readily with enol ester-type electrophiles (*e.g.* isopropenyl acetate) having chemical features resembling PEP-K structure (Suihko et al., **2001**). On the other hand, the equally unexpected formation of IdoA units could be explained by an epimerization of some of the GlcA methyl ester units of starting polysaccharide **42**, plausibly activated by protic species present in the reaction mixture (PEP-K, TBAHS and the species afforded by their reaction) (Domon et al., **2020**). Indeed, the amount of IdoA units in CP derivatives was found to be directly dependent on PEP-K/TBAHS equivalents, with a marked increase from a 6% value in **CP-18** to 29% and 41% in **CP-19** and **CP-20**, respectively, as detected by relative integration of signals at δ 5.08 and 4.49-4.43 in the ^{1}H-NMR spectra.

Further investigations on the mechanism and the scope of such GlcA to IdoA epimerization are currently underway.

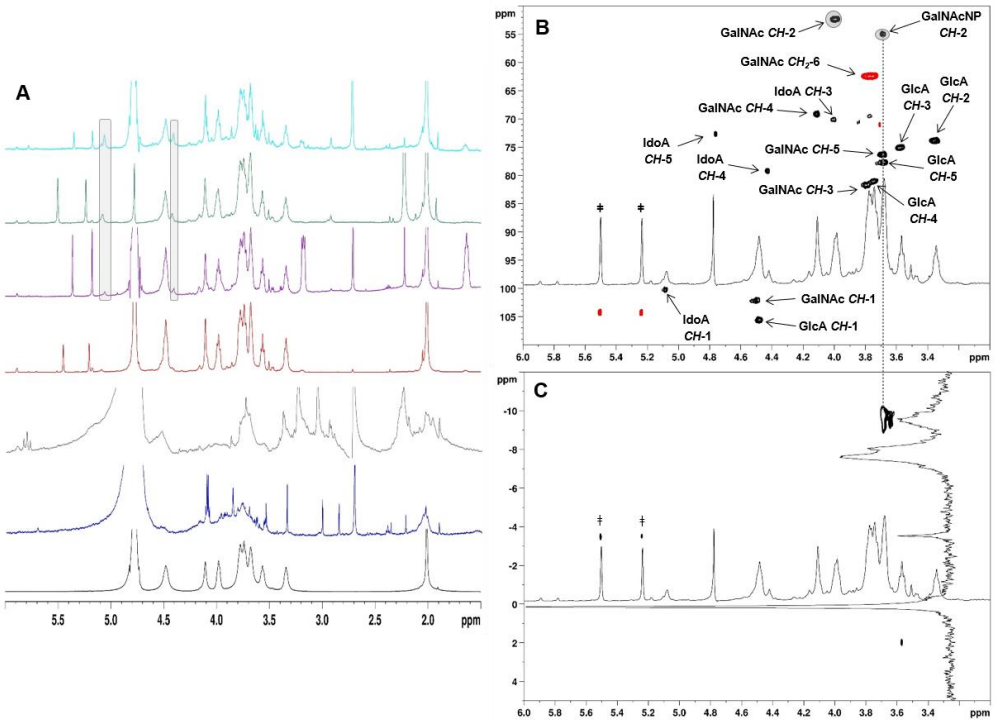

Figure 3.7. (a) ^{1}H-NMR spectra (400 MHz, 298K, D_2O) of CS-0 (black), **CP-14** (blue), **CP-15** (grey), **CP-16** (pink), **CP-17** (red), **CP-18** (purple), **CP-19** (green) and **CP-20** (light blue) (the grey stripes highlight the main differences among the spectra of CS-0 and **CP-18-20**); (b) superimposed ^{1}H-NMR and ^{1}H,^{13}C-DEPT-HSQC 2D-NMR spectra (600 MHz, 298K, D_2O, zoom) of **CP-19** (densities enclosed in grey circles were integrated for GalNAcNP *vs.* GalNAc relative amount estimation); (c) superimposed ^{1}H-, ^{31}P-NMR and ^{1}H,^{31}P-HSQC 2D-NMR spectra (400 and 162 MHz, 298K, D_2O, zoom) of **CP-19** (signals marked with ‡ symbol are relative to residual PEP-K)

The employed phosphorylation protocols were also tested on partially protected derivative **41,** which had free hydroxyls at position *O*-4 and *O*-6 GalNAc residues with other positions protected by esters moieties, and on **43,** which had a single, free hydroxyl at position *O*-2 of GlcA residues with other positions protected by CPGs.

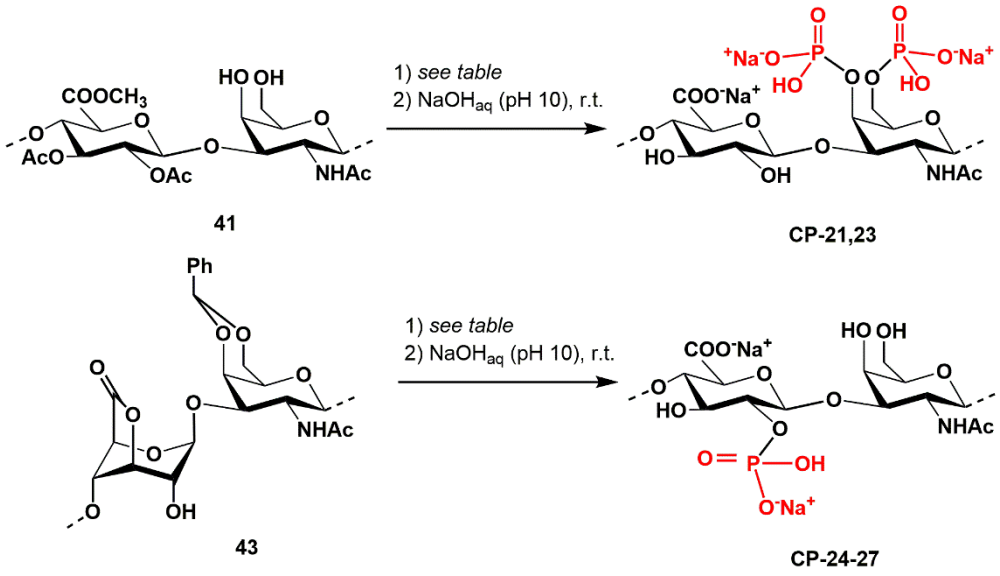

entry	product	precursor	phosphorylation conditions[a]	phosphorylation position (DPh)
1	**CP-21**	**41**	H_3PO_4, urea, 150°C, 3h	n.d.[b]
2	**CP-22**	**41**	$POCl_3$, pyridine, rt, 18h	n.d.[b]
3	**CP-23**	**41**	PEP-K (50 eqs), TBAHS (2.0 eqs), 100°C, 48h	GalNAc *O*-6 (80%)
4	**CP-24**	**43**	H_3PO_4, urea, 150°C, 3h	n.d.[b]
5	**CP-25**	**43**	$POCl_3$, pyridine, rt, 18h	n.d.[b]
6	**CP-26**	**43**	Ψ^O, DBU, rt, 1h	--
7	**CP-27**	**43**	PEP-K (50 eqs), TBAHS (2.0 eqs), 100°C, 48h	GlcA *O*-2 (19%) GalNAc *O*-6 (4%)

[a] Reactions were all conducted in dry DMF

[b] Not determined

Table 3.6. Phosphorylation tests on precursors **41** and **43** with different reagents

Standard methods gave highly heterogeneous derivatives or negligible phosphorylation (Table 3.6, entries 1, 2, 4, 5), while Ψ^O-based procedure gave no reaction at all (Table 3.6, entry 6). Conversely, by treating **43** with PEP-K and TBAHS in DMF at 100°C, the targeted phosphorylation at GlcA *O*-2 site was clearly detected

by $^{1}H,^{1}H$-, $^{1}H,^{13}C$- and $^{1}H,^{31}P$-2D-NMR analysis of the obtained derivative **CP-27** (Table 3.6, entry 7; Figure 3.8), but a low DPh (19%) was calculated by $^{1}H,^{13}C$-DEPT-HSQC integration. Furthermore, a trace amount (4%) of phosphate groups attached at GalNAc *O*-6 site could be detected too. This could be ascribed to residual, unprotected GalNAc units along the polysaccharide backbone of starting **43** and/or to the cleavage of some of the benzylidene rings protecting GaNAc units during the reaction.

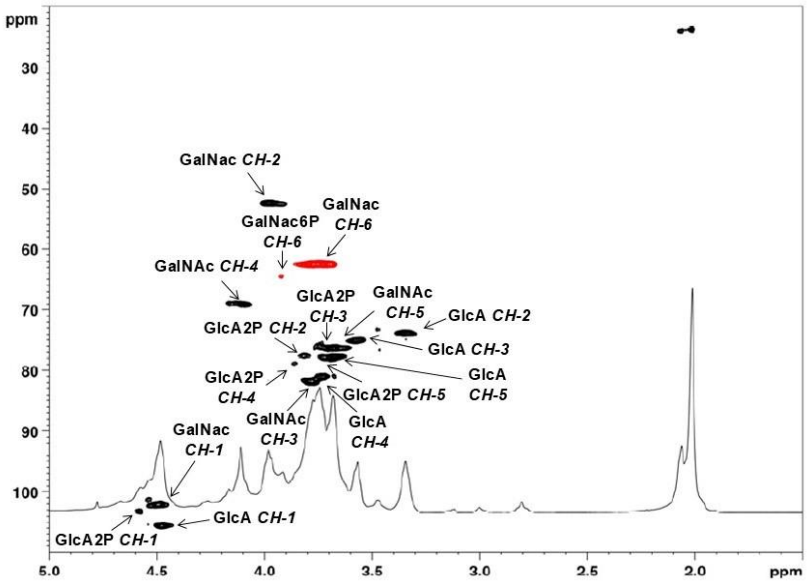

Figure 3.8. Superimposed ^{1}H-NMR and $^{1}H,^{13}C$-DEPT-HSQC 2D-NMR spectra (600 MHz, 298K, D_2O, zoom) of **CP-27**

A much higher DPh (80%) was measured for GalNAc *O*-6 sites of derivative **CP-23**, obtained by treatment of precursor **1** with PEP-K and TBAHS (Table 3.6, entry 3). The $^{1}H,^{31}P$-HSQC spectrum of **CP-23** (Figure 3.10) showed no further cross-peaks other than the one at $\delta_{H/P}$ 3.99/1.43, that was assigned to GalNAc *O*-6 phosphorylation, thus suggesting no phosphate group insertion at GalNAc *O*-4 sites, in agreement with the results described above for the phosphorylation of precursor **41**.

Nonetheless, the presence of a $^{1}H,^{13}C$-downfield shifted, non-anomeric signal at $\delta_{H/C}$ 4.76/77.1 in the $^{1}H,^{13}C$-DEPT-HSQC spectrum of **CP-23** (Figure 3.9) suggested the derivatization of some GalNAc units with a sulfate group at their *O*-4 site. This was confirmed by comparison with the chemical shift values reported for GalNAc4S *CH*-4 in A-type subunits of both natural (Mucci, Schenetti, & Volpi, **2000**) and semi-synthetic (Vessella et al., **2021a**) CS polysaccharides. Noteworthy, a detailed study of COSY, TOCSY and $^{1}H,^{13}C$-DEPT-HSQC spectra as well as the superimposition of the $^{1}H,^{13}C$-heterocorrelated spectra of **CP-23** and semi-synthetic CS-A (Vessella et al., **2021a**) revealed that *O*-4 sulfation could be detected only in GalNAc units also carrying a phosphate group at *O*-6 position.

Thus, **CP-23** polysaccharide was composed of GalNAc, GalNAc6P and GalNAc4S6P residues in a 20%:50%:30% relative amount, as estimated by relative integration of 6-*O*-phosphorylated *vs.* 6-*O*-underivatized GalNAc *CH*-6 and 4-*O*-sulfated *vs.* 4-*O*-underivatized GalNAc *CH*-4 couple of signals in the $^{1}H,^{13}C$-DEPT-HSQC at $\delta_{H/C}$ 3.99/65.2, 3.78/62.4 and $\delta_{H/C}$ 4.76/77.1, 4.16/68.6, respectively.

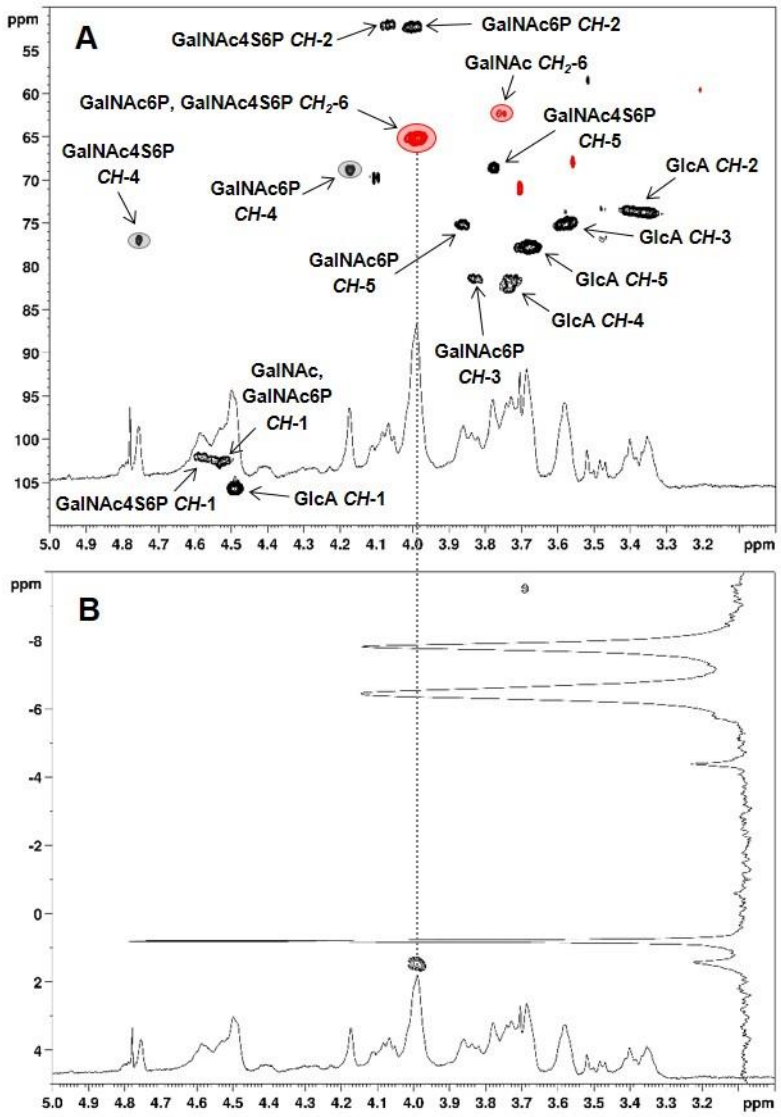

Figure 3.9. (a) Superimposed ^{1}H-NMR and ^{1}H,^{13}C-DEPT-HSQC 2D-NMR spectrum (600 MHz, 298K, D_2O, zoom) of **CP-23** (densities enclosed in red and grey circles were integrated for GalNAc:GalNAc6P:GalNAc4S6P relative amount estimation); (b) superimposed ^{1}H-, ^{31}P-NMR and ^{1}H,^{31}P-HSQC 2D-NMR spectra (400 MHz, 298K, D_2O, zoom) of **CP-23**

The simultaneous presence of both a phosphate and a sulfate group as decoration of GalNAc units in **CP-23** is, to the best our knowledge, unprecedented in any GAG mimic. This unexpected structural feature could be explained with the mechanism proposed for phosphorylation with PEP-K/TBAHS reagents (Domon et al., **2020**). Indeed, after phosphosulfophosphate (POSOP) has formed as active phosphate donor in the reaction mixture, its reaction with the primary alcohol group at GalNAc *O*-6 site allows the insertion of a phosphate moiety at this position and the simultaneous release of phosphosulfate (POS), that can act not as phosphate but as sulfate donor on the proximal alcohol at *O*-4 position (Figure 3.10). Such sulfation process was not detected on *O*-4 and/or *O*-6 sites of GalNAc units other than GalNAc6P, due to the competition of PEP-K for reaction on POS migrated far from its generation site to form POSOP again.

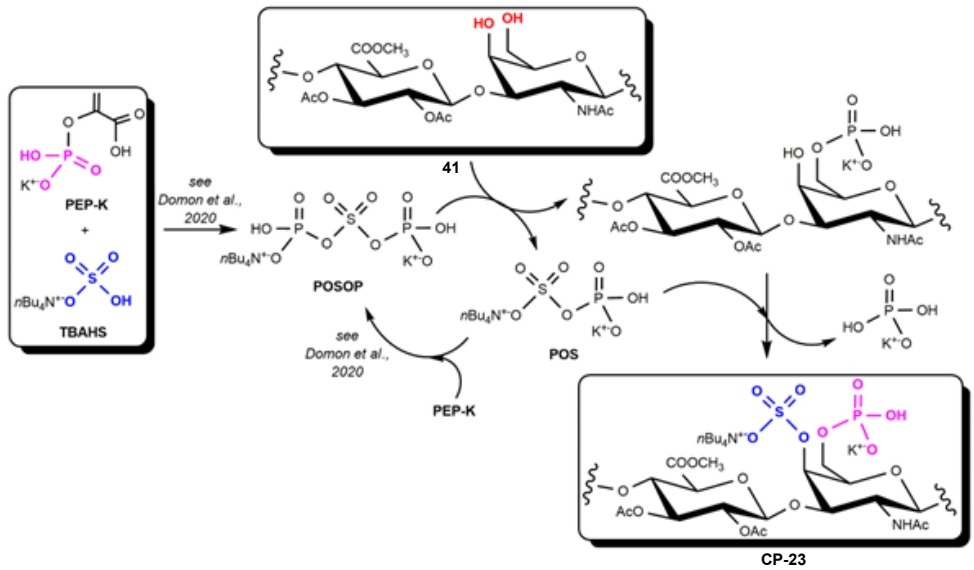

Figure 3.10. Proposed mechanism for the obtainment of GalNAc4S6P as major units in **CP-23** by treating **41** with PEP-K/TBAHS

The successful obtainment of regioselectively chondroitin-6-phosphate derivatives (from now named also as CP-C) prompted a preliminary study of their behavior in the

presence of bovine testicular hyaluronidase (BTH), an endonuclease enzyme known for catalysing the hydrolysis of hyaluronic acid and showing activity towards chondroitin and CS polysaccharides too (Wang et al., **2023**), in order to open a direct access to low molecular weight species, *i.e.* CP oligosaccharides, that to the best of our knowledge are completely missing in literature. Noteworthy, several studies have demonstrated that low molecular weight chondroitin sulfate (LMW-CS) species have enhanced bioavailability and biological activities, including antioxidant, anticoagulation, anti-inflammatory and neuroprotective effects, together with a safer profile in terms of absence of immunological responses (Lan et al., **2020**; Li et al., **2021**). Therefore, a future evaluation of LMW-CP-C biological properties would be surely worth being pursued. By incubating **CP -5** with BTH in a NaOAc/AcOH buffer (pH=5) at 37°C, three low molecular weight chondroitin phosphate species (named **LMW-CP-C-a**, **LMW-CP-C-b** and **LMW-CP-C-c**, respectively) could be obtained after purification of the crude reaction mixture by size-exclusion chromatography. Their characterization by a complete set of NMR experiments (^{1}H-NMR, ^{31}P-NMR, ^{1}H,^{13}C-DEPT-HSQC- and ^{1}H,^{31}P-HSQC-2D-NMR) confirmed a structure of LMW chondroitin species carrying phosphate groups at some of GalNAc *O*-6 sites. In particular, a comparison of **CP-5** and **LMW-CP-C-a-c** ^{1}H-NMR spectra clearly showed the presence of doublet signals at 5.13 and 4.59 ppm only in the latter case (Figure 3.11). Since these signals corresponded in the ^{1}H,^{13}C-DEPT-HSQC spectra to cross-peaks at δ_C 92.3 and 96.2, respectively, they could be assigned to the anomeric H atom of α- and β-configured GalNAc reducing end units, respectively. A comparison between the sum of their integral values and the area of the signal at 1.94 ppm related to the methyl group of (reducing and non-reducing) GalNAc units through Eq. 3.1, gave an estimation of the average chain length in the three LMW-CP samples: **LMW-CP-C-a** length distribution could be centered on a 23-mer species, while **LMW-CP-C-b** and **LMW-CP-C-c** could be estimated to be shorter (13-mer and 9-mer, respectively). Finally, the presence of GalNAc-6-phosphate units within **LMW-CP-C-a-c** structures was confirmed by the presence of a signal at $\delta_{H/P}$ 3.84/3.9

in their $^{1}H,^{31}P$-HSQC 2D-NMR spectra, corresponding to a ^{1}H- and ^{13}C-downfield shifted CH_2 signal at $\delta_{H/C}$ 3.84/63.0 in their $^{1}H,^{13}C$-DEPT-HSQC spectra (Figure 3.12).

$$\text{average chain length} = \frac{I(CH_3)/3}{I(\alpha-reducing) + I(\beta-reducing)} \times 2 \qquad \text{(Eq. 3.1)}$$

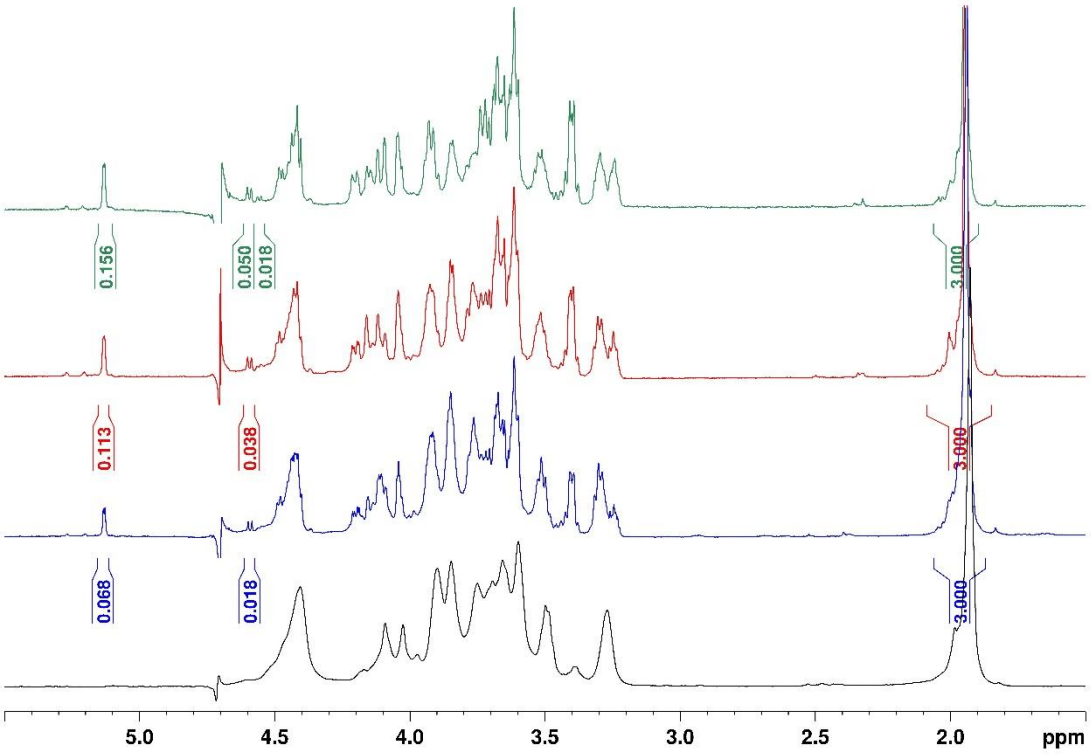

Figure 3.11. ^{1}H NMR spectra (D_2O, 600 MHz, 298K) of **CP-5** (black), **LMW-CP-C-a** (blue), **LMW-CP-C-b** (red), and **LMW-CP-C-c** (green)

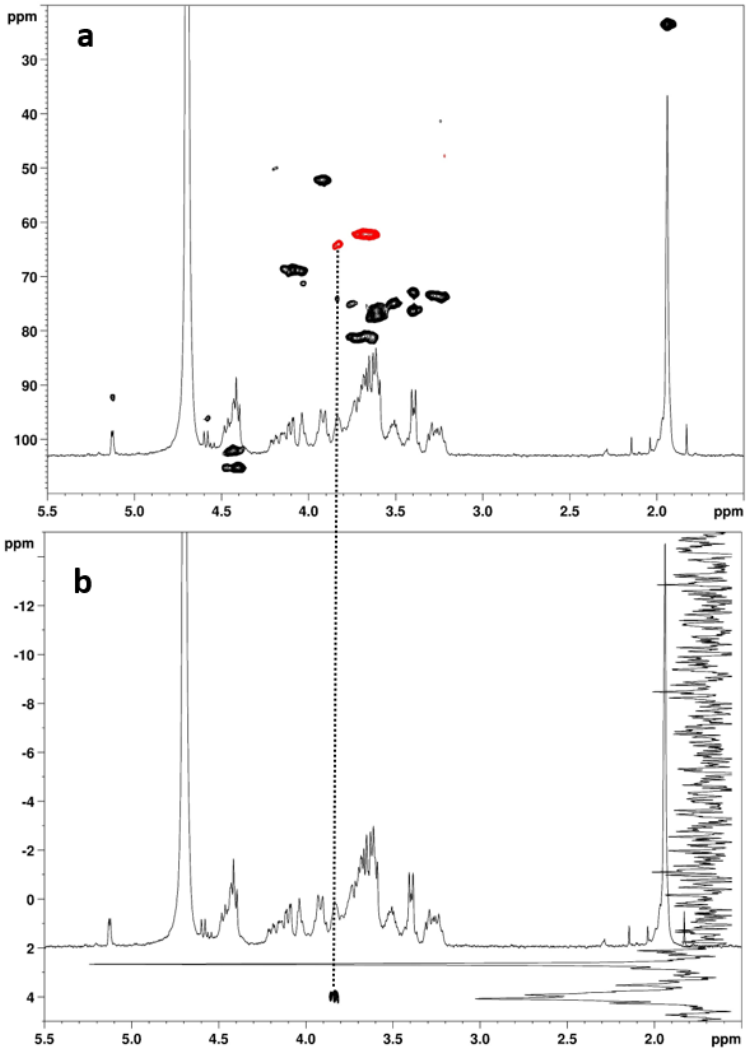

Figure 3.12. Superimposed (a) ^{1}H and $^{1}H,^{13}C$-DEPT-HSQC and (b) ^{1}H, ^{31}P, $^{1}H,^{31}P$-HSQC NMR spectra (D_2O, 400 MHz, 298K) of **LMW-CP-C-c**

In order to compare the structural features and the properties of CP-C with respect to its sulfated counterpart (CS-C), a semi-synthetic access to the latter from CS-0 was attempted. Although some procedures have been already reported to this aim (Bedini et al., **2016**), some of them did not report any NMR analysis of the obtained product

(Valoti et al., **2014**). Therefore, a screening of different reaction conditions was performed and the resulting CS derivatives were characterized by ^{1}H-NMR and ^{1}H,^{13}C-DEPT-HSQC 2D-NMR spectroscopy (Table 3.7).

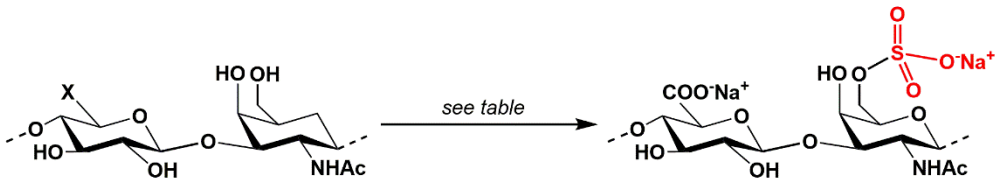

44: X = $COO^{-+}N(n\text{-}Bu)_4$
45: X = COOH

CS-1,9

entry	product	starting compound	conditions	DS-6S[a]	DS-2S[b]
1	**CS-1**	**45**	SO_3·py (2.2 eqs.), DMF, 25°C, 120 min	0	0
2	**CS-2**	**45**	SO_3·py (1.1 eqs.), DMF, 80°C, 330 min	0.06	0
3	**CS-3**	**44**	SO_3·py (2.2 eqs.), DMF, 25°C, o.n.	0.06	0
4	**CS-4**	**44**	SO_3·py (4.4 eqs.), DMF, 25°C, 120 min	1.00	0.43
5	**CS-5**	**44**	SO_3·py (3 eqs.), DMF, 4°C, 75 min	0.27	0
6	**CS-6**	**44**	SO_3·DMF (3 eqs.), DMF, 4°C, 75 min	0.16	0
7	**CS-7**	**44**	SO_3·py (7 eqs.), DMSO, 25°C, 75 min	1.00	0.14
8	**CS-8**	**44**	SO_3·py (4 eqs.), DMSO, 25°C, 75 min	0.55	0
9	**CS-9**	**44**	SO_3·py (1.1 eqs.), DMF, 80°C, 330 min	0.09	0

[a] Degree of sulfation at GalNAc O-6 site, measured by relative integration of CH_2 signal at 4.22/68.9 and 3.76/62.4 ppm assigned to GalNAc-6S and GalNAc CH_2-6, respectively, in the ^{1}H,^{13}C-DEPT-HSQC 2D-NMR spectrum

[b] Degree of sulfation at GlcA O-2 site, measured by relative integration of CH signal at 4.11/80.9 and 3.35/73.8 ppm assigned to GlcA-2 sulfate and GlcA CH-2, respectively, in the ^{1}H,^{13}C-DEPT-HSQC 2D-NMR spectrum

Table 3.7. Regioselective sulfation reactions on **44** and **45** towards CS-C derivative

Firstly, we performed the sulfation on polysaccharide **45**, *i.e.* CS-0 in its acid form (Table 3.7), under the mild conditions reported by Valoti et al. (2014) who used

SO_3·py complex as sulfating agent in DMF at 25°C (Table 3.7, entry 1), and under the stronger conditions employed in literature (Benito-Arenas et al., **2018**) but with a very slight stoichiometric excess of the same sulfating agent (entry 2). In the former case, no derivatization could be detected at all by ^{1}H-NMR spectroscopy. Conversely, a ^{1}H,^{13}C-DEPT-HSQC 2D-NMR spectrum (Figure 3.13) measured on the latter, *i.e.* derivative **CS-2**, showed the presence of sulfate groups located at position *O*-6 of some GalNAc subunits, as highlighted by comparison with literature data (Mucci et al., **2000**). By relative integration of the CH_2 signal at $\delta_{H/C}$ 4.22/68.9 and 3.76/62.4, that could be assigned to GalNAc-6 sulfate and GalNAc residues, respectively (Mucci et al., **2000**), a very low DS value could be estimated. Since a scarce solubility was observed for **45** in DMF during the sulfation reactions under the employed conditions, the latter were replicated on the more DMF-soluble, *n*-tetrabutylammonium salt polysaccharide **44**. In this case, mild sulfation conditions gave a regioselective sulfation at GalNAc CH_2-6 sites, but an unsatisfying DS was detected again (entry 3). By doubling the stoichiometric amount of SO_3·py, a remarkable increase in the sulfation efficiency was detected (entry 4). Indeed, the ^{1}H,^{13}C-DEPT-HSQC 2D-NMR spectrum of **CS-4** showed a quantitative DS for GalNAc CH_2-6 positions (DS-6S), together with additional sulfate groups located at position O-2 of some GlcA units. By relative integration of the signals at $\delta_{H/C}$ 4.11/80.9 and 3.35/73.8, that could be assigned to GlcA-2 sulfate and unsulfated GlcA CH-2 atoms, respectively, a DS-2S value of 0.43 was estimated. In order to restore a higher control of sulfation regiochemistry, the reaction was conducted at a lower temperature, but a too low DS-6S was obtained both in the case of SO_3·py or the more reactive SO_3·DMF as employed sulfating agent (Table 3.7, entries 5 and 6, respectively). A satisfying DS-6S without detectable sulfate groups at any of the secondary alcoholic functionalities was finally obtained by restoring 25°C as reaction temperature but conducting the reaction in DMSO rather than DMF (entry 8).

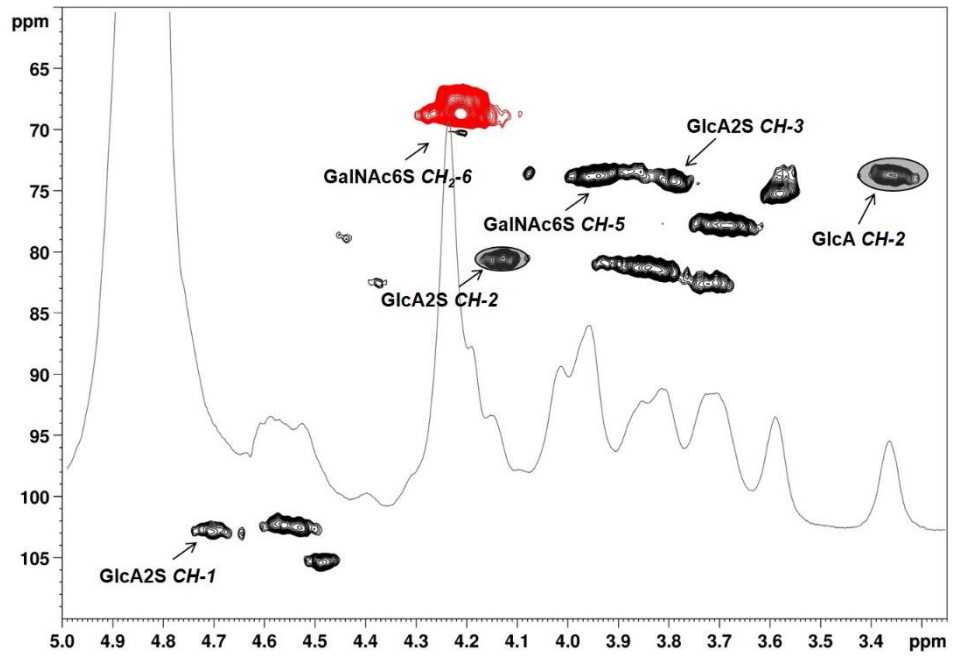

Figure 3.13. Superimposed ^{1}H and $^{1}H,^{13}C$-DEPT-HSQC NMR spectra (D_2O, 600 MHz, 298K, zoom) of **CS-4** (densities enclosed in grey circles were integrated for DS-2S estimation)

Since **CS-4** and **CS-8** derivatives showed a CS-D and CS-C structure, having sulfate groups decorating *O*-6 site of every GalNAc residue of the polysaccharide with or without additional sulfate groups at *O*-2 position of GlcA units, respectively, they could be considered as sulfated counterparts of **CP-6** and **CP-11**, that had phosphate groups at (almost) every *O*-6 site of the polymer with or without additional phosphorylation at some secondary alcoholic functionalities, respectively. This set of sulfated and phosphorylated chondroitin derivatives will be subjected to a comparison in terms of some chemical and biological features in collaboration with our partner groups.

3.1.3. Conclusions

This section was focused on the construction of a library of semi-synthetic chondroitin phosphate derivatives, testing different phosphorylating agents under several reaction conditions, in order to have access for the first time to the semi-synthesis of regioselectively phosphorylated GAG mimics. Direct strategies, involving conventional heating and microwave irradiation techniques, were tested on the *n*-tetrabutylammonium salt of CS-0 to access a chondroitin-6-phosphate polysaccharide. A detailed ^{1}H-, ^{13}C- and ^{31}P- one- and two-dimensional NMR analyses of the resulting polysaccharides revealed that both standard and novel phosphorylating agents were able to achieve the regioselective phosphorylation of the primary hydroxyl of GalNAc units on unprotected chondroitin. In particular, by using H_3PO_4 as phosphorylating agent, significant phosphorylation at the GalNAc *O*-6 site was achieved with both conventional heating and microwave irradiation. Noteworthy, by increasing the DPh at quantitative values under conventional heating eroded the desired phosphorylation regioselectivity, while the reaction conducted under microwave irradiation did not. In the case of the partially protected substrates, this study revealed the higher versatility of a new, biomimetic phosphorylation method based on the combination of PEP-K and TBAHS, in comparison to standard reagents such as $POCl_3$ and H_3PO_4. In particular, only the former couple of reagents reacted on partially protected polysaccharide derivatives in a controlled, regioselective fashion, affording a set of CP species with different derivatization patterns. Noteworthy, some of these products displayed an unexpected chemical structure, with the combined insertion of a sulfate and a phosphate group at GalNAc O-4 and O-6 positions, respectively, or with a GlcA to IdoA epimerization. Encouraged by the here presented results, an expansion of the screening of phosphorylation procedures on regioselectively protected chondroitin derivatives is planned for a near future, by using, for example, P(III) reagents.

Furthermore, in addition to phosphorylation strategies, some regioselectively sulfated chondroitin polysaccharides were also semi-synthesized from *E. coli* sourced CS-0, in order to compare, in the future, the structural features and biological properties of two derivatives with the highest DPh related to GalNAc *O*-6 site – with or without additional phosphate groups at GlcA *O*-2 position (**CP-6** and **CP-11**, respectively) with respect to their sulfated counterparts (**CS-4** and **CS-8**, respectively). Moreover, methods for the controlled depolymerization of chondroitin-6-phosphate derivatives were investigated. In this context, ^{1}H-NMR analysis revealed that CP-C depolymerization via hyaluronidase enzymatic hydrolysis is effective in obtaining a mixture of chondroitin phosphate oligosaccharides. These compounds will be subjected firstly to a detailed structural analysis by combining NMR and computational techniques to allow the prediction of an accurate 3D model of protein–glycan complexes and perform an investigation of the interactions of these **LMW-CP** compounds with protein growth factors. The structural characterization of all **CP** compounds will be also completed with molecular weight measurements, which will be evaluated by HP-SEC-TDA in collaboration with our partner group (prof. Schiraldi and collaborators at the Department of Experimental Medicine of the University of Campania "L. Vanvitelli"). These experiments are currently in progress.

3.1.4. Experimental section

General methods. E. coli-sourced CS-0 (42±3 kDa, 1.34 dispersity) was a kind gift of Prof. C. Schiraldi (Department of Experimental Medicine, Università della Campania "L.Vanvitelli"). Commercial grade reagents and solvents were used without further purification, except where differently indicated. Microwave-irradiated reactions were performed with a CEM Discover 908010 instrument. Dialyses were conducted on Spectra/Por 3.5 kDa cut-off membranes at 4°C. Centrifugations were performed with an Eppendorf Centrifuge 5804R instrument at 4°C (4600 g, 5 min). Freeze-dryings

were performed with a 5Pascal Lio 5P 4K freeze dryer. NMR spectra were recorded on a Bruker Avance-III HD (^{1}H: 400 MHz, ^{13}C: 100 MHz, ^{31}P: 162 MHz) or on a Bruker Avance-III (^{1}H: 600 MHz, ^{13}C: 150 MHz) instrument – the latter equipped with a cryo-probe – in D_2O (acetone as internal standard, ^{1}H: $(CH_3)_2CO$ at δ 2.22; ^{13}C:$(CH_3)_2CO$ at δ 31.5; H_3PO_4 as external standard, ^{31}P: δ 0.0). Data were processed using the data analysis packages integrated with Bruker TopSpin® 4.0.5 software. ^{31}P-NMR spectra were obtained by typically accumulating 512 transients. ^{1}H- and ^{31}P-1D-DOSY experiments were measured using a stimulated echo sequence with bipolar gradient pulses and one spoil gradient (stebpgp1s1d) with a diffusion time Δ of 100 ms, a gradient duration of 2 or 4 ms (for ^{1}H- and ^{31}P-1D-DOSY, respectively) and accumulating 64 or 2048 transients (for ^{1}H- and ^{31}P-1D-DOSY, respectively). ^{1}H,^{13}C-DEPT-HSQC experiments were measured in the ^{1}H-detected mode via single quantum coherence with proton decoupling in the ^{13}C domain, using data sets of 2048 × 256 points and typically 64 increments. ^{1}H,^{31}P-HSQC experiments were measured in the ^{1}H-detected mode via a phase sensitive gradient selection with decoupling during acquisition, using data set of 2048 × 256 points and typically 64 increments.

Typical procedure for phosphorylation with H_3PO_4. A mixture of chondroitin *n*-tetrabutylammonium salt **44** (99.0 mg, 0.159 mmol) and urea (1.48 g, 24.6 mmol) was dried under vacuum, purged under argon, then treated with dry DMF (3.0 mL) and heated to 100°C. The resulting solution was treated with 85% H_3PO_4 (257 μL). The suspension was stirred at 80-150°C under conventional heating or microwave irradiation for 1-3 hours. The obtained yellowish suspension was then cooled to room temperature and methanol (30 mL) was added to form a white precipitate. The mixture was cooled in freezer for 1h, then the precipitate was collected by centrifugation. The solid was dissolved in HPLC-grade H_2O (6.0 mL; pH ~ 2) and treated with a few drops of aqueous 33% NaOH to neutral pH (for reactions on **41**-**43**, a pH ≥ 12 was reached and the alkaline solution was stirred at rt overnight and then neutralized with 1M HCl; for reaction on **43**, additional 2h stirring at 50°C was performed before

NaOH addition). After dialysis and freeze-drying, phosphorylated product **CP-1** was obtained (73.4 mg, 74% mass yield).

Typical procedure for phosphorylation with $POCl_3$. A solution of **44** (56.4 mg, 90.6 μmol) in dry DMF (2.2 mL) was treated with a freshly prepared 9:1 v/v pyridine-$POCl_3$ mixture (2.2 mL). After overnight stirring at rt, the resulting brownish mixture was diluted with 33% NaOH and stirred for 1h (overnight for reactions on **41, 42, 43**). Dialysis and freeze-drying afforded **CP-2** (36.2 mg, 64% mass yield). In the case of reaction on **43**, the product was further treated with 1M HCl (pH ~ 2), stirred at 50°C for 2h, then neutralized with 33% NaOH, dialyzed and freeze-dried.

Typical procedure for phosphorylation with PEP-K. Compound **44** (127 mg, 0.204 mmol) was mixed with *n*-tetrabutyl-ammonium bisulfate (TBAHS, 41.4 mg, 0.122 mmol) and the monopotassium salt of phosphoenolpyruvate (PEP-K, 421 mg, 2.04 mmol). Dry DMF (5.6 mL) was then added under argon atmosphere. The resulting suspension was stirred at 80 °C (or 100°C: see Table 1) for 48h, then cooled to rt and treated with acetone saturated with NaCl (7 mL) to form a yellowish precipitate. The mixture was cooled in freezer for 1h, then the precipitate was collected by centrifugation, and subsequently dissolved in HPLC-grade H_2O (10 mL). The solution was neutralized with a few drops of a 33% NaOH solution (for reactions on **41, 42, 43**, a pH ≥ 12 was reached and the alkaline solution was stirred at rt overnight and then neutralized with 1M HCl; for reaction on **43**, additional 2h stirring at 50°C was performed before NaOH addition). After dialysis and freeze-drying, phosphorylated product **CP-4** was obtained (123 mg, 97% mass yield). An aliquot (18.8 mg) was further purified by size-exclusion chromatography (11.7 mg purified product recovered).

Typical procedure for phosphorylation with Ψ^O. A mixture of compound **44** (21.3 mg, 32.7 μmol) and (2*S*,3a*S*,6*R*,7a*S*)- -methyl-2-((4-bromophenyl)thio)-6-(prop-2-

yl)hexahydrobenzo[*d*][1,3,2]oxathiaphosphole 2-oxide (Ψ^0, 43.8 mg, 98.1 μmol) was suspended in dry DMF (1.2 mL) under Ar atmosphere. A freshly prepared 1.68 mM solution of 1,8-Diazabicyclo(5.4.0)undec-7-ene (DBU) in dry DMF (58.5 μL, 98.5 μmol) was then added and the resulting mixture was stirred at rt for 1h. Thereafter, double-distilled water (2.5 mL) and then some drops of 1M NaOH (till pH > 10) were added. After overnight stirring at rt, the resulting precipitate was collected by centrifugation and discarded, while the supernatant was dialyzed and then freeze-dried to afford product **CP-3** (23.1 mg, 108% mass yield).

Phosphorylation with P_2O_5. Derivative **42** (63.7 mg, 0.110 mmol repeating unit) was dissolved in dry DMF (2.3 mL). The reaction flask was sonicated in an ultrasound bath for a long time to homogenize the reaction mixture, which was then treated with phosphorus pentoxide (P_2O_5, 311 mg, 2.19 mmol). The resulting orange solution was treated with dry pyridine (1.14 mL), forming an orange suspension, which was stirred at 50 °C overnight. For the deprotection procedure, the suspension was diluted with pure H_2O (~ 8.2 mL), treated with few drops of 4M aqueous NaOH until reaching an alkaline pH (~ 10/12). The mixture was stirred at room temperature for additional 24h. The resulting brown solution was neutralized with 1M aqueous HCl. After dialysis and freeze-drying, the phosphorylated product **CP-12** was obtained (142 mg, 223 % weight yield).

Phosphorylation with P_2O_5, H_3PO_4, $(CH_3O)_3PO$. Derivative **42** (42.9 mg, 74.1 μmol repeating unit) was treated with P_2O_5 (2.145 g, 15.11 mmol). The mixture was dried under vacuum, purged under argon, and then treated with dry DMF (1.4 mL), trimethyl phosphate ($(CH_3O)_3PO$, 1.60 mL) and 85% aqueous H_3PO_4 (1.80 mL added portionwise). After each addition, the mixture was sonicated in an ultrasound bath. The resulting suspension was stirred at 80 °C for 2h and then at room temperature (rt) overnight. The obtained yellow viscous mixture, containing putative undissolved P_2O_5, was treated with acetone saturated with NaCl (12 mL) and cooled in the freezer

for 2h. The resulting precipitate and any undissolved material were collected by centrifugation and subsequently dissolved in the minimum amount of pure water (~ 6 mL). For the deprotection procedure, the solution was treated with few drops of 4M aqueous NaOH until reaching an alkaline pH (pH ~ 10/12) and stirred at room temperature overnight. Finally, the solution was neutralized with aqueous 1M HCl, dialyzed, and freeze-dried to yield the compound **CP-13** (99.2 mg, 231% weight yield).

*Enzymatic depolymerization of **CP-5**.* A suspension of **CP-5** (20.4 mg) in a 0.15M NaCl, 0.10M NaOAc solution (1.0 mL) was buffered to pH=5 by adding a drop of acetic acid. The mixture was incubated at 37°C for 1 h, then a solution of bovine testicular hyaluronidase (BTH, 1.9 mg) in pure water (950 μL) was added. The production of oligosaccharide species was detected in progress by silica-gel thin-layer chromatography (TLC; eluent: 1:1:1:0.05 v/v/v/v *n*-butanol/ethanol/water/acetic acid). After 165 hours incubating at 37°C, the reaction was quenched by heating it at 100°C for 15 minutes. By successive cooling and freeze-drying, a white solid residue (33.3 mg) was obtained. It was dissolved in the minimum amount of water and purified by size-exclusion chromatography to give three fractions (**LMW-CP-C-a**, 4.9 mg; **LMW-CP-C-b**, 5.7 mg; **LMW-CP-C-c**, 2.6 mg).

Typical procedure for regioselective sulfation reaction. Polysaccharide **44** (or **45**) (Vessella et al., **2021b**) (88.7 mg, 0.143 mmol) was suspended in dry DMF or DMSO (3.2 mL) and the mixture was then treated with SO_3·py (68.3 mg, 0.428 mmol) or SO_3·DMF (65.6 mg, 0.428 mmol). After 75, 120 or 330 minutes or overnight stirring at 4°, 25° or 80° C, the resulting clear solution was cooled/heated to rt and then diluted with pure water (10 mL) and then a saturated $NaHCO_3$ aqueous solution was dropwise added until neutralization. Purification by dialysis, followed by freeze-drying afforded CS products (50.5 mg, 57% mass yield).

References

Amhare, A.F., Lei, J., Deng, H., Lv, Y., Han, J., Zhang, L., **2021**. *J. Drug Target. 29*, 259–268.

Bedini, E., Laezza, A., Iadonisi, A., **2016**. *Eur. J. Org. Chem. 2016(18)*, 3018-3042.

Benito-Arenas, R., Doncel-Pérez, E., Fernández-Gutiérrez, M., Garrido, L., García-Junceda, E., Revuelta, J., Bastida, A., Fernández-Mayoralas, A., **2018**. *Carbohydr. Polym. 202*, 211-218.

Cimini, D., Bedini, E., Schiraldi, C., **2023**. *Biotechnol. Adv. 67*, 108185.

Cimini, D., Boccella, S., Alfano, A., Stellavato, A., Paino, S., Schiraldi, C., Guida, F., Perrone, M., Donniacuo, M., Tirino, V., Desiderio, V., Rinaldi, B., **2022.** *Front. Bioeng. Biotechnol. 10*, 934997.

Cimini, D., Restaino, O. F., Schiraldi, C., **2018.** *Emerg. Top. Life Sci. 2*, 349–361.

Collin, E.C., Carroll, O., Kilcoyne, M., Peroglio, M., See, E., Hendig, D., Alini, M., Grad, S., Pandit, A., **2017**. *Signal Transduction Targeted Ther. 2*, 17049–17056.

Crich, D., Dudkin, V., **2001**. *JACS 123*, 6819−6825.

Domon, K., Puripat, M., Fujiyoshi, K., Hatanaka, M., Kawashima, S. A., Yamatsugu, K., Kanai, M., **2020**. *ACS Cent. Sci. 6*, 283−292

Dudley, G. B.; Richert, R.; Stiegman, A. E., **2015**. *Chem. Sci. 6*, 2144-2152

Esposito, F., Traboni, S., Iadonisi, A., Bedini, E., **2024**. *Carbohydr. Polym. 324*, 121517.

Granja, P.L., De Jéso, B., Bareille, R., Rouais, F., Baquey, C., Barbosa, M.A., **2006**. *React. Funct. Polym. 66 7*, 728-739.

Knouse, K. W., Flood, D. T., Vantourout, J. C., Schmidt, M. A., Mcdonald, I. M., Eastgate, M. D., Baran, P. S., **2021**. *ACS Cent. Sci. 7*, 1473–1485.

Lan, R., Li, Y., Shen, R., Yu, R., Jing, L., Guo, S., **2020**. *Carbohydr. Polym. 241*, 116302.

Li, H., Yuan, Q., Lv, K., Ma, H., Gao, C., Liu, Y., Zhang, S., Zhao, L., **2021**. *Carbohydr. Polym. 251*, 117034.

Liao, L., Auzanneau, F. I., **2005**. *J. Org. Chem. 70*, 6265–6273.

Lin, H., Leman, L. J., Krishnamurthy, R., **2022**. *Chem. Sci. 13*, 13741–13747.

Lowman, D., Ensley, H., Williams, D., **1998.** *Carbohydr. Res. 306*, 559–562.

Mikami, T., Kitagawa, H., **2013**. *Biochim. Biophys. Acta 1830*, 4719–4733.

Mizumoto, S., Yamada, S., Sugahara, K., **2015**. *Curr. Opin. Struct. Biol. 34*, 35–42.

Mucci, A., Schenetti, L., Volpi, N., **2000**. *Carbohydr. Polym. 41*, 27-35.

Ociepa, M., Knouse, K. W., He, D., Vantourout, J. C., Flood, D. T., Padial, N. M., Chen, J. S., Sanchez, B. B., Sturgell, E. J., Zheng, B., Qiu, S., Schmidt, M. A., Eastgate, M. D., Baran, P. S., **2021**. *Org. Lett. 23*, 9337–9342.

Pomin, V. H., **2014**. *Anal. Chem. 86*, 65–94.

Pomin, V.H., **2013**. Chondroitin Sulfate: Structure, Uses and Health Implications, 1st ed. Nova Science Publishers, New York (NY).

Ponedel'kina, I.Y., Khaibrakhmanova, E.A., Kozyrev, S.V., Tyumkina, T.V., **2023**. *Chem. Nat. Compd. 59*, 625–628.

Qingshan, S., Yujie, G., Kangyu, W., Chunhui, Z., Yanli, M., **2023**. *Molecules 28*, 7093.

Silbert, J.E., Sugumaran, G., **2002**. *IUBMB Life 54*, 177–186.

Sudo, M., Sato, K., Chaidedgumjorn, A., Toyoda, H., Toida, T., Imanari, T., **2001**. *Anal. Biochem. 297*, 42–51.

Suihko, M., Ahlgrén, M., Aulaskari, P., Rouvinen, J., **2001**. *Carbohydr. Res. 334*, 337–341.

Uebelhart, D., Malaise, M., Marcolongo, R., de Vathaire, F., Piperno, M., Mailleux, E., Fioravanti, A., Matoso, L., Vignon, E., **2004**. *Osteoarthr. Cartil. 12*, 269–276.

Uyama, T., Ishida, M., Izumikawa, T., Trybala, E., Tufaro, F., Bergström, T., Sugahara, K., Kitagawa, H., **2006**. *J.Biol. Chem. 281*, 38668–38674.

Valoti, E., Miraglia, N., Bianchi, D., Valetti, M., Bazza, P., **2014.** US8664196B2

Vassallo, V., Stellavato, A., Russo, R., Cimini, D., Valletta, M., Alfano, A., Pedone, P.V., Chambery, A., Schiraldi, C., **2022a.** *Int. J. Mol. Sci. 23 24*, 15865–15880

Vassallo, V., Tsianaka, A., Alessio, N., Grübel, J., Cammarota, M., Tovar, G.E.M., Southan, A., Schiraldi, C. **2022b**., *J. Biomed. Mater. Res. A 110 6*, 1210–1223.

Vessella, G., Marchetti, R., Del Prete, A., Traboni, S., Iadonisi, A., Schiraldi, C., Silipo, A., Bedini, E., **2021a**. *Biomacromolecules 22*, 5151–5161.

Vessella, G., Traboni, S., Cimini, D., Iadonisi, A., Schiraldi, C., Bedini, E., **2019a.** *Biomacromolecules 20*, 3021–3030.

Vessella, G., Traboni, S., Pirozzi, A. V. A., Laezza, A., Iadonisi, A., Schiraldi, C., & Bedini, E., **2019b**. *Mar. Drugs 17*, 655.

Vessella, G., Vázquez, J. A., Valcárcel, J., Lagartera, L., Monterrey, D. T., Bastida, A., Garcia-Junceda, E., Bedini, E., Fernández-Mayoralas, A., Revuelta, J., **2021b**. *Polymers 13*, 313.

Wang, K., Qi, L., Zhao, L., Liu, J., Guo, Y., Zhang, C., **2023**. *Carbohydr. Polym. 301*, 120361.

Yamada, S., Morimoto, H., Fujisawa, T., Sugahara, K., **2007**. *Glycobiology 17*, 886–894.

SECTION 3.2 – PRELIMINARY STUDIES FOR THE SEMI-SYNTHESIS OF CHITOSAN PHOSPHATE DERIVATIVES

3.2
PRELIMINARY STUDIES FOR THE SEMI-SYNTHESIS OF CHITOSAN PHOSPHATE DERIVATIVES

3.2.1. Chitosan: structure and activities

Chitosan is a linear polysaccharide derived from the deacetylation of chitin (Figure 3.14), composed of randomly distributed β-(1→4)-linked D-glucosamine (deacetylated unit) and *N*-acetyl-D-glucosamine (acetylated unit) (Fedel et al., **2012**; Lima et al., **2022**). This structure gives a range of properties that make chitosan suitable for several applications, especially in the biomedical fields. In particular, the degree of acetylation affects the solubility and biological activity of chitosan. For example, high deacetylation values lead the increase of solubility, also independence of the pH of the solution.

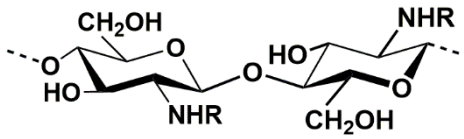

Figure 3.14. Repeating unit of chitosan polysaccharide

Additionally, chitosan exhibits conformational flexibility, which can be modulated by environmental conditions such as pH and ionic strength, allowing it to adopt various structural forms, including flexible rod-like macromolecules in solution (Skovstrup et al., **2010**). This flexibility is crucial for its interactions with other biomolecules and

materials, enhancing its functionality in applications such as drug delivery and tissue engineering (Sharifianjazi et al., **2022**). It has been shown to form hydrogels with excellent biocompatibility and mechanical properties, making it suitable for use in biomedical applications (Duan et al., **2015**; Sacco et al., **2018**). Furthermore, the presence of functional groups allows for easy chemical modifications, enabling the development of chitosan derivatives with tailored properties for specific applications (Sacco et al., **2020**). For example, in the pharmaceutical field it has been extensively studied for its potential as a drug delivery system. Its ability to form nanoparticles allows for the encapsulation of therapeutic agents, enhancing their bioavailability and controlled release (Grenha et al., **2009**). For instance, chitosan nanoparticles have been shown to improve the delivery of poorly soluble drugs, thereby increasing their therapeutic efficacy (Ahmed & Aljaeid, **2016**). Additionally, chitosan mucoadhesive properties facilitate prolonged retention of drug formulations at the site of action, which is particularly beneficial for oral and nasal drug delivery systems (Sogias et al., **2008**). The conjugation of chitosan with other polysaccharides, such as inulin, has been reported to enhance its antimicrobial properties, making it suitable for applications against biofilms formed by pathogenic bacteria (Zhang et al., **2018**). Chitosan has been extensively studied also for applications in tissue engineering and regenerative medicine. Its biocompatibility and ability to promote cell adhesion and proliferation make it an ideal candidate for scaffolding materials in tissue engineering applications. Chitosan hydrogels, formed through ionic or covalent cross-linking, have been developed for controlled drug release and as matrices for cell culture (Moura et al., **2011**). The versatility of chitosan allows for the incorporation of bioactive molecules, enhancing its functionality in biomedical applications (Elgadir et al., **2015**).

3.2.2. Results and discussion

This section was carried out in collaboration with the BioGlycoChem group of the Institute of General Organic Chemistry of the Spanish National Research Council and was focused on the semi-synthesis of phosphorylated derivatives of chitosan. The final goal aimed to obtain chitosan phosphate hydrogels in order to compare their properties with the sulfated ones and to obtain new promising candidates for advanced therapeutic strategies. Indeed, in the past years the members of the BioGlycoChem group performed a comprehensive study on the development and characterization of chitosan sulfate-lysozyme hybrid hydrogels. Lysozyme is a glycoside hydrolase with high enzymatic specificity for the hydrolysis of the glycosidic bonds of chitosan and is widely used to modulate the properties of chitosan-based biomaterials. These hydrogels are engineered to possess tailored degradability and sustained inherent antibiotic and antioxidant activities, making them promising candidates for biomedical applications. The dual functionality of these hydrogels was demonstrated, providing both antimicrobial and antioxidant effects, and they could be particularly useful in wound healing and tissue regeneration applications (Aguanell et al., **2022**). As anticipated, their studies were here extended to the possibility to obtain a phosphorylated counterpart.

As preliminary studies, standard phosphorylation methods on an unprotected substrate were used (Wang and Liu, **2022**). In particular, H_3PO_4 and urea in DMF were employed by performing a screening of heating conditions in order to compare the results of microwave irradiation to the conventional heating technique. The starting material was a commercial chitosan polysaccharide with a degree of deacetylation greater than 90%. Firstly, it was subjected to the standard protocol (Wang and Liu, **2022**) using conventional heating at 150°C for 1h. Then, the same reaction was conducted also at 120°C and 135°C both using conventional heating and microwave irradiation (Table 3.8).

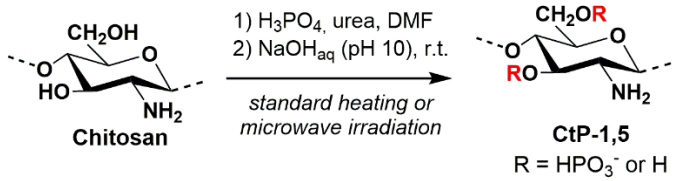

entry	product	conditions	DPh[a]
1	**CtP-1**	conventional heating: 150°C, 1h	0.70
2	**CtP-2**	microwave irradiation: 120°C, 1h, 100W, 300 psi	0
3	**CtP-3**	conventional heating: 120°C, 1h	0
4	**CtP-4**	microwave irradiation: 135°C, 1h, 100W, 300 psi	0.39
5	**CtP-5**	conventional heating: 135°C, 1h	0.16

[a] Degree of phosphorylation at O-6 site, measured by relative integration of CH_2 signal at 3.92/62.4 and 3.69/60.1 ppm assigned to CH_2-6 phosphate and CH_2-6, respectively, in the ^1H,^{13}C-DEPT-HSQC 2D-NMR spectrum

Table 3.8. Phosphorylation tests on n with H_3PO_4, urea and DMF under different reaction conditions

A set of 1D- and 2D-NMR experiments, comprising ^1H-, ^{31}P-, ^1H,^{31}P-HSQC and ^1H,^{13}C-DEPT-HSQC spectra have been recorded in order to perform the structural characterization of derivatives **CtP-1,5**. As showed in the ^{31}P-NMR spectra (Figure 3.15a) of derivatives **CtP-2,3** obtained at 120°C through microwave irradiation and conventional heating respectively, no derivatization was detected under these conditions. By increasing the temperature to 135-150°C a signal at δ_P 3.35 ppm was detected for both heating conditions.

The analysis of the ^1H,^{13}C-DEPT-HSQC 2D-NMR spectra of derivatives **CtP-1,4,5** (Figure 3.15b) revealed the presence of two methylene signals, at $\delta_{H/C}$ 3.92/62.4 and 3.69/60.1. The former could be assigned to the CH_2 group at position O-6 of 6-phosphorylated GlcN (GlcN6P) units by the main signal detected at $\delta_{H/P}$ 3.92/3.35 in the ^1H,^{31}P-HSQC 2D-NMR spectrum (Figure 3.15c), while the latter was due to unsubstituted GlcN 6-*O*-CH_2 moieties as confirmed by comparison with spectra of starting chitosan. The relative integration of the two methylene signals volumes in the

^{1}H,^{13}C-DEPT-HSQC spectra of **CtP-1,4,5** returned the DPh values resumed in Table 3.8. In all cases, this approach was found regioselective on *O*-6 position since no derivatization on either GlcN-*N*-2 or *O*-3 position was detected.

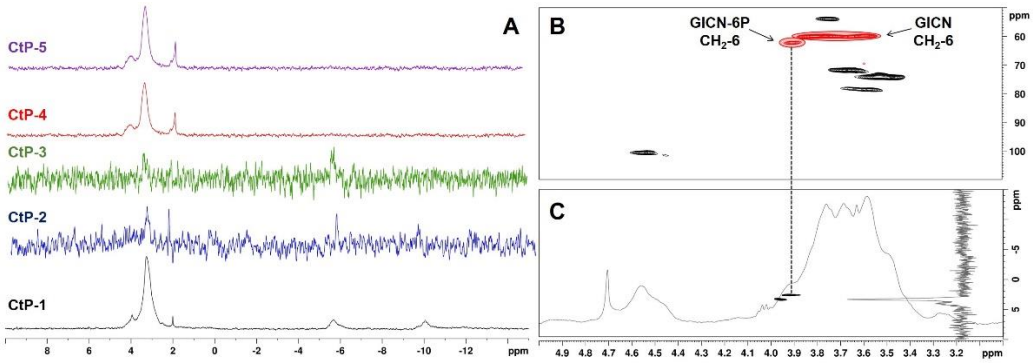

Figure 3.15. (A) ^{31}P-NMR spectra (162 MHz, 298K, D_2O) of **CtP-1** (black), **CtP-2** (blue), **CtP-3** (green), **CtP-4** (red) and **CtP-5** (purple); (B) superimposed ^{1}H-NMR and ^{1}H,^{13}C-DEPT-HSQC 2D-NMR spectra (400 MHz, 298K, D_2O, zoom) of **CtP-4** (densities enclosed in red circles were integrated for DPh estimation); (C) superimposed ^{1}H-, ^{31}P-NMR and ^{1}H,^{31}P-HSQC 2D-NMR spectra (400 and 162 MHz, 298K, D_2O) of **CtP-4**

The reactions were also tested working under the same conditions which afforded highly phosphorylated CP-C derivatives (see Section 3.1). Unfortunately, in the case of chitosan polysaccharide an increasing of the DPh value was not detected in both cases (Table 3.9). Therefore, on the basis of these preliminary studies, **CtP-1,4** were found to be the most promising products.

Further investigations testing other phosphorylating agents are planned for a near future and the most interesting compounds will be tested in the labs of BioGlycoChem group to study the bioactivity of CtP compounds in comparison with their sulfated counterparts.

entry	product	conditions	DPh[a]
1	**CtP-6**	conventional heating: 150°C, 3h	0.25
2	**CtP-7**	microwave irradiation: 120°C, 3h, 100W, 300 psi	0

[a] Degree of phosphorylation at *O*-6 site, measured by relative integration of CH_2 signal at 3.92/62.4 and 3.69/60.1 ppm assigned to CH_2-6 phosphate and CH_2-6, respectively, in the $^{1}H,^{13}C$-DEPT-HSQC 2D-NMR spectrum

Table 3.9. Semi-synthesis of **CtP-6,7**

3.2.3. Conclusions

This section was focused on the semi-synthesis of phosphorylated derivatives of chitosan working under a set of different reaction conditions. In particular, direct strategies, involving conventional heating and microwave irradiation techniques, were tested. A detailed structural characterization was carried out by performing a set of ^{1}H-, ^{13}C- and ^{31}P- one- and two-dimensional NMR experiments. These analyses revealed that both methods were able to achieve the regioselective phosphorylation of the primary hydroxyl of GlcN units on unprotected chitosan with different DPh values. Encouraged by these initial results, an expansion of the screening to further protocols, by testing for example other phosphorylating agents or by developing multi-step methods to have access to other phosphorylation patterns, has been planned for a near future. The final goal is to build a library of CtP derivatives. The most interesting compounds will be subjected to some biological investigations in the labs of BioGlycoChem group in order to compare the bioactivity of CtP compounds with their sulfated counterparts.

3.2.4. Experimental section

General methods. Commercial grade reagents and solvents were used without further purification, except where differently indicated. Starting chitosan was purchased from Biosynth (Thal, Switzerland). Microwave-irradiated reactions were performed with a CEM Discover 908010 instrument. Dialyses were conducted on Spectra/Por 3.5 kDa cut-off membranes at 4°C. Centrifugations were performed with an Eppendorf Centrifuge 5804R instrument at 4°C (4600 g, 5 min). Freeze-dryings were performed with a 5Pascal Lio 5P 4K freeze dryer. NMR spectra were recorded on a Bruker Avance-III HD (^{1}H: 400 MHz, ^{13}C: 100 MHz, ^{31}P: 162 MHz) or on a Bruker Avance-III (^{1}H: 600 MHz, ^{13}C: 150 MHz) instrument – the latter equipped with a cryo-probe – in D_2O (acetone as internal standard, ^{1}H: $(CH_3)_2CO$ at δ 2.22; ^{13}C:$(CH_3)_2CO$ at δ 31.5; H_3PO_4 as external standard, ^{31}P: δ 0.0). Data were processed using the data analysis packages integrated with Bruker TopSpin® 4.0.5 software. ^{31}P-NMR spectra were obtained by typically accumulating 512 transients. ^{1}H- and ^{31}P-1D-DOSY experiments were measured using a stimulated echo sequence with bipolar gradient pulses and one spoil gradient (stebpgp1s1d) with a diffusion time Δ of 100 ms, a gradient duration of 2 or 4 ms (for ^{1}H- and ^{31}P-1D-DOSY, respectively) and accumulating 64 or 2048 transients (for ^{1}H- and ^{31}P-1D-DOSY, respectively). ^{1}H,^{13}C-DEPT-HSQC experiments were measured in the ^{1}H-detected mode via single quantum coherence with proton decoupling in the ^{13}C domain, using data sets of 2048 × 256 points and typically 64 increments. ^{1}H,^{31}P-HSQC experiments were measured in the ^{1}H-detected mode via a phase sensitive gradient selection with decoupling during acquisition, using data set of 2048 × 256 points and typically 64 increments.

Typical procedure for phosphorylation with H_3PO_4. A mixture of chitosan (45.3 mg, 0.268 mmol) and urea (227 mg, 3.78 mmol) was dried under vacuum, purged under argon, then treated with dry DMF (1.8 mL) and heated to 100°C. The resulting solution was treated with 85% H_3PO_4 (454 μL). The suspension was stirred at 120-

150°C under conventional heating or microwave irradiation for 1 hour. The obtained yellowish suspension was then cooled to room temperature and methanol (15 mL) was added to form a white precipitate. The mixture was cooled in freezer for 1h, then the precipitate was collected by centrifugation. The solid was dissolved in HPLC-grade H_2O (6.0 mL; pH ~ 2) and treated with a few drops of aqueous 33% NaOH to neutral pH. After dialysis and freeze-drying, phosphorylated product **CtP-1** (or **CtP-2,5**) was obtained (44.7 mg, 99% mass yield).

References

Aguanell, A., del Pozo, M. L., Perez-Martin, C., Pontes, G., Bastida, A., Fernandez-Mayoralas, A., García-Junceda, E., Revuelta, J., **2022**. *Carbohydr. Polym. 291*, 11961.

Ahmed, T., Aljaeid, B., **2016**. *Drug. Des. Devel. Ther. 10,* 483-507.

Duan, J., Liang, X., Cao, Y., Wang, S., Zhang, L., **2015**. *Macromolecules 48*, 2706-2714.

Elgadir, M., Uddin, M., Ferdosh, S., Adam, A., Chowdhury, A., Sarker, Z., **2015**. *J. Food Drug Anal. 23*, 619-629.

Fedel, M., Endogan, T., Hasirci, N., Maniglio, D., Morelli, A., Chiellini, F., Motta, A., **2012**. *J. Bioact. Compat. Polym. 27*, 295-312.

Grenha, A., Gomes, M. E., Rodrigues, M., Santo, V. E., Mano, J. F., Neves, N. M., Reis, R. L., **2009**. *J. Biomed. Mater. Res. A 92A*, 1265-1272.

Moura, M., Faneca, H., Lima, M., Gil, M., Figueiredo, M., **2011**. *Biomacromolecules, 12*, 3275-3284.

Sacco, P., Cok, M., Scognamiglio, F., Pizzolitto, C., Vecchies, F., Marfoglia, A., Donati, I., **2020**. *Molecules 25*, 1534.

Sacco, P., Furlani, F., Marzo, G., Marsich, E., Paoletti, S., Donati, I., **2018**. *Gels 4*, 67.

Skovstrup, S., Hansen, S., Skrydstrup, T., Schiøtt, B., **2010**. *Biomacromolecules 11*, 3196-3207.

Sogias, I., Williams, A., Khutoryanskiy, V., **2008**. *Biomacromolecules 9*, 1837-1842.

Wang, K., Liu, Q., **2022**. *Carbohydr. Res. 386*, 48-56.

Zhang, G., Liu, J., Li, R., Jiao, S., Feng, C., Wang, Z., Du, Y., **2018**. *Mar. Drugs 16*, 151.

CHAPTER 4

DEVELOPMENT OF COVALENTLY CROSS-LINKED INJECTABLE GELS DERIVED FROM RENEWABLE NATURAL BIOPOLYMERS FOR THERAPEUTIC APPLICATIONS

4

DEVELOPMENT OF COVALENTLY CROSS-LINKED INJECTABLE GELS DERIVED FROM RENEWABLE NATURAL BIOPOLYMERS FOR THERAPEUTIC APPLICATIONS

4.1. Cross-linked gels: an overview

This PhD fellowship was granted by PON project "Ricerca e Innovazione" 2014-2020 – Azione IV.5 "Dottorati di ricerca su tematiche Green" and included a period of work in collaboration with IBSA Italia Farmaceutici Srl. In this frame, a part of this thesis work was focused on the structural characterization of new cross-linked gel derived from sustainable sources for applications in pharmaceutical field. The general project aimed to develop a pre-filled syringe medical device based on a cross-linked formulation for osteoarthritis drugs or dermocosmetic applications. The final goal is to obtain a device with optimal performance in terms of rheological behavior and *in vivo* residence time. In particular, through the use of innovative biopolymers, both in terms of specific macromolecular constituents and the chemical modification and cross-linking technologies implemented on them, it is possible to increase process yields and reduce the environmental impact compared to existing commercially devices. The synthesis of cross-linked gels can be achieved through various methods, including ionic and covalent cross-linking. The choice of cross-linking agent significantly impacts the mechanical properties and swelling behavior of the resulting hydrogels. The versatility of these materials makes them suitable for a wide range of applications, from injectable gels for localized drug delivery to scaffolds for tissue regeneration. The exploration of new cross-linked gels derived from sustainable

sources, particularly hyaluronic acid (HA) cross-linked with 1,4-butanediol diglycidyl ether (BDDE), has garnered significant attention in the pharmaceutical field. HA is a naturally occurring polysaccharide that plays a crucial role in various biological processes, including tissue hydration, cellular signaling, and wound healing. Its biocompatibility and biodegradability make it an ideal candidate for applications in drug delivery systems, tissue engineering, and regenerative medicine. The use of BDDE as a cross-linking agent enhances the mechanical properties and stability of HA gels, allowing for controlled release of therapeutic agents and improved structural integrity (Sturabotti et al., **2022**).

This type of modification affects the hydroxyl groups of polysaccharides, inducing the cross-linking of polymeric chains through ether bond formation. This reaction preserves the polyanionic nature of the polysaccharides, promoting the formation of hydrogels with elevated hydrophilicity with a consequent impact on their hydration capacity in a physiological environment. Recent studies have demonstrated that the cross-linking density of HA gels can be finely tuned by varying the concentration of BDDE, which directly influences the gels physicochemical properties, such as viscosity, injectability, and degradation rates (Del Olmo et al., **2022**).

Besides, commercially available hydrogels are known to contain two different 1,4-butanediol di-(propan-2,3-diolyl) ether (BDPE) functionalizations. Indeed, part of BDDE reacts with both its ends with HA, bridging the two disaccharide units (BDPE bridging) and forming cross-linked HA. Another portion of the di-epoxide reacts with water/hydroxide at one end and with the polymer at the other, thus installing only an ether-linked appendage to HA (BDPE pendant) and forming branched HA (Figure 4.1) (La Gatta et al., **2022**).

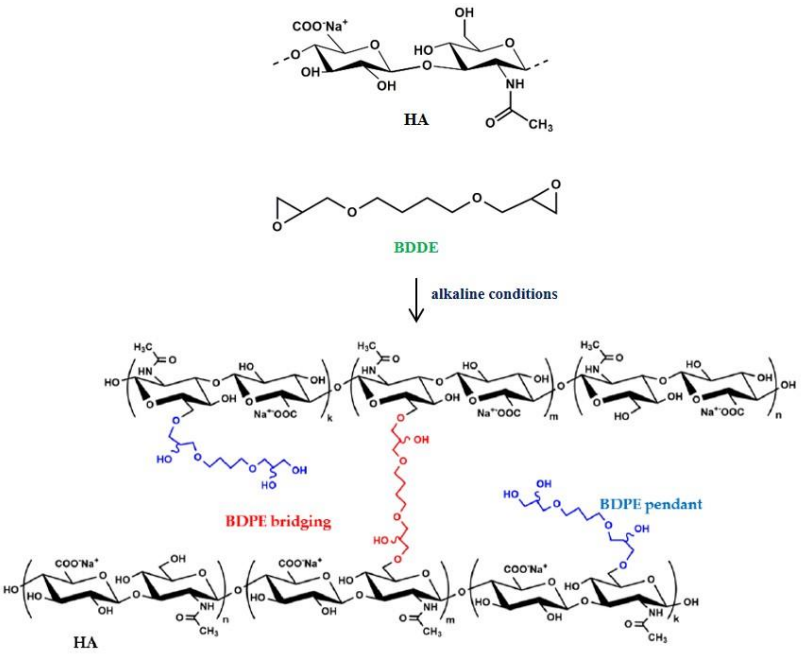

Figure 4.1. Structure of the HA network obtained through the reaction with BDDE (La Gatta et al., **2022**)

The rheological properties of HA-BDDE gels have been shown to exhibit favorable characteristics, such as shear-thinning behavior, which is essential for injectable applications. The incorporation of BDDE not only improves the mechanical strength of HA gels but also enhances their resistance to enzymatic degradation, a critical factor for maintaining the longevity of drug delivery systems *in vivo* (Choi et al., **2015**; Al-Sibani et al., **2015**). Studies have indicated that HA gels cross-linked with BDDE can effectively encapsulate a variety of therapeutic agents, including antibiotics and anti-inflammatory drugs, thereby providing a dual function of drug delivery and tissue augmentation (Varga, **2024**). This capability underscores the potential of these gels in addressing clinical challenges related to localized drug delivery and tissue repair. Moreover, the sustainability aspect of using HA derived from natural sources aligns with the growing demand for environmentally friendly materials in the pharmaceutical industry. The development of cross-linked gels represents a significant

advancement in the field, combining the benefits of biocompatibility, mechanical robustness, and controlled drug release, while also adhering to sustainable practices (Khunmanee et al., **2017**). As research progresses, these species are expected to play a pivotal role in the future of regenerative medicine and targeted therapy.

4.2. Results and discussion

Based on these premises, the polymers selected for this project were hyaluronic acid (HA) of different molecular weights and biotechnological chondroitin (BC), both from bio-fermentative sources. In particular, they were used in different combinations through the use of a heterogeneous-phase polysaccharide cross-linking technology, using BDDE as a cross-linking agent (Figure 4.2). This reaction technology has been recently developed by IBSA Italia Farmaceutici Srl and its details cannot be described here due to trade secrets. The aim was to develop different hydrogels obtained by modulating the relative ratio of HA and BC and using HA samples with different molecular weights. In particular, a high molecular weight derivative (Mw ≥ 1 MDa) and a low molecular weight one (HA ~ 200kDa) were used. Indeed, previous studies (La Gatta et al., **2020**) showed that the combinations of different molecular weights allow to design gels with specific performance. In particular, it was expected that to decrease the length of the polymer chains would decrease the swelling of the hydrogels, allowing the realization of formulations capable of releasing a greater amount of HA/BC while maintaining the rigidity of the hydrogel unaltered and, therefore, preserving its injectability. The final intent is to obtain more concentrated formulations that persist longer in tissues and have better cohesiveness with a relative positive impact on tissue integration. Furthermore, by appropriately modulating the ratios between the two molecular weights of HA and between HA and BC, the aim is to create hydrogels with specific performances.

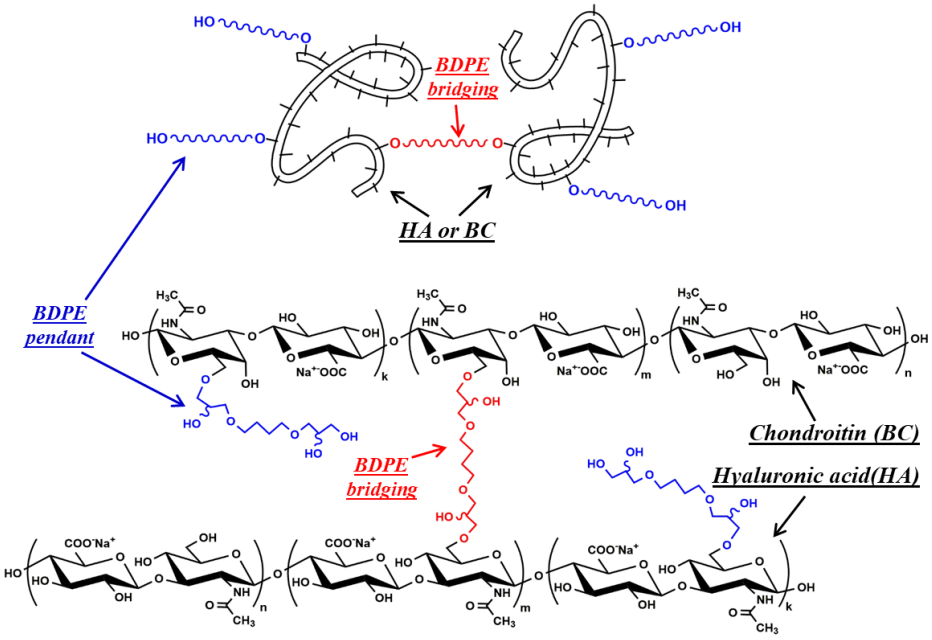

Figure 4.2. Schematic representation of the co-cross-linking of GAGs from bio-fermentative sources

Within this frame, the main part of the experiments performed within this PhD thesis work were to analyze and characterize through NMR techniques the most promising formulations in order to determine their network structure.

In particular, for all the selected samples, one-dimensional ^{1}H NMR spectra were first recorded, both under standard conditions and in diffusion-ordered (DOSY) mode. The former provided general information on the chemical structure of the analytes, showing the presence of signals characteristic of biopolymers and, if present, of semi-synthetically introduced functionalities, whether derived from BDPE cross-linking agents or from any other modification. DOSY spectra, on the other hand, allowed to distinguish between the covalent chemical conjugation of cross-linkers from their simple physical mixing with the biopolymers. The presence of any low molecular weight organic contaminant (cross-linking agents, derivatization reagents, solvent residues, etc.) in quantities comparable in scale (from 5% by weight upwards) with

the biopolymer under analysis, could be also deduced by comparing ^{1}H-NMR spectra recorded under standard conditions and in DOSY mode. For all the investigated cross-linked biopolymers, these spectra were also measured on some chemically partially degraded derivatives thereof, in order to facilitate the recognition of characteristic signals in the NMR spectra. In fact, the resolution of NMR spectra, under the same instrumental conditions, decreases as the molecular weight of the analyte increases. For this purpose, an analytical method was developed based on the coupling of a chemoselective, chemical degradation reaction of the analytes followed by measurements of their one-dimensional ^{1}H- and ^{13}C-NMR spectra. The reaction involves a partial depolymerization of the biopolymers, aimed to obtain a mixture of oligomers that are completely soluble in deuterated water (for NMR experiments). Optimization of the reaction required the use of sufficiently mild conditions to cleave some of the glycosidic bonds that hold the monomeric units of the biopolymers together without affecting the ether functionalities that act as cross-linking or branching points (Figure 4.3). By using dilute acidic conditions (0.01 M HCl in water) and carrying out the reaction at a temperature of 70°C under magnetic stirring for 72 hours (La Gatta et al., **2022**), the complete disappearance of the initial solid material constituting the biopolymer and the formation of a clear solution was observed. After neutralization with solid NaH_2PO_4 and freeze-drying, a material was obtained that was completely soluble at high concentrations in D_2O ($\geq$ 100 mg/mL) in all cases treated during this work.

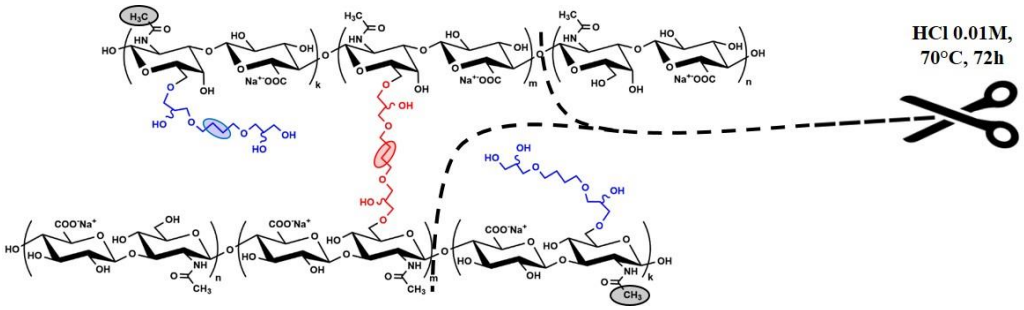

Figure 4.3. Schematic representation of partial depolymerization reaction of cross-linked HA and BC biopolymers with BDDE (atoms enclosed in ellipses are the ones related to the ^{1}H-NMR signals employed for quantifying BDDE derivatization: see text for details)

^{1}H-NMR analysis of the obtained products allowed the evaluation of the total degree of functionalization with BDPE units resulting from cross-linking reactions with BDDE. Indeed, the relative integration of the CH_3 signal at 1.95 ppm, attributable to the *N*-acetyl in the repeating disaccharide unit of the biopolymer (HA and/or BC), and the CH_2CH_2 aliphatic signal of BDPE at 1.55 ppm, allowed for the quantitative evaluation of the degree of biopolymer derivatization with BDDE, through equation 4.1 (Wende et al., **2017**).

$$\text{Degree of derivatization with BDPE (mol\%)} = (\text{integral } CH_2CH_2/4) / (\text{integral } CH_3/3) * 100 \qquad \text{(Eq. 4.1)}$$

For instance, Figure 4.4 shows a comparison between the ^{1}H-NMR spectra of the partially degraded derivatives of two unmodified biopolymers (HA and BC) and of a product containing both of them cross-linked with BDDE.

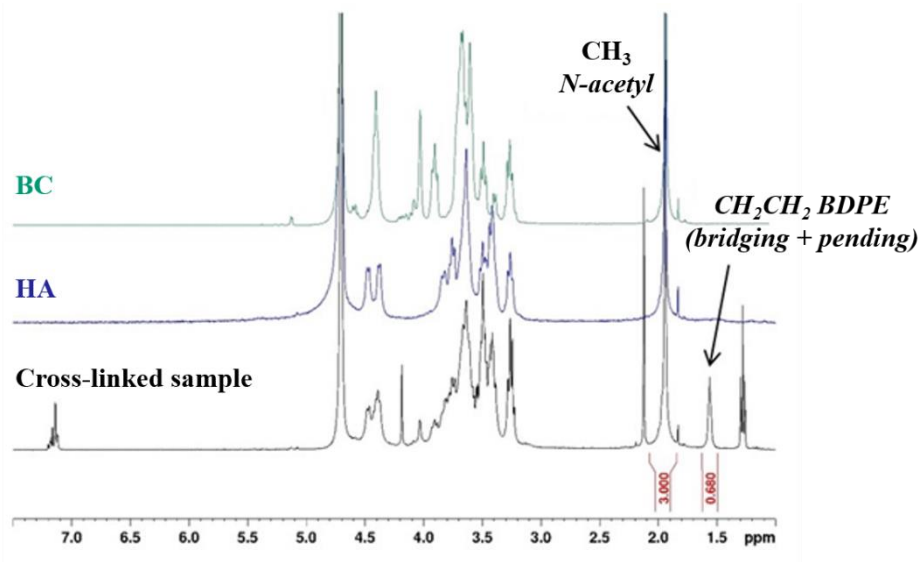

Figure 4.4. ^{1}H-NMR spectra (400 MHz, 298K, D_2O) of the chemically partially degraded derivatives of unmodified chondroitin (**BC**, green) and hyaluronic acid (**HA**, blue) and of a cross-linked sample (black)

This method was also validated by performing ^{1}H-NMR analysis on low molecular weight cross-linked biopolymers (≤ 100 kDa), which were therefore soluble in D_2O even before partial depolymerization. In such cases, the degree of derivatization with BDPE, calculated according to equation 4.1, was found to be very similar whether calculated on the intact biopolymer (either HA or BC), or after partial depolymerization, demonstrating that the latter does not significantly affect the BDPE functionalities that derivatize the biopolymer (Table 4.1).

Sample	***Degree of derivatization with BDPE***	
	pre-depolymerization	*post-depolymerization*
cross-linked-HA	15.5%	14.8%
cross-linked-BC	10.7%	10.0%

Table 4.1. Degree of derivatization with BDPE pre- and post-depolymerization

Figure 4.5 shows a comparison between the two spectra measured on samples pre- and post-depolymerization, respectively, in the case of a cross-linked BC biopolymer.

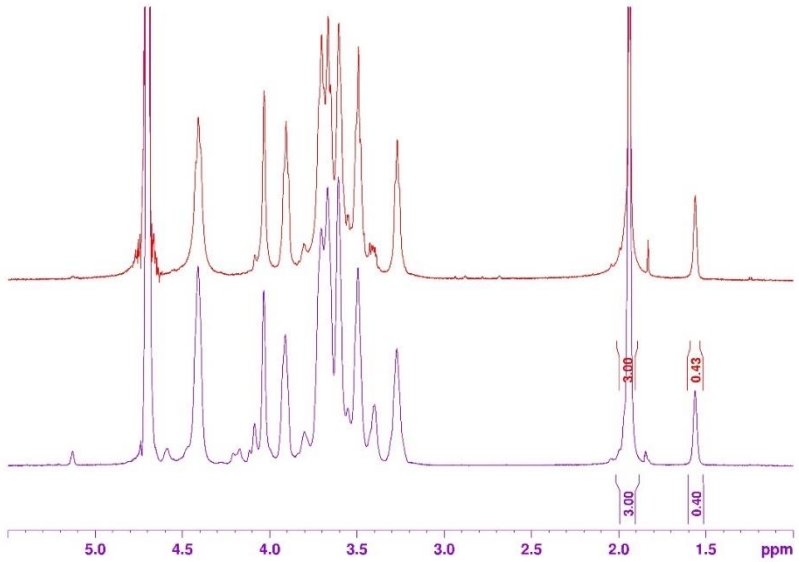

Figure 4.5. ^{1}H-NMR spectra (400 MHz, 298K, D_2O) of cross-linked BC pre- (red) and post-depolymerization (purple)

Further analysis by ^{13}C-NMR spectroscopy allowed for the quantitative determination of further structural parameters of biopolymers functionalized with BDPE units. Specifically, ^{13}C-NMR spectra of post-depolymerization biopolymers enabled differentiation between BDPE units present on the biopolymer as either branching or cross-linking moieties. By acquiring ^{13}C-NMR spectra in inverse-gated mode with a sufficiently long delay time (15 s), the influence of relaxation times and the nuclear Overhauser effect (nOe) on peak integrals was minimized, correlating them solely to the amount of atomic nuclei generating them. Thus, by integrating the signal at 22.5 ppm, corresponding to the CH_3 of the *N*-acetyl groups in the repeating units of both HA and BC, and the signal at 62.7 ppm, corresponding to the terminal CH_2OH group of the branched BDPE units, and using equations 4.2 and 4.3 (Wende et al., **2017**), it

was possible to obtain quantitative data of the branching or cross-linking BDPE units relative to the total degree of derivatization:

Degree of branching with BDPE (mol%) = (integral of the terminal CH_2OH BDPE) / (integral CH_3 NAc) * 100) (Eq. 4.2)

Degree of cross-linking with BDPE (mol%) = Degree of derivatization with BDPE (mol%) – Degree of branching with BDPE (mol%) (Eq. 4.3)

Figure 4.6 shows the ^{13}C-NMR spectrum in inverse-gated mode of the partially degraded derivative of a product containing both HA and BC cross-linked with BDDE.

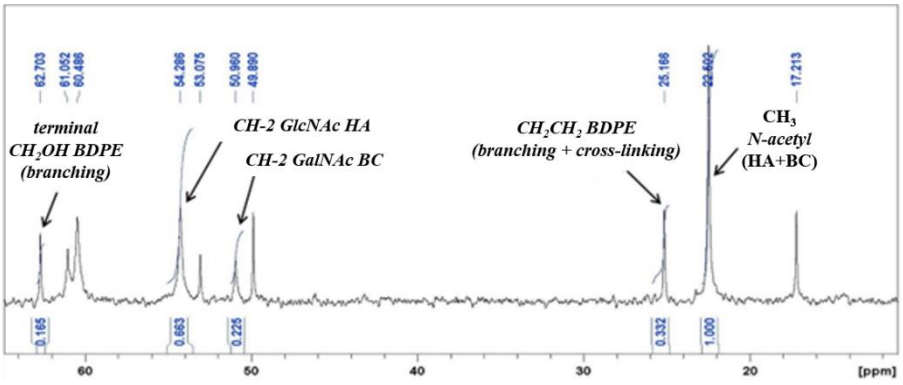

Figure 4.6. ^{13}C-NMR spectrum (100 MHz, 298K, D_2O, zoom) of the chemically partially degraded derivative of HA and BC derivatized with BDDE

The described approach was used for the analysis of the most promising gel formulations obtained in the laboratories of IBSA Italia Farmaceutici Srl. The results are resumed in the following table.

Sample	BDPE/HA-BC (mol%)[a]	BDPE pend./HA-BC (mol%)[b]	BDPE-brid/HA-BC (mol%)[c]	BDPE-brid/tot BDPE[d]	BDPE/HA-BC (wt%)[e]	Total BDPE in the gel (wt%)[f]
	A	**B**	**C**	**D**	**E**	**F**
Sample 1	17.0	16.5	0.5	2.9	8.7	3.46
Sample 2	17.0	16.6	0.4	2.4	8.7	3.46
Sample 3	8.1	7.6	0.5	6.2	4.1	1.65
Sample 4	8.1	7.3	0.8	9.9	4.1	1.65
Sample 5	5.9	4.7	1.2	20.3	3.0	n.d.
Sample 6	19.9	18.3	1.6	8.0	10.1	3.23

[a] see equation 4.1
[b] see equation 4.2
[c] see equation 4.3
[d] (C)/(A)*100
[e] (A)*[(M_W BDPE) /(M_W HA_d)]
[f] [HA wt% in the gel × (E)] /100

Sample	Cross-linked-HA-BC/HA-BC (mol%)[g]	Branched-HA-BC/HA-BC (mol%)[h]	Modified-HA-BC/HA-BC (mol%)[i]	HA-BC ratio[j]
	G	**H**	**I**	**J**
Sample 1	1	16.5	17.5	2.9
Sample 2	0.8	16.6	17.4	3.1
Sample 3	1	7.6	8.6	3.0
Sample 4	1.6	7.3	8.9	3.0
Sample 5	2.4	4.7	7.1	n.d.
Sample 6	3.2	18.3	21.5	total HA

[g] (C)*2
[h] = (B)
[i] (G) + (H)
[j] ^{13}C-NMR (integral GlcNAc-CH-2 HA / integral GalNAc-CH-2 BC)

Table 4.2. Structural characterization data for the most promising cross-linked biopolymers formulations obtained in the laboratories of IBSA Italia Farmaceutici Srl

The BDPE/HA-BC (mol%) values (A) calculated from the ^{1}H-NMR analyses ranged widely. It varied between a lower amount (5.9%), which was detected for **Sample 5**, up to 19.9%, which was recorded for **Sample 6**. As regards the BDPE/HA-BC weight ratio (E), the values ranged from 3 (**Sample 5**) to 10 wt% (**Sample 6**), with **Sample-1,2** and **3,4** showing similar results. The total BDPE amount (wt%) in the gel (F) was in the range 1.65–3.46 wt%. Besides the ^{13}C-NMR spectra allowed to quantify the BDPE pendant/HA-BC molar ratio (B), the BDPE bridging/HA-BC (mol%) (C) and the BDPE bridging/$BDPE_{tot}$ (mol%) values (D). The data indicate that BDPE cross-linking disaccharide units varied from 2.4 to 20.3% compared to the total BDPE amount, with the highest value recorded for **Sample 5** (D). Therefore, most of the BDDE-derived functionalizations were present on HA-BC chains as pendant groups, rather than as cross-linking moieties. The amount (mol%) of cross-linked HA-BC disaccharide units (G) and the amount of branched HA-BC (mol%) (H) are also showed. Finally, the amount (mol%) of HA-BC that were chemically modified by BDPE, which describes the total HA/BC modification level (cross-linked + branched) (I), is indicated. **Sample 6** turned out to be the most cross-linked gel (3.2 mol% (G)) and the product that presented the highest percentage of branched disaccharide units (18.3 mol%) (H). It also showed the highest overall modification degree (I), reaching a 21.5% value.

4.3. Conclusions

This section was focused on the structural characterization of new cross-linked gel derived from sustainable sources for applications in pharmaceutical field in collaboration with IBSA Italia Farmaceutici Srl. In this frame, cross-linked GAGs-based products were synthesized, starting from a mixture of hyaluronic acid (HA) and biotechnological chondroitin (BC), both from bio-fermentative sources. These

biopolymers were cross-linked with BDDE as cross-linking. The obtained samples were subjected to a protocol involving a partial depolymerization step under mild acidic conditions to improve the gel solubility in D_2O and ^1H and ^{13}C NMR analysis for structural characterization were performed. In particular, it was possible to determine a series of structural parameters including the degree of derivatization, the degree of branching, and the degree of cross-linking with BDPE. The investigated samples will be subjected to further studies concerning the *in vitro* and *in vivo* biochemical and biological characterization of the developed formulations, also with the aid of novel methodologies such as cultures on three-dimensional (3D) scaffolds.

4.4. Experimental section

General methods. The cross-linked HA and/or BC samples were synthetized by IBSA Italia Farmaceutici Srl. Freeze-dryings were performed with a 5Pascal (Trezzano sul Naviglio, Italy) Lio 5P 4K freeze dryer. NMR spectra were recorded on a Bruker (Billerica, MA, USA) Avance-III HD (^1H: 400 MHz, ^{13}C: 100 MHz) or on a Bruker Avance-III (^1H: 600 MHz, ^{13}C: 150 MHz) instrument – the latter equipped with a cryo-probe – in D_2O (acetone as internal standard, ^1H: $(CH_3)_2CO$ at δ 2.22 ppm; ^{13}C:$(CH_3)_2CO$ at δ 31.5 ppm) or DMSO-*d*$_6$ (^1H: CHD_2SOCD_3 at δ 2.49 ppm; ^{13}C: CD_3SOCD_3 at δ 39.5 ppm). Data were processed using the data analysis packages integrated with Bruker TopSpin® 4.0.5 software.

Partial depolymerization procedure. The samples were suspended in a 0.01M HCl solution (pH 2) and stirred at 70 °C for 3 days. The samples were neutralized by adding Na_2HPO_4 and freeze-dried. The dried samples were dissolved in D_2O and ^1H,^{13}C - NMR analyses were performed.

References

Al-Sibani, M., Al-Harrasi, A., Neubert, R., **2015**. *J. Drug Deliv. Sci. Technol. 29*, 24-30.

Choi, S., Yoo, M., Lee, S., Lee, H., Son, D., Jung, J., Noh, I., Kim, C., **2015**. *J. Biomed. Mater. Res. 103(9)*, 3072-3080.

Del Olmo, J., Pérez-Álvarez, L., Saez Martínez, V., Benito Cid, S., Pérez González, R., Vilas-Vilela, J. L., Alonso, J. M. **2022**. *Gels 8(4)*, 223.

La Gatta, A., Bedini, E., Aschettino, M., Finamore, R., Schiraldi, C., **2022**. *Polymers 14(12)*, 2402.

La Gatta, A., Salzillo, R., Catalano, C., Pirozzi, A. V. A., D'Agostino, A., Bedini, E., Cammarota, M., De Rosa, M., Schiraldi, C., **2020**. *Int. J. Biol. Macromol. 144*, 94–101.

Sturabotti, E., Consalvi, S., Tucciarone, L., Macrì, E., Lisio, V., Francolini, I., Minichiello, C., Piozzi, A., Vuotto, C., Martinelli, A. **2022**. *Gels 8(8)*, 480.

Varga, V., **2024**. *Int. J. Mol. Sci. 25(8)*, 4336.

Wende, F. J., Gohil, S., Nord, L. I., Helander Kenne, A., Sandström, C., **2017**. *Carbohydr. Polym. 157*, 1525.

APPENDIX
PhD COURSE ACTIVITY SUMMARY

PhD Course Activity Summary

Attended courses:

- "Natural phenolic compounds: structure, reactivity and applications", Prof. L. Panzella;

- "Synthetic glycochemistry", Proff. A. Iadonisi, E. Bedini;

- "Smart drug delivery systems", Prof. A. Guaragna

- "Advanced Climatology", Prof. N. Scafetta (transversal training course)

- "Persistent organic pollutions (POPs)", Prof. A. Andolfi

- "Protein Engineering", Prof. A. Duilio

- PhD course in the frame of arCHIMede project, title: "DNA beyond the double-helix" – Dr. Jean Louis Mergny

Attended seminars:

- January 10th, 2022: *"Il chimico: un'esperienza nell'industria"* by Dr. Vito Savino;

- January 21th, 2022: *"Research & development in a big company"* by Dr. Andrea di Matteo;

- March 9th, 2022: *"Chimici in ospedale"* by Dr. Rita Boenzi;

- April 11th, 2022: *"Developments in Green Catalytic Technologies for a Circular Economy of Water"* by Dr. Moisés Canle Lopez;

- April 14th, 2022: *"Protezioni dei contenitori metallici destinati ad uso alimentare"* by Dr. Biagio Leone;

- April 22th, 2022: *"Metabolic control of immunological self-tolerance: bridging the gap among susceptibility to autoimmunity infections and cancer"* by Prof. Giuseppe Materese;

- May 13th, 2022: *"Synthetic carbohydrates-based materials"* by Dr. Martina Delbianco;

- May 16th, 2022: *"Breaking the limits in understanding glycan recognition by NMR"* by Prof. Jesús Jiménez-Barbero;

- September 2th, 2022: *"A through the looking glass view of voltage-gated ion channel structure"* by Prof. Daniel Minor;

- September 22th, 2022: *"Adventures in Chemical Biology – from proteases to in vivo Chemistry"* by Prof. Mark Bradley.

- September 5th, 2023: *"On discovery and sensitivity in (photo)catalysis"* by Prof. Frank Glorius;

- December 1st, 2023: "*Staphylococcus aureus glycopolymers: sweet ispiration for synthetic methodology development*" by Prof. Jeroen Codèe;

- May 8th, 2024: *"Brewer's spent yeast polysaccharides – structural features and applications"* by Prof. Manuel Coimbra;

- May 8th, 2024: *"NMR characterization of biological therapeutics and nanosystem"* by Prof. Marco Fragai;

- May 16th, 2024: *"There and back again: from applications to theoretical modelling in Chemistry"* by Prof. Carlo Adamo

Visiting periods in Institutions different from University of Naples "Federico II":

Host Institution	Country	Start date	End date
Instituto de Quimica Organica General – Consejo Superior de Investigaciones Cientificas	Spain (Madrid)	25/02/2023	06/06/2023

Attended congresses/workshops/summer schools/contribution:

- July 2022 Flash and Poster Communication at 9th Biennial Meeting on Microbial Carbohydrates *(BMMC)*, Naples, Italy. Title: "*Glycosaminoglycan-like sulfated polysaccharides from Vibrio diabolicus bacterium: semi-synthesis and characterization*".

- September 2022 Poster Communication at Ischia Advanced School of Organic Chemistry (IASOC2022), Ischia, Italy. Title: "*Multi-step strategies for the regioselective sulfation of polysaccharides from eco-sustainable sources*".

- October 2022 Poster Communication at EPNOE workshop – "Polysaccharides in drug delivery: on the road to innovation", Rome, Italy. Title: "*Semi-synthesis of glycosaminoglycan-mimetics from bacterial sources for biomedical applications*".

- June 2023 Oral Communication at XVIII Convegno-Scuola sulla chimica dei carboidrati, Pontignano, Siena, Italy. Title: "*Regioselective sulfation of polysaccharides from sustainable sources*".

- July 2023 Oral Communication at NapOsaka Meeting, Naples, Italy. Title: "*Semi synthesis of glycosaminoglycans mimetics from sustainable sources"*.

- July 2023 Oral Communication 21th European Carbohydrate Symposium (EUROCARB), Paris, France. Title: "*Development of semi-synthetic methods to obtain glycosaminoglycans mimics from sustainable sources"*.

- September 2023 Oral Communication at 8th EPNOE International Polysaccharides Conference, Graz, Austria. Title: "*Semi-synthesis of glycosaminoglycans mimetics from sustainable sources"*.

- September 2024 Poster Communication at Ischia Advanced School of Organic Chemistry (IASOC2024), Ischia, Italy. Title: "*Semi-synthesis of glycosaminoglycans mimetics from sustainable sources"*.

Support for teaching activity:

- Laboratory assistant for students training in Fundamental Organic Chemistry, Department of Chemical Sciences, University of Naples Federico II – Naples, Italy

- Tutor for students in Organic Chemistry - Department of Chemical Sciences, University of Naples Federico II – Naples, Italy

UNIONE EUROPEA
Fondo Sociale Europeo

La borsa di dottorato è stata cofinanziata con risorse del
Programma Operativo Nazionale Ricerca e Innovazione 2014-2020,
risorse FSE REACT-EU
Azione IV.4 “Dottorati e contratti di ricerca su tematiche dell’innovazione”
e Azione IV.5 “Dottorati su tematiche Green”